CONF-871179--Vol. 2

*Research sponsored by the Office of Fusion Energy, U.S. Department of Energy, under contract DE-AC05-84OR21400 with Martin Marietta Energy Systems, Incorporated.

Proceedings of

U.S.–Japan Heliotron-Stellarator Workshop

Volume II

held at

Oak Ridge National Laboratory
Oak Ridge, Tennessee, U.S.A.

November 9-13, 1987

CONF-871179--Vol. 2

AGENDA FOR US-JAPAN STELLARATOR/HELIOTRON WORKSHOP

FUSION ENGINEERING DESIGN CENTER, OAK RIDGE

NOVEMBER 9–13, 1987

CONF-871179--Vol.2

DE88 004789

Table of Contents

Monday, November 9

8:30 A.M. Registration

8:45 A.M. Welcome - M. W. Rosenthal (ORNL)

Opening Remarks - K. Uo (Kyoto PPL)

9:00 A.M. Overviews - K. Uo, Chairman

Volume I

Overview of the Heliotron E Experiment - O. Motojima (Kyoto PPL)

Overview of CHS Program - K. Matsuoka (Nagoya IPP)

Status of ATF Project - G. H. Neilson (ORNL)

Status of W VII-AS - H. Renner (IPP Garching)

TJ-II Program Status - A. P. Navarro (CIEMAT, Madrid)

12:30 P.M. Lunch

2:00 P.M. Tour of ATF and private discussions, Fusion Energy Division

Tuesday, November 10

8:30 A.M. Programs, Device Preparation - J. L. Shohet, Chairman

ATF Experimental Plans - M. Murakami (ORNL)

ATF Diagnostics - R. C. Isler (ORNL)

Machine of Compact Helical System - K. Matsuoka (Nagoya IPP)

CHS Experimental Program and Diagnostics - S. Okamura (Nagoya IPP)

Transport Studies in IMS - J. L. Shohet (U. Wisc.)

11:30 A.M. Lunch

Tuesday, November 10

1:00 P.M. Confinement - O. Motojima, Chairman Volume II

Ripple Transport at Arbitrary Collision Frequency - W.N.G. Hitchon (U. Wisc.)

Transport Scaling in the Collisionless-Detrapping Regime - E. C. Crume (ORNL)

Transport Analysis for Heliotron E - T. Mutoh (Kyoto PPL)

Transport Analysis for ATF - H. C. Howe (ORNL)

Simulation Analysis of Heating and Transport - T. Amano (Nagoya IPP)

Analysis of W VII-A Data - H. Renner (IPP Garching)

7:00 P.M. Reception - Home of W. R. Wing

Wednesday, November 11

8:30 A.M. ECH and NBI - M. Murakami, Chairman

Numerical Study of Fast Ion Confinement - K. Hanatani (Kyoto, PPL)

Benchmarks of NBI Codes for Stellarators - R. H. Fowler (ORNL)

ECH Commissioning and Plans for ATF - T. L. White (ORNL)

ECH and ICH Startup Analysis - M. D. Carter (ORNL)

11:30 A.M. Lunch

1:00 P.M. Ion Cyclotron Heating - T. Amano, Chairman Volume III

Heliotron E ICRF Heating Experiment - T. Mutoh (Kyoto PPL)

CHS Heating Systems (NBI, ECH, ICH) - K. Nishimura (Nagoya IPP)

ICH Program for ATF - F. W. Baity (ORNL)

ICRF Wave Propagation - D. B. Batchelor (ORNL)

The HBQM Heliac Work - B. A. Nelson (U. Washington)

Thursday, November 12

Volume III (continued)

8:30 A.M. Configuration Studies - G. H. Neilson, Chairman

Configuration Studies – K. Nishimura (Nagoya IPP)

Compact Torsatron Studies – B. A. Carreras (ORNL)

Low Aspect Ratio Torsatron Design – J. Hanson (Auburn)

Optimized Small Stellarator Designs – D. T. Anderson (U. Wisc.)

Configuration Studies for ATF – J. H. Harris (ORNL)

11:30 A.M. Lunch

1:00 P.M. Configuration Studies - K. Matsuoka, Chairman

Currents in ATF – B. A. Carreras (ORNL)

Computations of 3-D Equilibria with Islands – A. Reiman (PPPL)

Magnetic Surface Mapping Studies – D. G. Swanson (Auburn)

Magnetic Field Alignment and Mapping on ATF – F.S.B. Anderson (U. Wisc.)

Divertor Experiments in IMS – D. T. Anderson (U. Wisc.)

Friday, November 13

8:30 A.M. General Experimental - H. Renner, Chairman

PMI Program and Wall Conditioning for ATF – P. K. Mioduszewski (ORNL)

Hard X-ray Suppression on ATF – D. A. Rasmussen (ORNL)

Plasma Rotation and Potential Measurement – O. Motojima, (Kyoto PPL)

Status of Heavy Ion Beam Probe for ATF – A. Carnevali (RPI)

11:30 A.M. Lunch

1:00 P.M. Private discussions, Fusion Energy Division

Visit to Large Coil Facility?

Ripple Transport At Arbitrary Collision Frequency.

C.D. Beidler, W.N.G. Hitchon, W.J. van Rij,* S.P. Hirshman* and J.L. Shohet.

Torsatron/Stellarator Laboratory, University of Wisconsin-Madison

* Fusion Energy Division, ORNL.

ABSTRACT.

The distribution function for ripple-trapped particles has been found in a series form valid for all collision frequencies, for standard and transport-optimized stellarators. The kinetic equation

$$\dot{\theta}\,\frac{\partial f}{\partial \theta} + \dot{r}\,\frac{dF_m}{dr} = \frac{\nu_{eff}}{A'(k^2)}\,\frac{\partial}{\partial k^2}\,A(k^2)\,\frac{\partial f}{\partial k^2}$$

where $A(k^2) = \frac{4}{\pi}\left[E(k) - (1-k^2)K(k)\right]$, has been solved by writing $f = \frac{dF_M}{dr}\left(X\cos\theta + Y\sin\theta\right)$ and expanding X and Y as series in k^2.

$$X = X_0 h - Y_0 g - \frac{v_d}{\Omega_E}\left[1 - \frac{\varepsilon_h}{\varepsilon_t}\sigma(1-k^2)\right],\quad Y = Y_0 h + X_0 g + \frac{v_d}{\Omega_E}\frac{\varepsilon_h}{\varepsilon_t}\sigma,$$

$$h = \sum_{n=0}^{\infty}(-1)^n\left[\left(\frac{k^2}{\hat{\nu}}\right)^n\frac{1}{2n!}\right]^2,\quad g = \frac{k^2}{\hat{\nu}}\sum_{n=0}^{\infty}(-1)^n\left[\left(\frac{k^2}{\hat{\nu}}\right)^n\frac{1}{(2n+1)!}\right]^2.$$

Here $B = B_0\left(1 + \varepsilon_t\cos\theta - \varepsilon_h(1-\sigma\cos\theta)\cos(\ell\theta + p\phi)\right)$, $\nu_{eff} \equiv \frac{\nu}{2\varepsilon_h}$, $\hat{\nu} = \frac{\nu_{eff}}{\Omega_E}$.

Boundary conditions $Y(k^2=1) = 0$ and $\frac{X'(k^2=1)}{X(k^2=1)} = -\frac{1}{\Delta k^2}$, $\Delta k^2 = \frac{\varepsilon_t + \sigma\varepsilon_h}{2\varepsilon_h}$ are used.

The Distribution Function obtained yields excellent agreement with the Diffusion coefficient given by a 'hybrid' Monte Carlo code, (which uses bounce-averaged equations for $k^2 < 1$, guiding centre for $k^2 \simeq 1$, and conservation of P_ϕ for $k^2 > 1$).

Ripple Transport at Arbitrary Collision Frequency.

C.D. Beidler *

W.N.G. Hitchon *

W.I. van Rij †

S.P. Hirshman †

J.L. Shohet *

* Torsatron/Stellarator Lab., University of Wisconsin-Madison

† ORNL.

Two Studies will be described :-

- 'Hybrid' Bounce-Averaged / Guiding Centre Monte Carlo Calculations.

  — A Monte Carlo code which is very efficient, and which includes an accurate description of the physical processes involved in transport, has been applied to a variety of 'stellarators'.

- The bounce-averaged kinetic equation has been solved, for arbitrary collision frequency, by a power-series expansion and using suitable boundary conditions.

Results for D agree very well in all cases tested.

Hybrid Monte Carlo :-

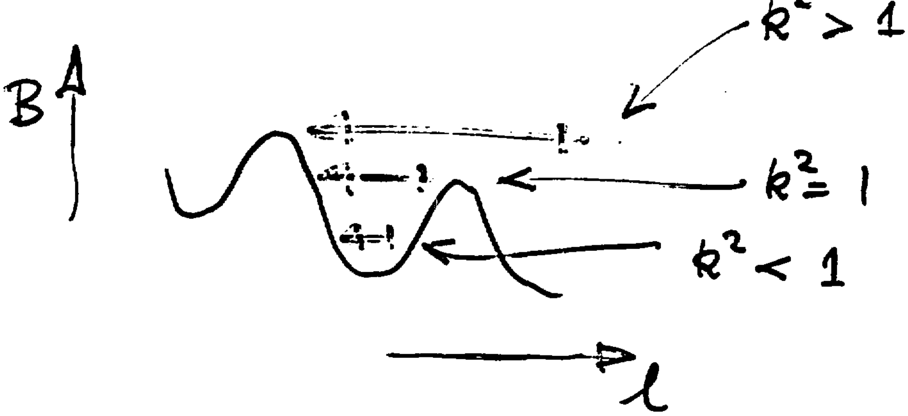

Classification of Orbits by 'Pitch-Angle' variable k^2 :-

- Below $k^2 = 1$, can describe orbits using bounce-averaged formulation;

$$J = \oint v_{\parallel}\, dl = \text{constant}$$

- Above $k^2 = 1$, an 'averaged' canonical momentum is approximately constant.

Use these constants to find $r(t)$, $\theta(t)$.

- Near $k^2 = 1$, need a careful, very accurate approach ~ use guiding-centre equations.

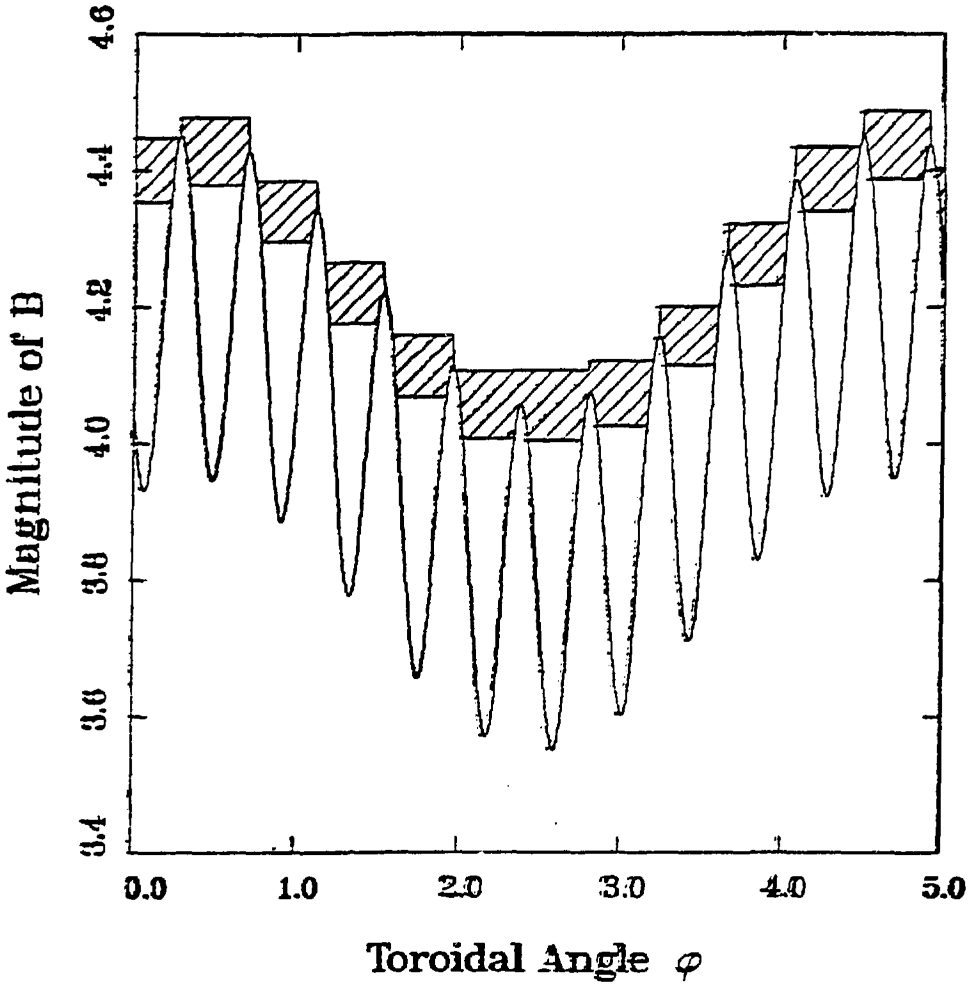

Figure 3–5. A typical partitioning of phase space relative to the model magnetic field. The guiding center region is hatched; the bounce–averaged and free–streaming regions lie below and above, respectively. The discontinuous definition of k^2 has been chosen for use in the free–streaming region.

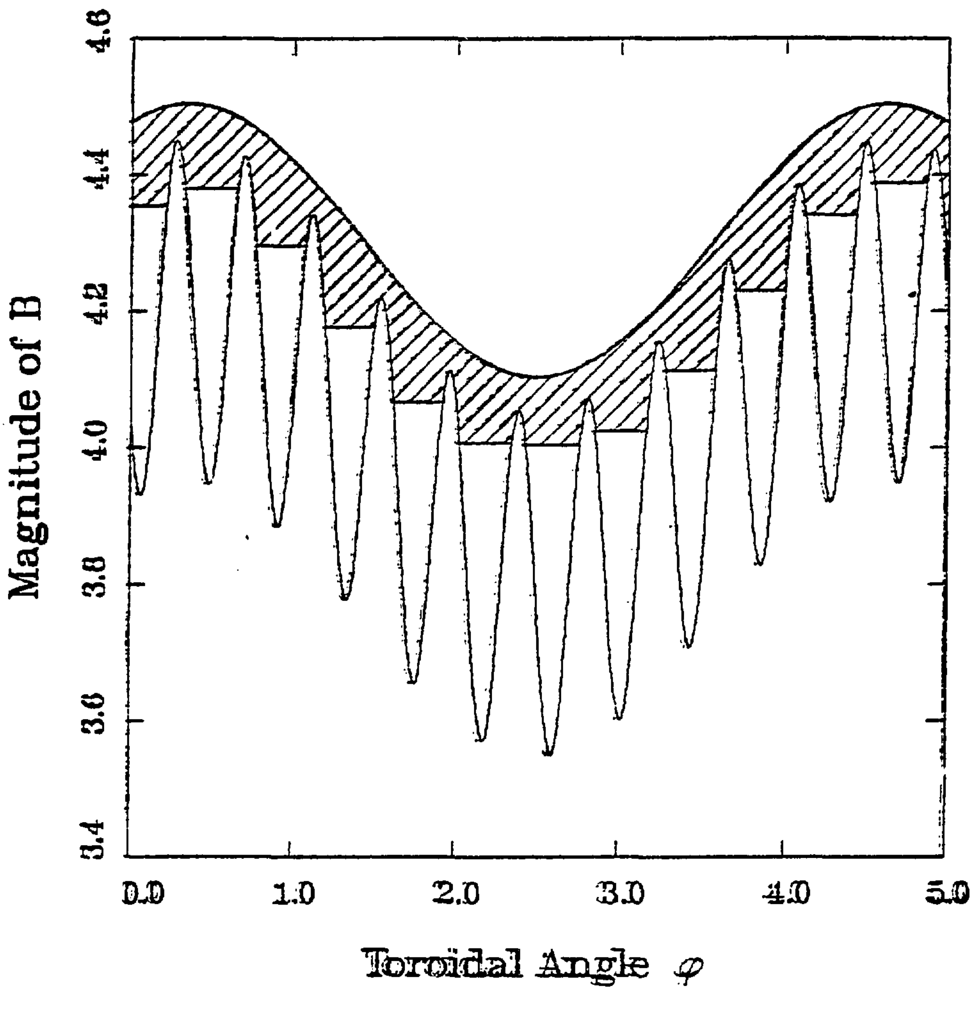

Figure 3–6. As for figure 3–5 with the continuous definition of k^2 chosen for use in the free–streaming region. In both figures k^2_{BA}=0.9 and k^2_{FS}=1.1.

Bounce-Averaged Kinetic Equation.

$$\dot{\theta} \frac{\partial f}{\partial \theta} + \dot{r} \frac{dF_M}{dr} = \bar{C}(f)$$

- This has already been bounce-averaged and linearised; previous solutions go on to order $\dot{\theta}$ relative to $\nu_{eff} \equiv \nu_{90°}/2\varepsilon_n$.

Three 'regimes' :-

- $\nu_{eff} \gg \dot{\theta}$; $D_{-1} \sim \nu^{-1}$.
- $\nu_{eff} \simeq \dot{\theta}$; $D_{1/2} \sim \nu^{1/2}$.
- $\nu_{eff} \ll \dot{\theta}$; $D_1 \sim \nu$.

These disparate 'regimes' are the result of the solution method. Problems:- a.) 3 regimes don't match; b.) D_1 only one which is believable.

We substitute

$$f = \frac{dF_m}{dr}\left[X(k^2)\cos\theta + Y(k^2)\sin\theta\right]$$

Technical Details:

$$B = B_0\left[1 + \varepsilon_t\cos\theta + \varepsilon_h(1-\sigma\cos\theta) \times \cos(l\theta + p\phi)\right]$$

which implies

$$k^2 = \frac{\mathcal{E}/\mu B_0 - 1 - \varepsilon_t\cos\theta}{2\varepsilon_h(1-\sigma\cos\theta)} + \frac{1}{2}$$

In general,

$$\overline{C}(f) = \frac{\nu_{eff}}{A'(k^2)}\frac{\partial}{\partial k^2}A(k^2)\frac{\partial f}{\partial k^2},$$

$$A(k^2) \equiv \frac{4}{\pi}\left[E(k) - (1-k^2)K(k)\right]$$

Approximating $\quad A/A' \simeq k^2,$

$$\frac{2E(k^2)}{K(k^2)} - 1 \simeq 1 - k^2$$

and expanding

$$X = \sum_{n=0}^{\infty} X_n (k^2)^n$$

$$Y = \sum_{n=0}^{\infty} Y_n (k^2)^n$$

Constants to be determined from b.c.s

$\dot{\theta} \simeq \Omega_E$

$$X(k^2) = X_0 h - Y_0 g - \frac{V_d}{\Omega_E}\left\{1 - \frac{\varepsilon_h}{\varepsilon_t}\sigma(1-k^2)\right\}$$

$$Y(k^2) = Y_0 h + X_0 g + \frac{V_d}{\Omega_E}\frac{\varepsilon_h}{\varepsilon_t}\sigma\hat{\nu}$$

$\hat{\nu} = \dfrac{\nu_{eff}}{\Omega_E}$

$$h = \sum_{n=0}^{\infty} (-1)^n \left[\left(\frac{k^2}{\hat{\nu}}\right)^n \frac{1}{2n!}\right]^2 \; ; \; g = \frac{k^2}{\hat{\nu}} \sum_{n=0}^{\infty} (-1)^n \left[\left(\frac{k^2}{\hat{\nu}}\right)^n \frac{1}{(2n+1)!}\right]^2$$

Boundary Conditions

Need Symmetry in θ at $k^2 = 1$;

$$Y(1) = 0 .$$

Most collisionless point

$$\frac{\partial f}{\partial k^2}\left(k^2 = 1^+, \theta = \pi\right) = -\frac{\partial f}{\partial \theta}\left[\frac{\partial k^2}{\partial \theta}\right]^{-1}$$

$$\simeq \frac{2\varepsilon_h X(1)}{\varepsilon_t + \sigma \varepsilon_h}\frac{dF_m}{dr}$$

$$\frac{\partial f}{\partial k^2}\left(k^2 = 1^-, \theta = \pi\right) = -X'(1)\frac{dF_m}{dr}$$

$$\Downarrow$$

$$\frac{X'(1)}{X(1)} = -\frac{2\varepsilon_h}{\varepsilon_t + \sigma \varepsilon_h}$$

i.e. have a layer of width $\Delta k^2 = \dfrac{\varepsilon_t + \sigma \varepsilon_h}{2\varepsilon_h}$ at 1^+, as expected.

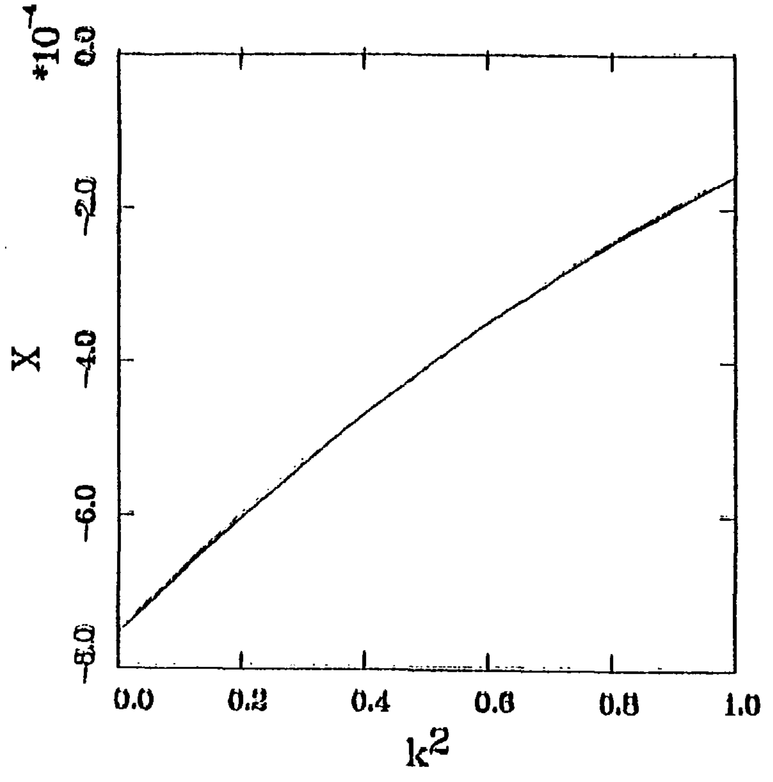
*10^-4
X
0.0
-2.0
-4.0
-6.0
-8.0
0.0
0.2
0.4
0.6
0.8
1.0
k^2

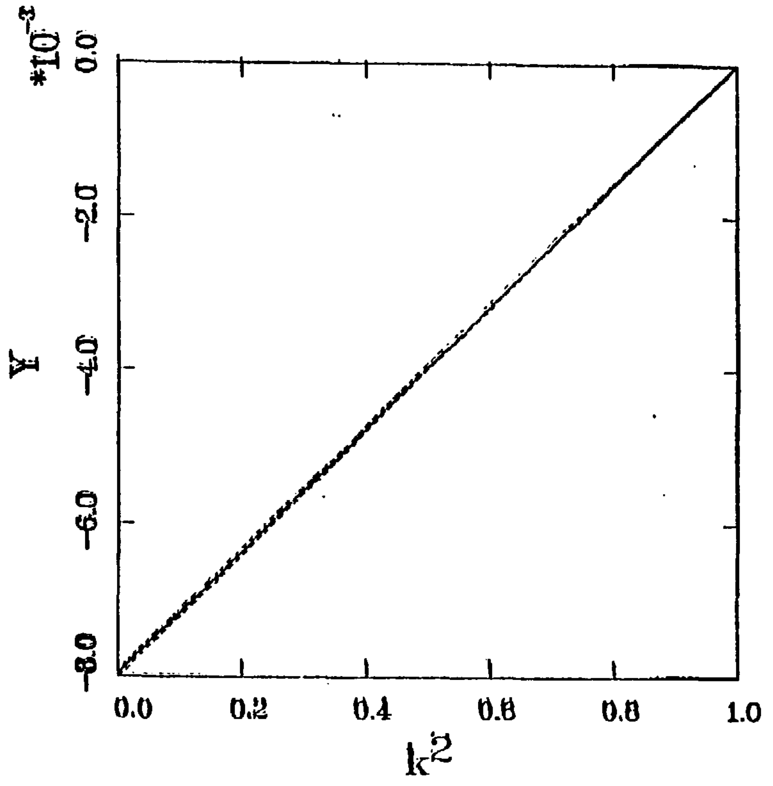
*10^-3
Y
0.0
-2.0
-4.0
-6.0
-8.0
0.0
0.2
0.4
0.6
0.8
1.0
k^2

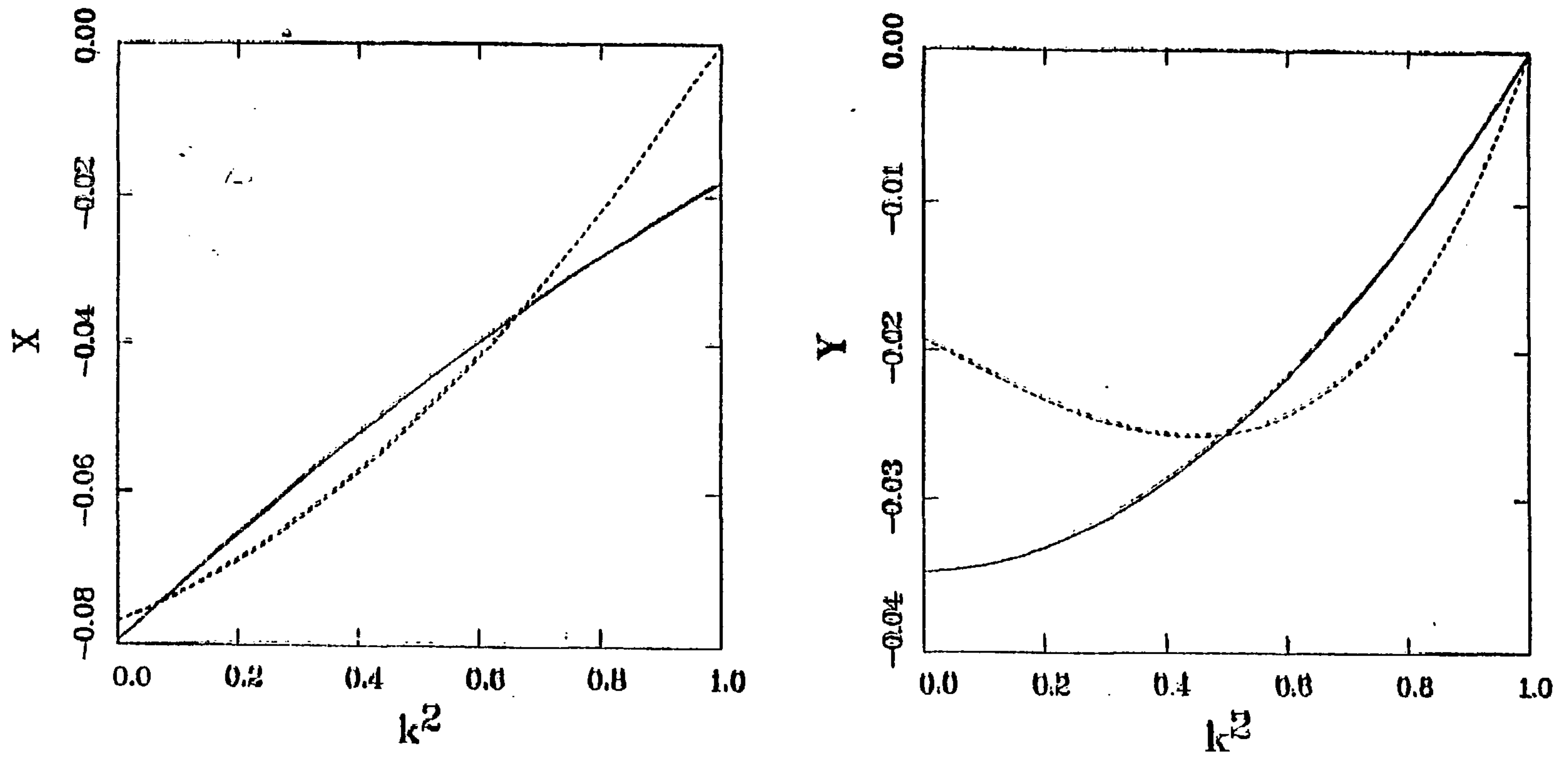

X
0.00
-0.02
-0.04
-0.06
-0.08
0.0
0.2
0.4
0.6
0.8
1.0
k2
Y
0.00
-0.01
-0.02
-0.03
-0.04
k2

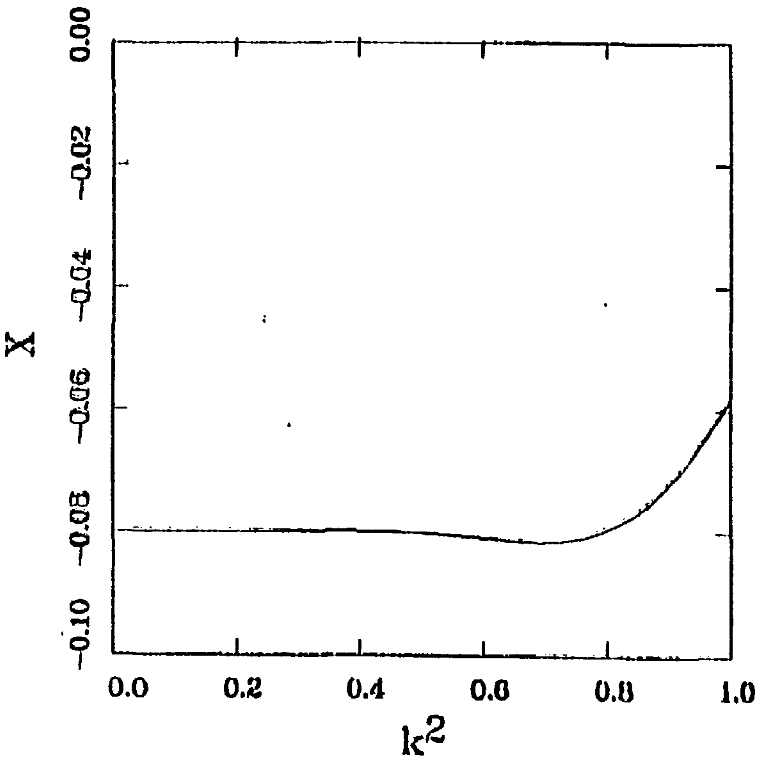

X
0.00
-0.02
-0.04
-0.06
-0.08
-0.10
0.0
0.2
0.4
0.6
0.8
1.0
k2

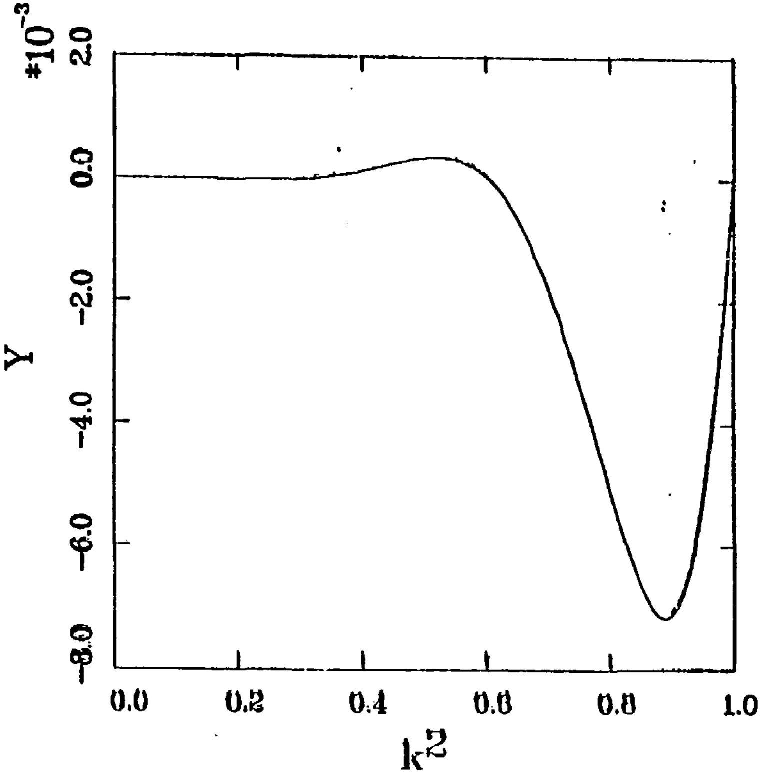

Y
*10-3
2.0
0.0
-2.0
-4.0
-6.0
-8.0
0.0
0.2
0.4
0.6
0.8
1.0
k2

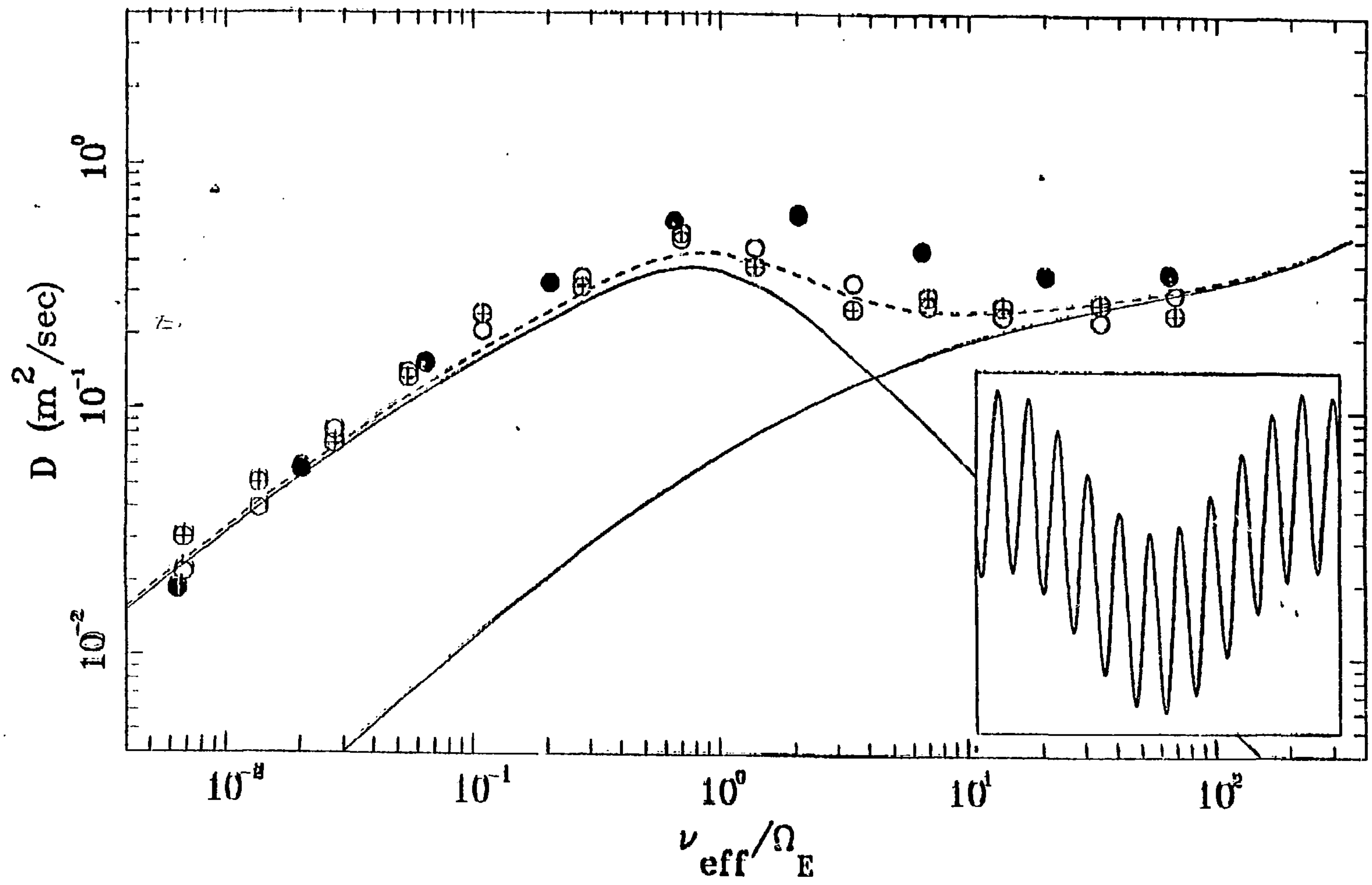

D (m^2/sec)
10^0
10^-1
10^-2
10^-2
10^-1
10^0
10^1
10^2
ν_eff/Ω_E

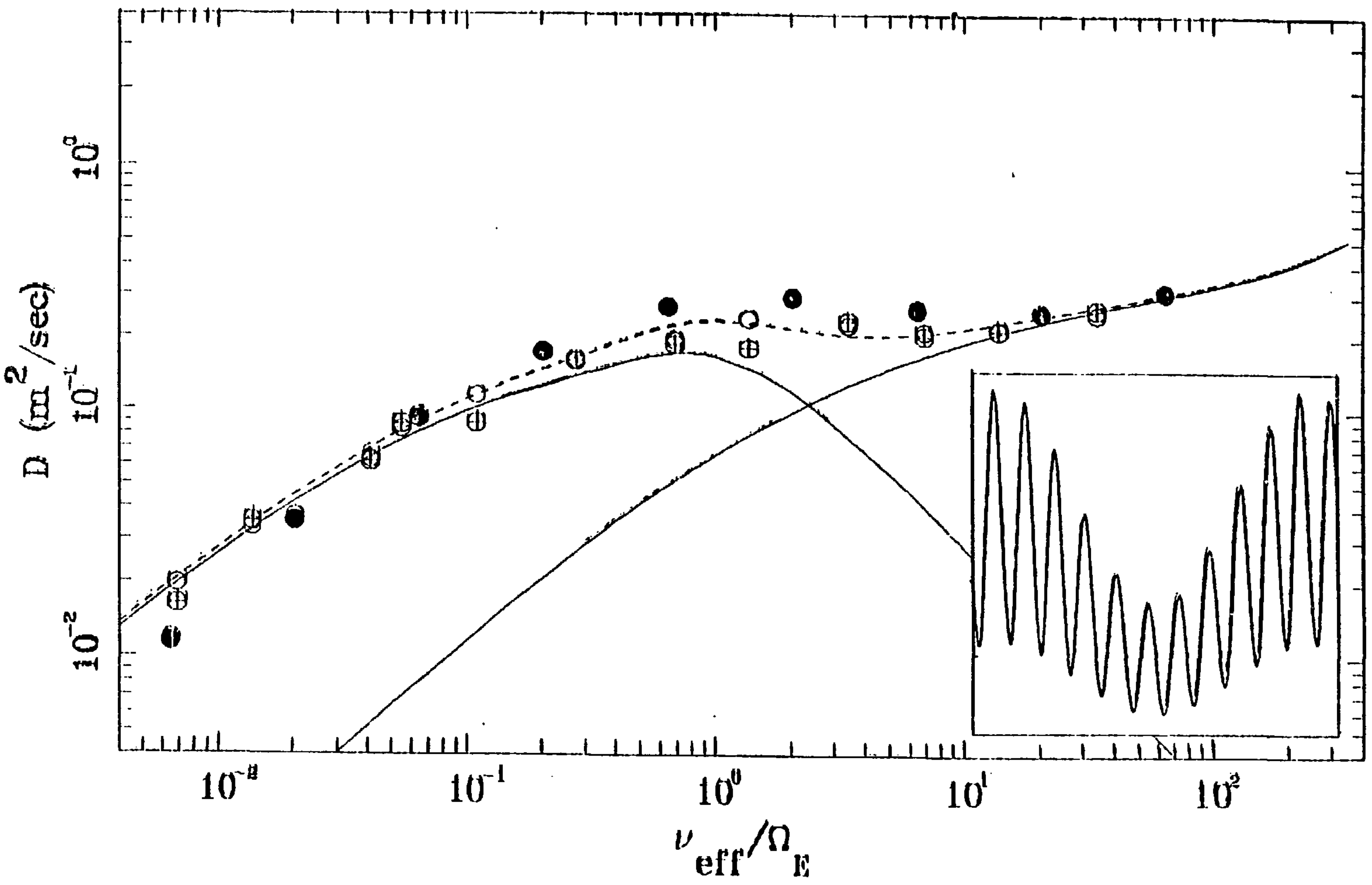
D (m²/sec)
10^0
10^-1
10^-2
10^-2
10^-1
10^0
10^1
10^2
ν_eff/Ω_E

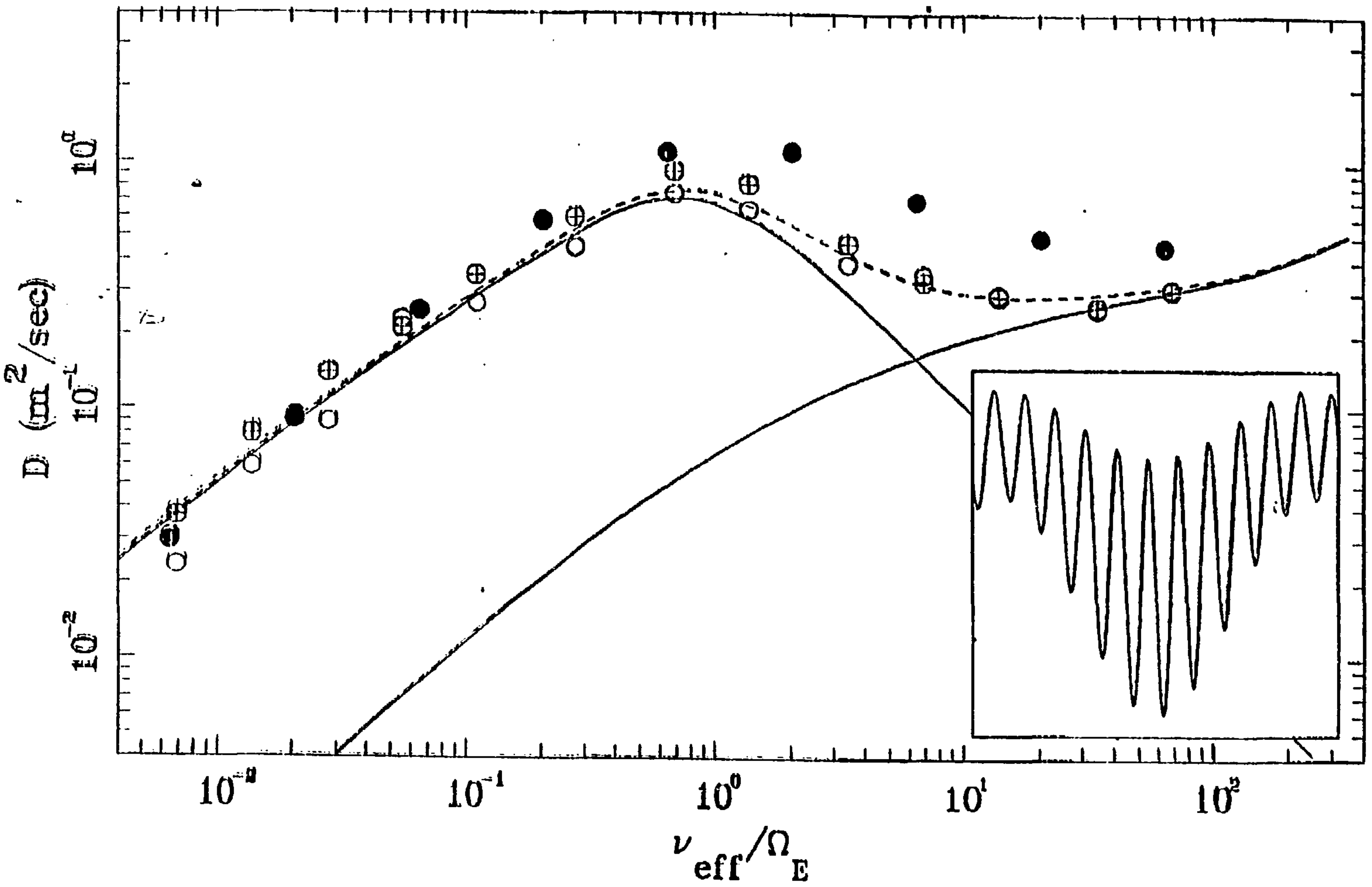
D (m^2/sec)
10^0
10^-1
10^-2
10^-2
10^-1
10^0
10^1
10^2
ν_eff/Ω_E

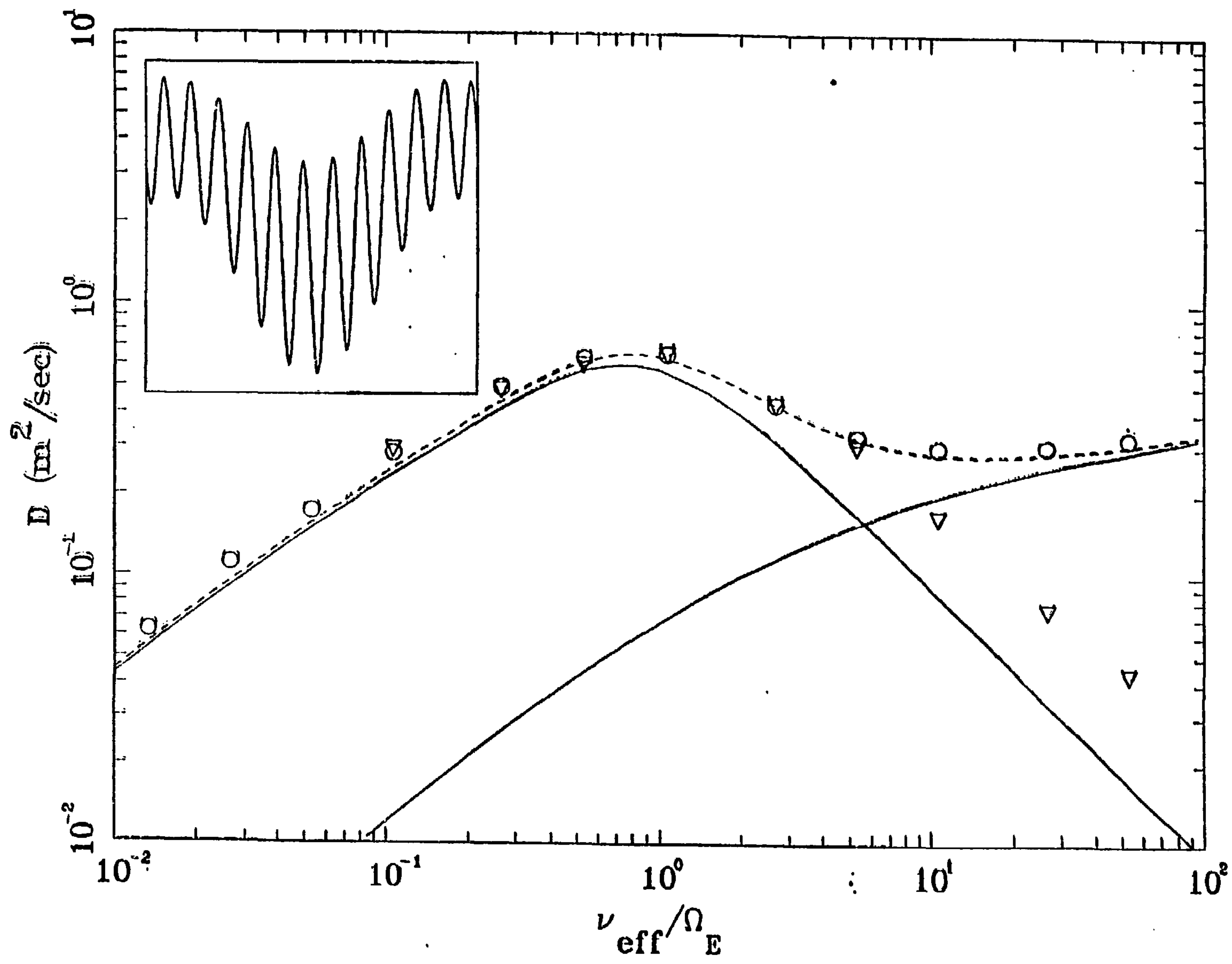

D (m^2/sec)
10^1
10^0
10^{-1}
10^{-2}
10^{-2}
10^{-1}
10^0
10^1
10^2
ν_{eff}/Ω_E

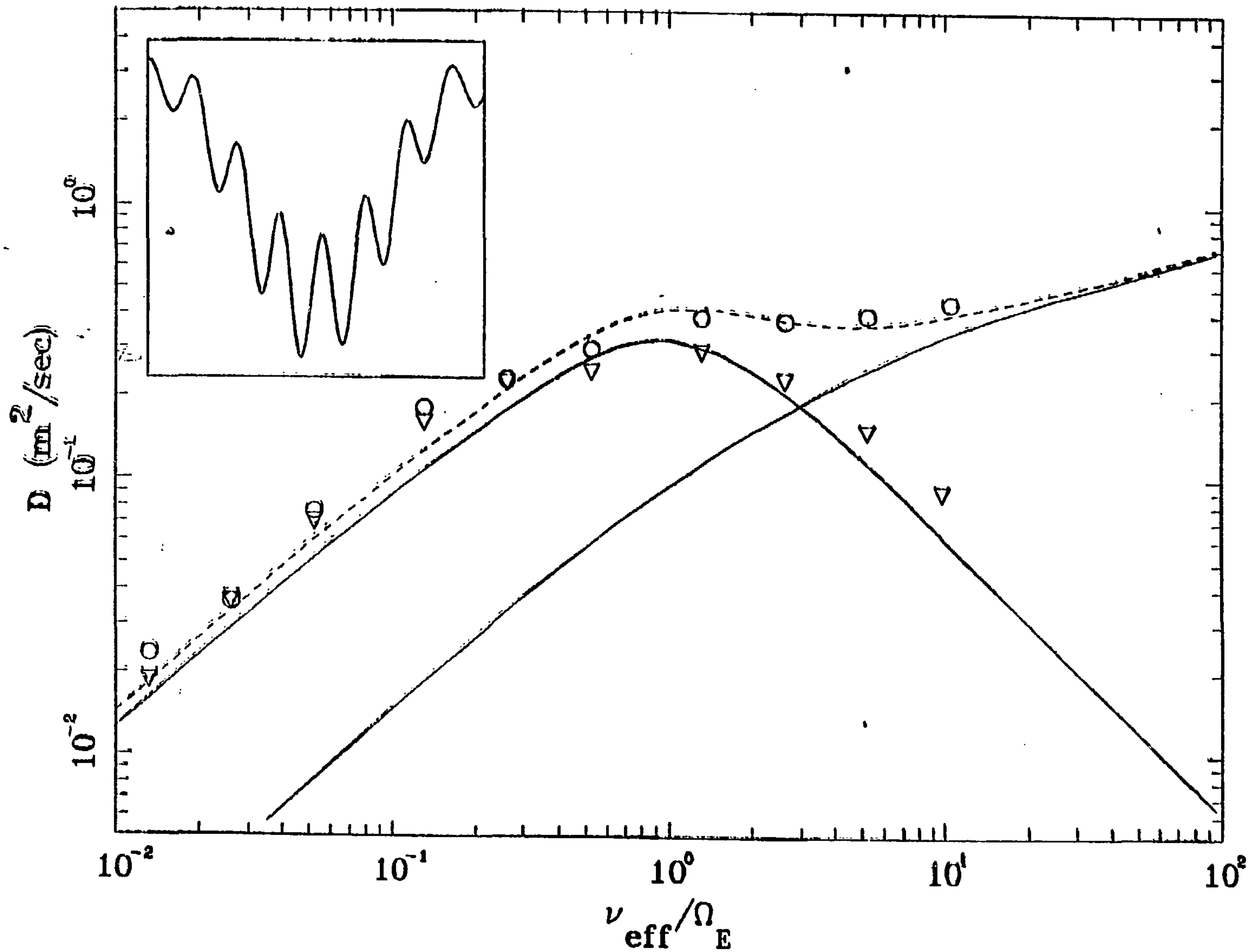

D (m²/sec)
10⁰
10⁻¹
10⁻²
10⁻²
10⁻¹
10⁰
10¹
10²
ν_eff/Ω_E

Conclusion:-

A fast, accurate 'hybrid' Monte Carlo code has been developed.

The bounce-averaged kinetic equation has been solved for arbitrary $\frac{\nu_{eff}}{\Omega_E}$, σ.

The diffusion coefficients predicted by the two approaches agree very well with each other ~ and fairly well with DKES ~ in all examples studied.

Future Work:- extend both calculations to more complex systems, such as WVII-AS.

TRANSPORT SCALING IN THE COLLISIONLESS-DETRAPPING REGIME

E. C. Crume

Fusion Energy Division

Oak Ridge National Laboratory

in collaboration with

K. C. Shaing

W. I. van Rij

S. P. Hirshman

U.S.-Japan Stellarator/Heliotron Workshop
Fusion Engineering Design Center, Oak Ridge, Tennessee
November 9–13, 1987

- For the collisionless-detrapping or ν-regime, we have determined stellarator transport scalings with:

E_ρ	(electric field)
ϵ_t and ϵ_h	(geometry)
ν	(collision frequency)

from numerical solutions to the DKE.

- We find a new geometrical scaling $\propto \epsilon_t$ independent of the helical ripple ϵ_h. Compare with Galeev-Sagdeev scaling $\epsilon_t \epsilon_h$

- We present integral expressions for Γ and Q that can be used in transport simulations, along with self-consistent determinations of E_ρ, to obtain, for example, confinement times for specific devices

OUTLINE

- Brief description of numerical techniques
- Deduction of the scalings from the numerical results.
- Expressions for Γ and Q
- Comparisons with other scalings

NUMERICAL TECHNIQUE

- Use DKES (Drift Kinetic Equation Solver) code to solve linearized DKE for f_1, the deviation from the Maxwellian

$$\vec{v} \cdot \nabla f_1 + \dot{\alpha}(\partial f_1/\partial \alpha) - C(f_1) = S,$$

where

$$\vec{v} = v\cos\alpha\,\hat{n} + \underline{E_\rho \nabla\rho \times \vec{B}/\langle B^2\rangle}$$

$$v_\parallel/v = \cos\alpha, \quad \hat{n} = \vec{B}/B, \quad E_\rho = -d\Phi/d\rho$$

$$\dot{\alpha} = -\frac{v}{2}\sin\alpha\,\vec{B}\cdot\nabla(VB)$$

$$S = f_M\left[-\vec{v}_d\cdot\nabla\rho\,(A_1 + x A_2) - Bv\cos\alpha\,A_3\right]$$

$$A_1 = \frac{n'}{n} - \frac{3T'}{2T} - \frac{eE_\rho}{T}$$

$$A_2 = \frac{T'}{T}$$

$$A_3 = -\frac{e\langle\vec{E}\cdot\vec{B}\rangle}{T\langle B^2\rangle}$$

$$x = \frac{Mv^2}{2T}$$

- No resonant superbanana orbits since the [redacted] curvature and ∇B drift term in $\vec{v} \cdot \nabla f_1$ neglected.

- Poloidal $\underline{\vec{E}_0 \times \vec{B}}$ drift retained for these calculations of collisionless detrapping/retrapping of particles in helically trapped orbits.

- $C(f_1)$ is a pitch-angle scattering operator

- The treatment of the boundary layer between trapped and circulating particles is exact; __no__ assumptions regarding boundary conditions on the distribution are made.

- Solve the linearized DKE in terms of Fourier-Legendre series for f_1 at a fixed value of the normalized energy x for a number of values of ν and E_ρ on a flux surface.

- Then obtain fluxes:

$$\langle \vec{\Gamma}\cdot\nabla\rho \rangle = \left\langle \int d^3v\, \vec{V}_d\cdot\nabla_\rho f_1 \right\rangle = -\sum_{n=1}^{2} L_{1n} A_n$$

$$\left\langle \frac{\vec{Q}\cdot\nabla\rho}{T} \right\rangle = \left\langle \int d^3v\, \vec{V}_d\cdot\nabla_\rho\, x f_1 \right\rangle = -\sum_{n=1}^{2} L_{2n} A_n$$

(Ignore A_3) [redacted]

- We use L_{22}, the coefficient of $A_2 = \frac{T'}{T}$ in the heat flux for illustrative purposes. Same scalings from L_{11} and $L_{12} = L_{21}$.

MAGNETIC SPECTRUM

- Use truncated spectrum on a flux surfac

$$B = B_0\left[1 - \epsilon_t \cos\theta + \epsilon_h \cos(\ell\theta - m\zeta)\right]$$

representative of vacuum B of ATF($\ell = 2$, $m = 12$)

- Investigated effects of multiple helicity using a more complete, eight-term spectrum

- NOTE: Truncated spectrum inappropriate for transport-optimized stellarators.

EFFECTS OF MULTIPLE HELICITY

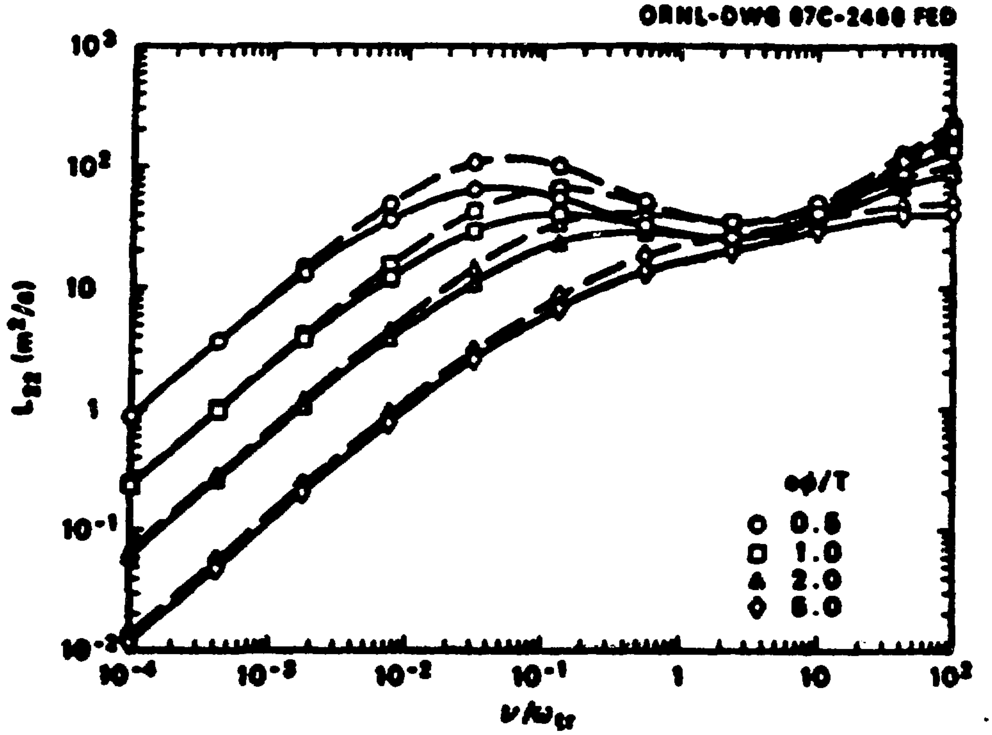

——— Truncated (three-term) spectrum

— — Eight-term spectrum

$\bar{a}$ = 0.3 m

- Effects not very important in ν-regime
- Factor of two for small $\frac{e\Phi}{T}$ in $1/\nu$ regime
- Less for larger $\frac{e\Phi}{T}$ and larger ν.

ELECTRIC FIELD SCALING AND RESONANC

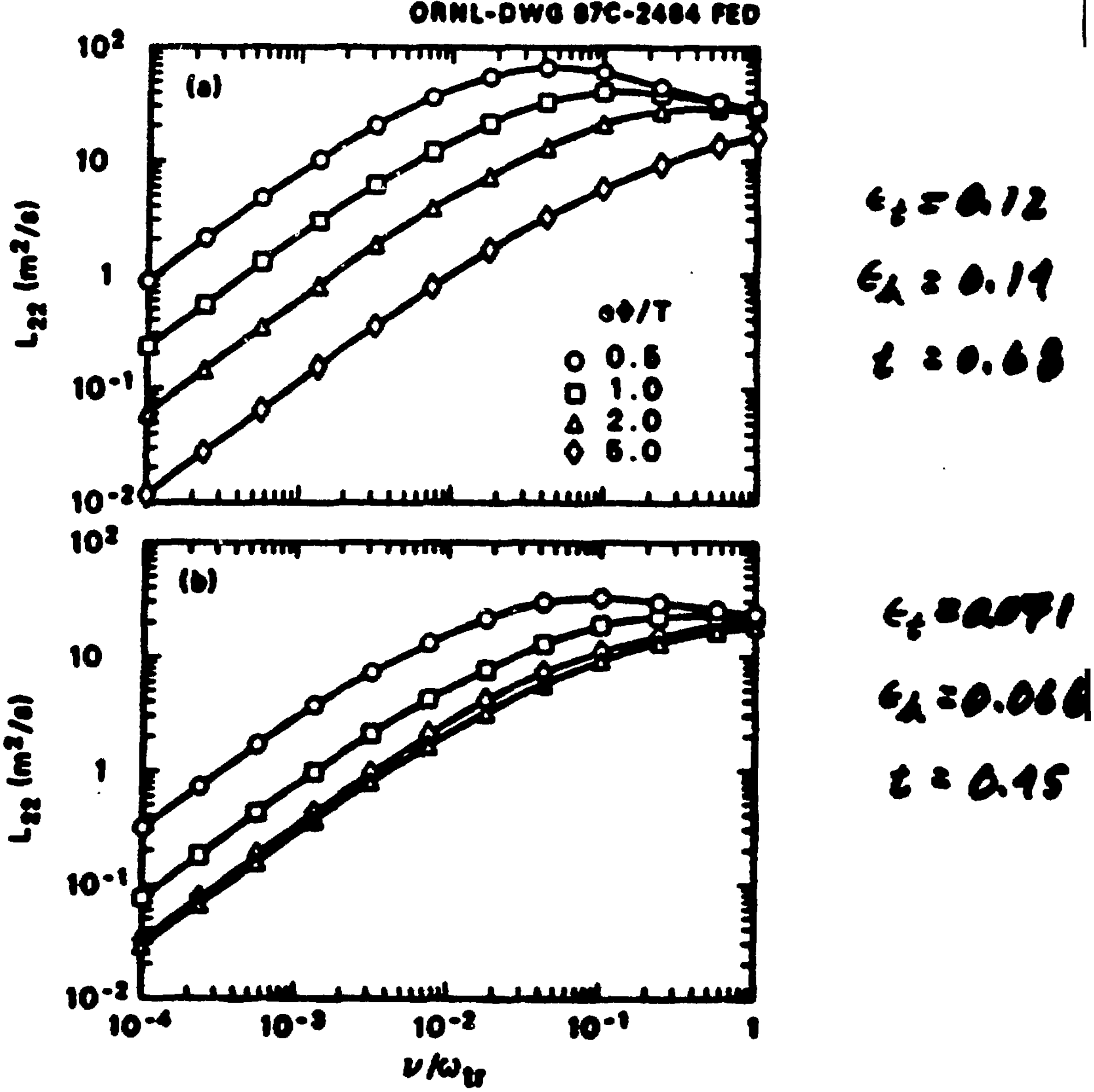

- In (a), for $\frac{\nu}{\omega_{tr}} \lesssim 10^{-3}$, $\underline{L_{22} \propto 1/\Phi^2}$

- In (b), resonance between $v_{\parallel}$ and poloidal $\vec{E}_0 \times \vec{B}$ drift causes scaling to deviate from $1/\Phi^2$ for $\frac{e\Phi}{T} \gtrsim 5$

- To obtain scalings, we avoided this resonance

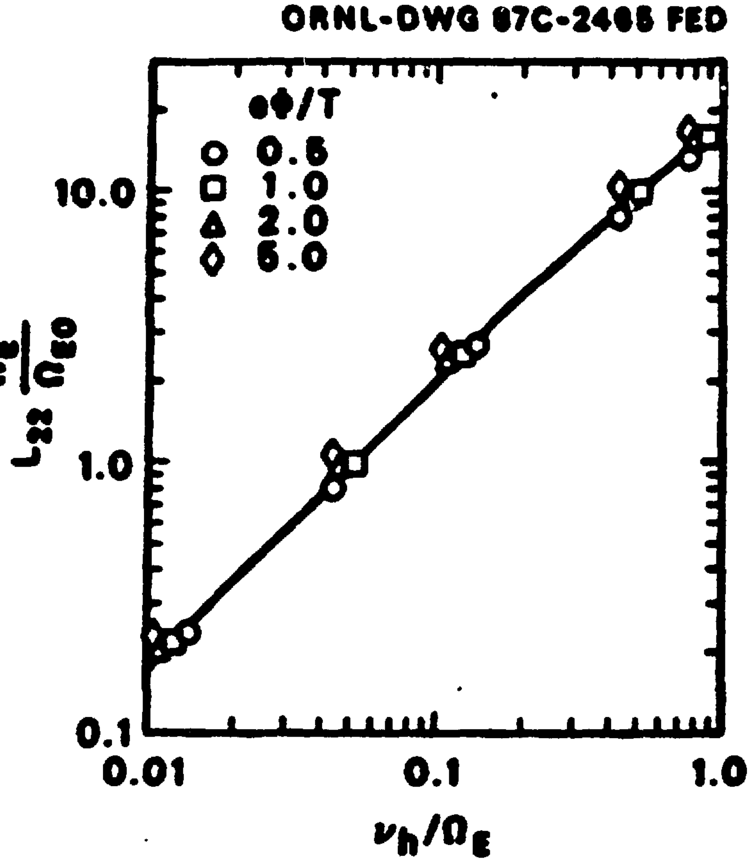

ϵ_t and ϵ_h fixed

Ω_E = poloidal $\vec{E} \times \vec{B}$ frequency.

$\Omega_{E0} = \Omega_E(e\Phi/T = 1)$.

$\nu_h = \nu/\epsilon_h$

- $L_{22} \propto \nu$ from unit slope

- $L_{22} \propto 1/\Omega_E^2 \propto 1/\Phi^2$ confirmed.

  from clustering of points.

GEOMETRICAL SCALING

ORNL-DWG 87C-2466 FED

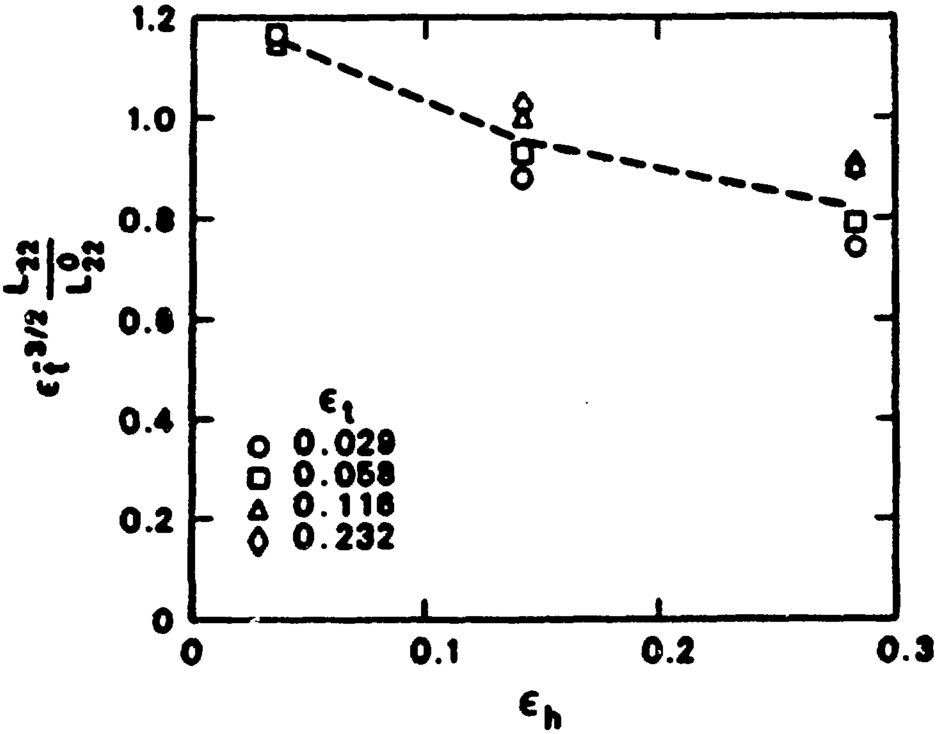

$$L_{22}^{0} = L_{22}\,(\epsilon_t = 0.12\,;\ \epsilon_h = 0.14)$$

- $\epsilon_t^{-3/2} \dfrac{L_{22}}{L_{22}^{0}}$ not very sensitive to ϵ_h

$\therefore$ dominant geometrical dependence is $L_{22} \propto \epsilon_t^{3}$

- Summarizing, the scaling we find is

$$L_{22}^{DKES} \propto \nu\, \epsilon_t^{3/2}\, G(\epsilon_t, \epsilon_h)/\Omega_E^2$$

where $G(\epsilon_t, \epsilon_h)$ is a weak function of ϵ_t, ϵ_h

ESTIMATION OF f, THE FRACTION OF PARTICLES INVOLVED IN THE TRANSPORT PROCESS

- In a random walk argument

$$D \sim f\,(\Delta r)^2/\Delta t$$

- In the ν-regime, the step size Δr is determined by the helically trapped particles

$$\Delta r \approx \frac{V_d}{\Omega_E} \approx \frac{\epsilon_t\, T}{M\Omega r \Omega_E}$$

- The effective time between collisions Δt is

$$\Delta t \approx (\nu/f^2)^{-1}$$

- Therefore,

$$D \sim \nu\, \epsilon_t^2\, T^2 / M^2 \Omega^2 r^2 \Omega_E^2\, f$$

and, using the scaling found above

$$f \approx \sqrt{\epsilon_t}\; G^{-1}(\epsilon_t, \epsilon_h)$$

EXPRESSIONS FOR THE FLUXES

- Shaing has given integral expressions for flux[es]

$$\begin{bmatrix} \Gamma_a \\ Q_a \end{bmatrix} = -\epsilon_t^2 \sqrt{\epsilon_h}\, v_a^2 \begin{bmatrix} n_a \\ n_a T_a \end{bmatrix} \int_0^\infty dx_a \begin{bmatrix} x_a^{1/2} \\ x_a^{3/2} \end{bmatrix} e^{-x_a} \frac{\nu_{ah}(x_a)(A_{a1} + x_a A \ldots}{\omega_a^2(x_a)}$$

where:
$$v_a = \frac{v_{da}}{\epsilon_t}$$

$$\nu_{ah}(x_a) = \begin{cases} \dfrac{\nu_{ii}(x_i)}{\epsilon_h} & \text{ions} \\[2ex] \dfrac{\nu_{ee}(x_e) + \nu_{ei}(x_e)}{\epsilon_h} & \text{electrons} \end{cases}$$

- Here, recalling ∇B drift not included in $\vec{v} \cdot \nabla f$

$$\omega_a^2(x_a) = 1.5 \sqrt{\epsilon_t \epsilon_h}\, \Omega_E^2 + 3 \nu_{ah}^2(x_a)$$

Previously, Galeev-Sagdeev geometrical scaling

$$\left[\omega_a^2(x_a)\right]_{OH} = 1.67 \frac{\epsilon_t}{\epsilon_h} \Omega_E^2 + 3 \nu_{ah}^2(x_a)$$

- **NOTE:** Superbanana terms must be added to $\omega_a^2(x_a)$ for device transport simulation[s]

CONVERGENCE STUDIES

- To ascertain the reliability of our numerical results, we have run convergence studies in which the number of poloidal, toroidal, and pitch-angle harmonics were varied.

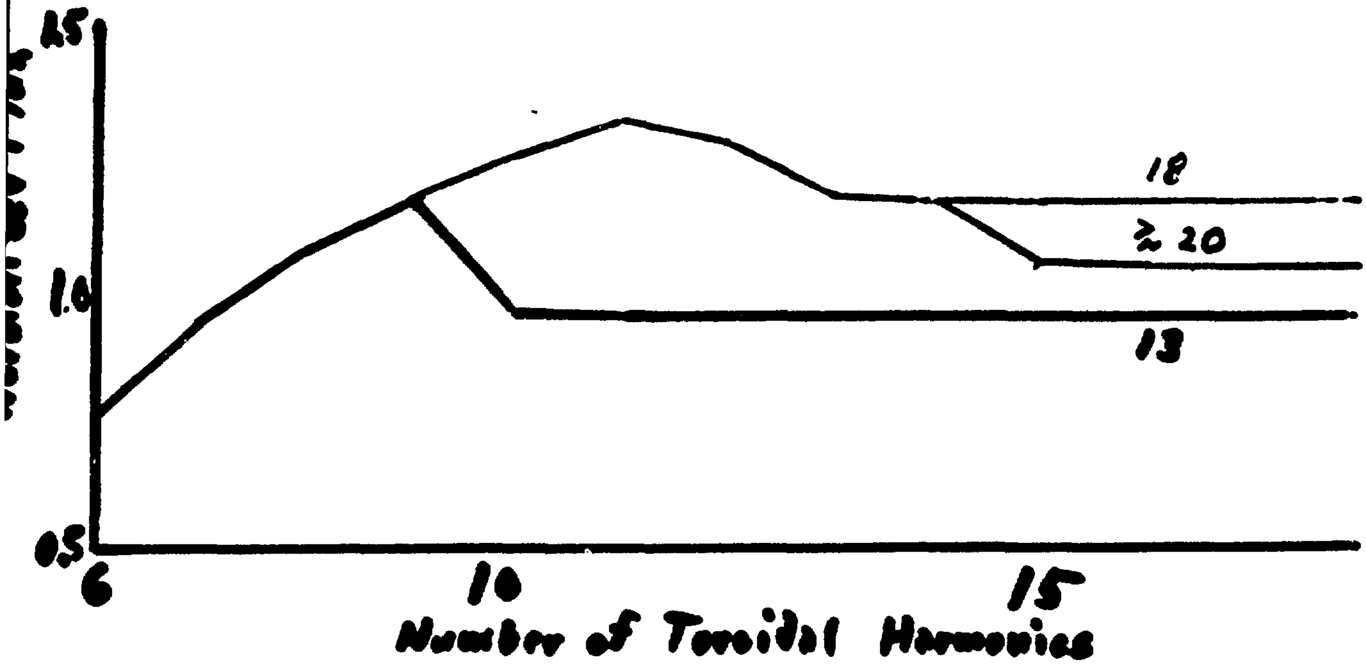

- Conclude that scalings with ν and $E_\parallel$ accurate to a few percent, scalings with ϵ_t and ϵ_h accurate to variation illustrated.

- Coefficient of 1.5 accurate to 10-20%.

COMPARISON OF SCALINGS

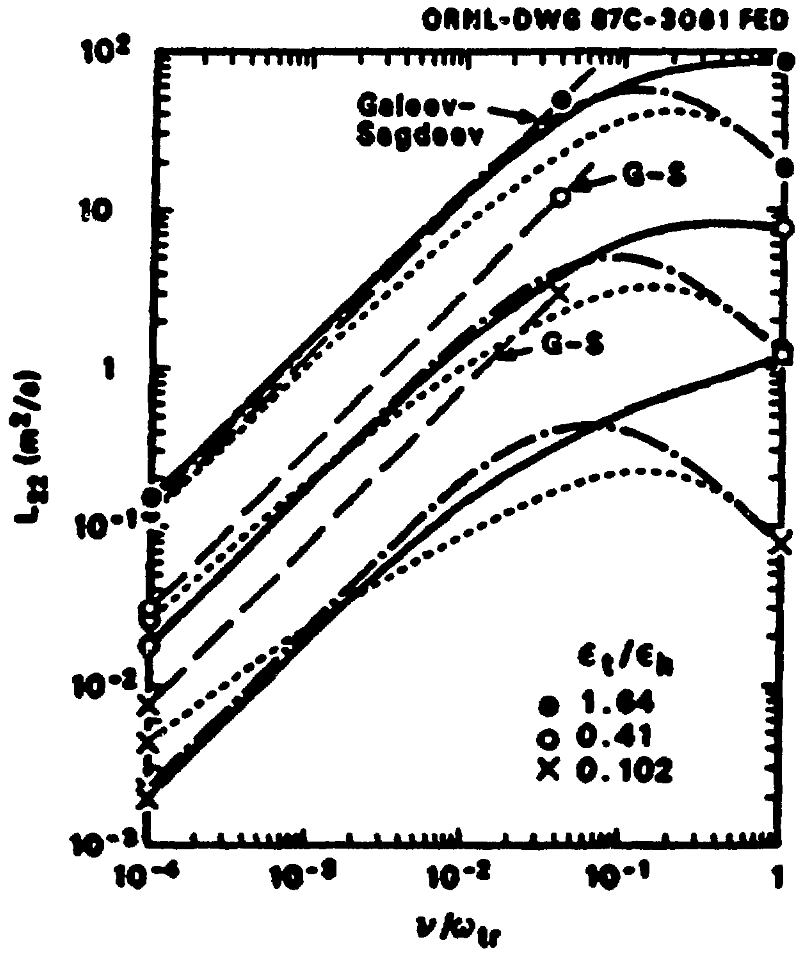

ϵ_h fixed

- For $\nu/\omega_{tr} \lesssim 10^{-2}$ agreement between DKES (— and integral expressions (—·—·) very good. For larger ν/ω_{tr} DKES has plateau-Pfirsch-Schlüte
- Galeev-Sagdeev results (— —) show same collision frequency scaling, but not ϵ_t scaling
- Beidler et al. results (- - -) [excluding symmetric] show different ν and geometrical scalings, but within a factor of 2 for these cases.

CONCLUSIONS

- From numerical solutions to the full, linearized DKE, we find a geometrical scaling of transport coefficients in the collisionless-detrapping regime different from scalings found using other analytic or numerical treatments.

- The discrepancies probably result from approximate boundary conditions imposed in other treatments; <u>no</u> such conditions are imposed here

- The new scaling is in the direction of providing more flexibility in stellarator design, since it is independent of the magnitude of the helical ripple.

- The results are incorporated into integral expressions for particle and heat fluxes useful for transport simulations.

RECENT TRANSPORT ANALYSIS FOR HELIOTRON E

T. Mutoh
Heliotron group

<u>ECH</u>

- Profile study between $P_{abs}(r)$ & $T_e(r)$
  (H. Zushi, et al)
- Scaling of τ^e_{decay}, τ^G_E
  (H. Zushi, et al)
- Energy balance
  $\chi_e^{neo\ classical}$
  $\chi_e^{anomaly}$
  (K. Itoh, M. Sato)

<u>NBI</u>

- Carbonization effect on energy balance
  (Y. Takeiri)
- Off-set linear law scaling
  (F. Sano)

<u>ICRF</u>

- Energy balance & scaling study
  (Y. Takeiri, T. Mutoh)

Fig. 2

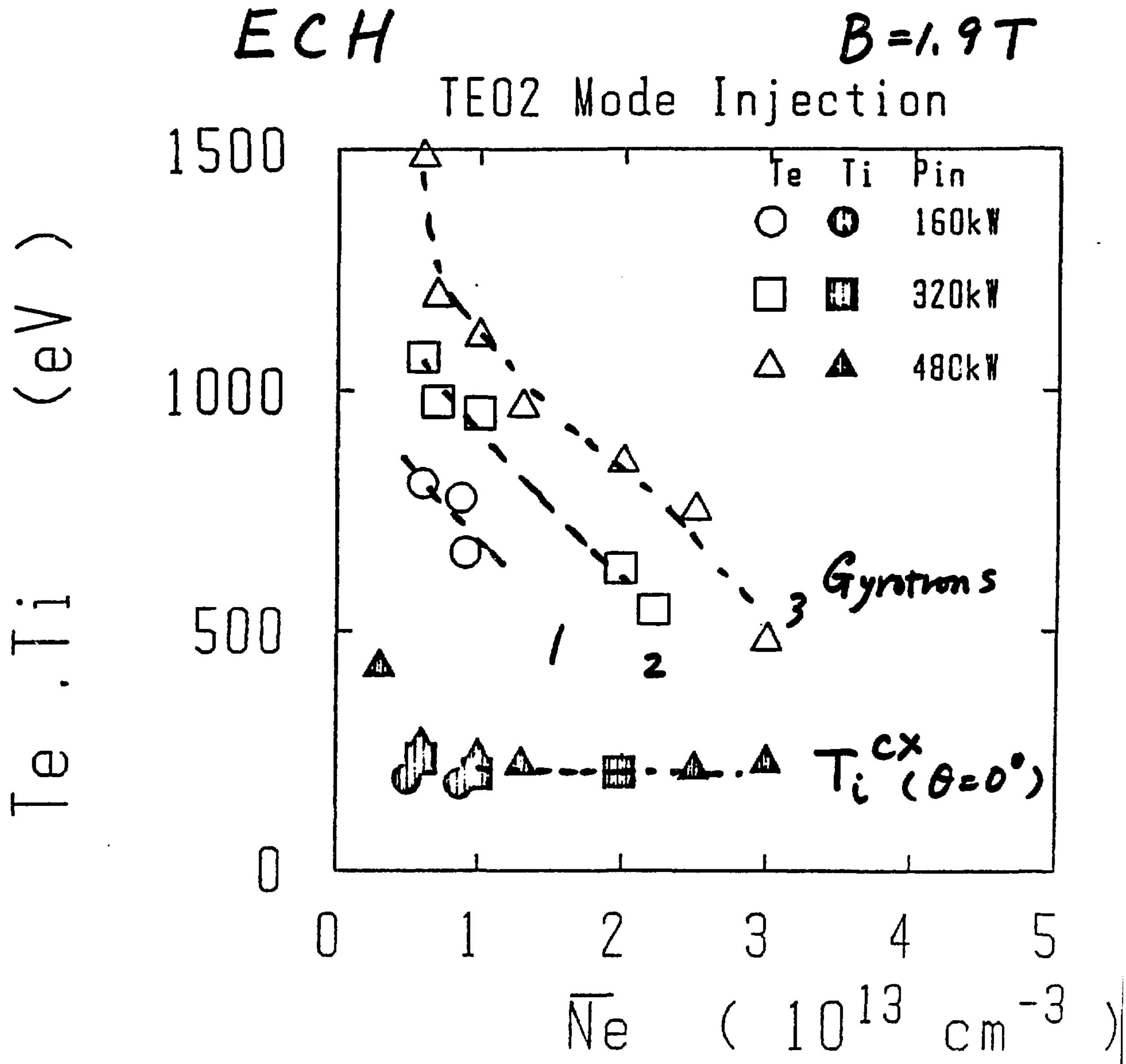

ECH
B=1.9T
TE02 Mode Injection
1500
1000
500
0
Te .Ti (eV)
Te Ti Pin
160kW
320kW
480kW
Gyrotrons
1
2
3
T_i^{cx} (θ=0°)
0
1
2
3
4
5
$\overline{Ne}$ (10^{13} cm^{-3})

H. Zushi

ECH $P_{abs}(r)$ measurement

Fig. 6

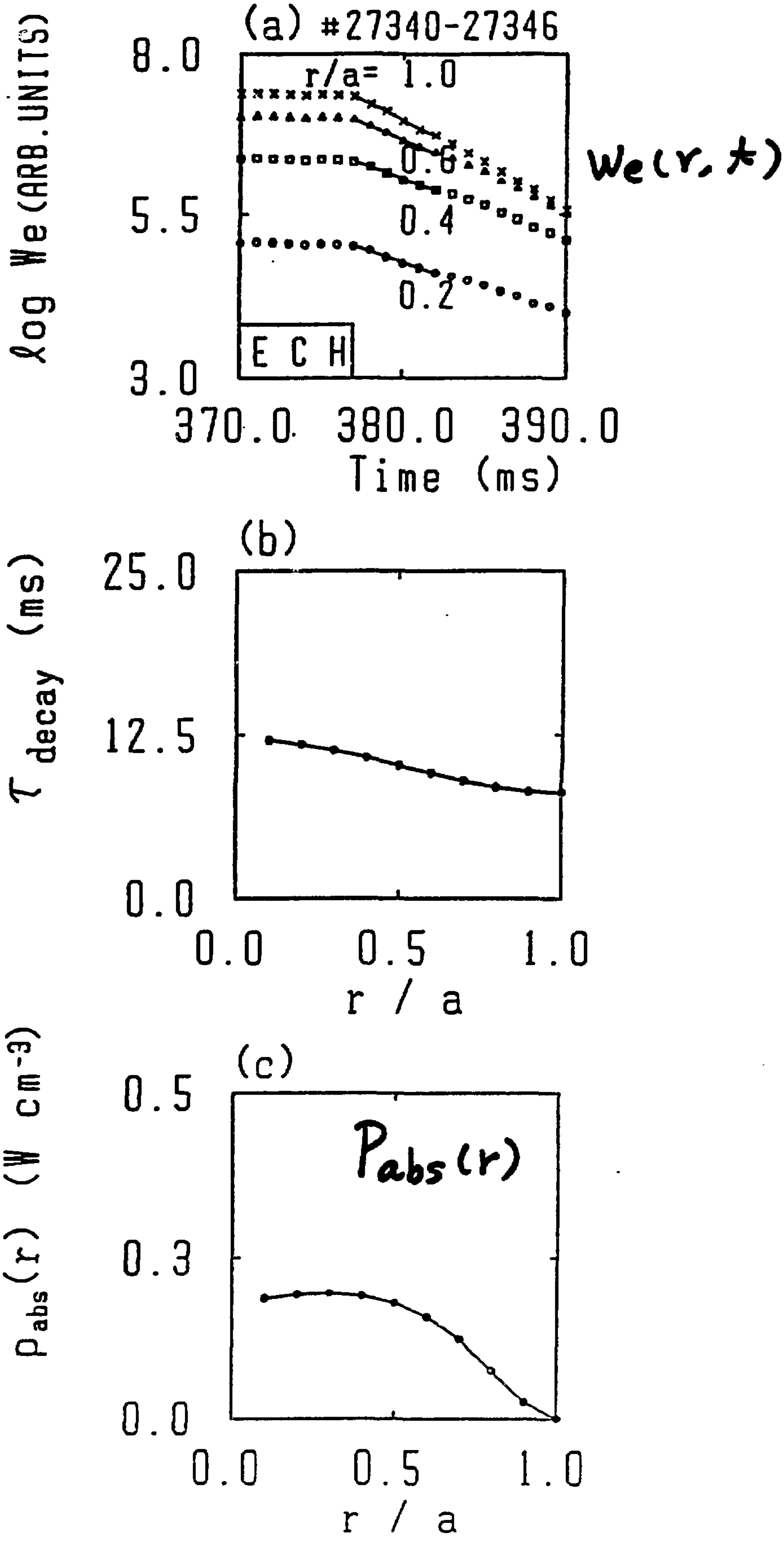

Fig. 7

ECH $T_e(r)$, $P_{abs}(r)$ vs. B

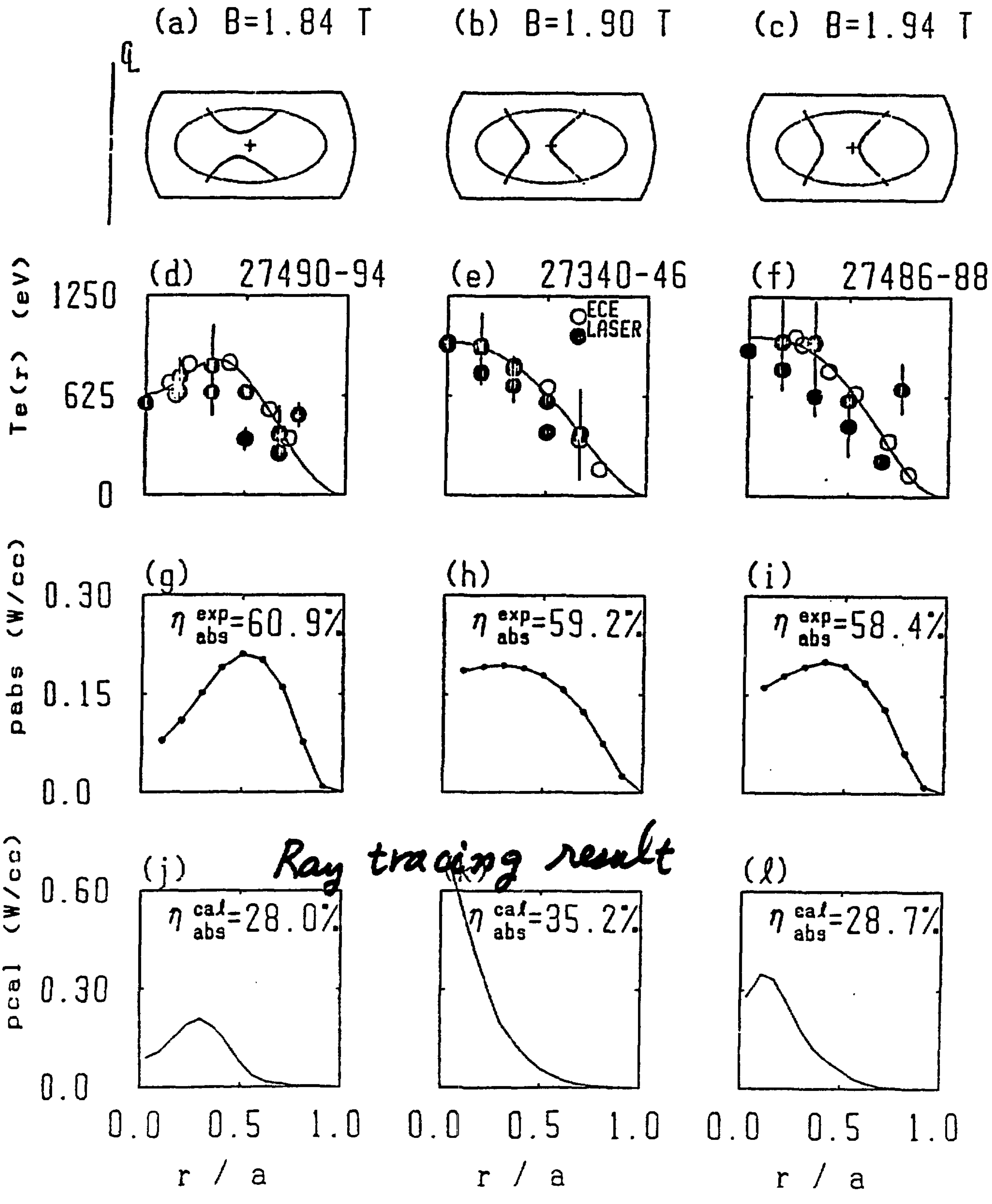

H. Zushi

ECH

Fig. 11

B=1.9T

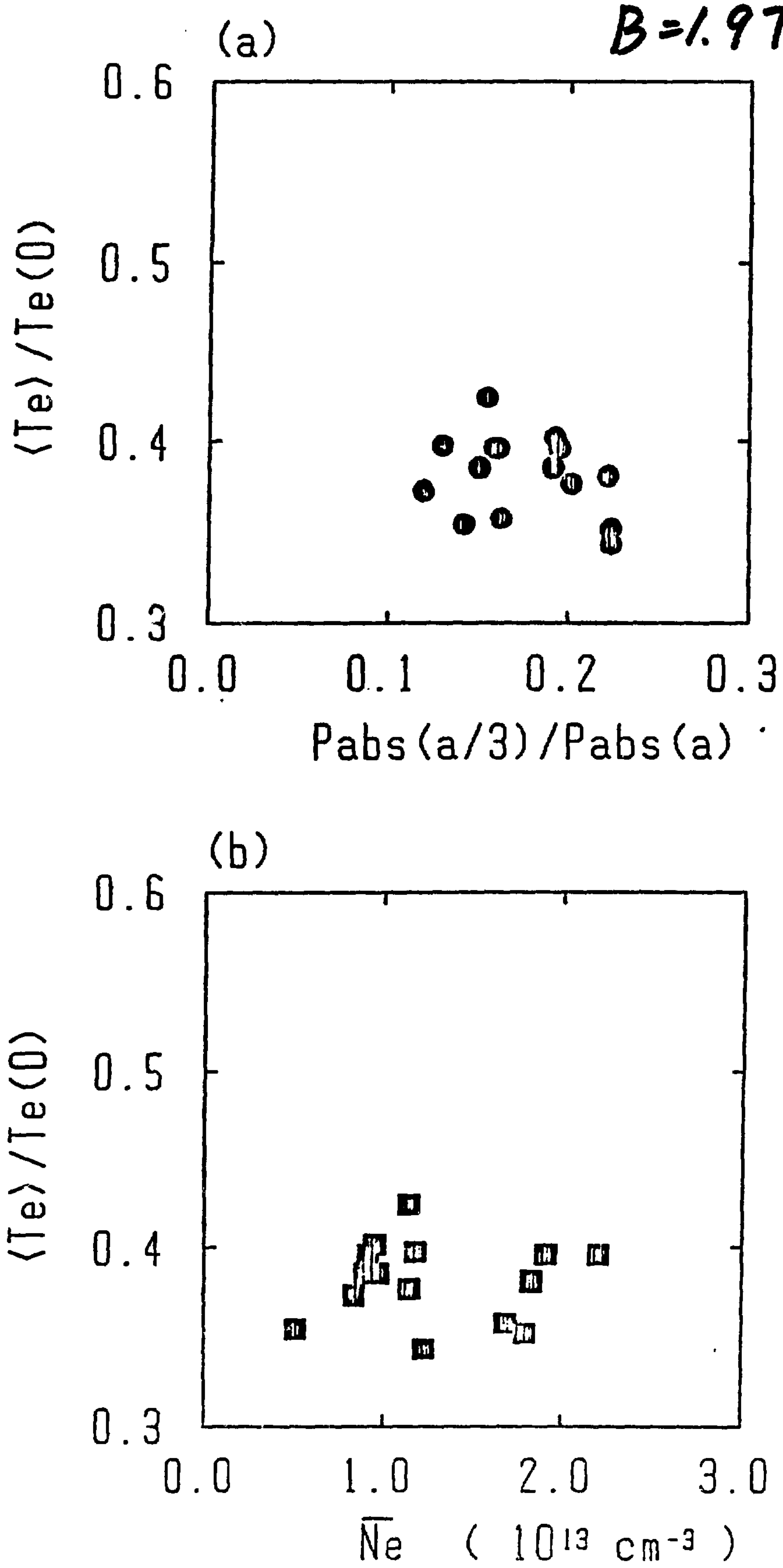

ECH

H. Zushi Fig. 16

B = 1.9 T

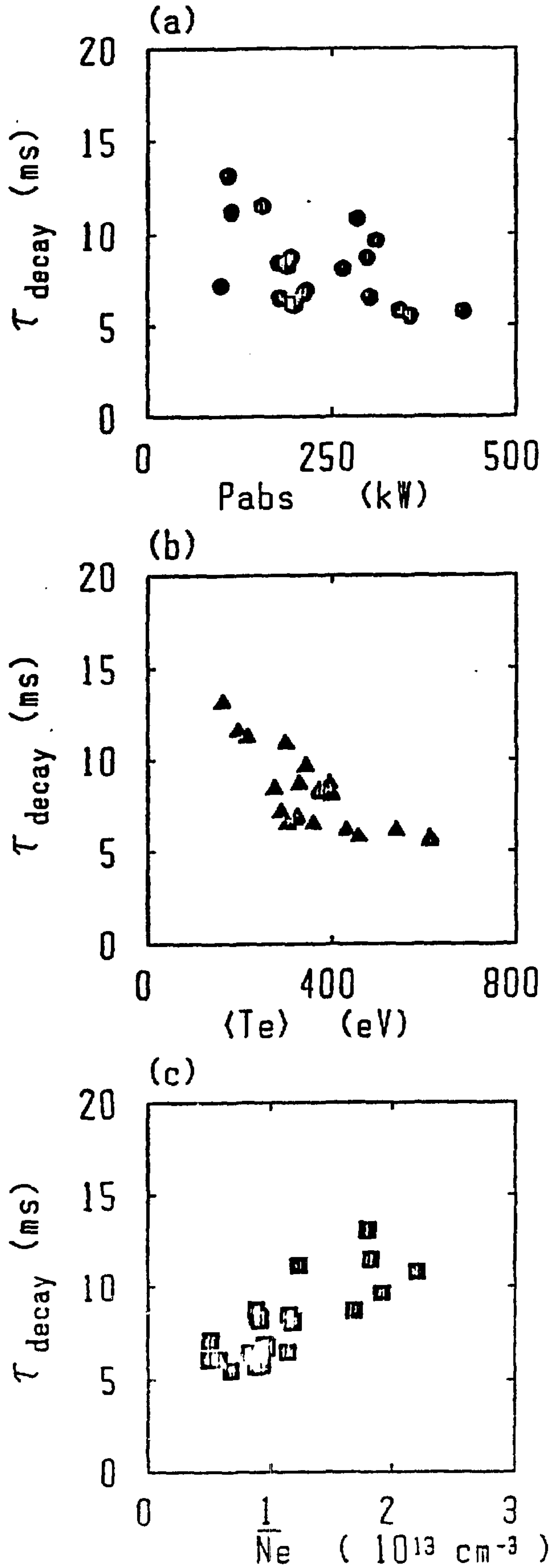

decay time of We(a)

vs.

P_{abs}, $\langle T_e \rangle$, $\overline{n_e}$

Fig. 17

ECH

Empirical scaling of τ_E^{decay}

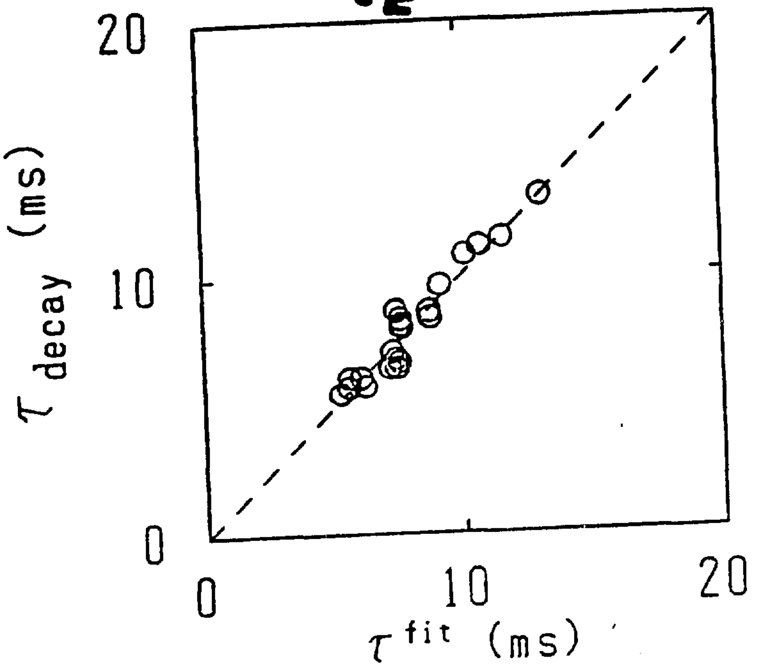

$P^{-0.3}\ \bar{n}_e^{\ 0.5}$

ECH

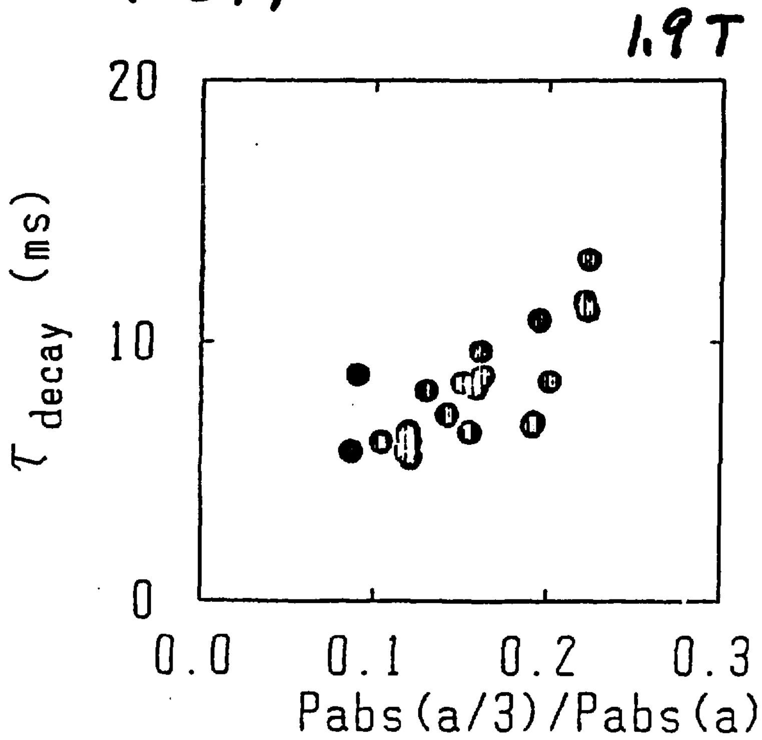

Pabs

Fig. 14

ECH

H. Zushi

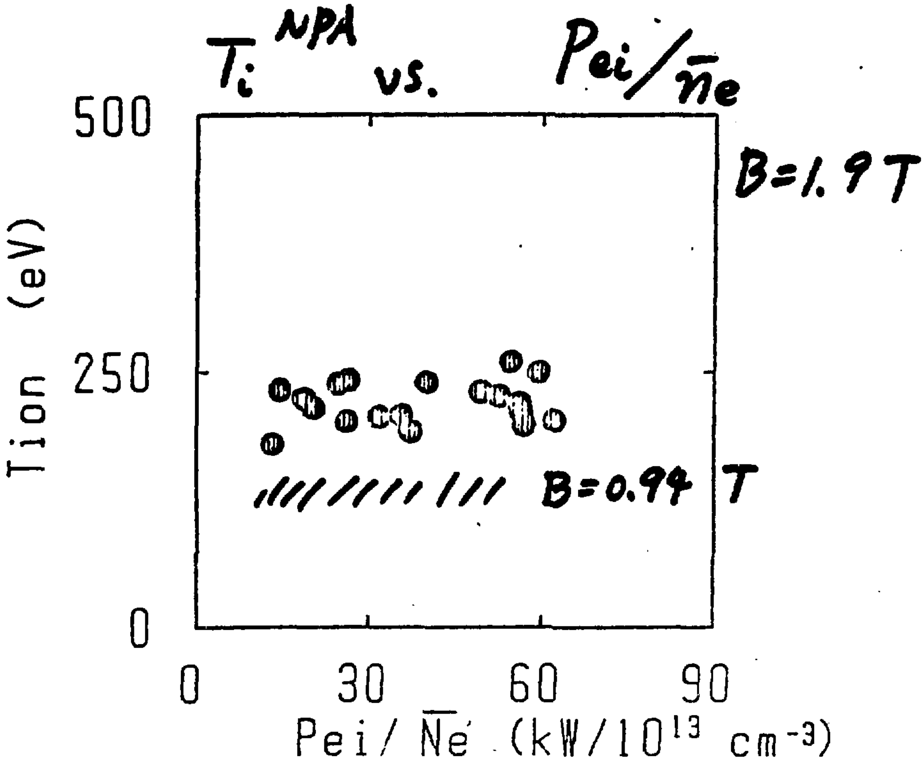

ion transport : anomalous?

Fig. 19

18

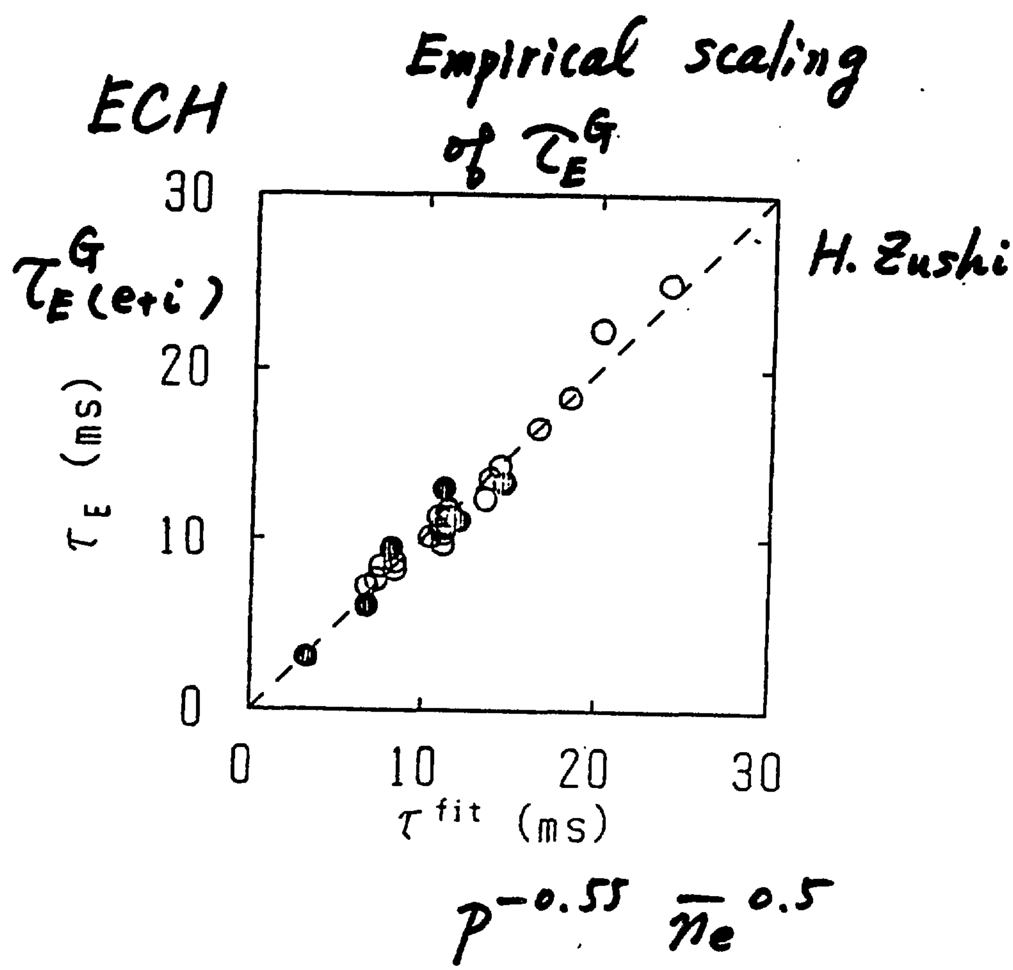

ECH
Empirical scaling of τ_E^G
H. Zushi
$\tau^G_{E(e+i)}$
τ_E (ms)
τ^{fit} (ms)
0
10
20
30
$P^{-0.55}\ \bar{n}_e^{0.5}$

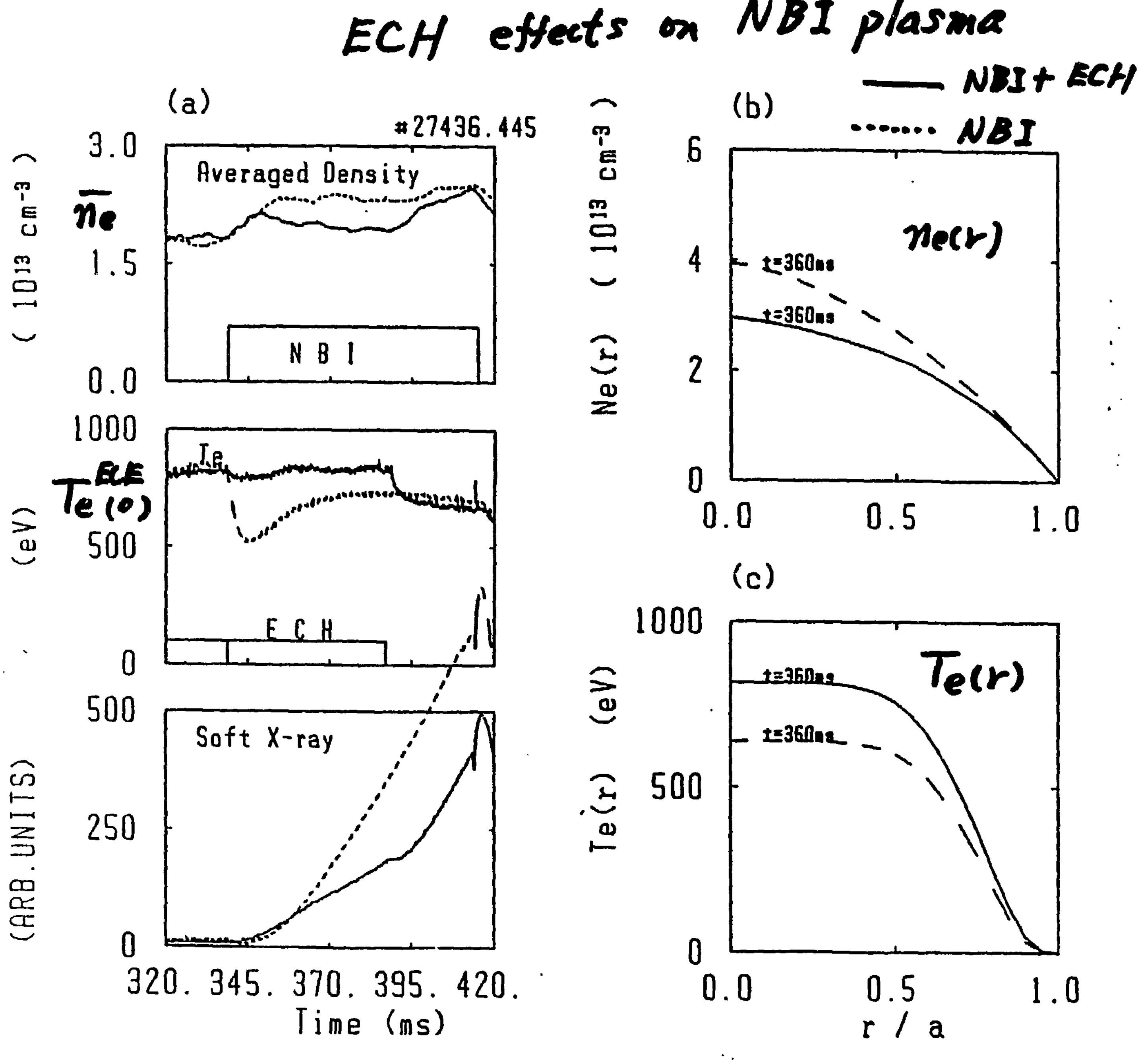

ECH effects on NBI plasma
NBI+ ECH
NBI
(a)
#27436.445
Averaged Density
NBI
$\overline{ne}$
(10^{13} cm^{-3})
3.0
1.5
0.0
1000
500
0
T_e
$T_e^{ECE}(0)$
(eV)
ECH
500
250
0
Soft X-ray
(ARB.UNITS)
320. 345. 370. 395. 420.
Time (ms)
(b)
ne(r)
Ne(r) (10^{13} cm^{-3})
6
4
2
0
t=360ms
t=360ms
0.0 0.5 1.0
(c)
Te(r)
Te(r) (eV)
1000
500
0
t=360ms
t=360ms
0.0 0.5 1.0
r / a

Fig. 20

US-Japan workshop on anomalous transport in toroidal fusion devices '87 Feb. Sandiego. Cal.

by . K. Itoh. et al.

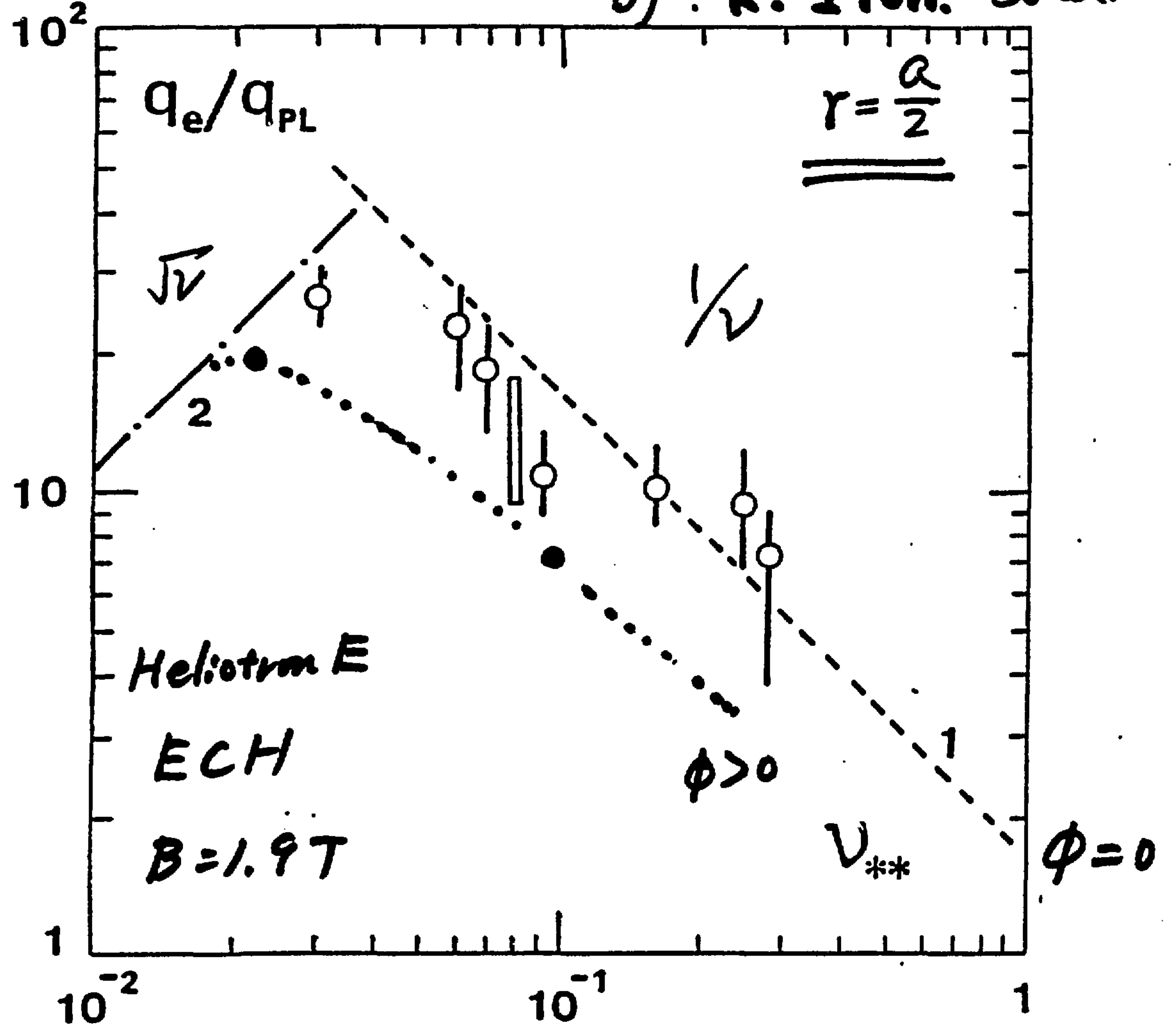

Not for Reference

M. Sato

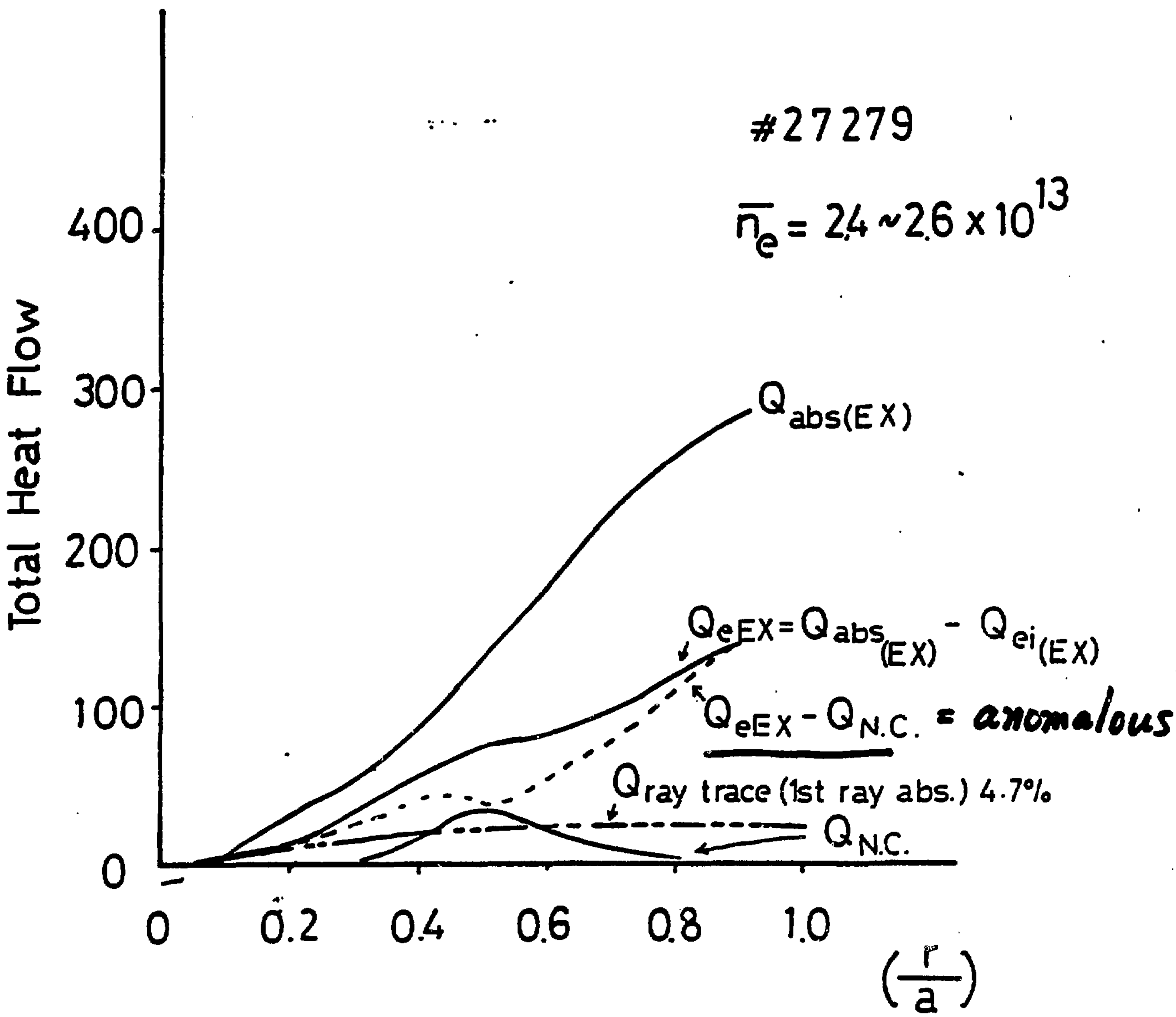

#27279
$\bar{n}_e = 2.4 \sim 2.6 \times 10^{13}$
Total Heat Flow
0
100
200
300
400
0
0.2
0.4
0.6
0.8
1.0
$(\frac{r}{a})$
$Q_{abs(EX)}$
$Q_{eEX} = Q_{abs_{(EX)}} - Q_{ei_{(EX)}}$
$Q_{eEX} - Q_{N.C.}$ = anomalous
$Q_{ray\ trace}$ (1st ray abs.) 4.7%
$Q_{N.C.}$

M. Sato

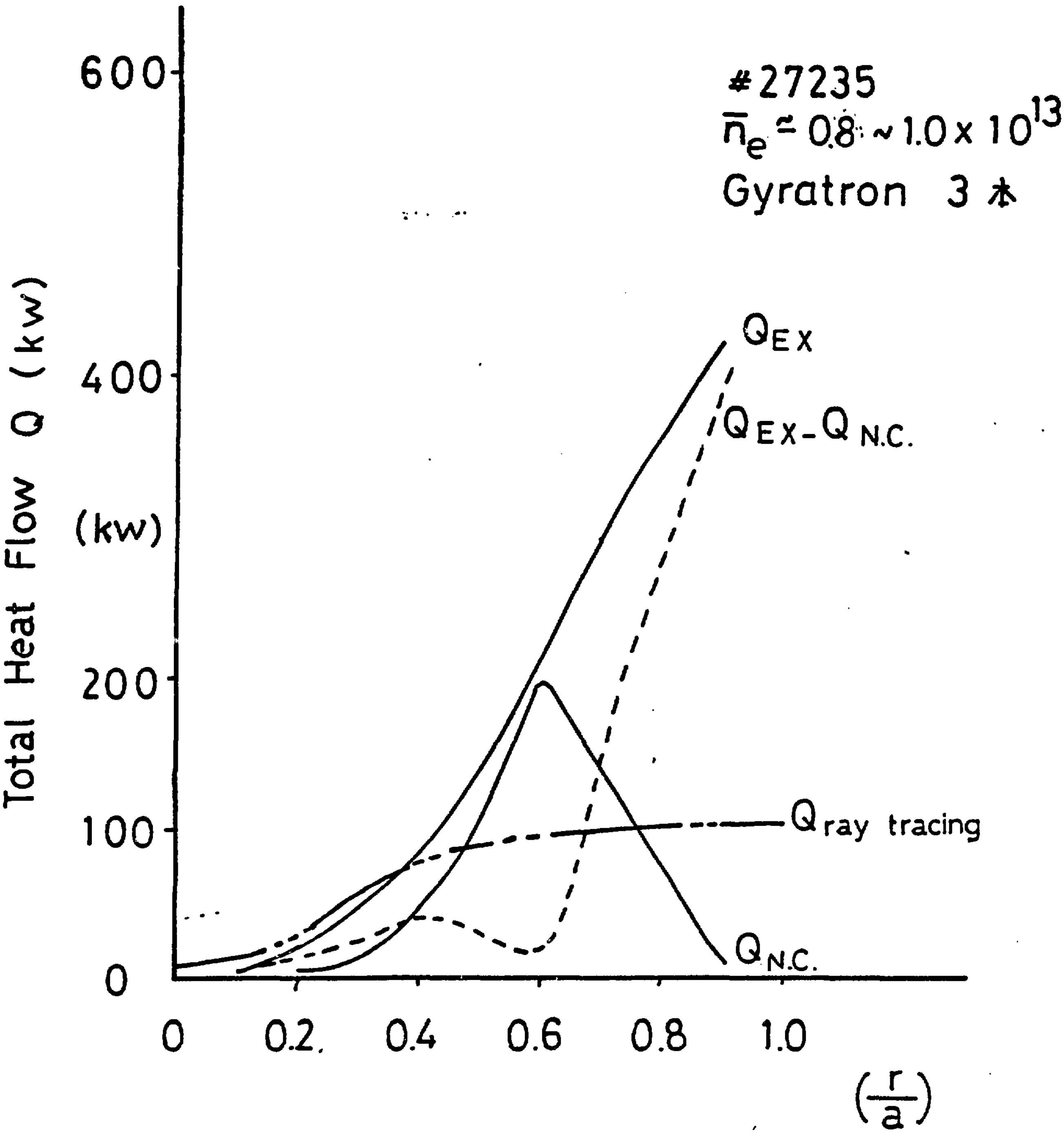

#27235
$\bar{n}_e \simeq 0.8 \sim 1.0 \times 10^{13}$
Gyratron 3 本
Total Heat Flow Q (kw)
(kw)
600
400
200
100
0
Q_{EX}
$Q_{EX} - Q_{N.C.}$
$Q_{ray\ tracing}$
$Q_{N.C.}$
0.2
0.4
0.6
0.8
1.0
$\left(\frac{r}{a}\right)$

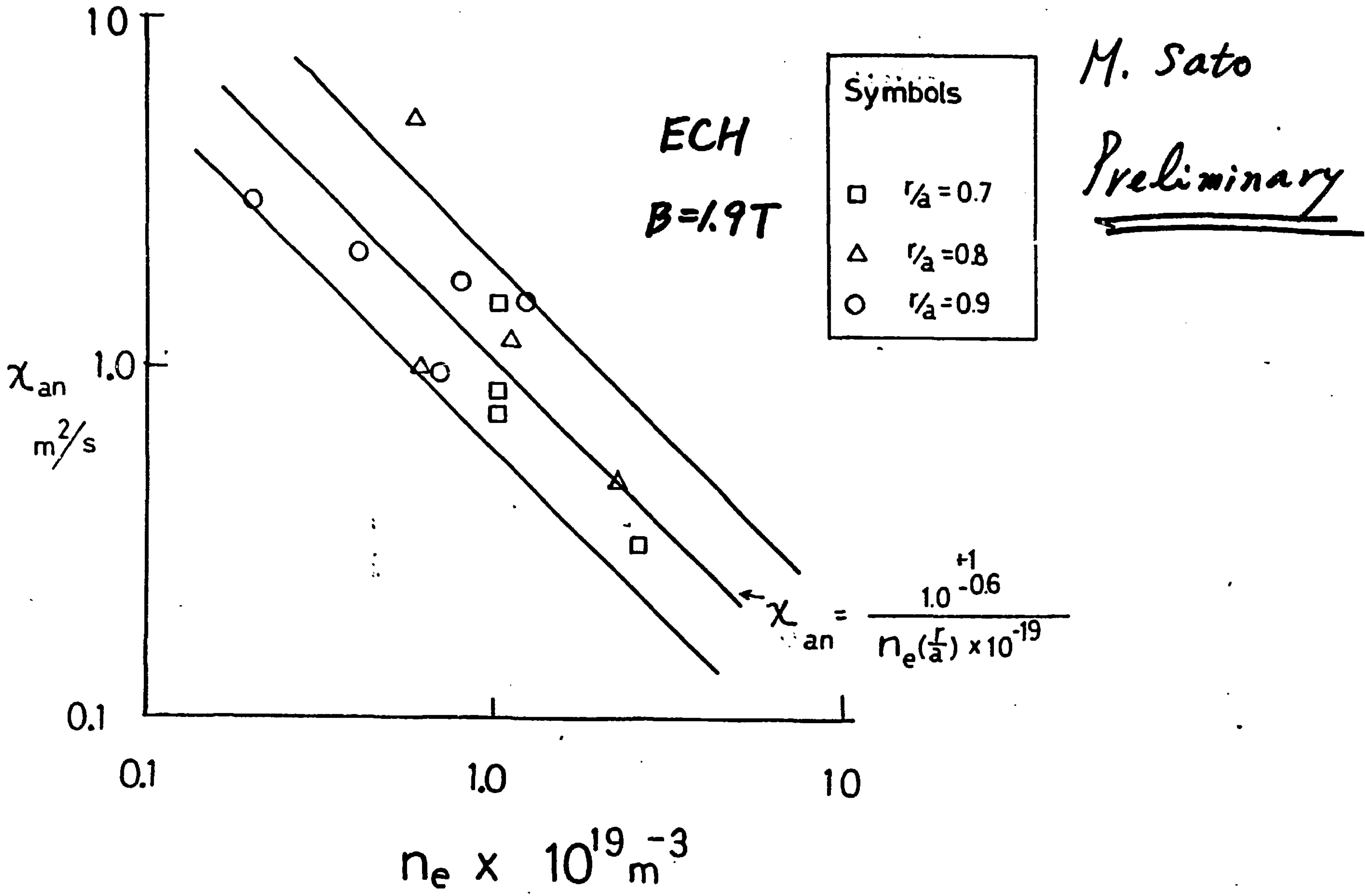
M. Sato
Preliminary
ECH
B=1.9T
Symbols
□ r/a = 0.7
△ r/a = 0.8
○ r/a = 0.9
χ_{an} m^2/s
10
1.0
0.1
0.1
1.0
10
$n_e \times 10^{19} m^{-3}$
$\chi_{an} = \frac{1.0^{+1}_{-0.6}}{n_e(\frac{r}{a}) \times 10^{-19}}$

χ_e of ECH plasma

$r < 0.3\ a_p$: anomalous (∇T_e measurement is not accurate)

$T_{eo} \propto P^{0.4}$: plateau like

(but worse than simulation)

island effect?

($\iota \sim 0.5$)

$r \sim 0.5\ a_p$: same order with the neoclassical ripple transport

$r > 0.7\ a_p$: anomalous

$\chi_e = 1 \sim 3\ m^2/S$

(Alcator like? $1/3 \sim 1/5$)

E_r : neoclassical behaviour

CONFINEMENT SCALING STUDY FOR NBI PLASMA

Y. Takeiri, F. Sano
M. Murakami, H.C. Howe (ORNL)

- Steady-state profile analysis is performed with the ORNL-developed transport-analysis code, PROCTR.

  Input profiles for PROCTR are:
  - Te(r): Thomson scattering,
  - ne(r): FIR interferometer,
  - Ti(r): Ti(r) calculated from Ti^{CX}(NPA).

- Results are analyzed with the PPPL-developed LOCUS database system for scaling study.

NBI

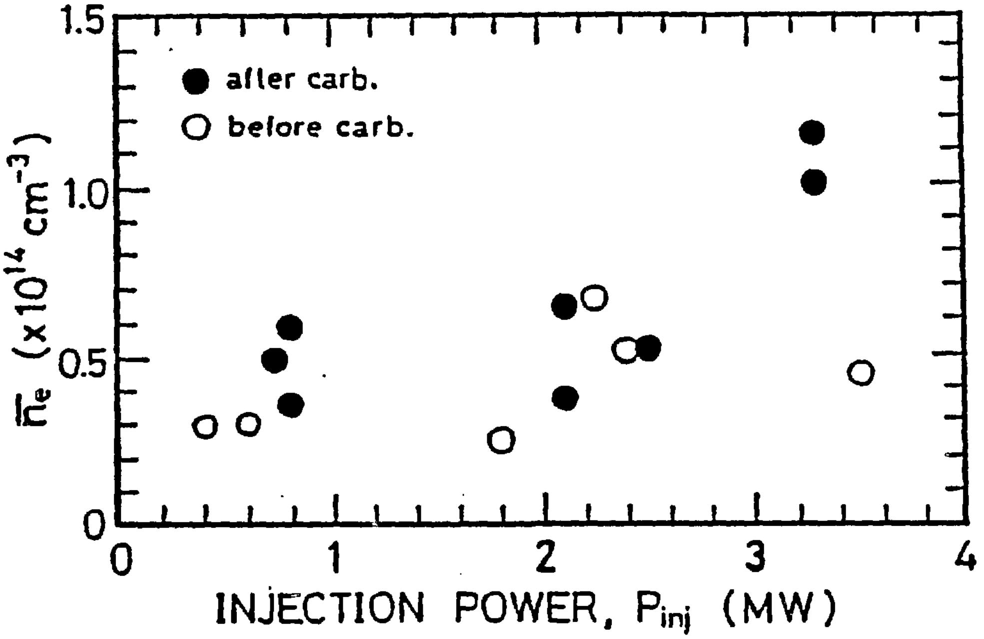

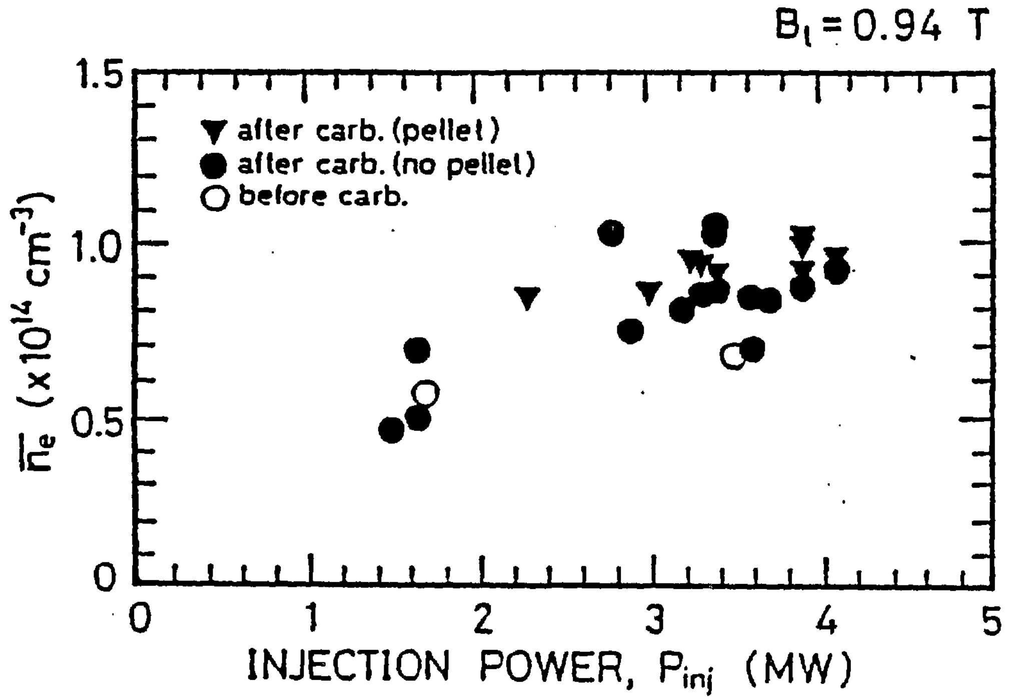

- $\overline{n_e}$ seems to be an increasing function of P_{inj}.
- High density plasmas are obtained after carbonization.
- At B_t=0.94T, operation is restricted to high power and high density regime after carbonization.

NBI

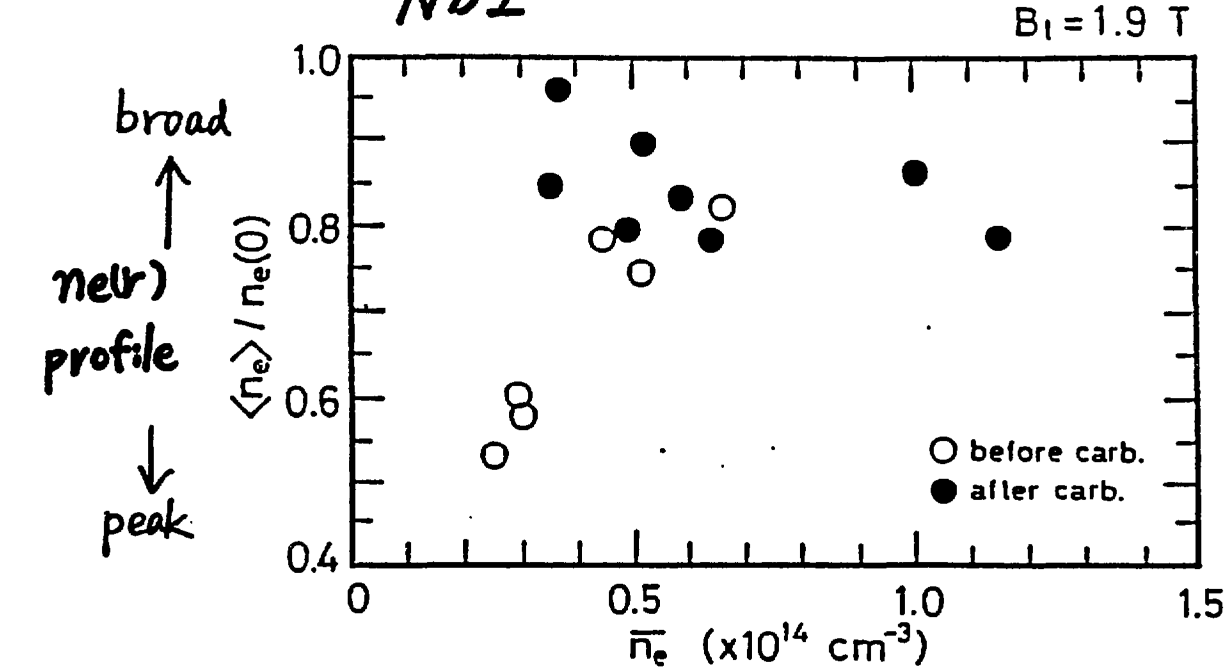

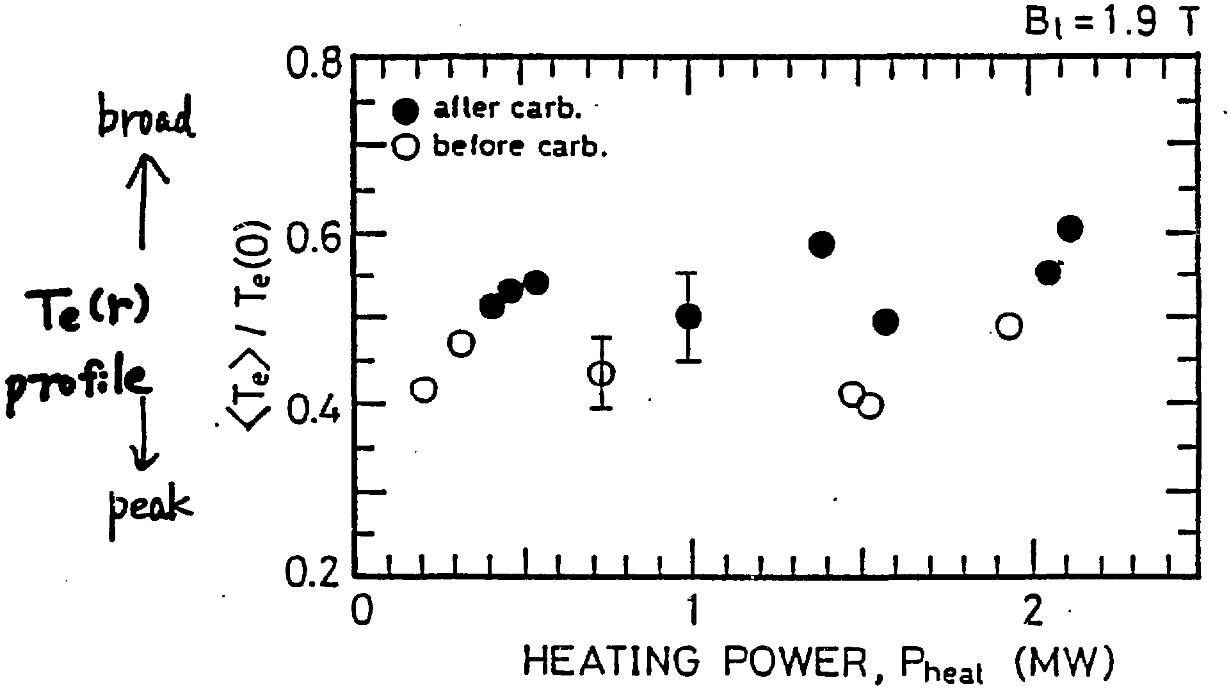

After carbonization :

- Electron temperature and density profiles become broader.
- Plasma pressure profile and calculated power deposition profile of NBI are also broader.

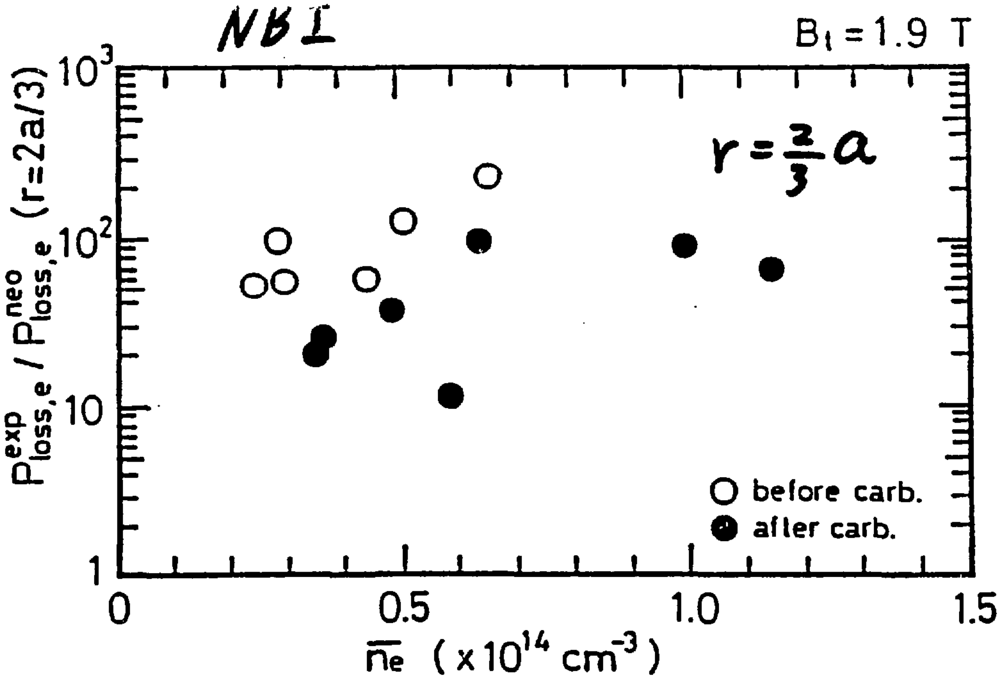

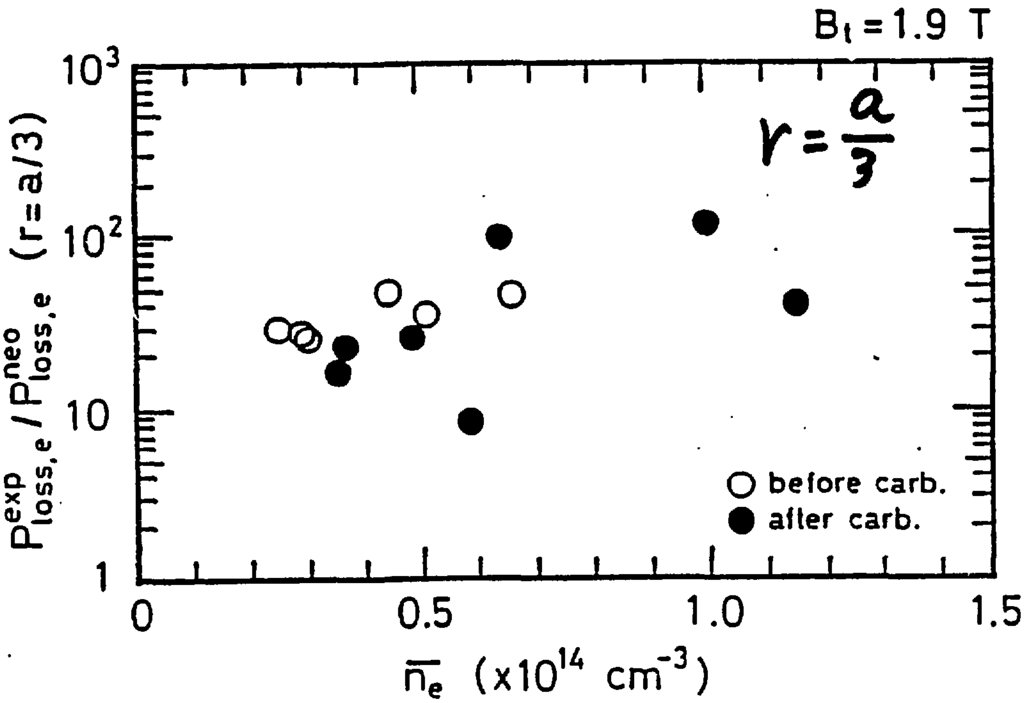

- $P^{exp}_{loss,e}$: Experimentally-inferred electron power loss (including radiation loss).
  $P^{neo}_{loss,e}$: neoclassically-calculated electron power loss (including helical ripple transport).

- Electron transport losses (including radiation loss) substantially exceed neoclassical predictions at high-power and high-density.

- At r=2a/3, electron-loss anomaly factor (including radiation loss) is reduced with carbonization. However, it is almost unchanged at r=a/3.

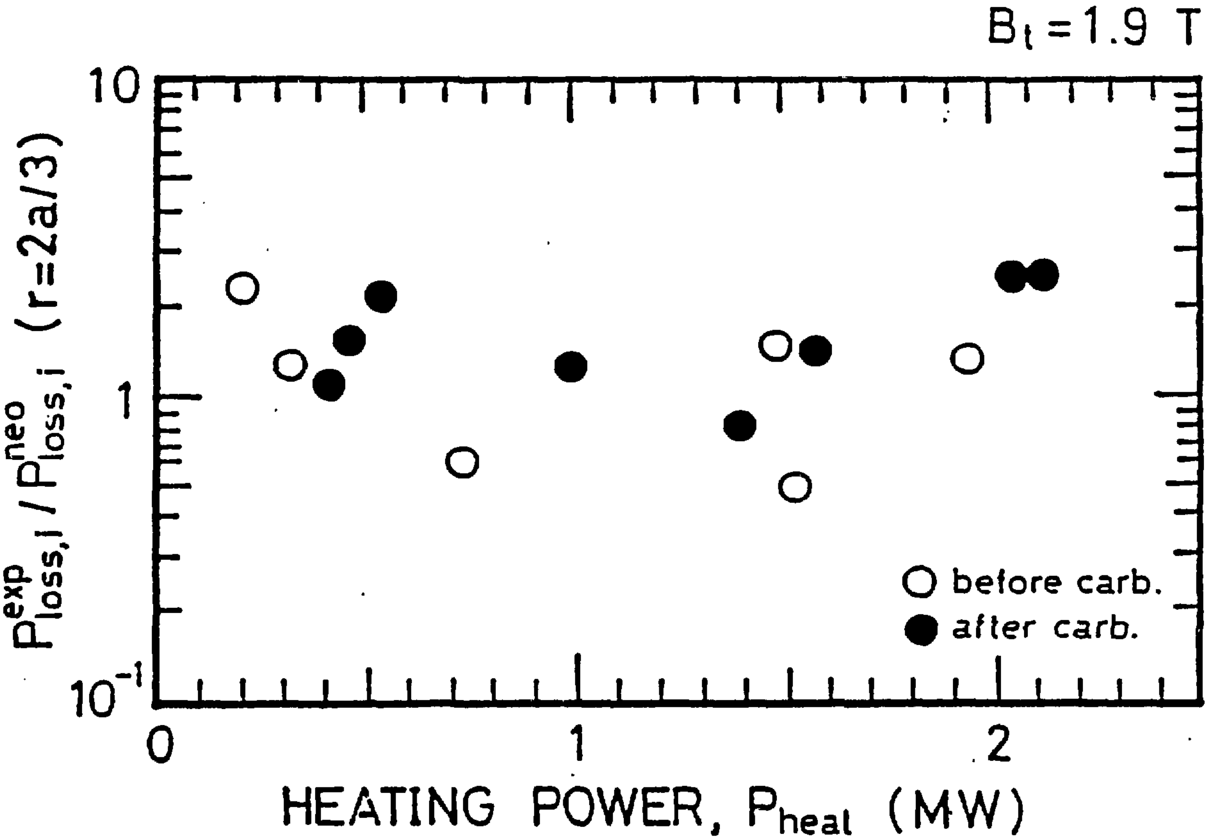

- $P^{exp}_{loss,i}$: Experimentally-inferred ion power loss.
  $P^{neo}_{loss,i}$: neoclassically-calculated ion power loss (including helical ripple transport).

- Ion heat transport is approximately in the neoclassical range (including helical ripple transport).

- Ion heat transport is not influenced by the carbonization.

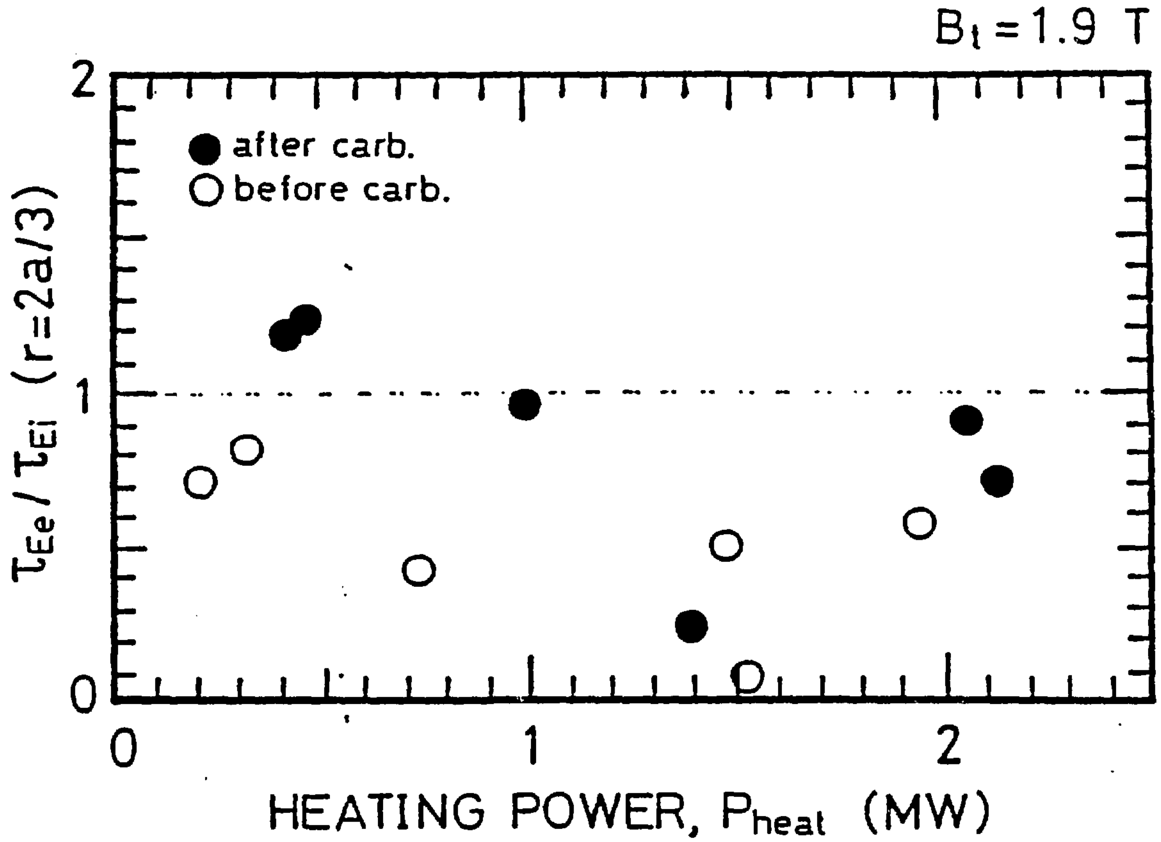

- τ_{Ee} : Electron confinement time

  τ_{Ee} = (electron energy)/(electron-loss power including radiation loss)

  τ_{Ei} : Ion confinement time

  τ_{Ei} = (ion energy)/(ion-loss power)

- At r=2a/3, electron confinement time seems to become comparable to ion confinement time with carbonization.

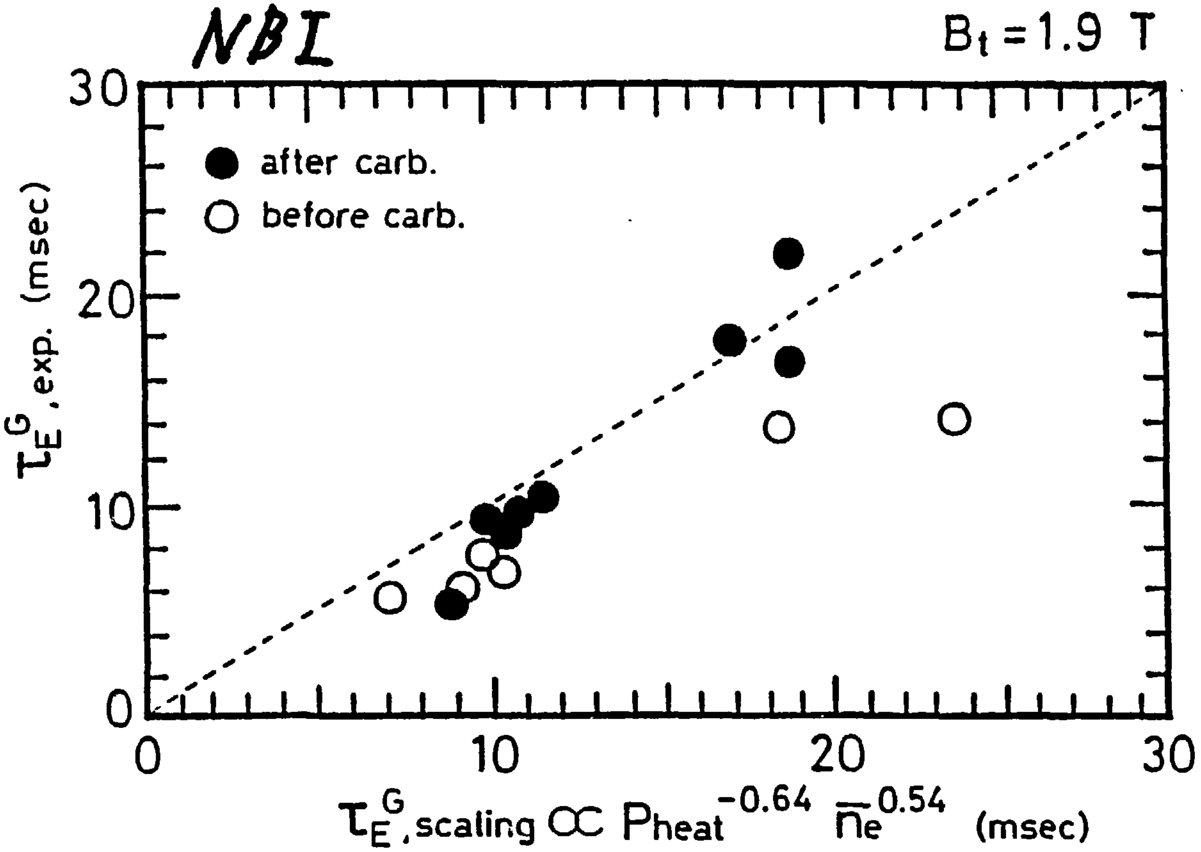

- τ_E^G = W_p(plasma internal energy)/P_{heat}(plasma heating power).
- $\tau_E^G \propto (P_{heat})^{-0.64} \cdot (\overline{n_e})^{0.54}$.
- τ_E^G is improved by about a factor of 1.3 after carbonization.

Energy Confinement Scaling

F. Sano

Confinement degrades with power

(1) Continuous degradation law.

Kaye-Goldston

$$\tau_E \propto \kappa^{0.28} B_t^{-0.09} I_p^{1.24} \bar{n}_e^{0.26} P^{-0.58} a^{-0.49} R^{1.65}$$

(2) Off-set linear law.

$$\tau_E \propto \sqrt{\kappa} \cdot I_p \cdot \left(\alpha + \frac{\beta}{P} \right)$$

Heliotron-E · NBI scaling

ⓐ $\tau_E \propto \bar{n}_e^{\alpha} \cdot P^{\beta} \cdot B^{\gamma}$

ⓑ $\tau_E \propto \alpha(B_h) + \beta(B_h) \cdot \dfrac{\langle n_e \rangle_v}{P_{heat}}$

$$\Downarrow$$

$$\alpha * B_h + \beta * \frac{\langle n_e \rangle_v}{P_{heat}} + \text{const.}$$

$$\tau_E^q \propto \bar{n}_e^{\alpha} \cdot P^{\beta} \quad ; \quad \alpha \approx -\beta$$

$B = 1.9\,T$

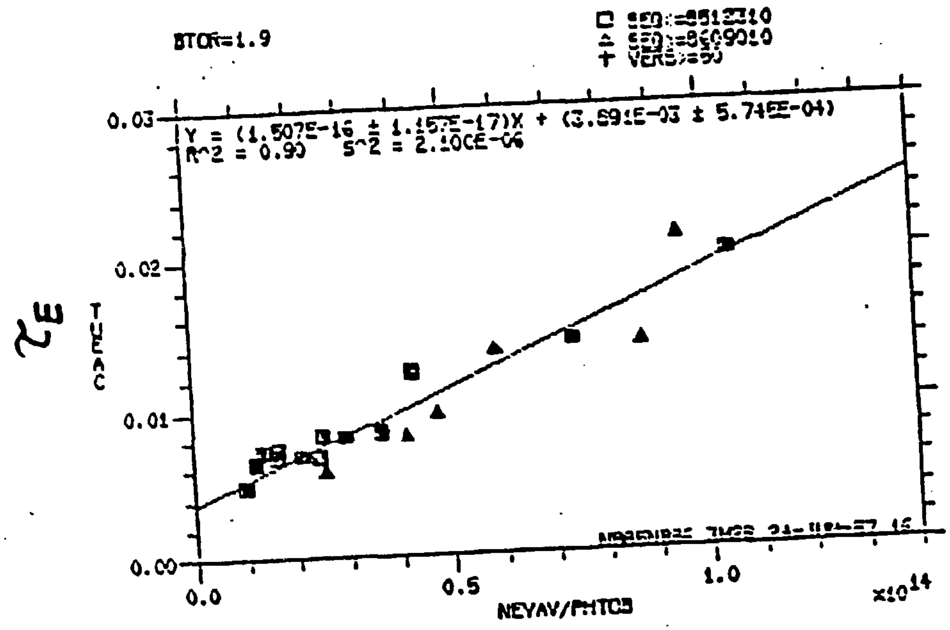

$\langle n_e \rangle_v / P_{heat}$

B = 0.94 T

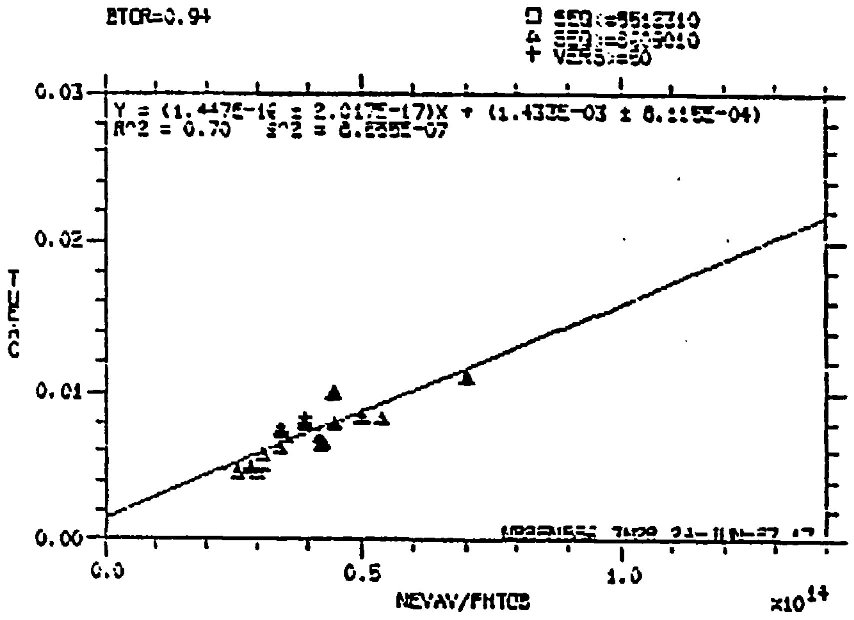

$$\tau_E^G = \alpha' \cdot B_h + \beta' \cdot \frac{\langle n_e \rangle}{P_{heat}} + \text{const.}$$

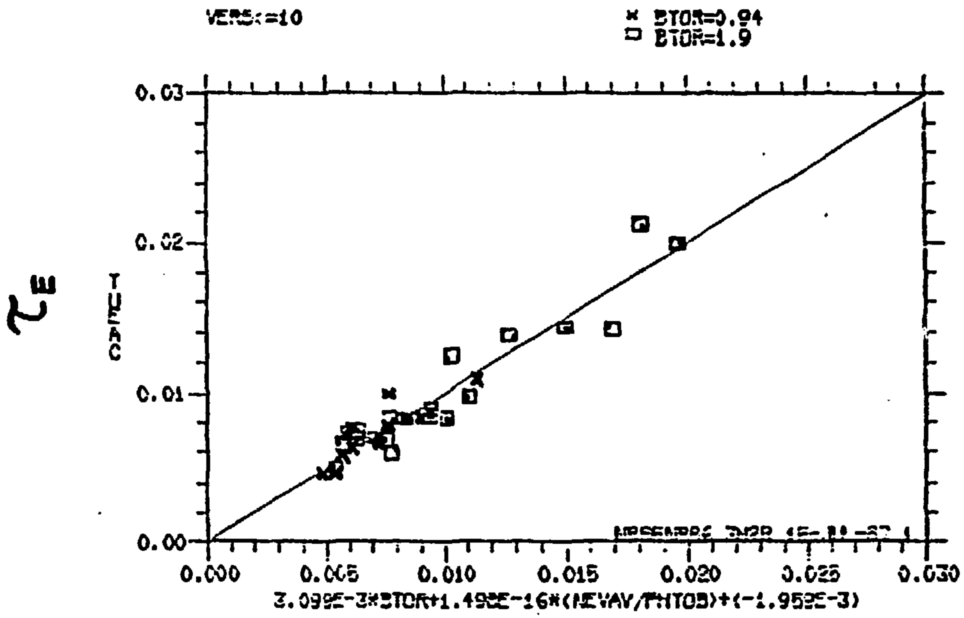

$$3.1\times10^{-3} * B + 1.5\times10^{-16}(\langle ne\rangle_v/P) - 2.0\times10^{-3}$$

Off-set linear scaling

samp. = 2

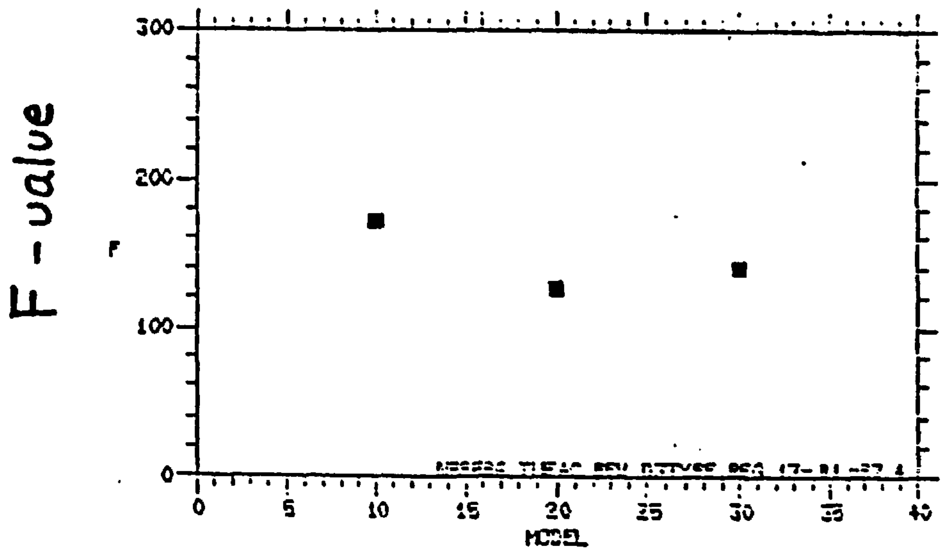

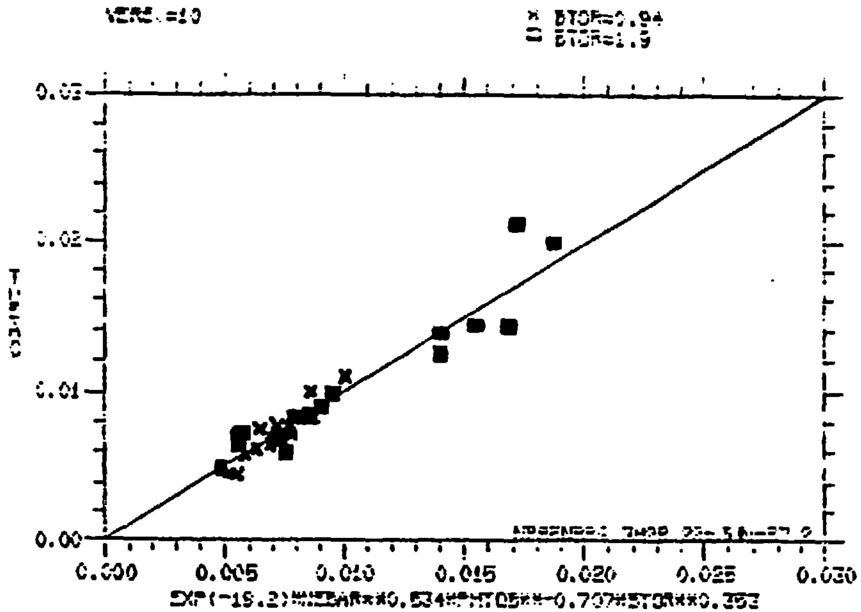

τ_E

$\exp(-19.2) \times \bar{n}_e^{0.534} \times \bar{P}^{-0.707} \times B^{0.353}$

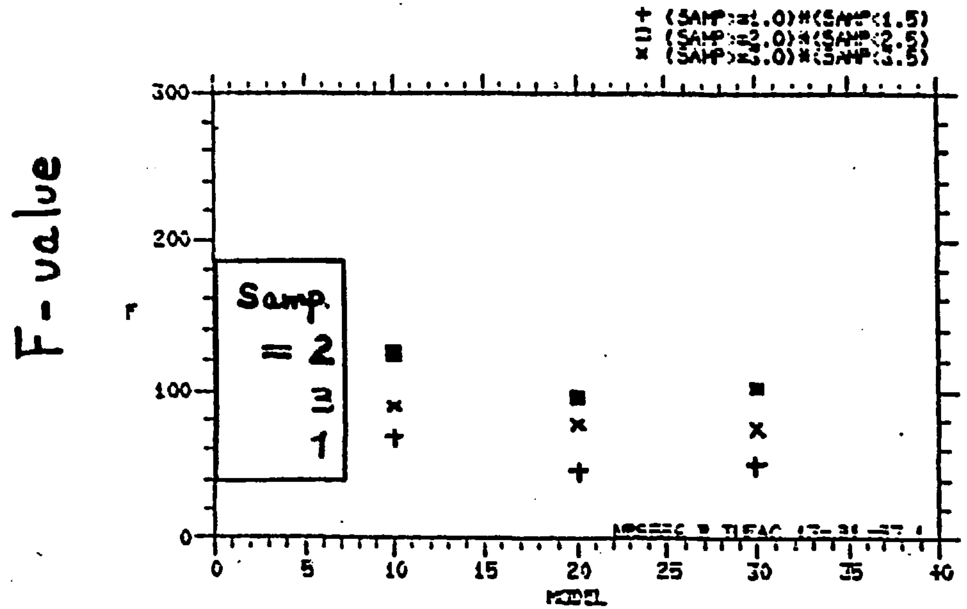
F- value
F
Samp.
= 2
3
1
MODEL
0
100
200
300
0
5
10
15
20
25
30
35
40

Goodness of Fit in Data Analysis

① Models of fitting curves ⇄ physical meanings

② Goodness of fit ⇄ physical meanings

<Test>

(i) t-test; (ii) χ^2-test; (iii) R^2-test; (iv) F-test; etc.

F-test ; F-value $\triangleq \dfrac{\chi_1^2/\nu_1}{\chi_2^2/\nu_2} = \dfrac{s_1^2/\sigma_1^2}{s_2^2/\sigma_2^2} \to \dfrac{s_1^2}{s_2^2}$ (≥ 1)

(exp. A) data $y_i \to y_i(t_i) = a_0 + \sum_{j=1}^{n_j} a_j X_j(t_i)$ variance ratio

$$\Sigma (y_i - \bar{y})^2 = \sum_{j=1}^{n_j} a_j \Sigma[(y_i - \bar{y})(x_j - \bar{x_j})] + \Sigma (y_i - y(x_i))^2$$

$$= R^2 \Sigma (y_i - \bar{y})^2 + (1 - R^2) \Sigma (y_i - \bar{y})^2$$

$$F^{n_j}_{N-n_j-1} = \frac{R^2 \Sigma (y_i - \bar{y})^2 / n_j}{(1-R^2)\Sigma (y_i - \bar{y})^2 / (N - n_j - 1)} = \frac{N - n_j - 1}{n_j} \cdot \frac{R^2}{1 - R^2}$$

↑ F-distribution, F-value Table

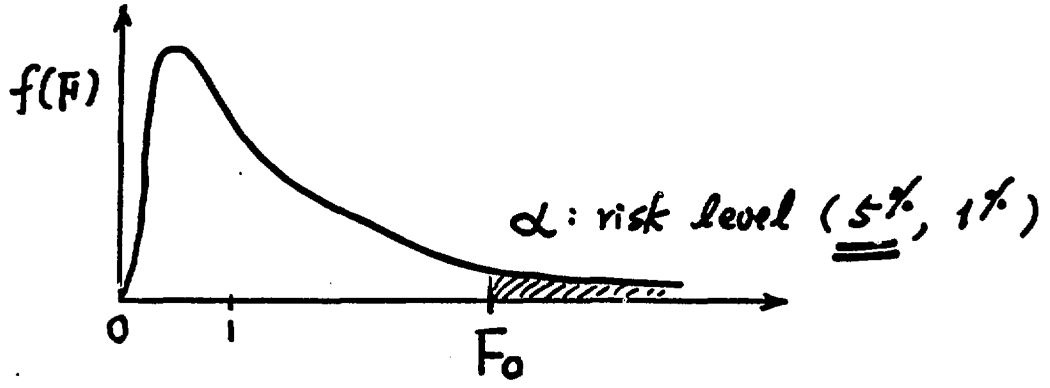

(exp. B)

$$F^{1}_{N-1} = \frac{(\bar{\alpha} - \alpha_0)^2}{(S^2/N)}$$

$$\tau_E\,(ms) = 3.1 \times B_{[T]} + 1.5 \cdot \frac{\langle n_e \rangle_{13}}{P_{[MW]}} - 2.0$$

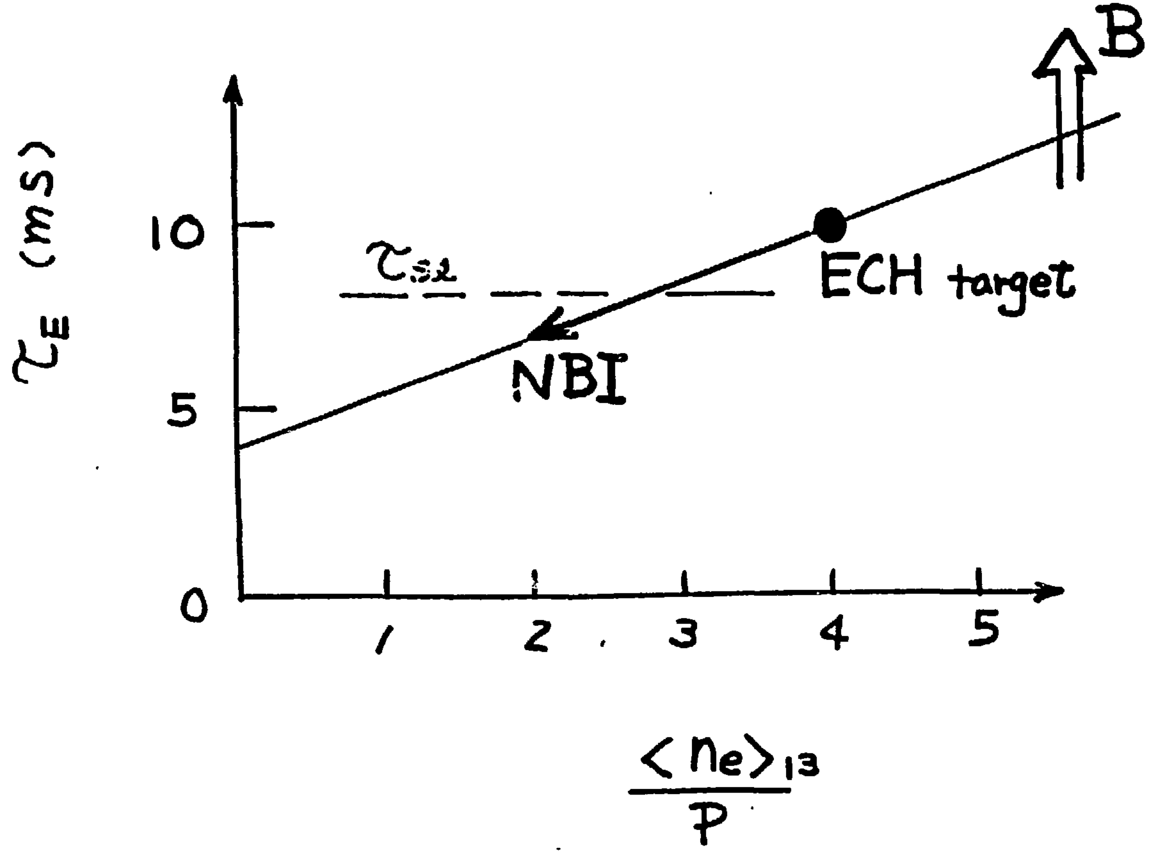

TRANSPORT ANALYSIS OF ICRF PLASMA

Measured Parameters $n_e(r)$, $T_e(r)$, $T_i(0)$

$P_{in}{}^{ICRF}$, $P_{abs}(r)^{ECH}$, P_{rad},

$f_H(E)$

Assumpsion τp: 7 msec

$T_i(r)$; calculated by Chan-Hinton χ_i

Energy Balance

$P_{abs}(r)$: calculated by Fukuyama code[1]

$P_e(r)$, $P_H(r)$, $P_D(r)$

Relaxation from P_H to electron and Deuteron is calculated by $f_H(D)$ distribution

Scaling

$P_{abs}=0.6 \times P_{in}$(emitted from antenna)

(1) Reviced version from Nuc. Fusion <u>26</u>, ('86) including Landau damping of fast wave, TTMP, ion cyclotron damping

. PROCTR code
. LOCUS code
are used

```
RF   = 28.220   BB   =  1.860   RRC =  0.270   IJ  AJ  PHASE      R           X
.RKZ =  4.318   RA   =  0.140   HI  =  4.318    1  1.0   0.0   1.904E-01 -6.776E-01
NNOD=    907    NELM=   1700    P= 1.904E-01

IS    PA         PZ     PN         PNS        PZCL    PTPR    PTPP    PTS    PABS
 1  5.446E-04  -1.   3.000E-01  1.000E-02  0.010   0.500   0.500   0.0   3.045E-02
 2  2.000E+00   1.   2.970E-01  9.900E-03  0.010   0.500   0.500   0.0   3.076E-02
 3  1.000E+00   1.   3.000E-03  1.000E-04  0.010   0.500   0.500   0.0   1.291E-01
```

by A. Fukuyama (Okayama Univ.) et al.

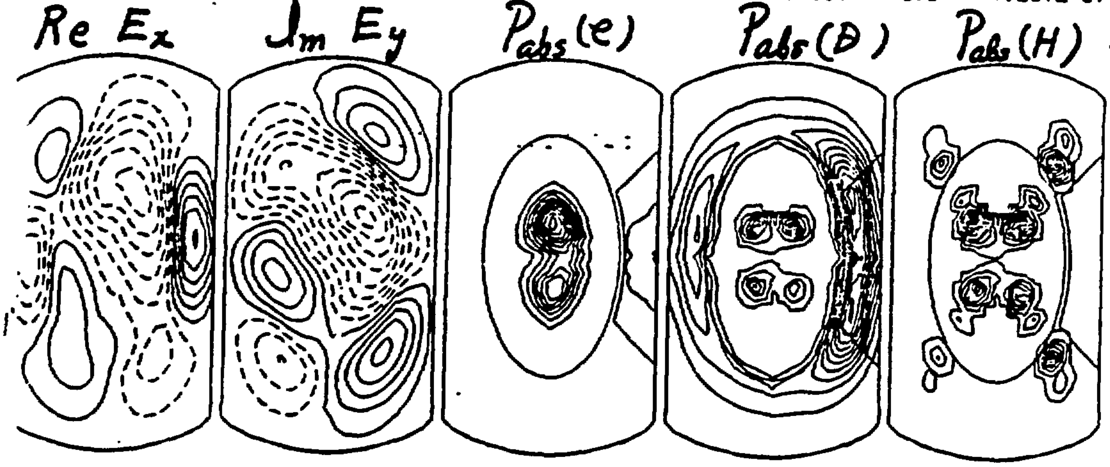


```
EX   REAL          EY   IMAG          PABS IS=     1     PABS IS=     2     PABS IS=     3
STP=         10    STP=         10    STP=         10    STP=         10    STP=         10
MAX= 2.29E+01      MAX= 1.42E+01      MAX= 2.09E+00      MAX= 6.31E-01      MAX= 8.75E+00
MIN=-2.44E+01      MIN=-2.34E+01      MIN= 9.62E-11      MIN=-7.64E-14      MIN=-1.05E-15
DLT= 4.07E+00      DLT= 2.99E+00      DLT= 2.08E-01      DLT= 6.31E-02      DLT= 8.75E-01
```

$B = 1.86\,T$ $T_e(0) = 500\,eV$
$f = 28.22\,MHz$ $T_i(0) = 500\,eV$
$n_e(0) = 3\times10^{19}\,m^{-3}$
$H/D = 0.01$

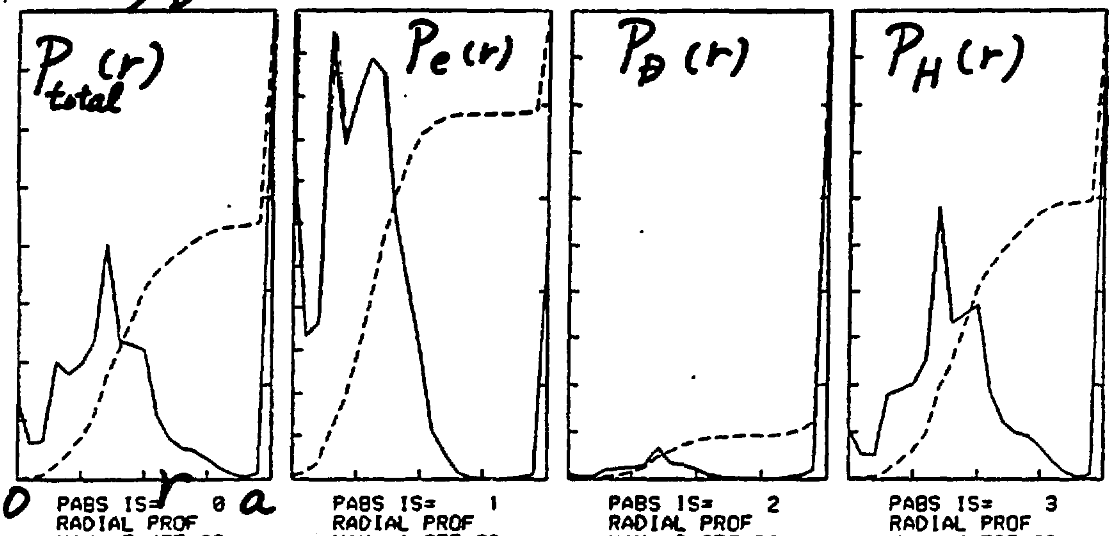


```
PABS IS=     0     PABS IS=     1     PABS IS=     2     PABS IS=     3
RADIAL PROF        RADIAL PROF        RADIAL PROF        RADIAL PROF
MAX= 7.47E-03      MAX= 1.05E-03      MAX= 2.35E-03      MAX= 4.56E-03
MIN= 4.16E-05      MIN= 1.50E-07      MIN= 1.86E-06      MIN= 1.60E-05
DLT= 1.00E-03      DLT= 1.00E-04      DLT= 2.50E-04      DLT= 5.00E-04
```

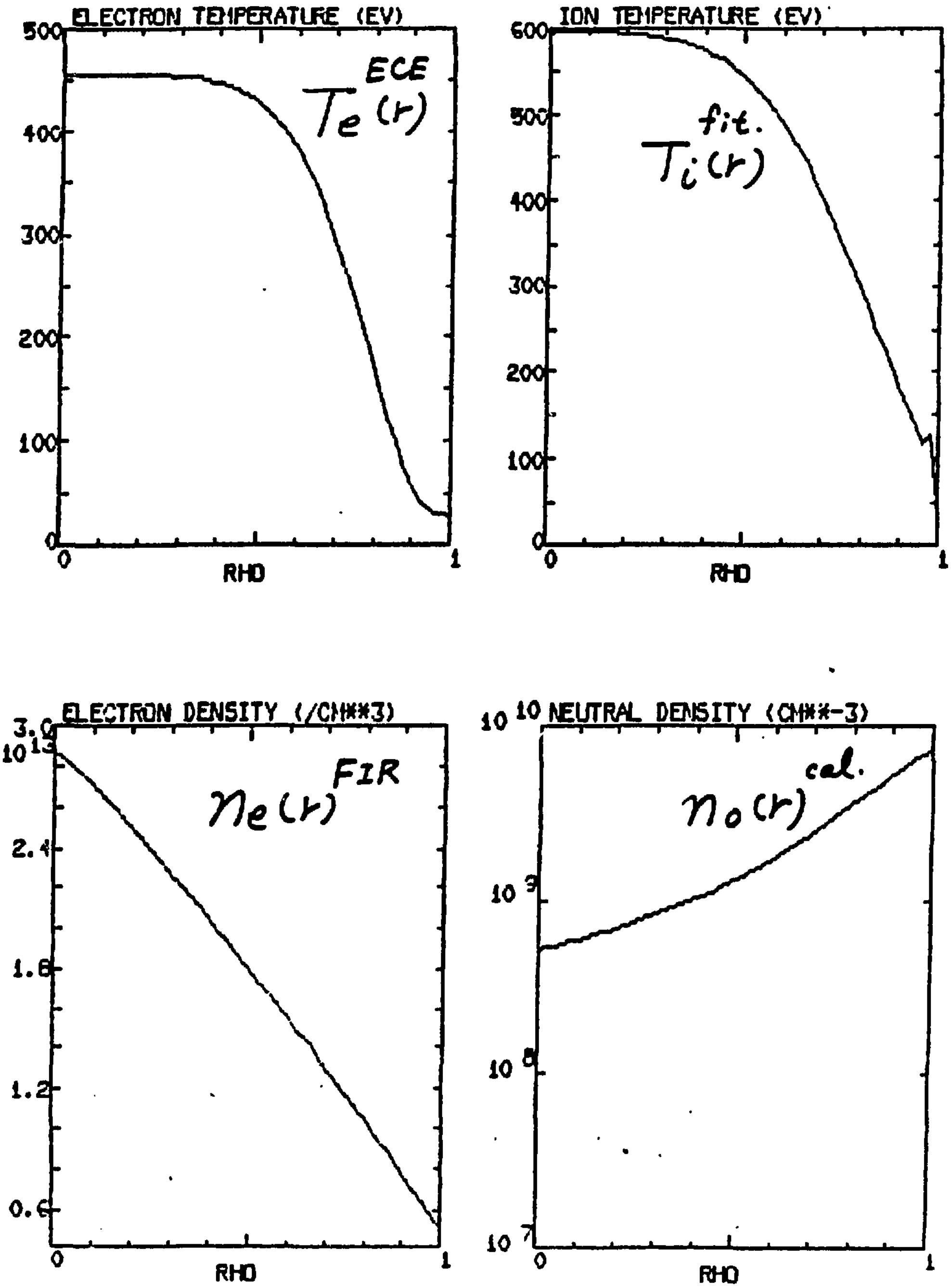
ELECTRON TEMPERATURE (EV)
500
400
300
200
100
0
RHO
1
$T_e^{ECE}(r)$
ION TEMPERATURE (EV)
600
500
400
300
200
100
0
RHO
1
$T_i^{fit.}(r)$
ELECTRON DENSITY (/CM**3)
3.0
10^{13}
2.4
1.8
1.2
0.6
0
RHO
1
$n_e(r)^{FIR}$
NEUTRAL DENSITY (CM**-3)
10^{10}
10^{9}
10^{8}
10^{7}
0
RHO
1
$n_0(r)^{cal.}$

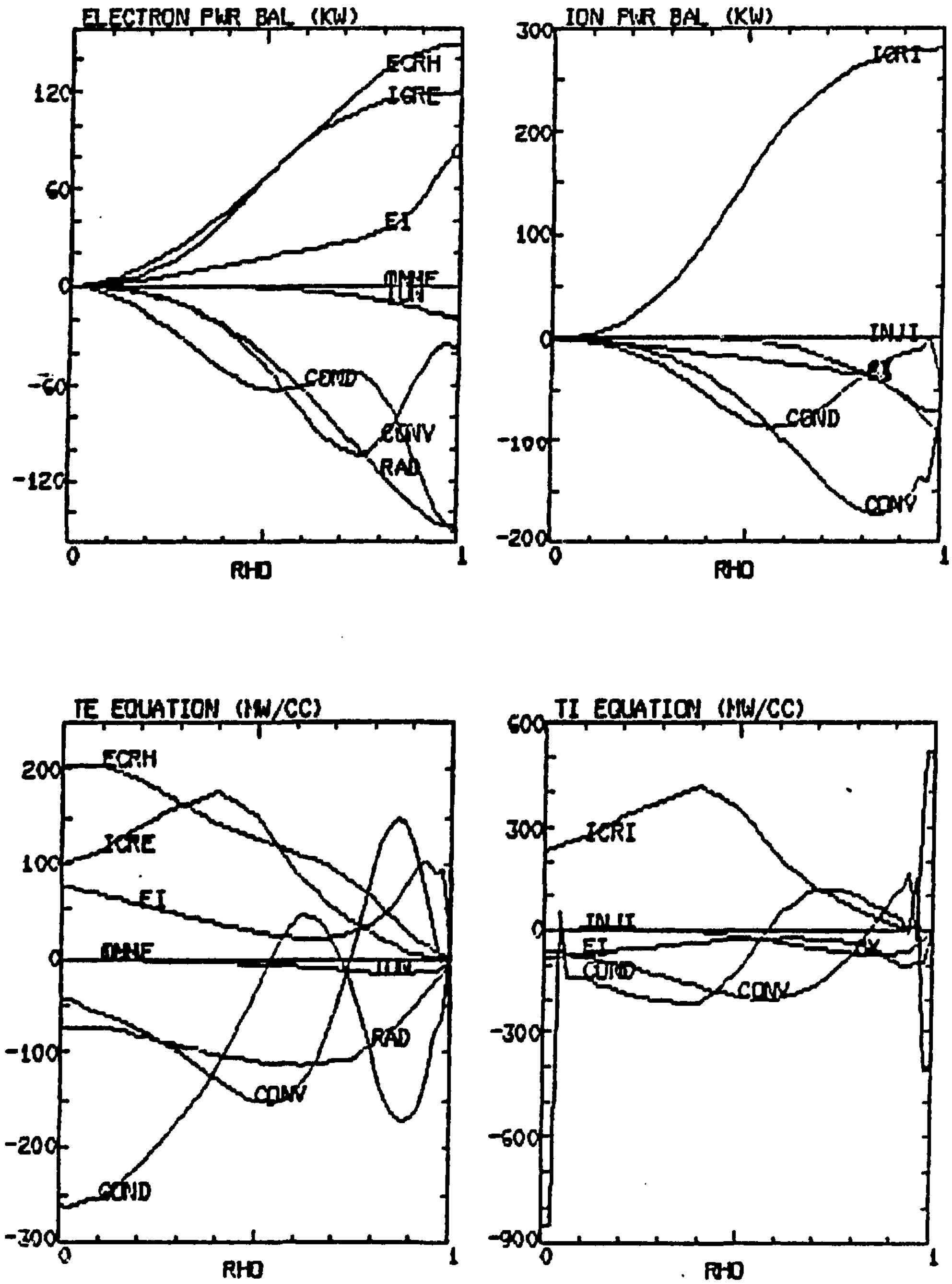

preliminary

preliminary

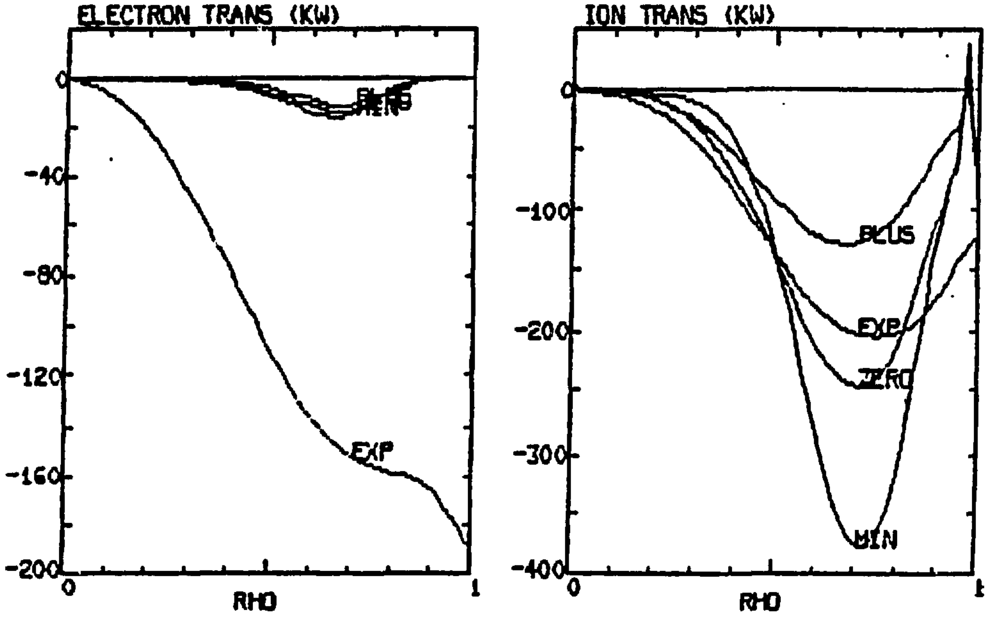

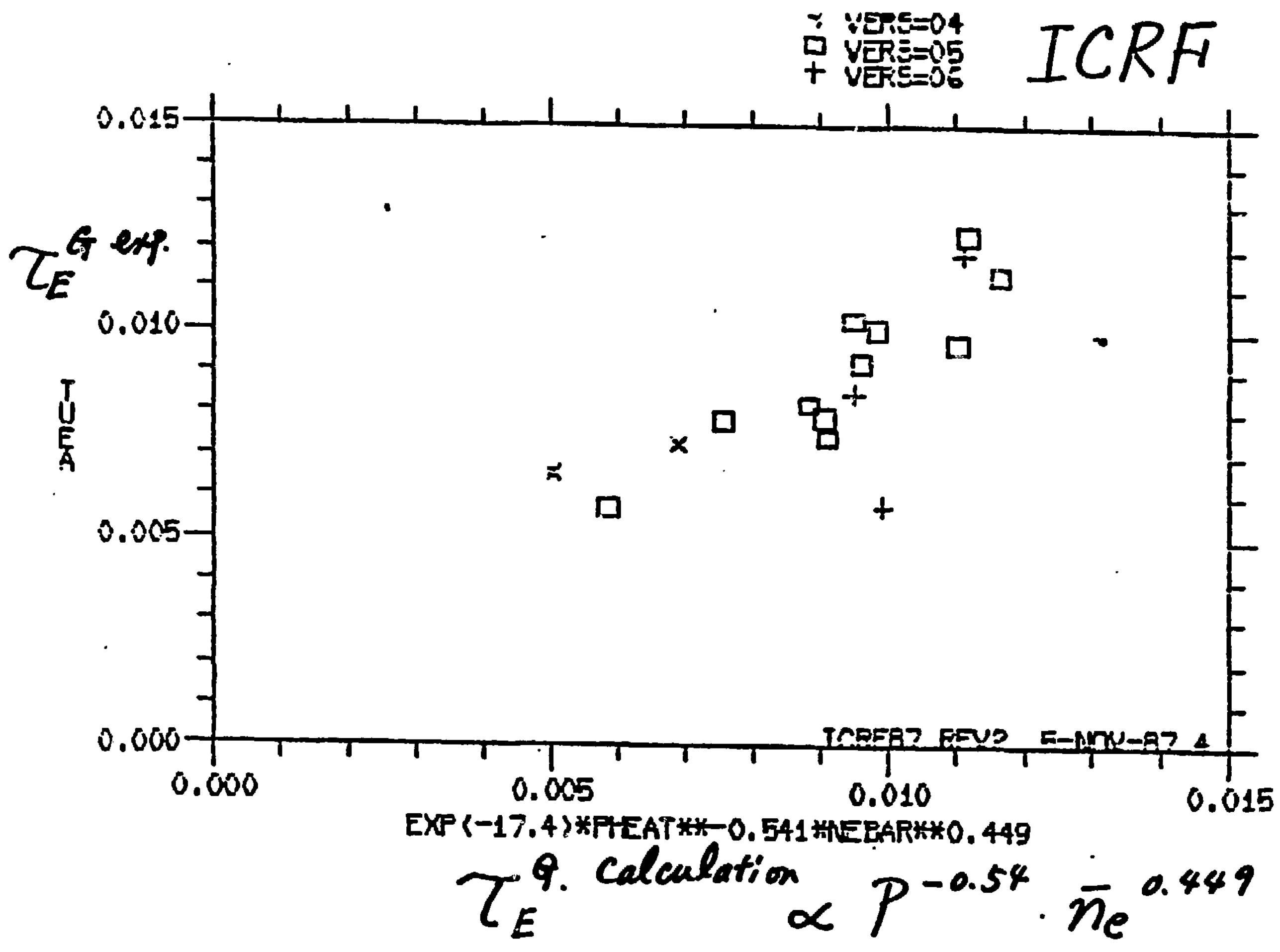

ICRF
VERS=04
VERS=05
VERS=06
$\tau_E^{G\ exp.}$
TUEA
0.015
0.010
0.005
0.000
0.000
0.005
0.010
0.015
ICRF87 REV2 5-NOV-87 4
EXP(-17.4)*PHEAT**-0.541*NEBAR**0.449
$\tau_E^{g.\ calculation} \propto P^{-0.54} \cdot \bar{n}_e^{0.449}$

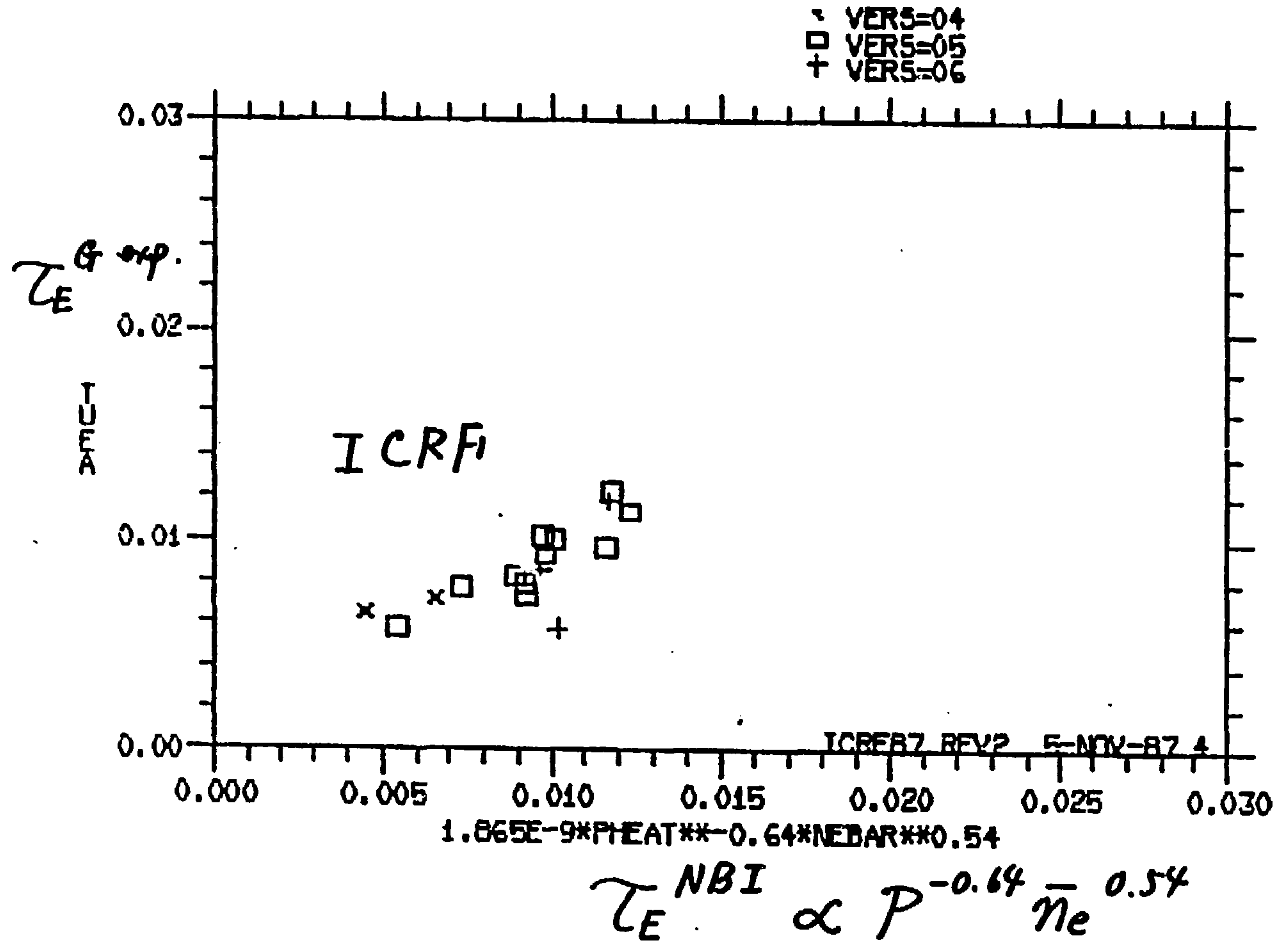
VERS=04
VERS=05
VERS=06
0.03
0.02
0.01
0.00
TUEA
$\tau_E^{G\ exp.}$
ICRF
ICREB7 REV2 5-NOV-87 4
0.000
0.005
0.010
0.015
0.020
0.025
0.030
1.865E-9*PHEAT**-0.64*NEBAR**0.54
$\tau_E^{NBI} \propto P^{-0.64}\, \bar{n}_e^{\,0.54}$

Transport Analysis for ATF

presented by H. Howe

Collaborators

- M. Murakami
- W. Houlberg, S. Attenberger – Chord tracker
- D. Lee, J. Harris – Vacuum flux surfaces
- B. Morris, R. Fowler, J. Rome – Neutral heating
- B. Morris, S. Hirshman – Finite-beta equilibrium
- K. Kannan – Data organization

US – Japan Stellerator/Heliotron Workshop
Oak Ridge, Tennessee, USA
November 10, 1987

Transport Analysis Flow

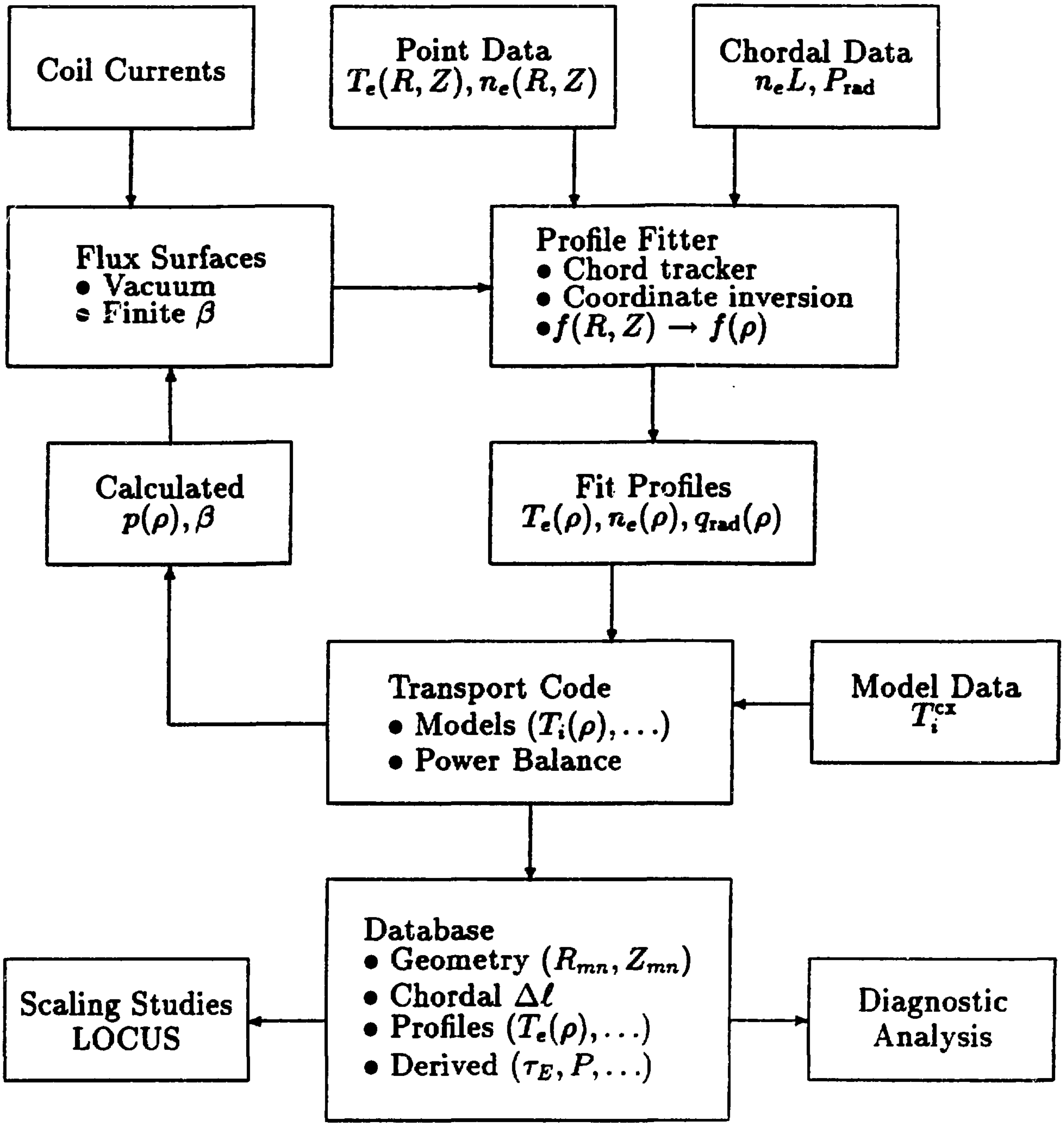

MAGNETIC REPRESENTATION

Flux surfaces are given by the inverse representation

$$R(\rho,\theta,\xi) = \sum_{m,n} R_{m,n}(\rho)\cos(m\theta - n\xi)$$
$$Z(\rho,\theta,\xi) = \sum_{m,n} Z_{m,n}(\rho)\sin(m\theta - n\xi)$$
$$\phi(\rho,\theta,\xi) = \xi$$

where the normalized radial coordinate ρ is specified by the enclosed toroidal flux Φ as

$$\rho = \sqrt{\Phi/\Phi_a}$$

The ATF geometry is adequately represented by 6–7 sets of (R_{mn}, Z_{mn}).

Two methods are used to determine the flux surface geometry:

- Field–line following for vacuum surfaces
- Free–boundary equilibrium (VMEC) for finite–beta

More description in talk by J. Harris Thursday morning.

For fast transport analysis, will use either:

- Functional representation $R_{mn}(\rho) = f(\Delta_v, \beta, \ldots)$ derived from results of above models.
- Large table lookup which interpolates between R_{mn}, Z_{mn} sets calculated with magnetics codes.

PROFILE FITTING

- Start with calculated geometry and a set of measurements (either point or chordal–array)
- Use assumed profile $X(\rho) = X_0(1-\rho^\alpha)^\beta$ or Gaussian
- Minimize total least–square difference between measured and calculated values to determine X_0, α, β
- Point measurements $X_{\mathrm{meas}}(R, Z)$
  - Use coordinate–invertor to find ρ for each (R, Z)
  - Minimize

$$\sum_{\mathrm{points}} \left(\frac{X_{\mathrm{meas}}(\rho) - X_{\mathrm{calc}}(\rho)}{\Delta X} \right)^2$$

  where ΔX may be $\langle X \rangle$ or experimental error
- Chordal measurments XL_{meas}
  - Use chord–tracker to find, for each chord,

$$XL_{\mathrm{calc}} = \int X(\rho)\, ds$$

  - Minimize

$$\sum_{\mathrm{chords}} \left(\frac{XL_{\mathrm{meas}} - XL_{\mathrm{calc}}}{\Delta XL} \right)^2$$

ATF TEST CASE

ORNL-DWG 86-2216 FED

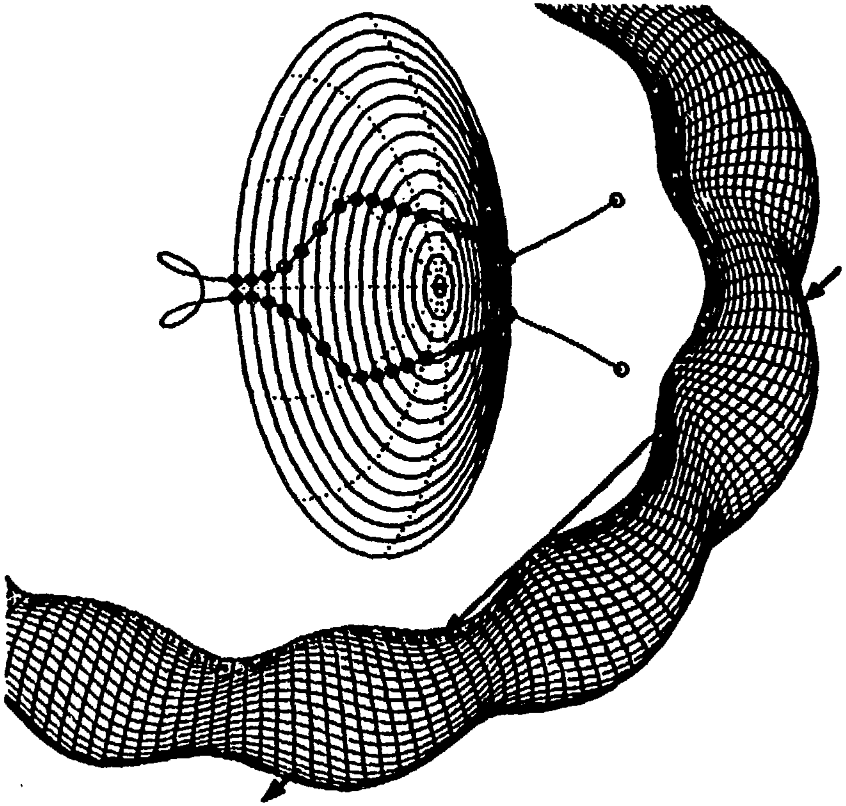

TRACK

HOULBERG & ATTENBERGER, ORNL

INPUT DATA

PLASMA GEOMETRY

MAJOR RADIUS	:	1.720 m
MINOR RADIUS	:	0.163 m
SCRAPE-OFF	:	0.000
ELONGATION	:	1.830
TRIANGUARITY	:	0.180
RADIAL NODES	:	16

RESULTS

SURFACES HIT	:	50
CHORD LENGTH	:	2.835 m

EXAMPLE OF POINT FIT

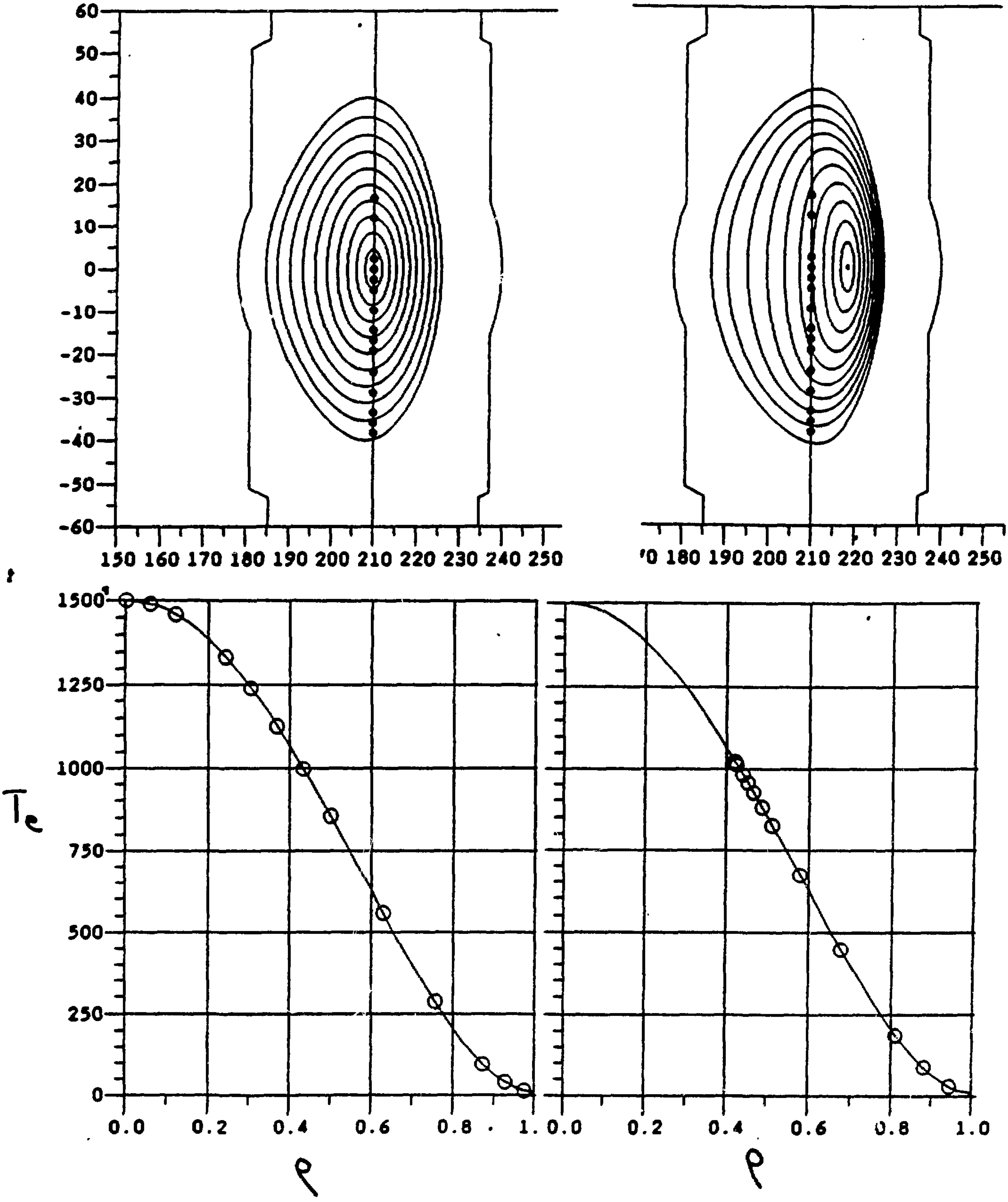

EFFECT OF GEOMETRY MISMATCH

- Simulated data generated with finite-beta surfaces
- Fit performed with vacuum surfaces
- Resulting T_e profile (solid line) is a poor fit to starting profile (dashed line)

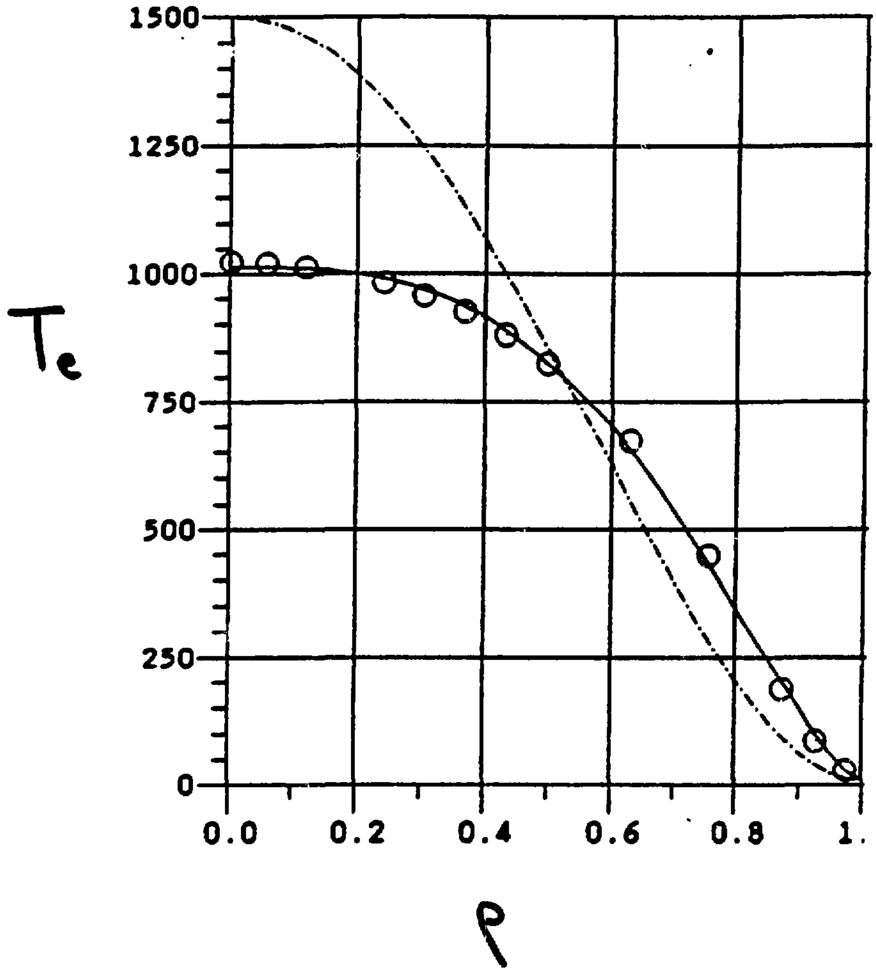

EXAMPLE OF CHORDAL FIT

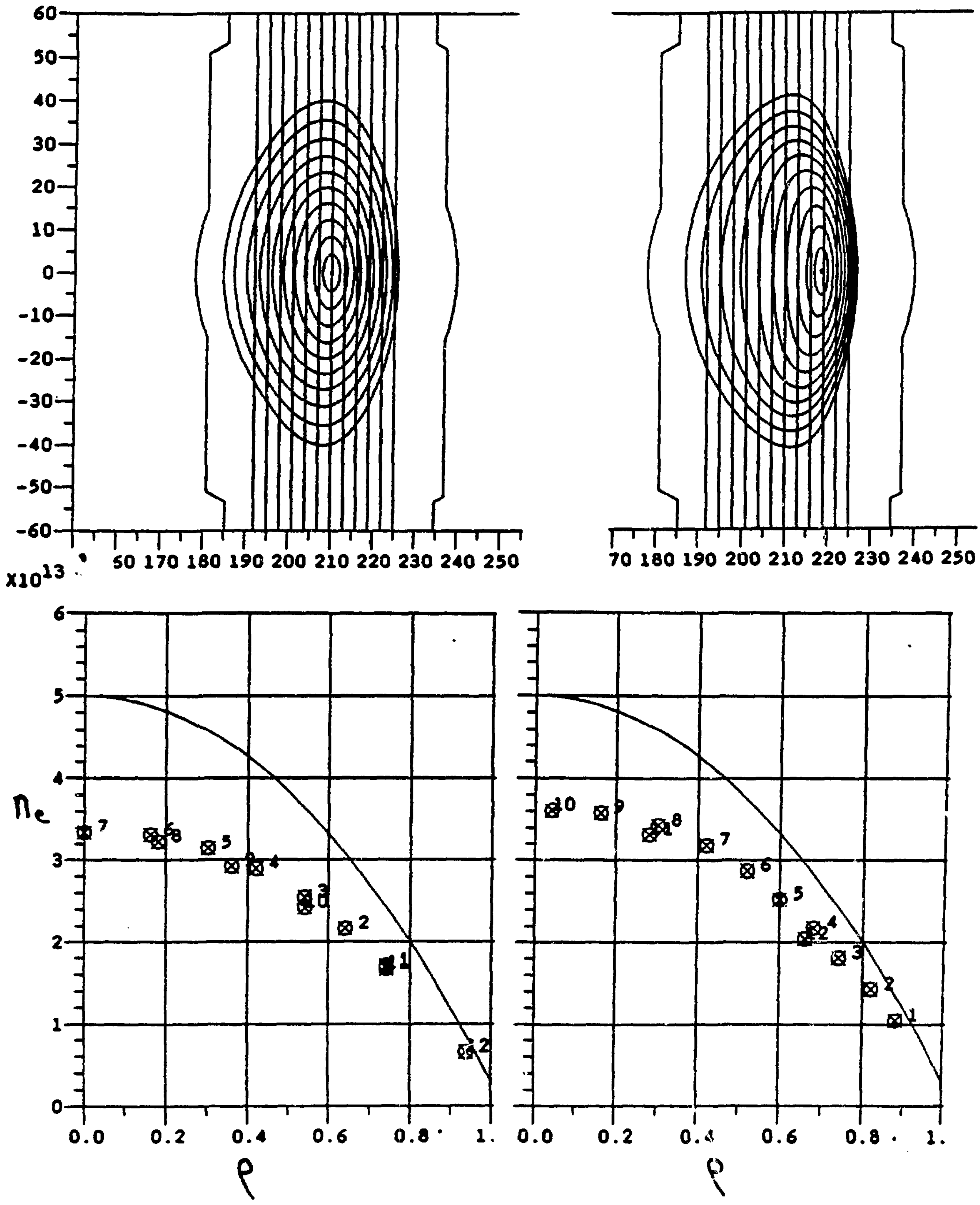

POWER BALANCE

Global parameters such as energy confinement time τ_E and β require an estimate of the total stored energy

$$\begin{aligned}
\tau_E(\rho) &= W(\rho)/P_{HEAT}(\rho) \\
W(\rho) &= \int_0^\rho (n_e(\rho')T_e(\rho') + n_i(\rho')T_i(\rho'))V'(\rho')\,d\rho' \\
P_{HEAT}(\rho) &= \int_0^\rho (q_{inj}(\rho') + q_{wave}(\rho'))V'(\rho')\,d\rho'
\end{aligned}$$

The volume integral is expressed as

$$\begin{aligned}
\int X\,dV &= \int_0^\rho X(\rho')V'(\rho')\,d\rho' \\
V'_\rho(\rho) &= \int_0^{2\pi} d\xi \int_0^{2\pi} d\theta\,\sqrt{g} \\
\sqrt{g} &= R\left(\frac{\partial R}{\partial \theta}\frac{\partial Z}{\partial \rho} - \frac{\partial R}{\partial \rho}\frac{\partial Z}{\partial \theta}\right)
\end{aligned}$$

which is particularly simple using the inverse representation

The electron profiles n_e and T_e are measured and an estimate of T_i may be obtained from the $\Longrightarrow$

ION–TEMPERATURE EQUATION

$$\frac{3}{2}n_T\frac{\partial T_i}{\partial t} = 3\frac{m_e}{m_p}\frac{n_e}{\tau_e}[Z](T_e - T_i) - \frac{1}{V'_\rho}\frac{\partial}{\partial \rho}\left(V'_\rho q_i\right)$$

$$- q_{cx}(\rho) + q^i_{inj}(\rho) + q^i_{ic}(\rho) - \frac{3}{2}T_i\frac{\partial n_T}{\partial t}$$

$$q_i = \sum_j \left(-\langle(\nabla\rho)^2\rangle_\psi n_{Hj}\chi_{Hj}\frac{\partial T_i}{\partial \rho} + q^{na}_{Hj} + \frac{5}{2}T_i\Gamma_{Hj}\right)$$

$$n_T = n_H + n_{He} + n_I$$

- Solve for $\partial T_i/\partial t = 0 \Rightarrow$ steady–state $T_i(\rho)$
- Feedback may be used to determine the M_χ for which $T_{cx} = T_i^{\mathrm{meas}}$ where T_i^{meas} is the experimentally–inferred T_i along some chord.
- Particle flux Γ_{Hj} balances ionization where total ionization rate is specified as N_H/τ_p^*; τ_p^* is assumed global particle confinement time.
- Volume–integrals of the terms in the T_i (and similar T_e) equation provide the experimental power balance estimate.

THERMAL–NEUTRAL TRANSPORT

- Slab model (SPUDNUT) $\Rightarrow s_{ion}, q_{cx}, n_0$
- Accurate for $\rho \geq 0.5$
- Two hydrogenic species
- Detailed energy/angle–dependent wall reflection
- Molecular dissociation and ionization

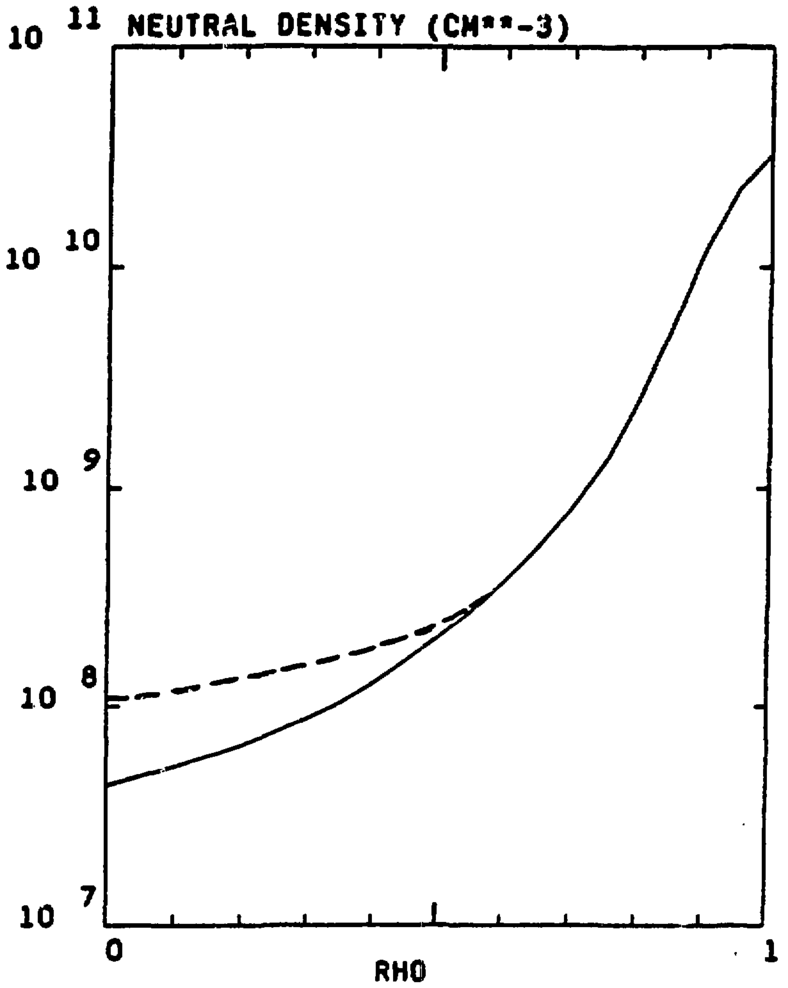

NEUTRAL–BEAM HEATING

$$q^i_{inj} = \frac{P_{inj}}{V_p} H(\rho) G_i$$

- Initial deposition $H(\rho)$ calculated for circularized, axisymmetric flux surfaces and diffuse beam
- Benchmark with Monte-Carlo deposition model (which uses real 3–D flux–surface geometry) shows good agreement
- Thermalization calculated with analytic moments of Fokker–Plank equation (G_e, G_i); orbits not included
- Comparison of G_e, G_i model with Monte–Carlo slowing-down code shows good agreement for tangential injection (ATF)
- Orbits broaden heating profile relative to G_e, G_i model for perpendicular injection (Heliotron–E)

COMPARISON OF CIRCULAR AND 3–D MONTE–CARLO FAST–NEUTRAL DEPOSITION

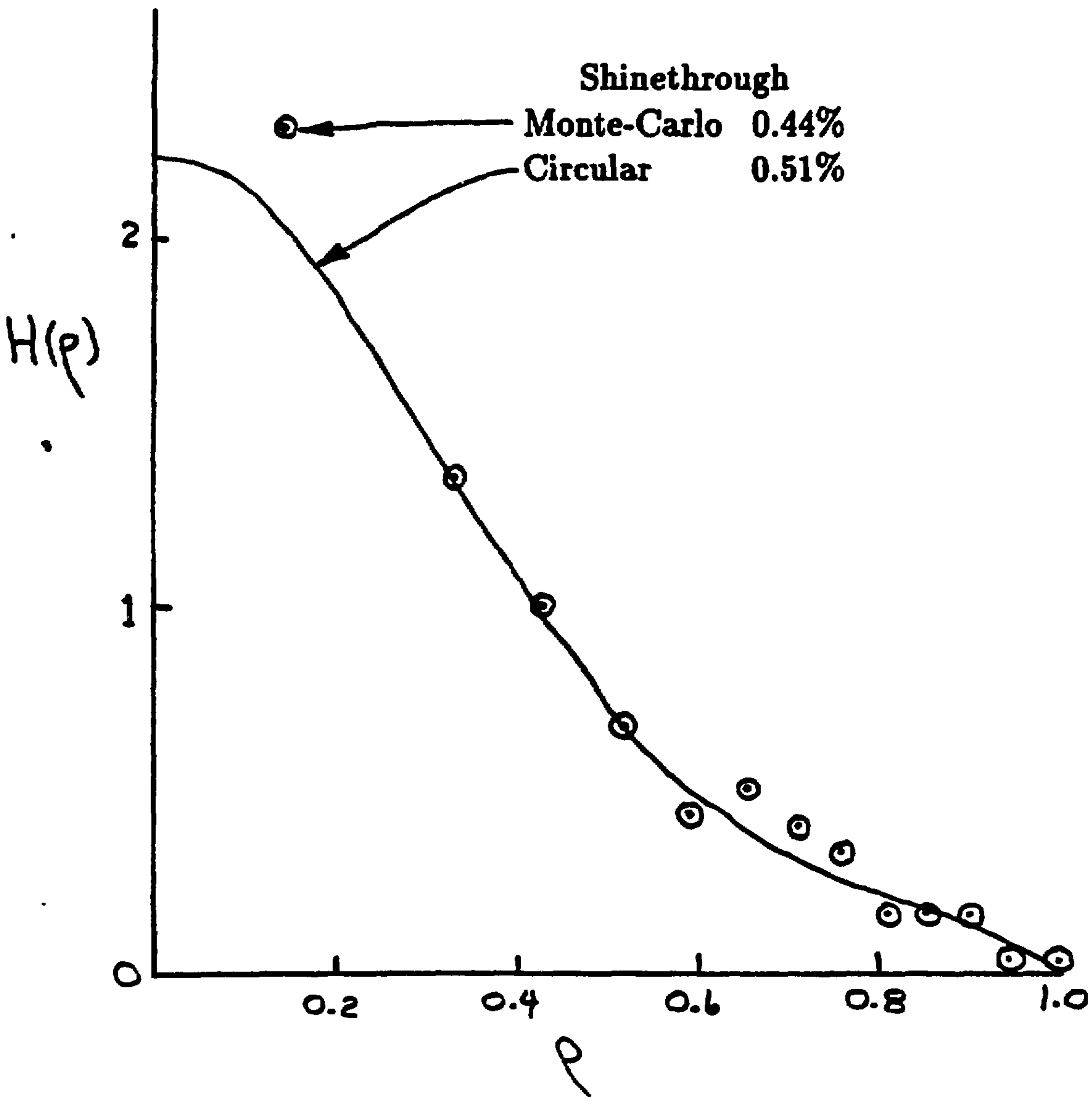

COMPARISON OF MOMENTS AND MONTE-CARLO THERMALIZATION FOR PARALLEL (ATF) INJECTION

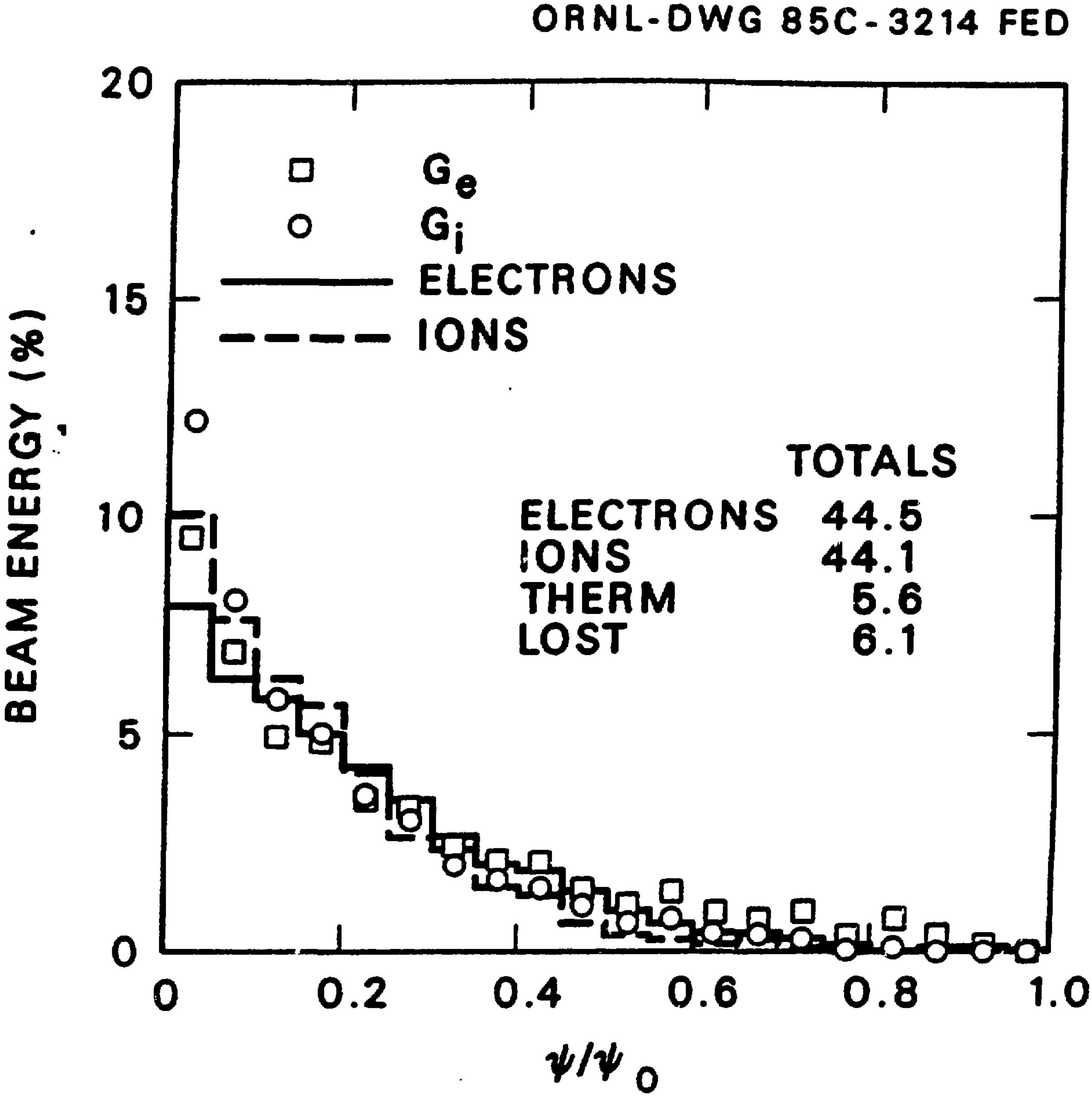

COMPARISON OF MOMENTS AND MONTE–CARLO THERMALIZATION FOR PERPENDICULAR (H–E) INJECTION

Finite–orbits broaden the energy deposition profile

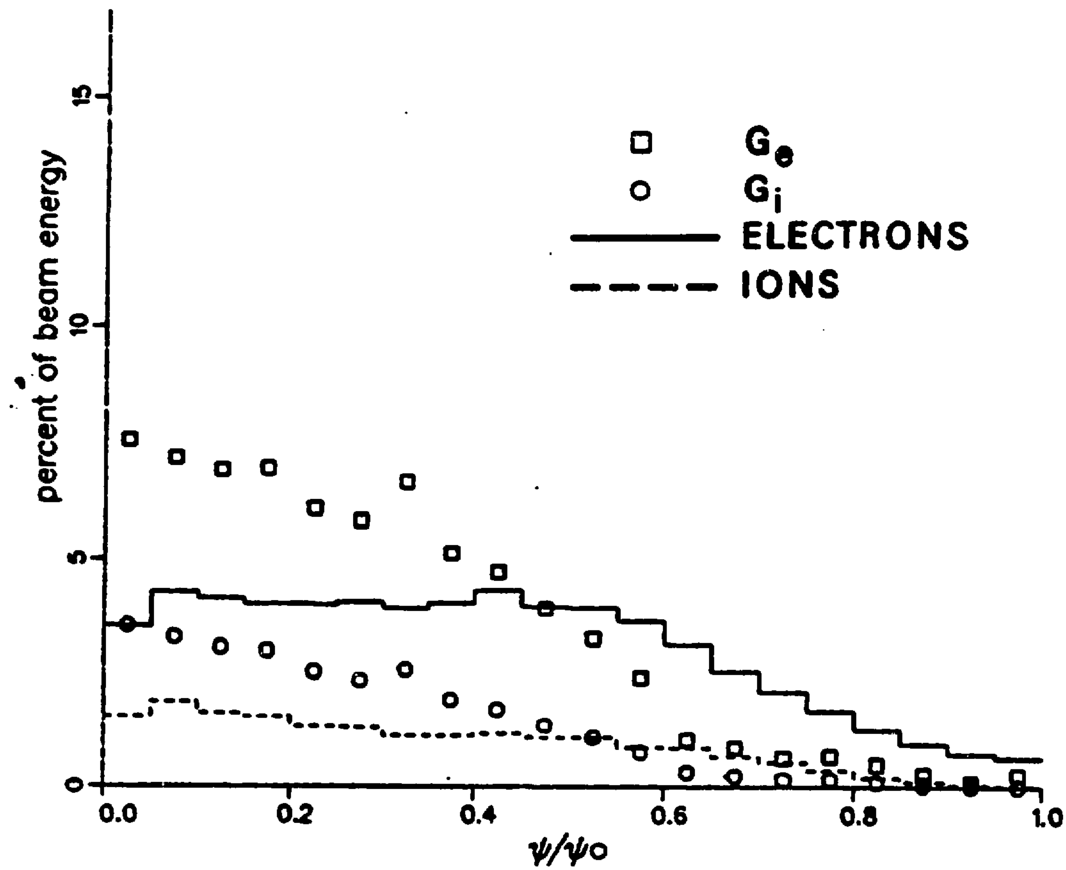

COMPARISON OF NEOCLASSICAL AND EXPERIMENTAL TRANSPORT

The non-ambipolar fluxes of particles Γ_a^{na} and heat q_a^{na} of plasma species a due to the helical ripple are given by Hastings, Houlberg, and Shaing, Nucl. Fus., 25 (1985):

$$\Gamma_a^{na} = -\epsilon_t^2 \sqrt{\epsilon_h}\, v_{d_a}^2 n_a \int_0^\infty dx\, x^{5/2} e^{-x} \frac{\tilde{\nu}_a(x) A_a(x)}{\omega_a^2(x)}$$

$$\left(q_a^{na} + \frac{5}{2}\Gamma_a^{na} T_a\right) = -\epsilon_t^2 \sqrt{\epsilon_h}\, v_{d_a}^2 n_a T_a \int_0^\infty dx\, x^{7/2} e^{-x} \frac{\tilde{\nu}_a(x) A_a(x)}{\omega_a^2(x)}$$

where

$$A_a(x) = \frac{1}{n_a}\frac{\partial n_a}{\partial \rho} + \frac{Z_a e}{T_a}\frac{\partial \Phi}{\partial \rho} + \left(x - \frac{3}{2}\right)\frac{1}{T_a}\frac{\partial T_a}{\partial \rho}$$

$$\tilde{\nu}_a(x) = \nu_a/(\epsilon_h x^{3/2}); \;\; x = \epsilon/T_a$$

$$\omega_a^2(x) = 3\tilde{\nu}_a^2(x) + (\epsilon_t/\epsilon_h)\left\{1.67\,(\omega_E + \omega_{B_a})^2 + \left(\frac{\epsilon_t}{\epsilon_h}\right)^{1/2}\left[\frac{(\omega_{B_a})^2}{4} + 0.6\,|\omega_{B_a}|\,\tilde{\nu}_a\left(\frac{\epsilon_h}{\epsilon_t}\right)^{3/2}\right]\right\}$$

$$\omega_E = \frac{1}{r_s \rho B}\frac{\partial \Phi}{\partial r_\rho}; \;\; \omega_{B_a} = -v_{d_a}\frac{\partial \epsilon_h}{\partial r_\rho} x$$

$$v_{d_a} = \frac{T_a}{Z_a e B \rho r_s}$$

- The radial electric field ($\partial\Phi/\partial\rho$) is specified arbitrarily.
- Helical ripple estimated by Fourier decomposition of magnetic representation (single–helicity approximation)
- Fluxes calculated using experimental and derived plasma profiles are compared with corresponding experimental estimates to determine level of agreement with neoclassical transport rates.

Simulation of Neutral Beam Heating and Transport of CHS

T. Amano, K.Matsuoka and T.S. Chen*
Institute of Plasma Physics,
Nagoya University, Nagoya, JAPAN

The CHS (Compact Helical System) is an l=2,m=8 low aspect ratio helical device whih will come to operation in April 1988. To evaluate the efficacy of neutral beam heating in such a low aspect ratio helical device in which a rather wide velocity space loss cone is expected, a Monte Carlo orbit code which calculates orbits and slowing down and pitch angle scattering of the fast ions. The charge exchange loss and reabsorption are included in the code. It is shown aboout 30 to 40 % of the injected beam energy is lost by the orbit and charge exchange losses. If the reabsorption process is not taken into account, the loss rate is a little higher.

A series of transport calculations of the CHS plasma has been carried out in order to predict the range of expected confinement time, electron and ion temperature etc., in the presence of 2 Mw level neutral beam injection. As for the neoclassical (ripple) transport coefficients, Oak Ridge groups' new scaling coefficients have been used.The multi-helicity helical field effect on the transport coefficients in the $1/\nu$ regime has been considerd. A comparison between the new and old scaling of the neoclassical transpotrt coefficients is made. Degradation of confinement with the increase of the beam power, a transition to the electron root ambipolar potential are discussed.

* on leave of absence from Institute of plasma physics,Hefei,China

SIMULATION OF NEUTRAL BEAM HEATING AND TRANSPORT OF CHS

T. AMANO, K. MATSUOKA

and T. S. CHEN *

INSTITUTE OF PLASMA PHYSICS

NAGOYA UNIVERSITY

NAGOYA, JAPAN

*INSTITUTE OF PLASMA PHISICS

HEFEI, CHINA

I. MONTE CARLO SIMULATION OF NBH

II. TRANSPORT SIMULATION

NEOCLASSICAL TRANSPORT COEEFICIENTS

NBH

III. SUMMARY

CHS (Compact Helical System) at IPPJ

$l=2$, $m=8$

$R=1m$, $a=0.2m$

$B=1.5T$

$\alpha^*=0.3$, $\Delta=-0.05m$

$\iota_0=0.3$, $\iota_a=1.0$

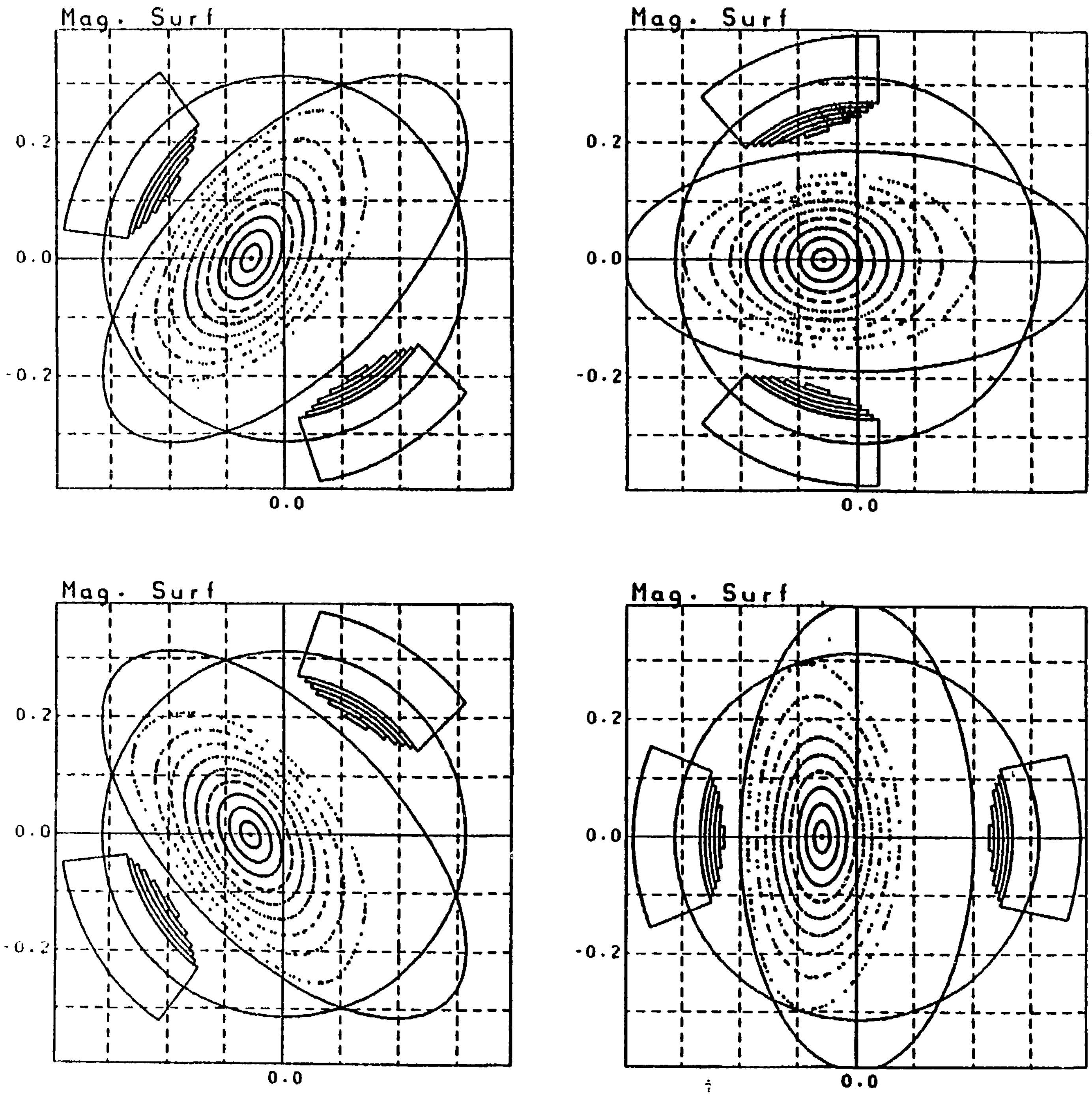

Mag. Surf
0.2
0.0
-0.2
0.0
Mag. Surf
0.2
0.0
-0.2
0.0
Mag. Surf
0.2
0.0
-0.2
0.0
Mag. Surf
0.2
0.0
-0.2
0.0

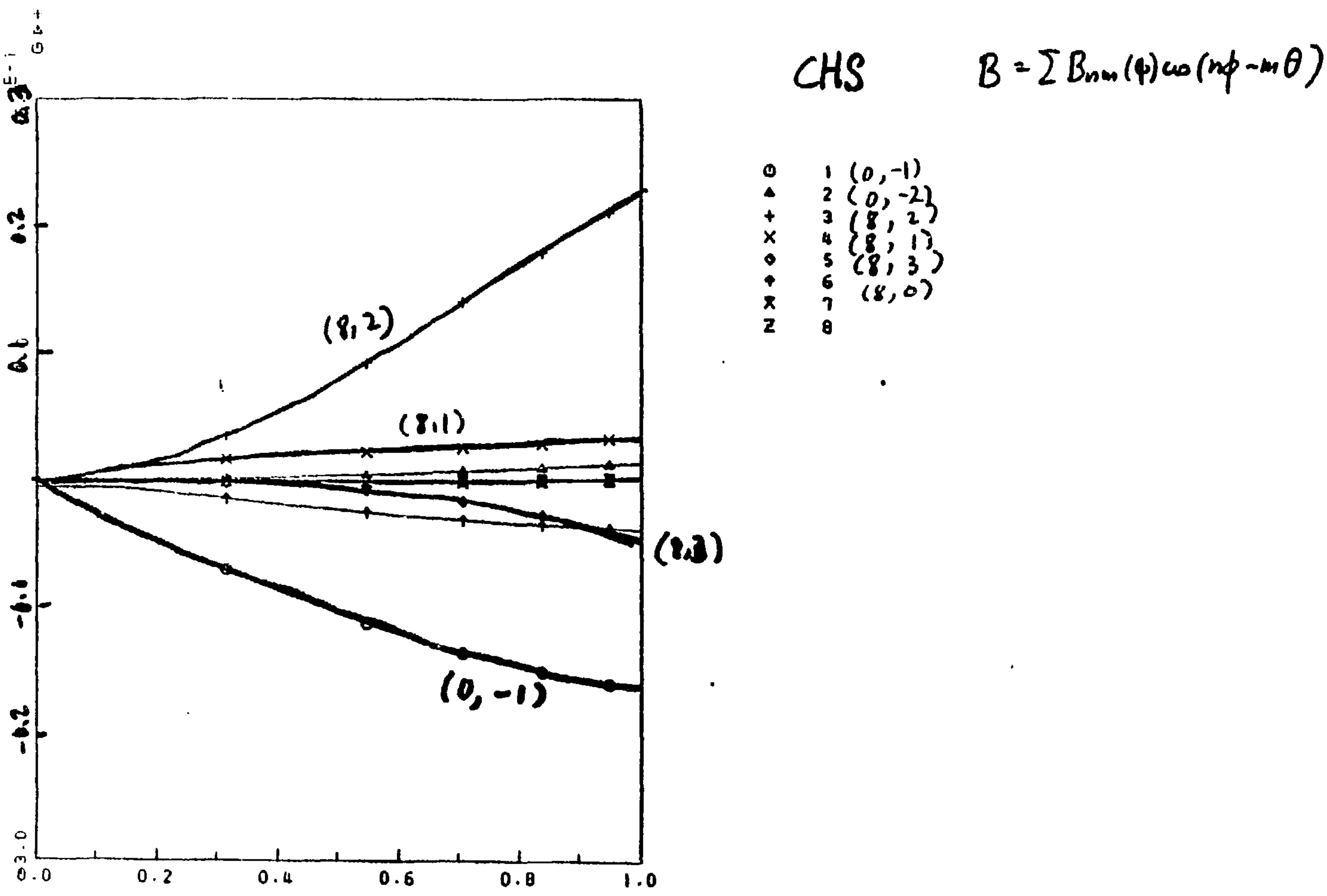

CHS
$B = \sum B_{nm}(\psi) \cos(n\phi - m\theta)$
1 (0, -1)
2 (0, -2)
3 (8, 2)
4 (8, 1)
5 (8, 3)
6 (8, 0)
7
8
(8, 2)
(8, 1)
(8, 3)
(0, -1)
0.0
0.2
0.4
0.6
0.8
1.0
E-1
-0.1
-0.2
0.1
0.2

MONTE CARLO SIMULATION

OF NEUTRAL BEAM HEATING

1. NEUTRAL BEAM INJECTION : FREYA

   FAST ION BIRTH

2. ORBIT : BOOZER HAMILTONIAN FORMULATION

3. SLOWING DOWN : MONTE-CARLO

   PITCH ANGLE SCATTERING

4. CHARGE EXCHANGE LOSS OF FAST IONS

5. RE-IONIZATION OF FAST NEUTRALS

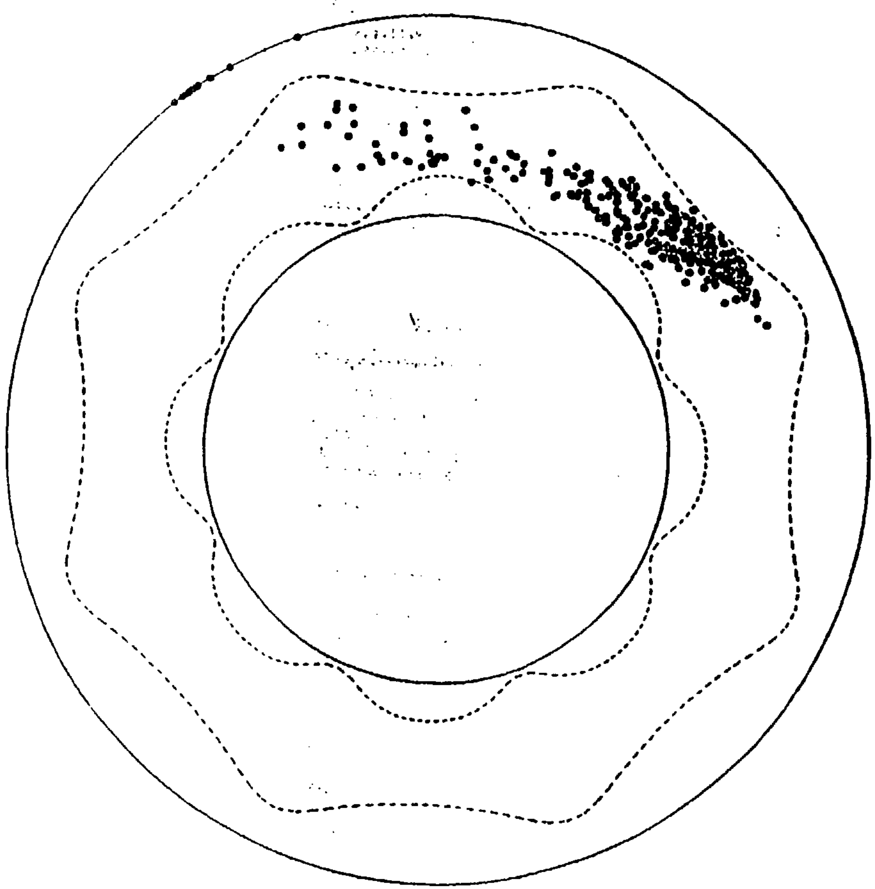

40KeV
beam

JOBNO = 200

MB = 1.0 E = 40.0 KEV
ANG = 40.00
Bo = 1.59 T
NEO = 1.00E14
TEO = 1.00 KEV
Ro = 0.9 M

--BOUNCE AVERAGED
—BIRTH DEPOSITION

TOTAL PARTICLES = 160
APERTURE LOSS = 3
MISSED CHAMBER = 0
PASSED THROUGH = 2
ORBIT LOSS = 23
DEPOSITED = 132
PCT LOST 17.5

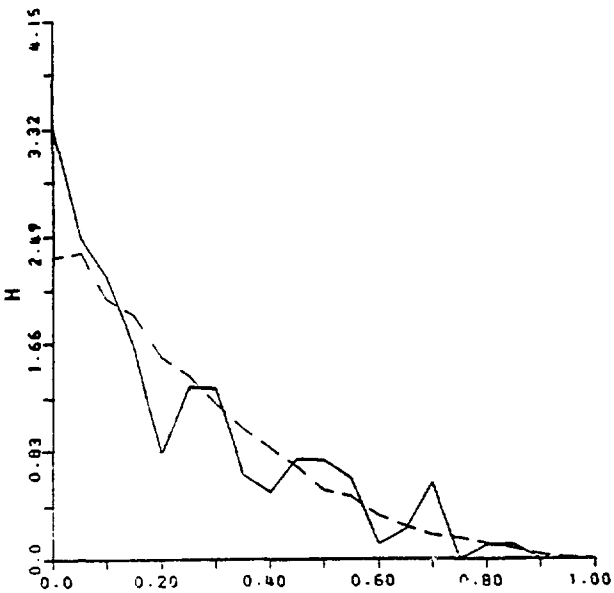

87-10-27

$$\left.\frac{\partial f}{\partial t}\right|_c = \frac{1}{\tau_s v^2}\frac{\partial}{\partial v}(v^3 + v_c^3) f + \frac{1}{\tau_s v^2}\frac{\partial}{\partial v}\left(\frac{v^2 T_e}{m_b} + \frac{v_c^3 T_I}{m_b v}\right)\frac{\partial f}{\partial v}$$

$$+ \frac{\nu_{ii}}{2}\frac{\partial}{\partial \zeta}(1-\zeta^2)\frac{\partial}{\partial \zeta} f,$$

$$\tau_s = \frac{6.32 \times 10^8 A_b T_e^{3/2}\,(\mathrm{eV})}{n_e Z_b^2 \ln \Lambda_e}, \qquad \nu_{ii} = \frac{\langle Z \rangle \bar{A}_I v_c^3}{\tau_s [Z] A_b v^3},$$

$$v_c^3 = 1.51 \times 10^{20}\, T_e^{3/2}(\mathrm{eV})\, [Z]/\bar{A}_I,$$

$$\langle Z \rangle = \frac{\sum_I n_I Z_I^2 \ln \Lambda_I}{n_e \ln \Lambda_e}, \qquad \frac{[Z]}{\bar{A}_I} = \frac{\sum_I n_I Z_I^2 \ln \Lambda_I / A_I}{n_e \ln \Lambda_e},$$

$$\zeta = v_{\parallel}/v.$$

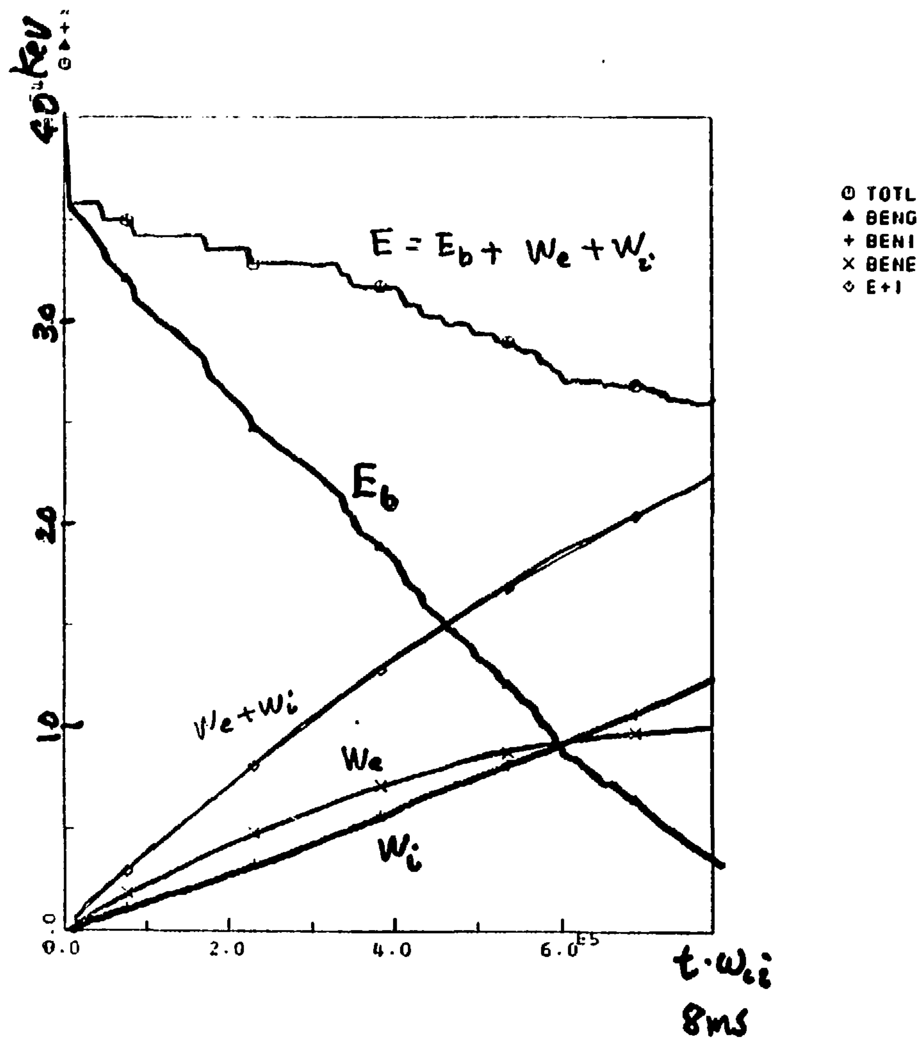

50 particles

$n_e = 5\times10^{13}(1-\psi)+10^{13}$

$T_e = 1.5\times10^{13}(1-\psi)+100$

$T_i = 10^3(1-\psi)+100$

$Z_{eff} = 2$

$B = 1.5T$

$\Phi = -2\times10^3(1-\psi)$

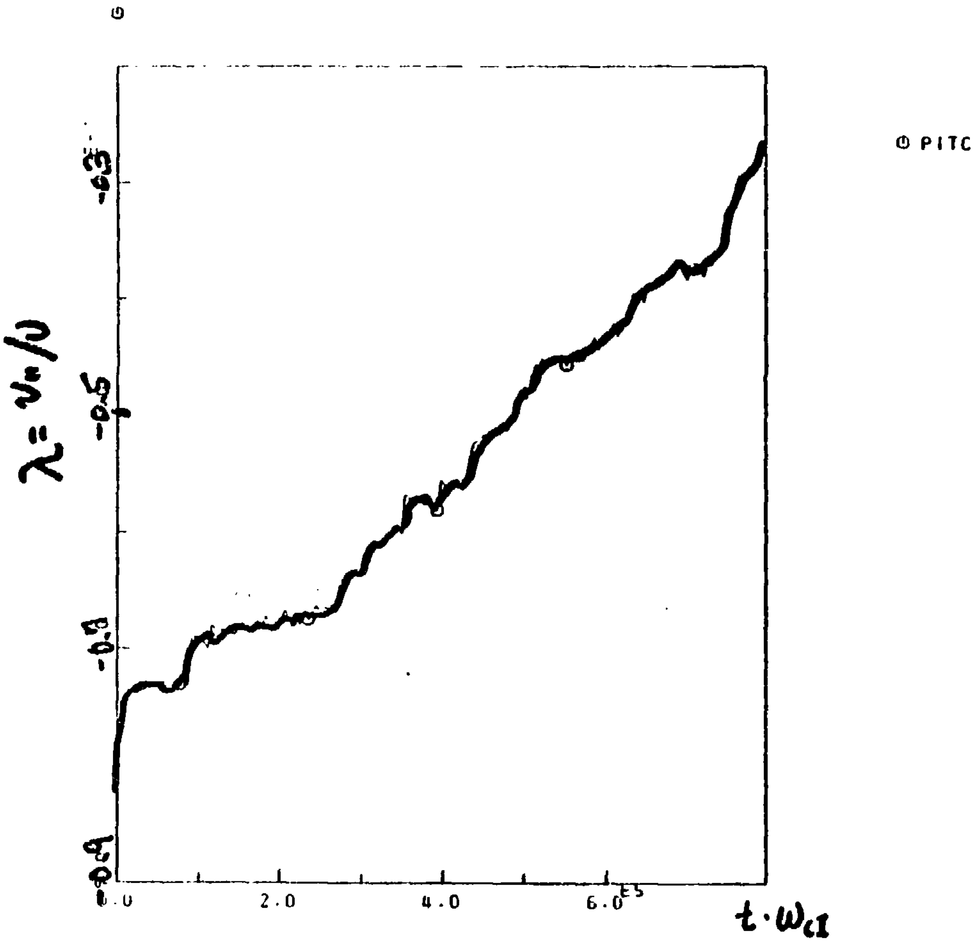
λ= v∥/v
-0.3
-0.5
-0.7
-0.9
0.0
2.0
4.0
6.0
E5
t·ωci
ⓘ PITC

BEAM ENERGY	40000.00 (	0.998)
ABSORBED BY E	9543.04 (	0.239)
ABSORBED BY I	11159.10 (	0.279)
BEAM COMP.	3035.60 (	0.076)
MISSED	1632.65 (	0.041)
ORBIT LOSS	14532.73 (	0.363)
FRACTION LOST	0.40	
C.X loss	?	

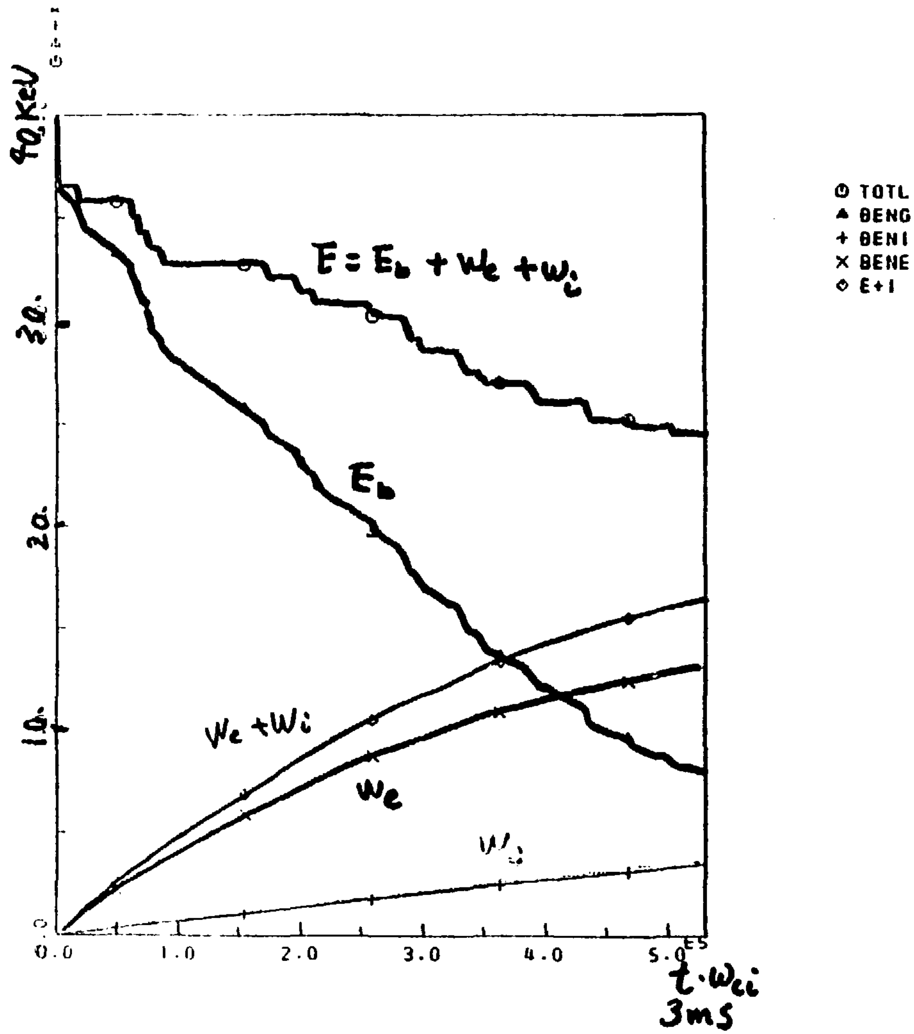

40 KeV

50 particles

$n_e = 5\times10^{13}(1-\psi)+5\times10^{12}$

$T_e = 10^3(1-\psi)+100$

$T_i = 10^3(1-\psi)+100$

$B = 1.5\,T$

$Z_{eff} = 1$

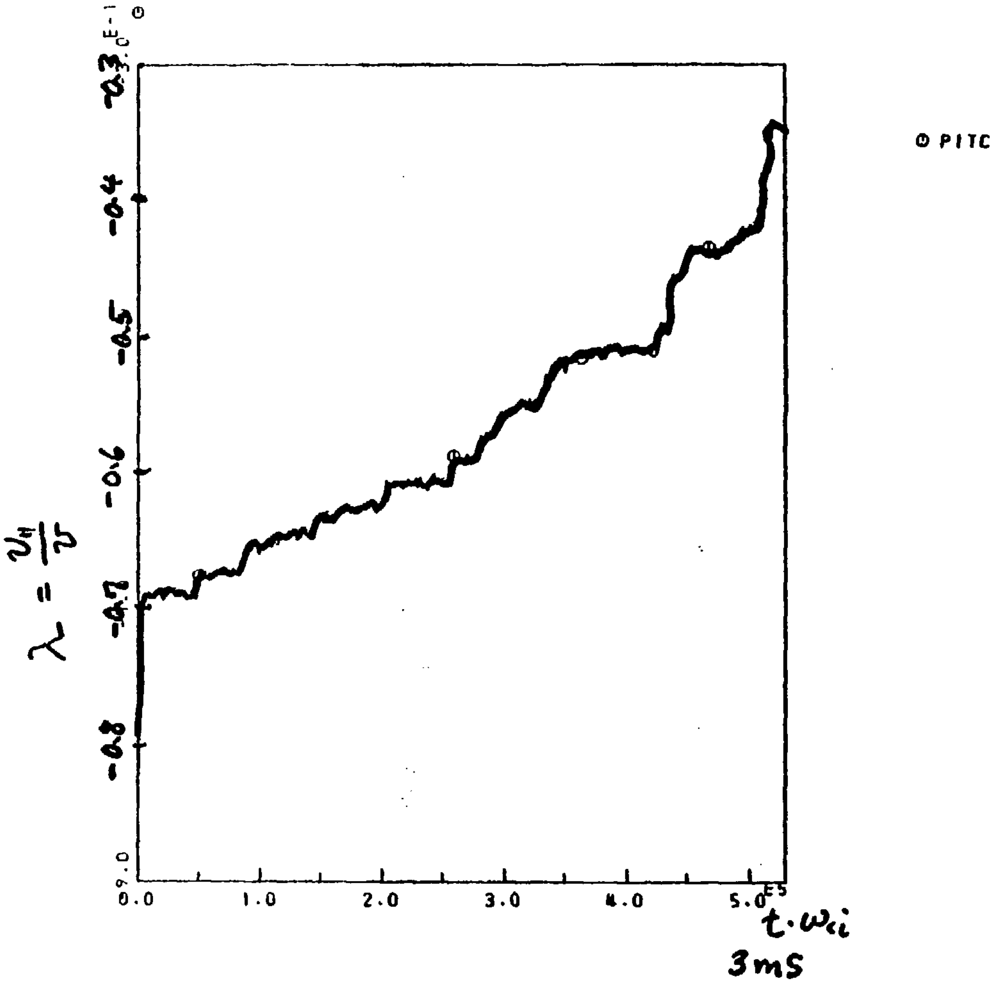

$\lambda = \frac{v_\parallel}{v}$
-0.3
-0.4
-0.5
-0.6
-0.7
-0.8
E-1
0.0
1.0
2.0
3.0
4.0
5.0
E5
$t \cdot \omega_{ci}$
3mS
⊙ PITC

deposition Profile

$\int H d\psi = 1$

40 KeV

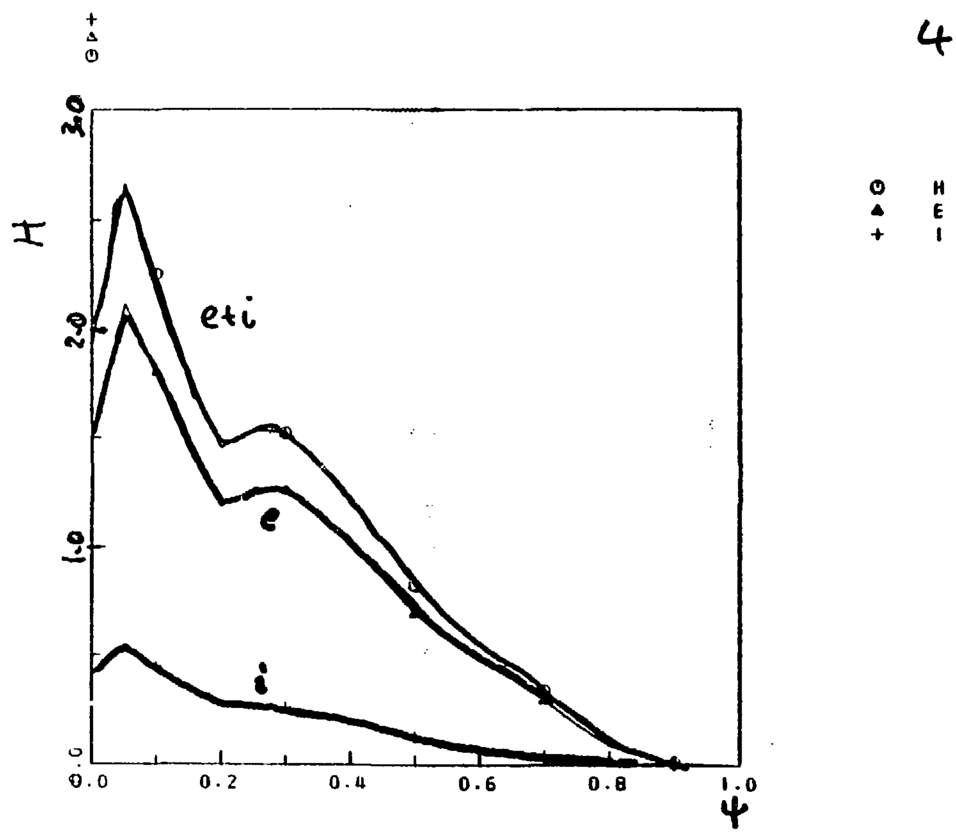

without re-absorption

BEAM ENERGY	40000.00 (	0.998)
ABSORBED BY E	12570.17 (	0.314)
ABSORBED BY I	3315.48 (	0.083)
BEAM COMP.	7553.92 (	0.189)
MISSED	1632.65 (	0.041)
ORBIT LOSS	7280.68 (	0.182)
CX LOSS	7581.81 (	0.190)
FRACTION LOST	0.41	

neutrals

$n_{ow} = 1.1 \times 10^{10}$

$n_{oc} = 9 \times 10^{8}$

with re-absorption

BEAM ENERGY	40000.00 (	0.970)
ABSORBED BY E	13061.92 (	0.327)
ABSORBED BY I	3567.01 (	0.089)
BEAM COMP.	9174.09 (	0.229)
MISSED	816.33 (	0.020)
ORBIT LOSS	9282.34 (	0.232)
CX LOSS	2911.21 (	0.073)
FRACTION LOST	0.33	

without reabsorption

BEAM ENERGY	20000.00 (	1.050)
ABSORBED BY E	3899.78 (	0.195)
ABSORBED BY I	6311.30 (	0.316)
BEAM COMP.	3100.66 (	0.155)
MISSED	0.00 (	0.000)
ORBIT LOSS	5144.18 (	0.257)
CX LOSS	2549.27 (	0.127)
FRACTION LOST	0.38	
no. charge exchange	0.29	

with reabsorption

BEAM ENERGY	20000.00 (	1.076)
ABSORBED BY E	4046.94 (	0.202)
ABSORBED BY I	6328.27 (	0.316)
BEAM COMP.	3783.02 (	0.189)
MISSED	759.49 (	0.038)
ORBIT LOSS	5718.84 (	0.286)
CX LOSS	879.31 (	0.044)
FRACTION LOST	0.37	

neutrals

$n_{ow} = 2\times10^{10}$

$n_{oc} = 6\times10^{8}$

SUMMARY I (NEUTRAL BEAM HEATING)

1. 30 ~ 40 % BEAM ENERGY LOSSES DUE TO ORBIT LOSS AND C.X.

2. C.X LOSS DOES NOT SEEM SIMPLY ADD UP TO THE ORBIT LOSS

3. ABOUT ONE HALF OF CHARGE EXCHANGED FAST NEUTRALS ARE REABSORBED

4. NEEDS MORE STUDY

   a) BETTER STATISTICS LARGER NUMBER OF TEST PARTICLES
   b) STEADY ATATE SIMULATION
   c) NEUTRAL PARTICLE DISTRBUTION
   d) COMBINE TO TRANSPORT CALCULATION (LIKE " TRANSP ")

TRANSPORT SIMULATION OF CHS PLASMAS

I. TRANSPORT COEFFICIENTS

1. SHAING : Phys. Fluids. 27, 1567(1984)

   A NEW GEOMETRICAL SCALING (DKES)

   $D \sim \varepsilon_h^{1.5}$ rather then $\varepsilon_t\varepsilon_h^{0.5}$ as $\nu \sim 0$

2. In the $1/\nu$ regime, multi helicity effects may be important

   Form factor $S = F_w/F_s$

3. Anomalous transport INTOR type

   also to add edge localized χ.

II. AMBIPOLAR POTENTIAL

$$\partial E_r/\partial t = -e(_r\Gamma_i - \Gamma_e)' + D_E\, \partial^2 E_r/\partial r^2$$

III. NEUTRALS : AURORA

HALO NEUTRALS ARE INCLUDED.

IV. NBH

FREYA + FIFPC

CX.LOSS : $-f/\tau_{cx}$

$$\Gamma_a^{na} = -\epsilon_t^2 \sqrt{\epsilon_h}\, v_{d_a}^2 n_a \int_0^\infty dx\, x^{5/2} e^{-x}\, \tilde{\nu}_a(x)\, \frac{A_a(x)}{\omega_a^2(x)}$$

where

$$A_a(x) = \frac{1}{n_a}\frac{\partial n_a}{\partial \rho} + \frac{Z_a e}{T_a}\frac{\partial \Phi}{\partial \rho} + \left(x - \frac{3}{2}\right)\frac{\partial T_a}{\partial \rho}\frac{1}{T_a}$$

$$\tilde{\nu}_a(x) = \frac{\nu_{th_a}}{\epsilon_h\, x^{3/2}}$$

$$x = \frac{\epsilon}{T_a}$$

$$\omega_a^2(x) = 3\tilde{\nu}_a^2(x) + (\epsilon_t/\epsilon_h)\Bigg[1.67\,(\omega_E + \omega_{B_a})^2$$
$$+\left(\frac{\epsilon_t}{\epsilon_h}\right)^{1/2}\left[\frac{(\omega_{B_a})^2}{4} + 0.6\,|\omega_{B_a}|\,\tilde{\nu}_a\left(\frac{\epsilon_h}{\epsilon_t}\right)^{3/2}\right]\Bigg]$$

$$\omega_E = \frac{1}{\rho B}\frac{\partial \Phi}{\partial \rho}$$

$$\omega_{B_a} = -\frac{T_a}{Z_a e B \rho}\frac{\partial \epsilon_h}{\partial \rho}\, x$$

$$v_{d_a} = -\frac{T_a}{Z_a e B\, \rho}$$

New Scaling

$$\omega_a^2(x) = 3\tilde{\nu}_a^2(x)/(F_m/F_s) + 1.5(\epsilon_t/\epsilon_h)^{1/2}\, \omega_E^2$$

F_m : multi-helicity form factor in $1/\nu$ regime

F_s : single helicity form factor

$$\Gamma = -\frac{4}{\pi}\frac{1}{M^{7/2}\Omega^2 r^2}\int_0^\infty dW \frac{W^{5/2}}{\nu}\frac{\partial f_M}{\partial r}$$

$$F = \boxed{\times\left\{\int_0^{2\pi} d\theta\, \epsilon_H^{3/2}\left[G_1\left(\frac{\partial \epsilon_T}{\partial \theta}\right)^2 - 2G_2\frac{\partial \epsilon_T}{\partial \theta}\frac{\partial \epsilon_H}{\partial \theta} + G_3\left(\frac{\partial \epsilon_H}{\partial \theta}\right)^2\right]\right\},}$$

where

$$G_1 = \int_0^1 dk^2 \frac{\int_0^{k^2} d(k^2)' K^2}{E-(1-k^2)K} = \frac{16}{9},$$

$$G_2 = \int_0^1 dk^2 \frac{\int_0^{k^2} d(k^2)' K^2 \int_0^{k^2} d(k^2)' (2E-K)}{E-(1-k^2)K} = \frac{16}{15},$$

$$G_3 = \int_0^1 dk^2 \frac{\int_0^{k^2} d(k^2)'(2E-K)^2}{E-(1-k^2)K} = 0.684.$$

Intor X 0.5

no ripple

JOB = 3000

RMAJC (CM)	94.14
RLIMC (CM)	12.38
RWALC (CM)	12.38
BZO (G)	1.50E+04
NEAV	5.00E+13
ELIP	2.17
LSER	1
NRIPLE	1
LCORR	T
HRIA	0.00E+00
DALPHE	1.00E+17
DBETAE	2.50E+17
DBETAI	1.00E+00
CDRIFT	0.00E+00
ETATH	2.00E+00

~~PNBI (MW)~~	~~2.00E+00~~
ANGLE3	4.00E+01
CLBCX	5.00E-01
PRFMW (MW)	0.00E+00
PECH (MW)	1.00E-01

TIME= 1.00E-01 JOB 3000

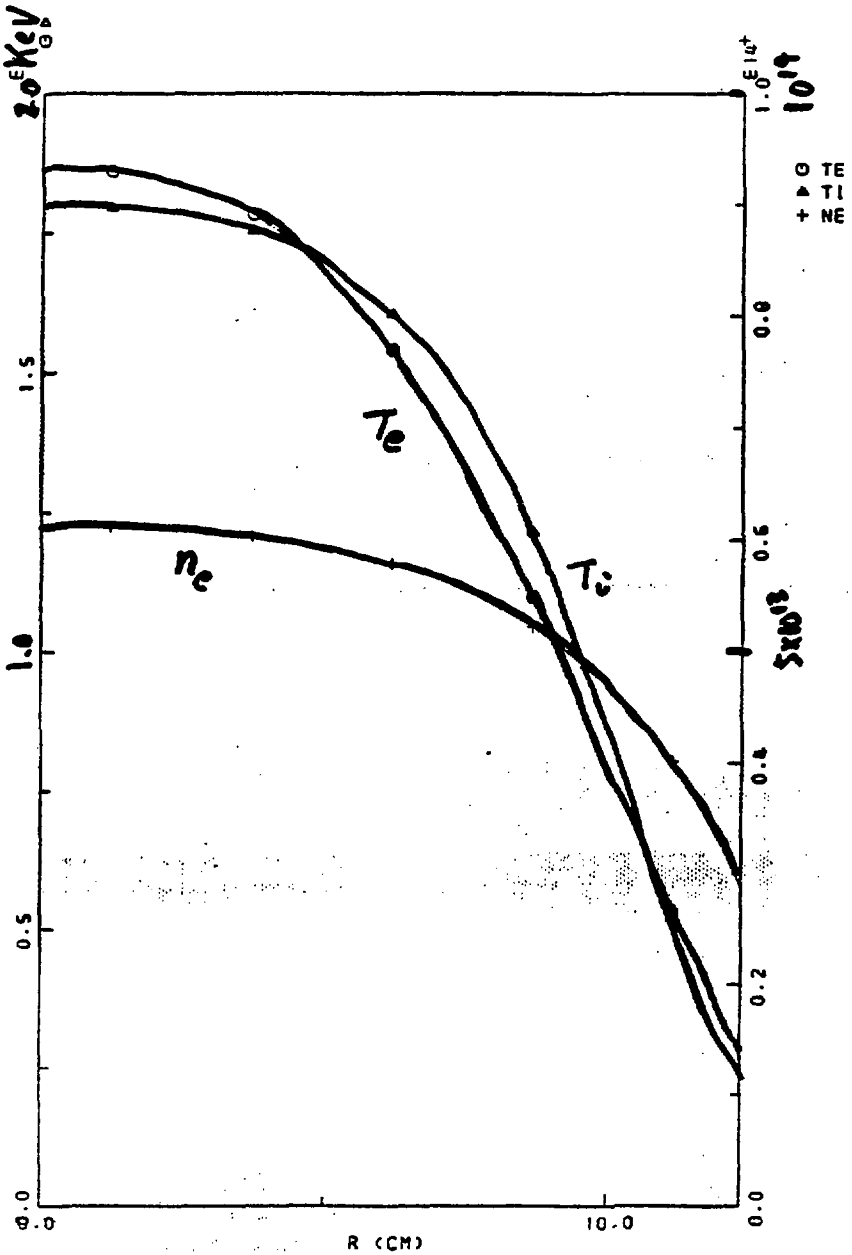

Intor x05
+ ripple

JOB - 3101

RMAJC (CM)	94.14	PNBI (MW)	2.00E+00
RLIMC (CM)	12.38	ANGLE3	4.00E+01
RWALC (CM)	12.38	CLBCX	5.00E-01
BZO (G)	1.50E+04	PRFMW (MW)	0.00E+00
NEAV	5.00E+13	PECH (MW)	1.00E-01
ELIP	2.17		
LSER	0		
NRIPLE	1		
LCORR	T		
HRIA	1.00E+00		
DALPHE	1.00E+17		
DBETAE	2.50E+17		
DBETAI	1.00E+00		
CDRIFT	0.00E+00		
ETATH	2.00E+00		

TIME= 1.00E-01 JOB 3101

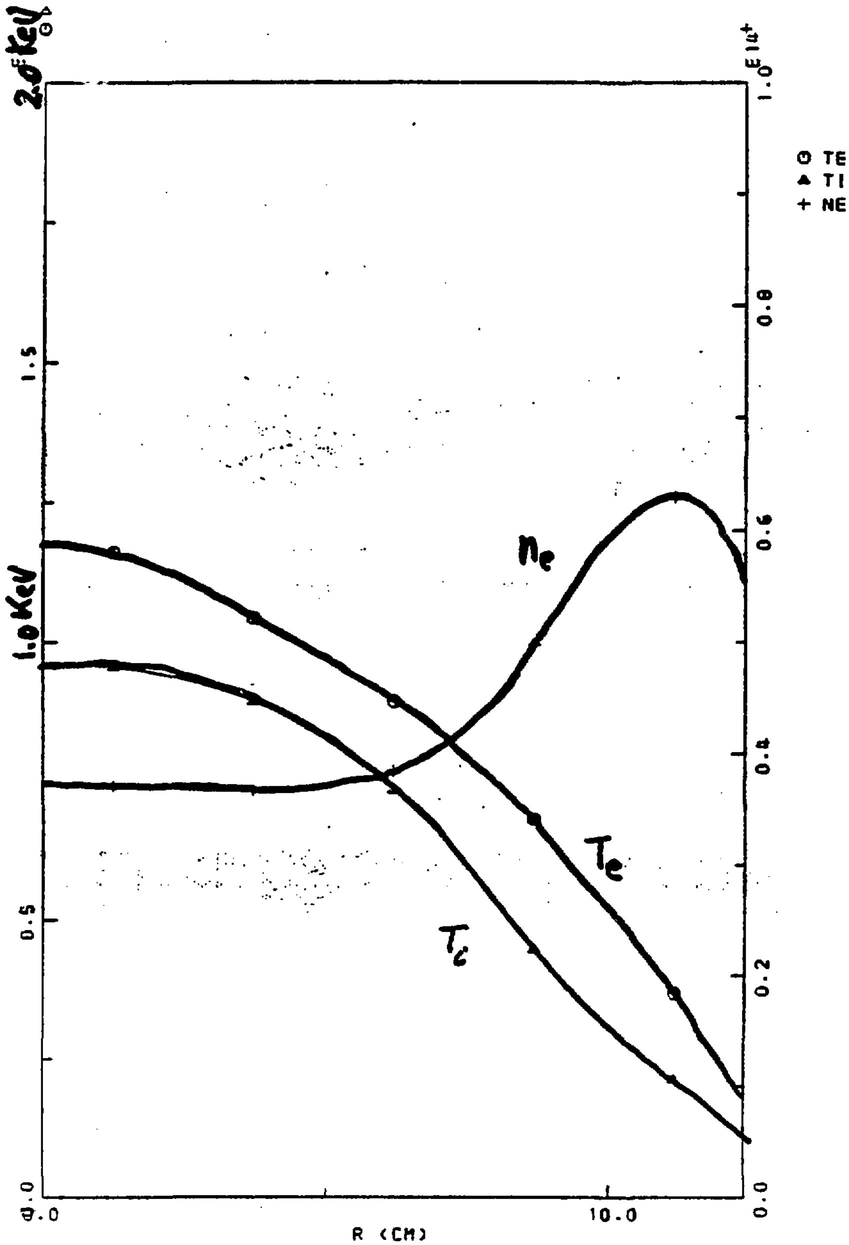

< JOB - 3101 >

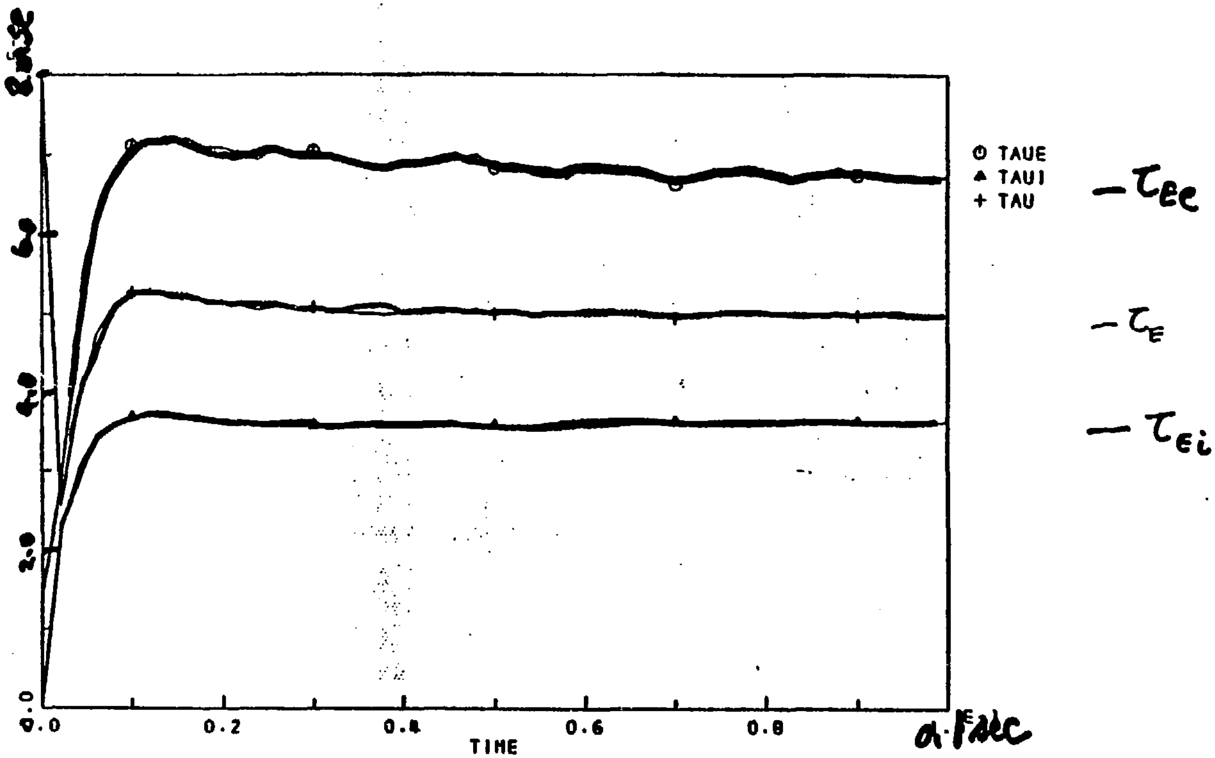

< JOB - 3101 >

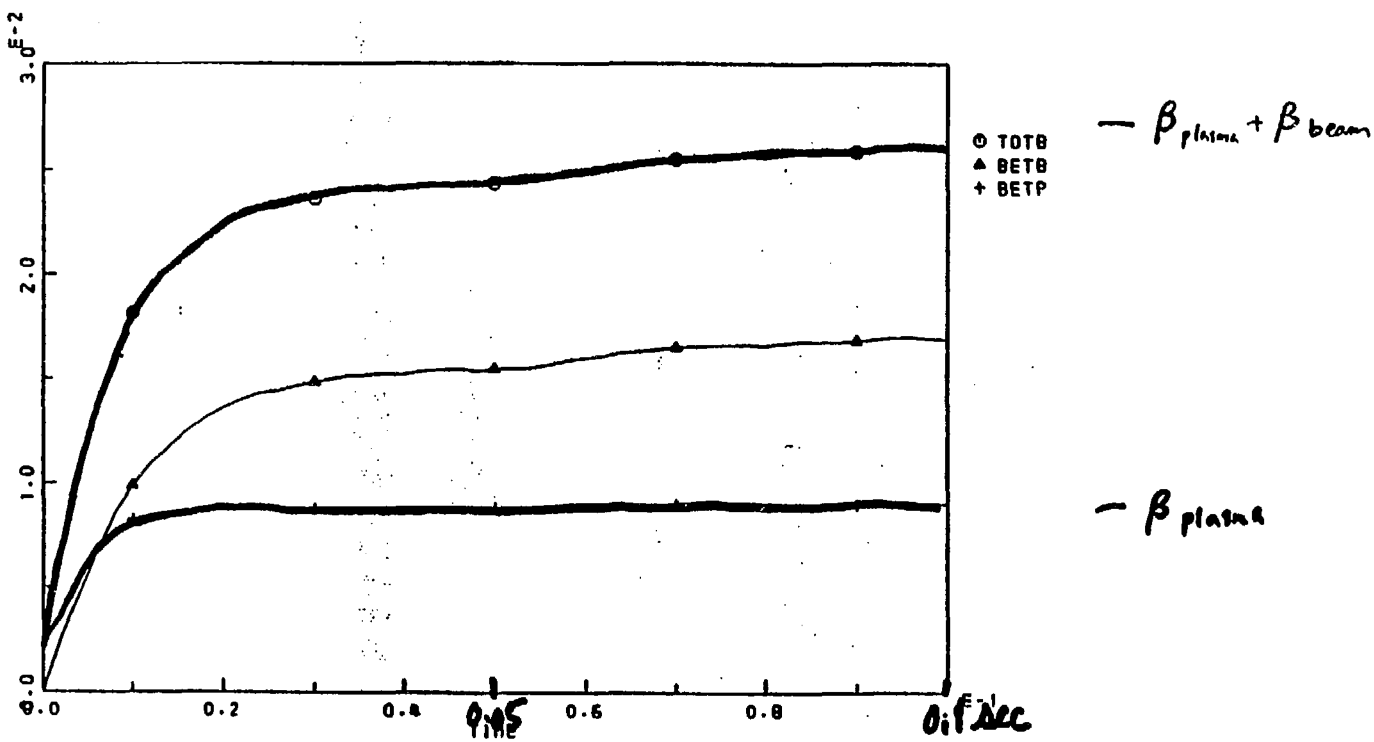
3.0 E-2
2.0
1.0
0.0
0.0
0.2
0.4
0.6
0.8
0.05
0.1 sec
E-1
TIME
⊙ TOTB
▲ BETB
+ BETP
— β plasma + β beam
— β plasma

TIME= 8.00E-02 JOB 3101

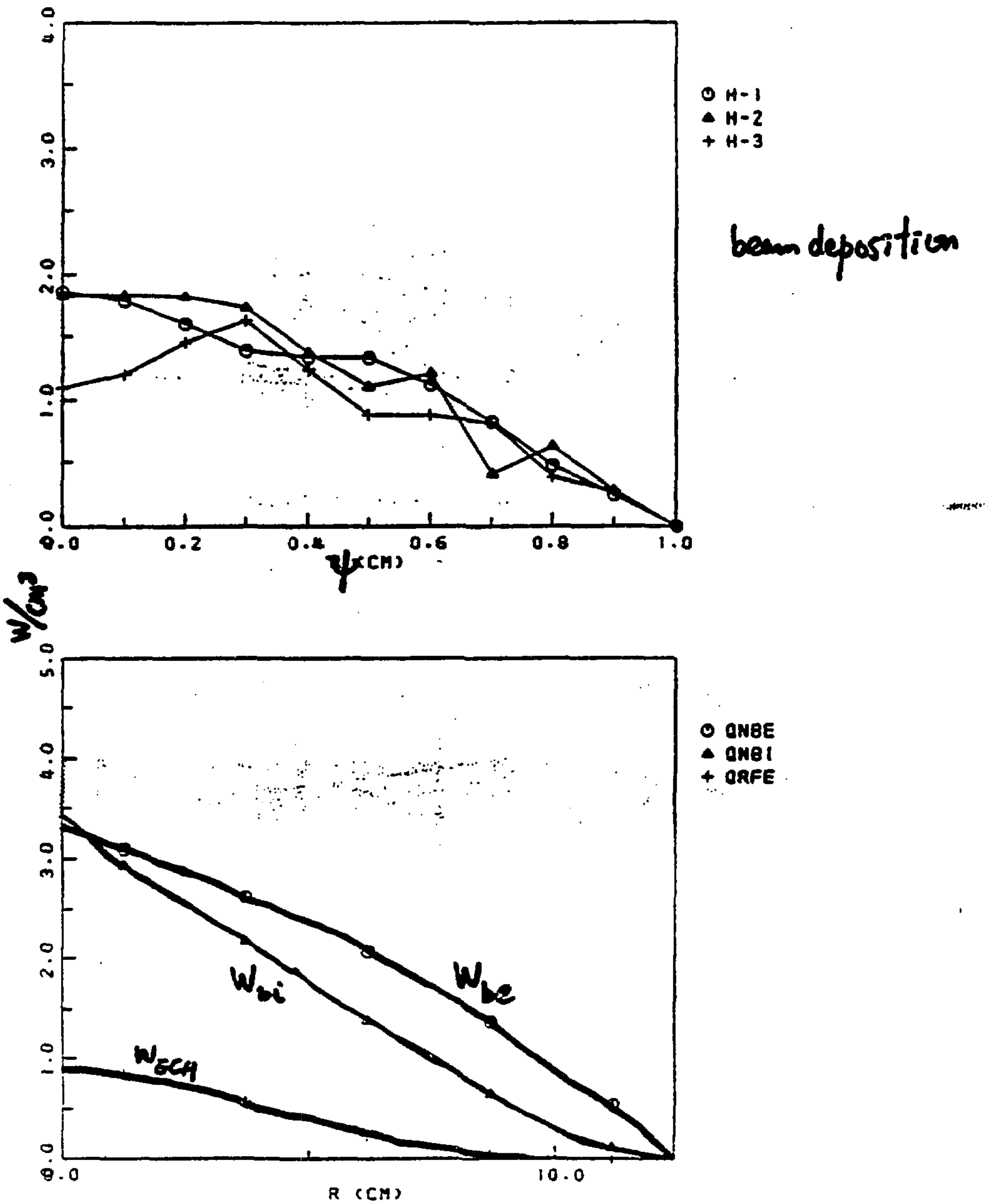

electron root case

JOB - 5000

RMAJC (CM)	94.14	~~PNBI (MW)~~	~~2.00E+00~~
RLIMC (CM)	12.38	ANGLE3	4.00E+01
RWALC (CM)	12.38	CLBCX	5.00E-01
BZO (G)	1.50E+04	PRFMW (MW)	0.00E+00
NEAV	2.00E+13	PECH (MW)	5.00E-01
ELIP	2.17		
LSER	0		
NRIPLE	1		
LCORR	T		
HRIA	1.00E+00		
DALPHE	5.00E+16		
DBETAE	5.00E+16		
DBETAI	1.00E+00		
CDRIFT	0.00E+00		
ETATH	2.00E+00		

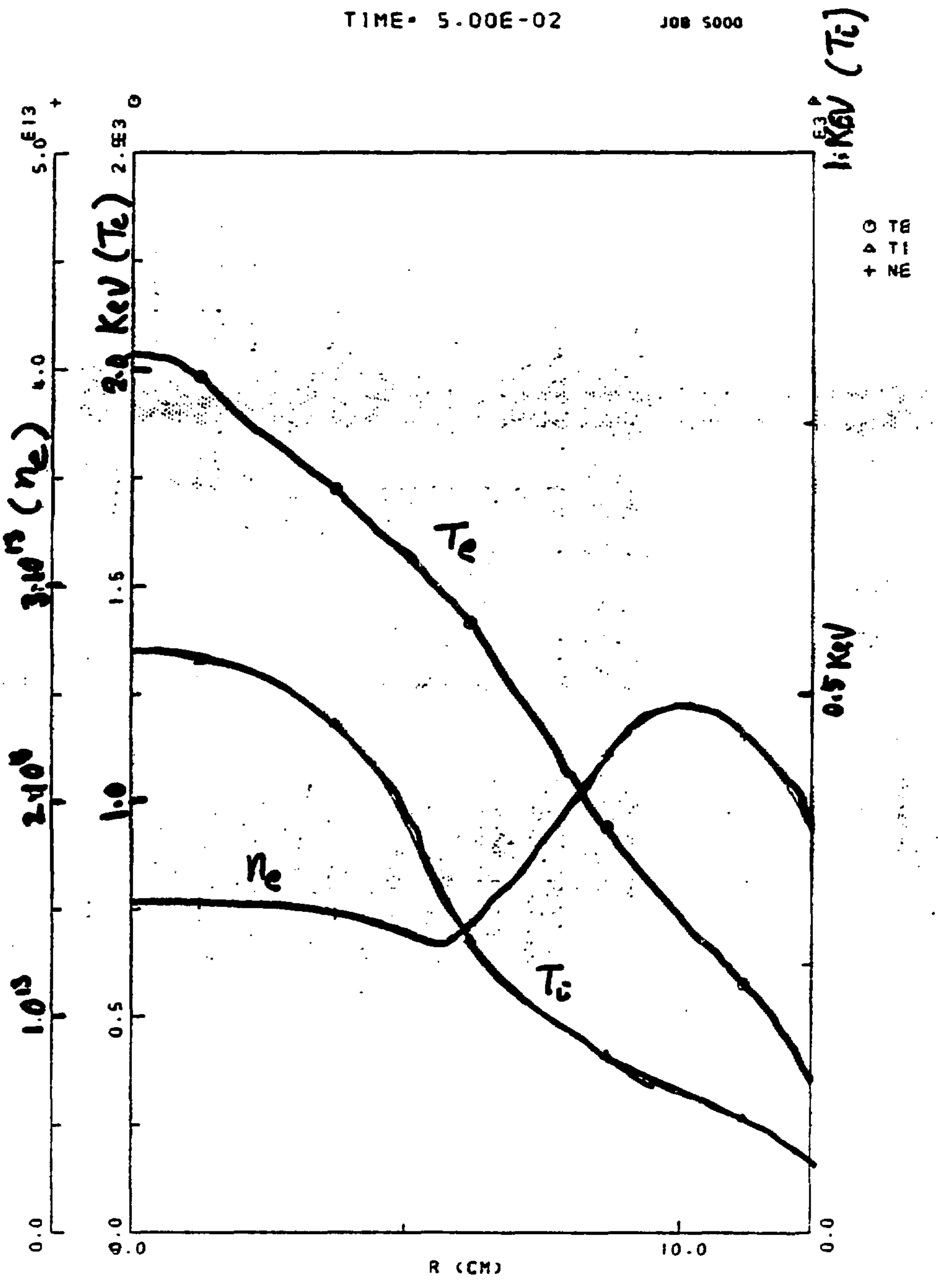

TIME= 5.00E-02
JOB 5000
O TE
Δ TI
+ NE
R (CM)
0.0
10.0
0.5
1.0
1.5
2.0
5.0 E13
2.5E3
Te
Ti
ne
2.0 KeV (Te)
1.KeV (Ti)
0.5 KeV

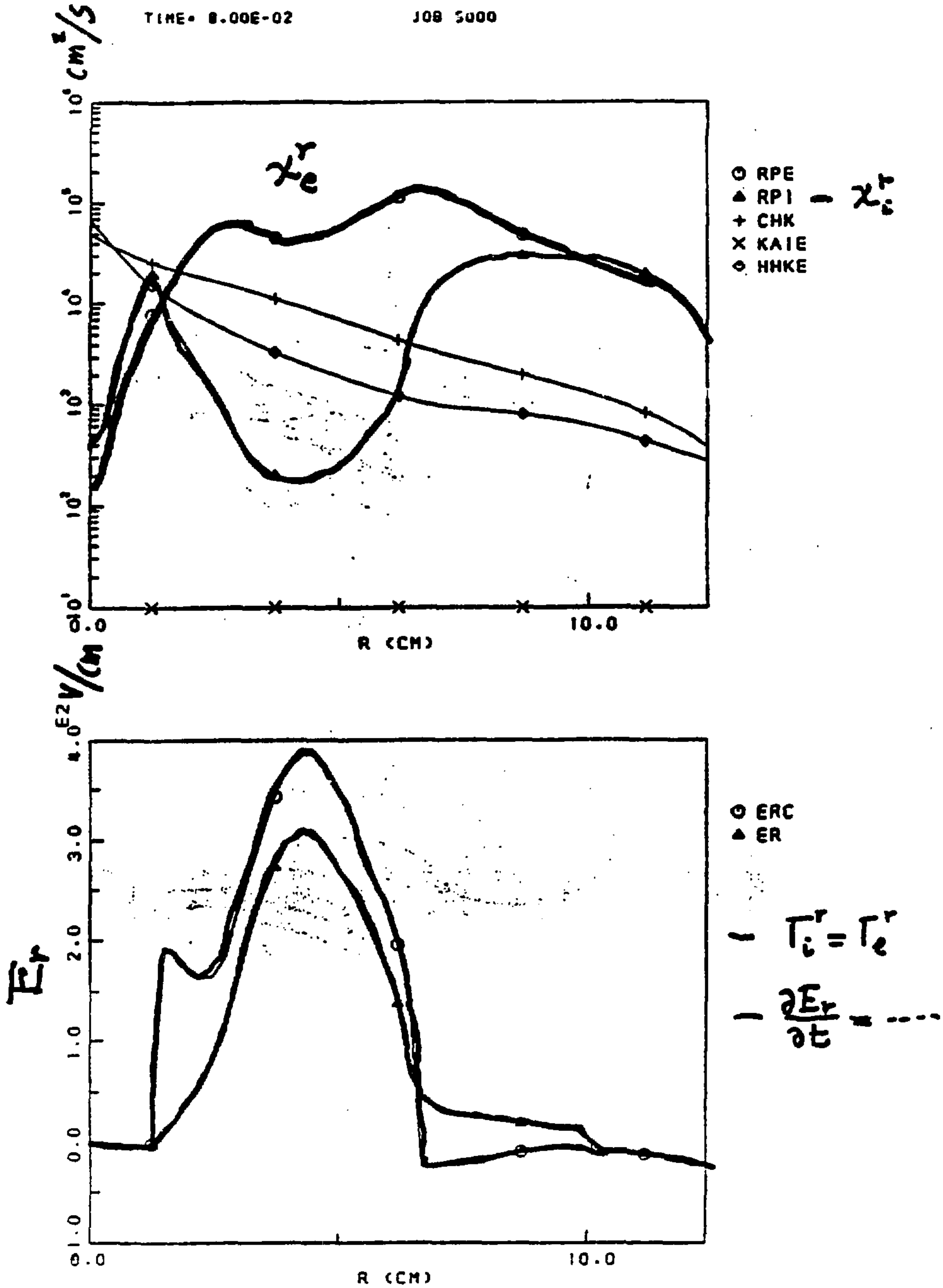

TIME= 8.00E-02
JOB 5000
10^6 cm²/s
χ_e^r
RPE
RPI — χ_i^r
CHK
KAIE
HHKE
0.0
10.0
R (CM)
4.0 E2 V/cm
3.0
2.0
1.0
0.0
-1.0
E_r
ERC
ER
— $\Gamma_i^r = \Gamma_e^r$
— $\frac{\partial E_r}{\partial t} = 0$

TIME= 6.00E-02 JOB 5000

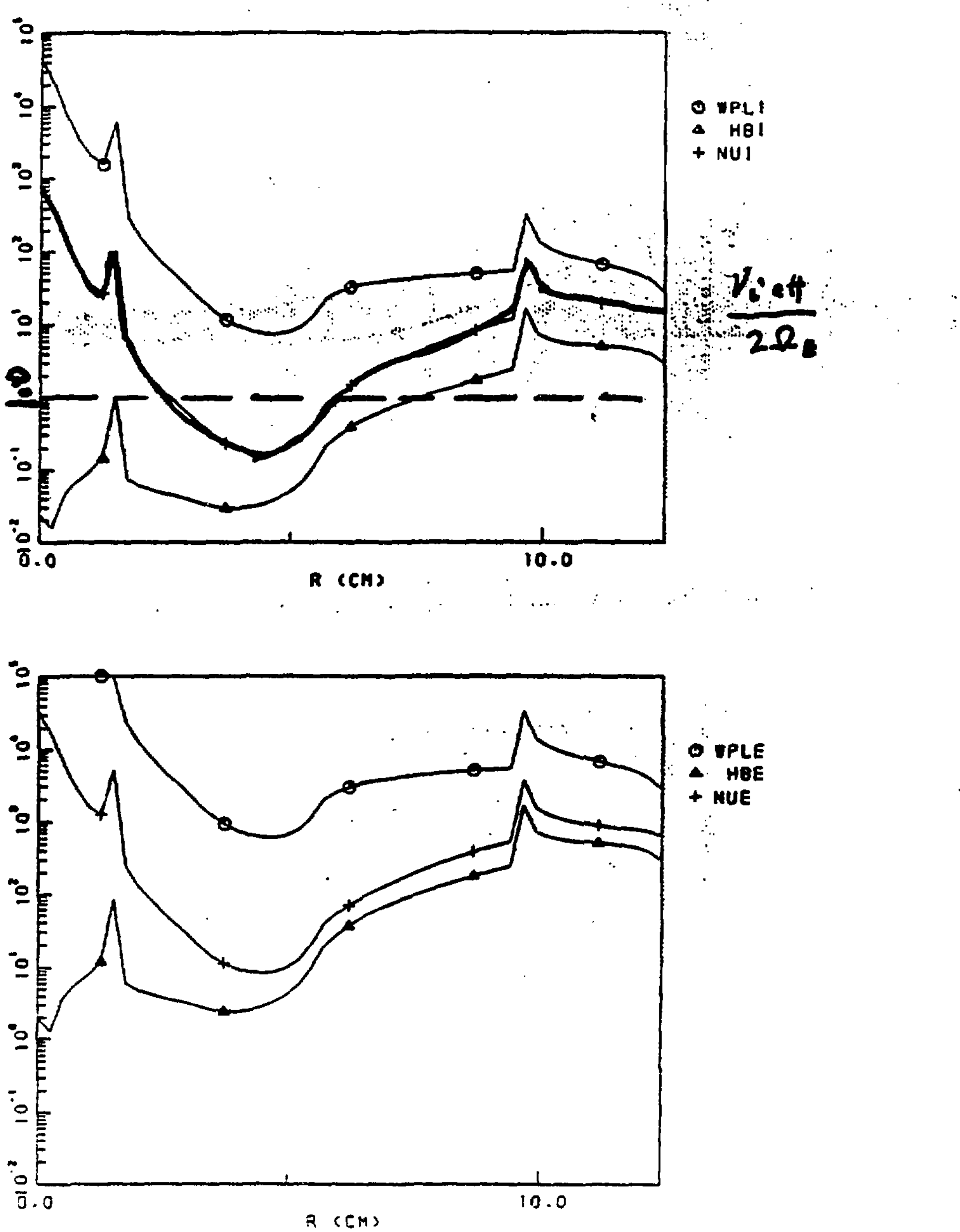

$n = 3\times10^{13}$
$B = 1.5\,T$

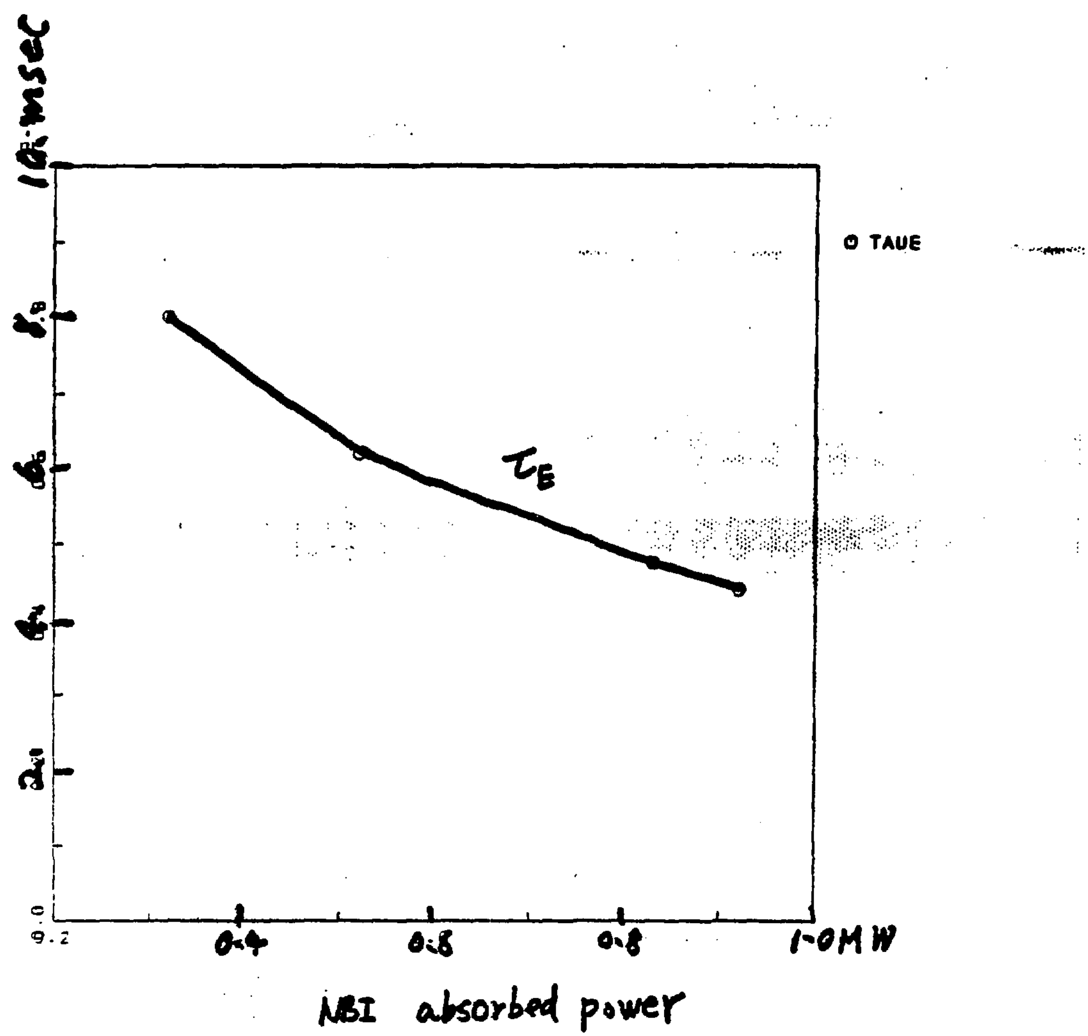

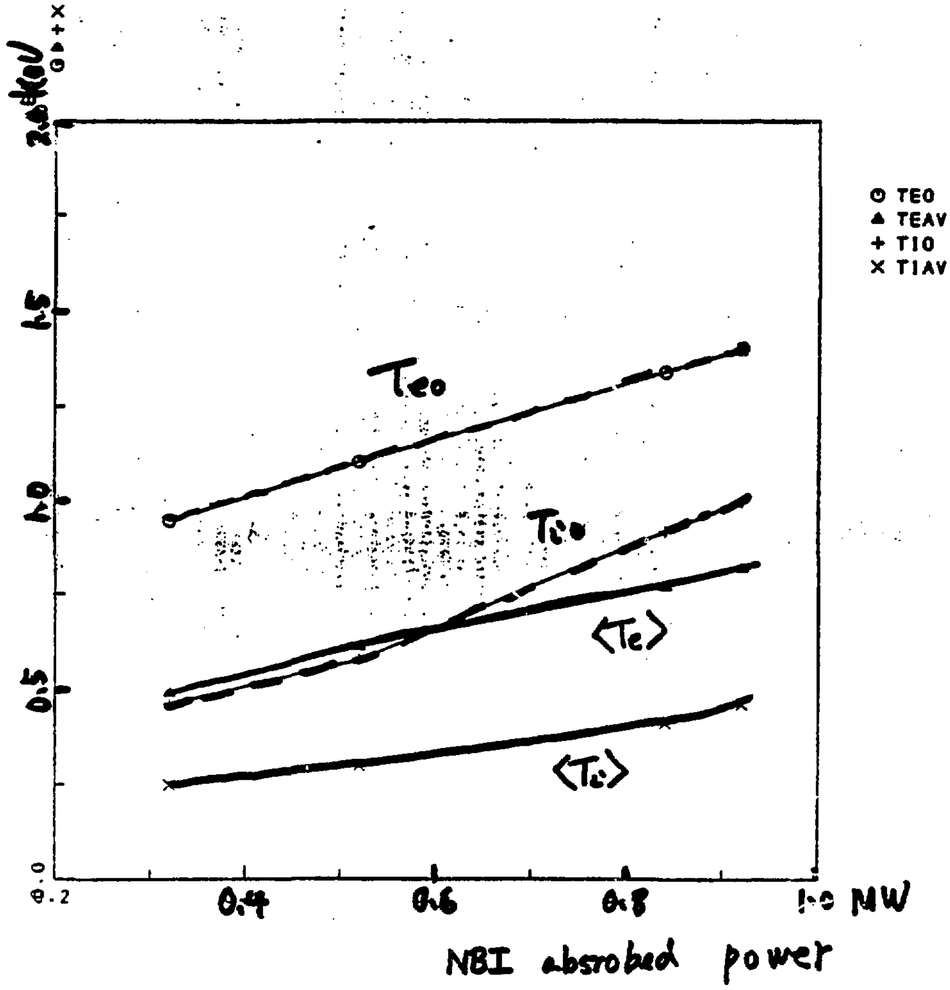

TEO
TEAV
TIO
TIAV
Teo
Tio
⟨Te⟩
⟨Ti⟩
keV
2.0
1.5
1.0
0.5
0.0
0.2
0.4
0.6
0.8
1.0 MW
NBI absrobed power

$\langle n_e \rangle$	B (T)	τ_e (ms)	T_{e0} (keV)	$\langle T_e \rangle$	T_{i0}	$\langle T_i \rangle$	β (%)	NBI ECH (MW)	remark
5×10^{13}	1.5	11.4	1.9	1.0	1.8	1.1	4.1 2.0	1.45 0.1	0.5·Intor
5×10^{13}	1.5	5.0	1.18	0.66	0.96	0.49	2.6 0.9	1.45 0.1	0.5 Intor + Neoc
3×10^{13}	1.0	3.8	1.14	0.67	0.69	0.34	5.7 4.7	0.85 0.1	Neoc
3×10^{13}	1.5	4.8	1.34	0.76	0.92	0.4	2.8 2.2	0.83 0.1	Neoc
3×10^{13}	2.0	5.4	1.49	0.83	1.12	0.47	1.6 1.3	0.83 0.1	Neoc
2×10^{13}	1.5	4.2	2.0	0.94	0.4	0.18	2.1 1.7	0.55 0.4	Neoc electron root

2MW NBI

$\epsilon_h \sim 0.22 \left(\frac{r}{a}\right)^2$

n_e	B (T)	τ_e (ms)	T_{e0} (keV)	$\langle T_e \rangle$	T_{i0}	$\langle T_i \rangle$	β (%)	NBI ECH (MW)	Remark
5×10^{13}	1.5	10. 28. 5.2	0.82	0.43	0.5	0.3	0.88 0.25	0.44* 0.1	E_r new scaling
5×10^{13}	1.5	8.7 20. 3.9	1.4	0.52	0.38	0.2	0.88 0.46	0.31* 0.1	$E_r=0$ new scaling
5×10^{13}	1.5	9.3 22. 4.1	1.42	0.54	0.4	0.2	0.94 0.47	0.33* 0.1	$E_r=0$ old scaling
3×10^{13}	1.5	4.8 6.4 3.7	1.34	0.76	0.92	0.4	2.8 2.3	0.83 0.1	NeoC
5×10^{13}	1.5	5.6 11.2 3.2	1.3	0.76	1.2	0.6	3.3 0.9	1.3 0.1	NeoC
10×10^{13}	1.5	7.3 20.0 4.0	0.95	0.59	0.69	0.43	2.3 0.65	1.87 0.1	NeoC

* NBI 0.5MW

SUMMARY II (TRANSPORT)

1. NEW SCALING VS. OLD SCALING (NEOCLASSICAL)

2. τ_E DEGRADADES WITH BEAM POWER

3. AMBIPOLAR POTENTIAL EFFECTS

4. ELECTRON ROOT FOR LOW DENSITY CASE

5. NEEDS GOOD ESTIMATION OF NEUTRAL BEAM ABSORPTION

US-JAPAN
STELLARATOR/HELIOTRON WORKSHOP
Oak Ridge, November 9-13, 1987

PLASMA CURRENT DURING ECF-HEATING IN THE WENDELSTEIN W7A STELLARATOR.

H. RENNER, W 7A-Team, ECRH-Group
MPI-Plasmaphysik, EURATOM-Ass.
8046 GARCHING, W.GERMANY
IPFder Universität STUTTGART
7000 STUTTGART, W.GERMANY

Plasma current has been observed during the experiments at the stellarator W7A dependent on the heating method and on plasma parameters. The main contributions to the current are related to the plasma pressure and current drive effects by application of heating.

In the almost shearless W7A (major radius 2m, minor radius 0.1m, main field <3.5T; helical windings l=2, m=5) the effect of "resonances" at rational values of the rotational transform $\iota = m/n$ has been demonstrated for the confinement.Optimum confinement was found very close to rational values of the transform, but at these values the containment became strongly degraded. The plasma current modifies the magnetic configuration and consequently even small currents can significantly affect the transform profile dependent on the current distribution.

The confinement properties have been shown strongly influenced by the current and the current density distribution. An aestimate of current density profiles for experiments with ECF heating is based on measured density and temperature profiles. Then, the ECF driven currents can be localized to the pressure gradient region where the maximum bootstrap current is expected.

The absorption of ECF power launched nearly perpendicular to the magnetic field, ECF current drive and generation of suprathermal electrons is analyzed using a 3-D ray tracing code in combination with a simplified Fokker-Planck solution for which the ECF energy source function is aestimated by means of quasilinear theory (1). Results have been found in rather good agreement with experimental data of W7A.Some degradation of the local power absorption is explainable by the deviation of the electron distribution function from the Maxwellian. So far, local current drive by application of ECF seems to be qualified to modify the current density profile and even to compensate the bootstrap current.

(1) U. Gasparino, H. Maaßberg, M. Tutter, W7A-Team, ECRH-Group
Studies on electron cyclotron heating at the W7A/AS stellarator.
EPS, 14. Europ. Conf., Madrid (1987)

US-JAPAN
STELLARATOR/HELIOTRON WORKSHOP
Oak Ridge, November 9-13, 1987

PLASMA CURRENT DURING ECF-HEATING IN THE WENDELSTEIN W7A STELLARATOR.

H. RENNER, W 7A-Team, ECRH-Group
MPI-Plasmaphysik, EURATOM-Ass.
8046 GARCHING, W.GERMANY
IPF der Universität STUTTGART
7000 STUTTGART, W.GERMANY

(1) U. Gasparino, H. Maaßberg, M. Tutter, W7A-Team, ECRH-Group
Studies on electron cyclotron heating at the W7A/AS stellarator.
EPS, 14. Europ. Conf., Madrid (1987)

STELLARATOR W 7A

R = 2 m
a = 0.1 m
helical windings: $l = 2$, $m = 5$
transform 0 - 0.6; shearless $\Delta \iota / \iota < 0.01$

" currentless " operation: NBI 1980

$P_{inj} < 500$ kW
injection angle: 6^{o} (radial injection)

ECF 28 GHz
70 Ghz 1985
200 kW, 0.1 sec
HE_{11}, o-mode and x-mode

RESULTS

confinement dependent on the magnetic configuration
island formation and ergodization

"resonances" : deterioration of containment at rational values of the transform $\iota = m/n$.
(boundary and plasma core)

influence of shear

optimal confinement with low shear ($\Delta \iota / \iota < 0.1$)
and with transform $\iota \neq m/n$

observation of plasma current
depending on energy content: bootstrap current $j_b \sim dp/dr$
induced by the heating method

CONTROL of current and current density distribution for optimal confinement

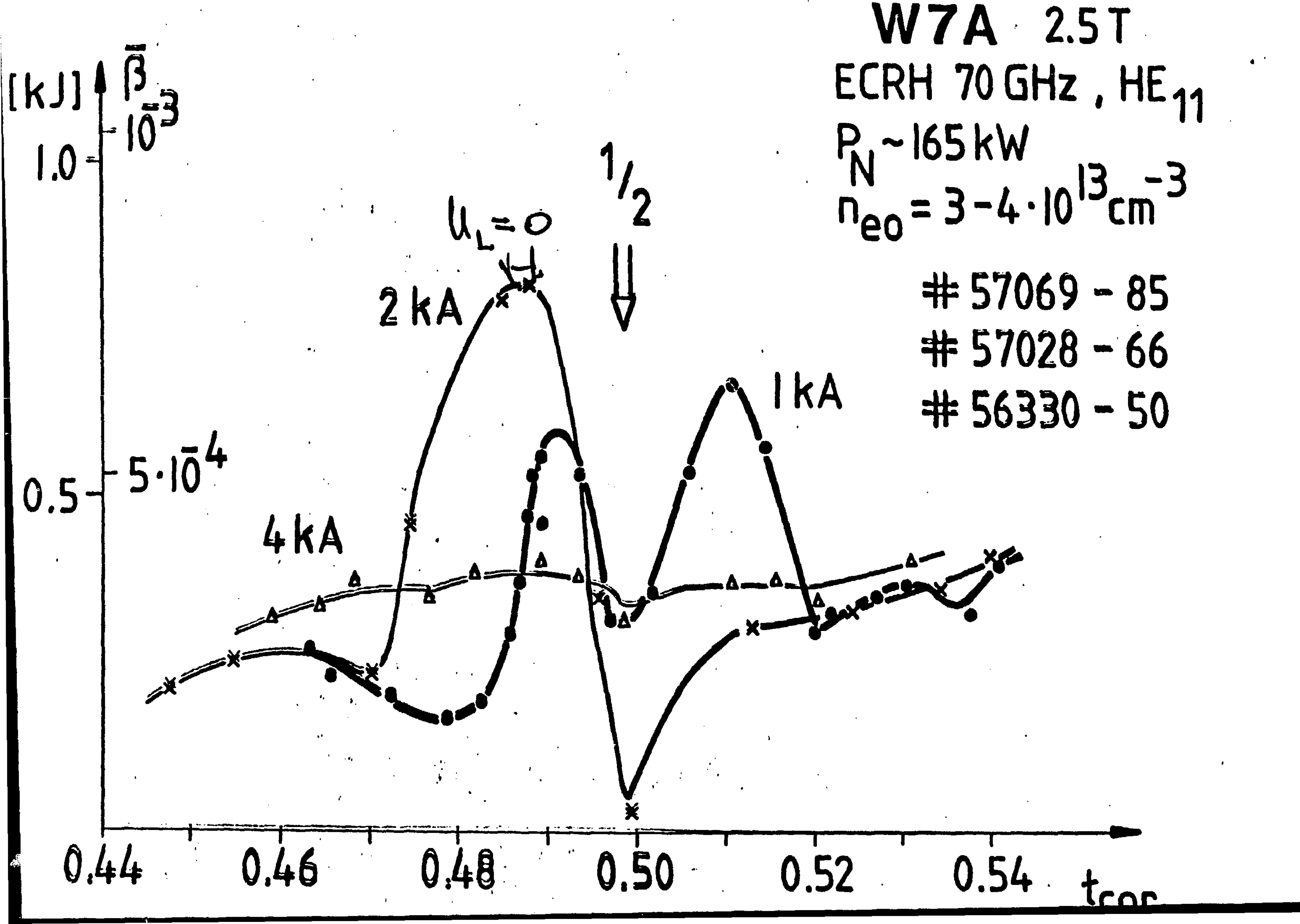

W7A 2.5 T
ECRH 70 GHz , HE11
PN ~ 165 kW
neo = 3 - 4 · 10^13 cm^-3
# 57069 - 85
# 57028 - 66
# 56330 - 50
[kJ]
β̄
10^-3
1.0
0.5
5 · 10^-4
UL = 0
1/2
2 kA
1 kA
4 kA
0.44
0.46
0.48
0.50
0.52
0.54
tcor

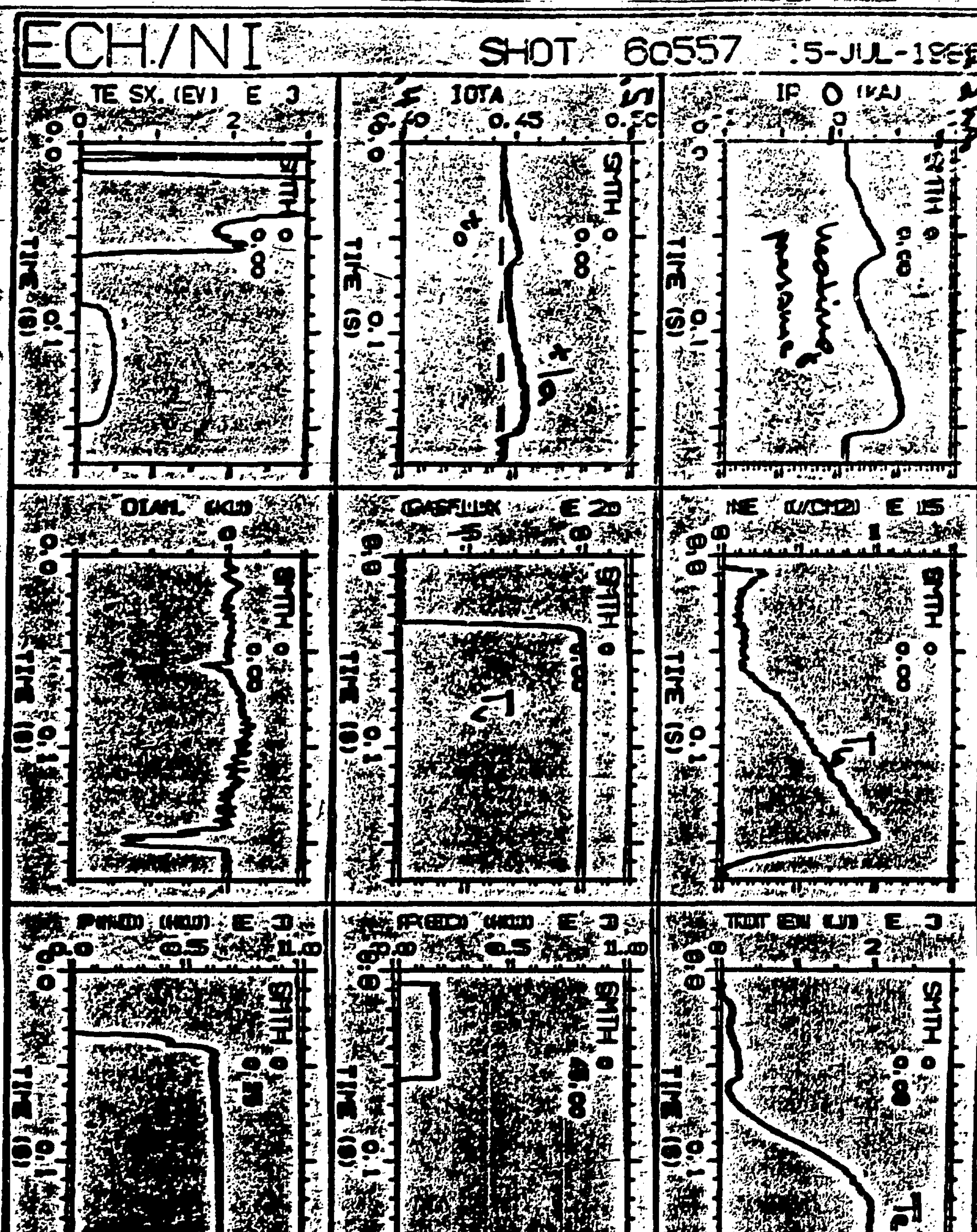
ECH/NI
SHOT 60557
TE SX. (EV) E 3
IOTA
IP (KA)
DIAM. (KJ)
GASFLUX E 20
NE (1/CM2) E 15
TOT EN (KJ) E 3
TIME (S)
SMITH

NBI - 6° 1 B

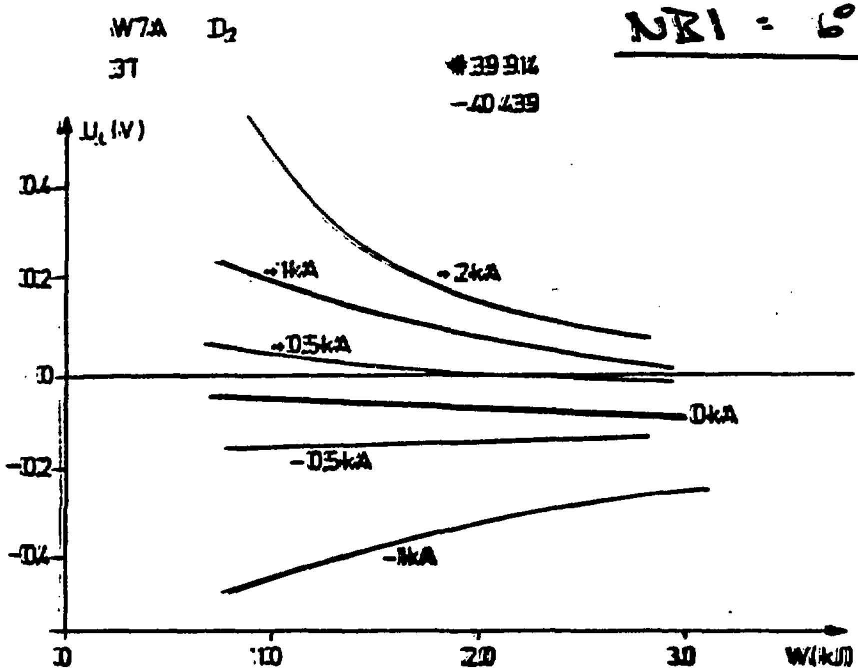

Loop voltage versus energy content W.
Programmed current I_p as parameter.

w/ counter
Ip changes
sign

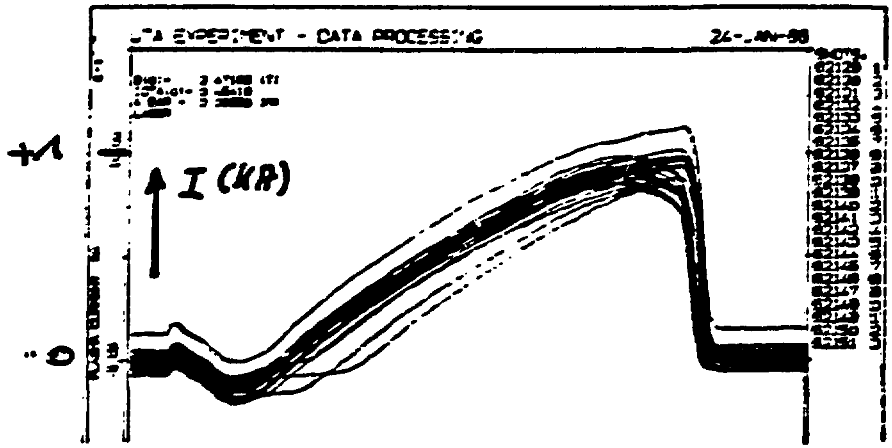

Toroidal current for B_0=2.47 T

J_6

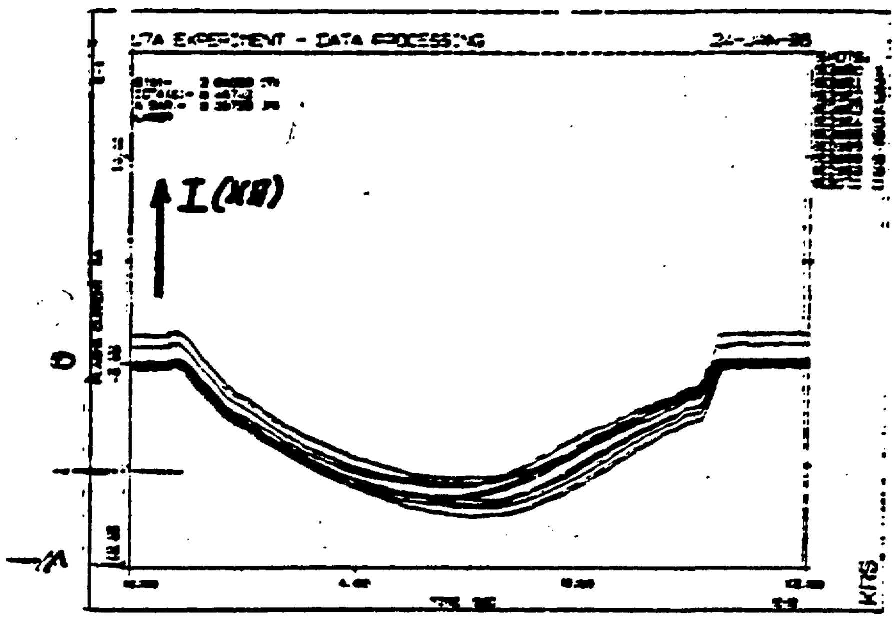

Toroidal current for B_0=2.60 T

$J_{47} + J_6$

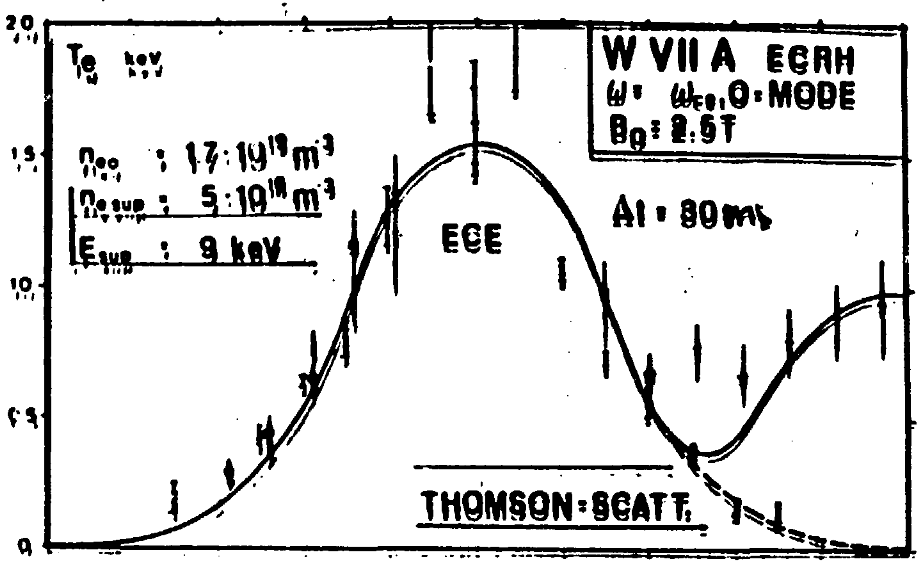

56 440 - 476

low field side
→ rel. m_e

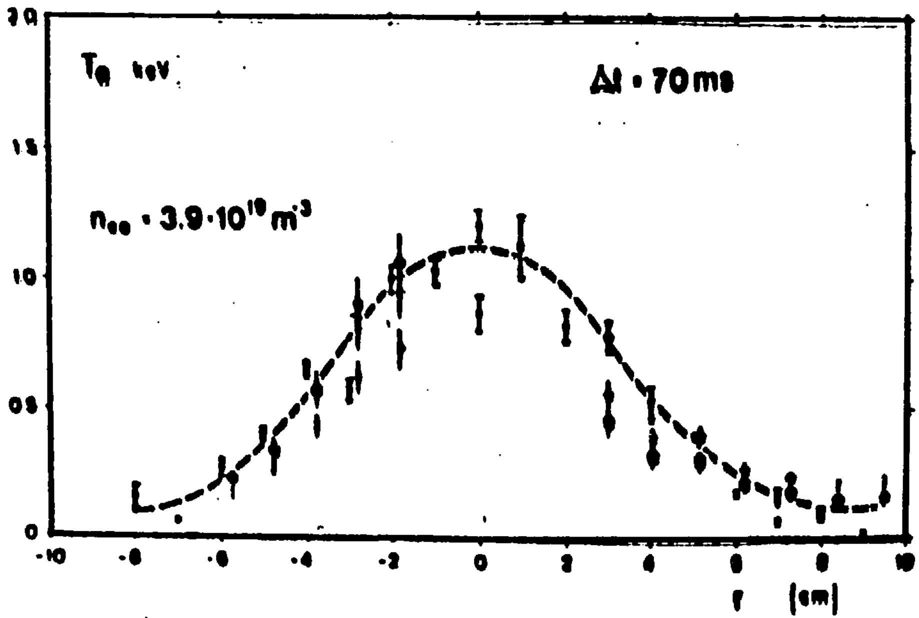

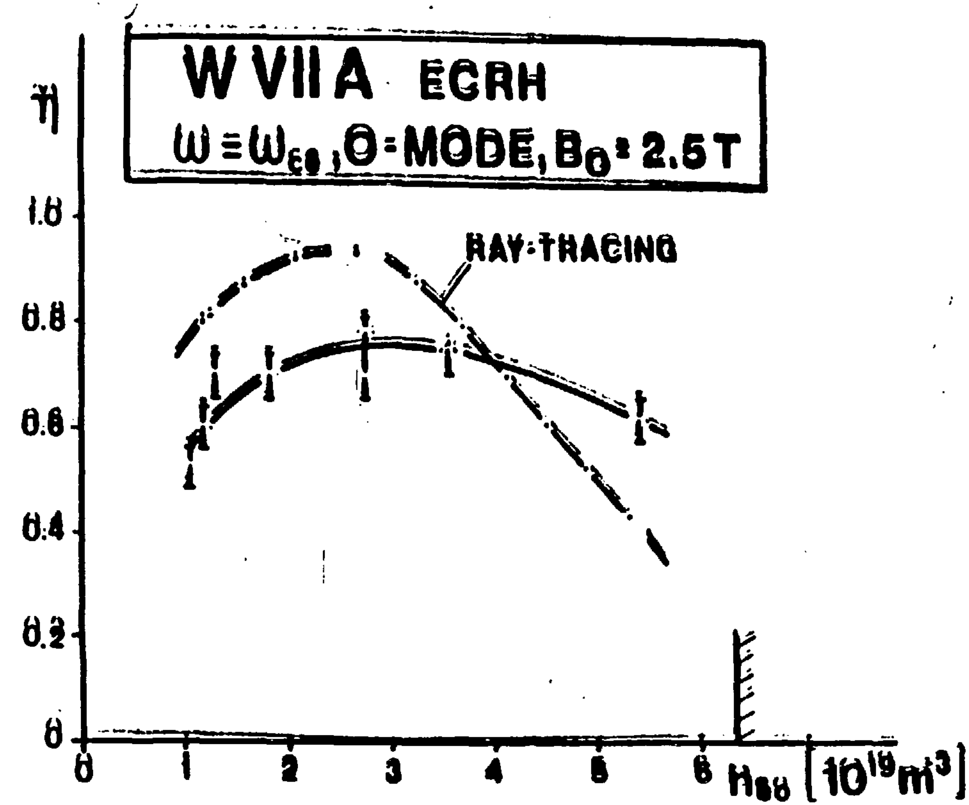

W VII A ECRH
ω = ω_ce, O-MODE, B_0 = 2.5 T
RAY-TRACING
η
1.0
0.8
0.6
0.4
0.2
0
0
1
2
3
4
5
6
n_e0 [10^19 m^-3]

investigations on plasma current for plasma heated by ECF 70 GHz

experiment	2.5 T 1.25 T variation of plasma parameters and power deposition ECE measurements suprathermal electrons heating efficiency
theory	3-D ray tracing code in combination with a simplified Fokker- Planck solution absorption current drive generation of suprathermal electrons on the basis of experimental density and temperature profiles

ECF HEATING AT THE W VII-A STELLARATOR

- major radius: 2 m; plasma radius: 10 cm
- injected ECF power: $P_{max} < 200$ kW at 70 GHz
- pulse length of ECF maintained discharges: < 100 ms
- ECF waves launched nearly perpendicular to the magnetic field ($\approx 92°$)
- current drive efficiency expected to be rather small for these conditions
- ECF driven, pressure driven (bootstrap current) and ohmic currents of the same order of magnitude

NUMERICAL FORMALISM

- Hamiltonian 3-D ray tracing calculations based on Maxwellian electron distribution function yield 0th order power deposition as a function of $k_\parallel$ and ω_{ce}
- Estimation of the flux surface averaged quasi-linear tensor element $Q_{\perp\perp}$
- Solution of flux surface averaged Fokker-Planck equation yields the deviation of the electron distribution function from the Maxwellian
- Estimation of the electron cyclotron emission (ECE) based on the flux surface averaged electron distribution function (Fokker-Planck equation) by means of the Hamiltonian 3-D ray tracing code

BASIC FORMULAE

absorption coefficient

$$\alpha(\underline{k},\omega) = \frac{1}{|\underline{S}(\underline{k},\omega)|}\,\frac{\omega}{4\pi}\Big\{ -\pi\,\frac{\omega_{pe}^2}{\omega} \sum_{n=-\infty}^{+\infty} \int d^3v\;\; \delta(\omega - k_\parallel v_\parallel - \frac{n\omega_{ce}}{\gamma})$$
$$v_\perp \,[\,(1 - N_\parallel \frac{v_\parallel}{c})\frac{\partial}{\partial v_\perp} + N_\parallel \frac{v_\perp}{c}\frac{\partial}{\partial v_\parallel}\,] f_e(\underline{v})$$
$$|\,\frac{1}{2}\,(E_x - iE_y)\;J_{n-1}(b) + \frac{1}{2}\,(E_x + iE_y)\;J_{n+1}(b) + \frac{v_\parallel}{v_\perp}\;E_z J_n(b)\;|^2 \Big\}$$

emission coefficient

$$\eta(\underline{k},\omega) = \frac{1}{|\underline{S}(\underline{k},\omega)|}\,\frac{\omega}{4\pi}\,(N_r^2\frac{\omega^2}{8\pi^3 c^2})\Big\{\,\pi\,\frac{\omega_{pe}^2}{\omega} \sum_{n=-\infty}^{+\infty} \int d^3v\;\; \delta(\omega - k_\parallel v_\parallel - \frac{n\omega_{ce}}{\gamma})$$
$$[\,m_e v_\perp^2 f_e(\underline{v})]$$
$$|\,\frac{1}{2}\,(E_x - iE_y)\;J_{n-1}(b) + \frac{1}{2}\,(E_x + iE_y)\;J_{n+1}(b) + \frac{v_\parallel}{v_\perp}\;E_z J_n(b)\;|^2 \Big\}$$

quasi-linear tensor

$$Q_{\perp\perp} = \frac{\pi e^2 \omega_{ce}^2}{m^2\omega^2}\,\Big\{\, \sum_{n=-\infty}^{+\infty} \int \frac{d^3k}{(2\pi)^3 V}\,\delta(\omega - k_\parallel v_\parallel - \frac{n\omega_{ce}}{\gamma})$$
$$n^2\,|\,\frac{1}{2}\,(E_x - iE_y)\;J_{n-1}(b) + \frac{1}{2}\,(E_x + iE_y)\;J_{n+1}(b) + \frac{v_\parallel}{v_\perp}\;E_z J_n(b)\;|^2 \Big\}$$

$\underline{S}(\underline{k},\omega)$: poynting vector with sloshing particles included

Fokker-Planck equation:

$$S^l(f) = C(f) + S^{rf}(f)$$

quasi-linear ECF energy source function:

$$S^{rf}(f) = \frac{1}{v_\perp}\frac{\partial}{\partial v_\perp} v_\perp Q_{\perp\perp}\frac{\partial f}{\partial v_\perp}$$

collision operator:

$$C(f) = \Gamma_e \frac{1}{v^2}\left\{ \frac{\partial}{\partial v}\left(\alpha_1(v) f + \frac{1}{2}\frac{\partial}{\partial v}(\alpha_2(v) f)\right) + \beta(v)\frac{\partial}{\partial p}(1-p^2)\frac{\partial}{\partial p} f\right\}$$

energy loss term:

$$S^l(f) \propto (v^2 - \langle v^2\rangle)\cdot f$$

to satisfy the energy balance for stationary conditions

W VII-A RAY TRACING CALCULATION

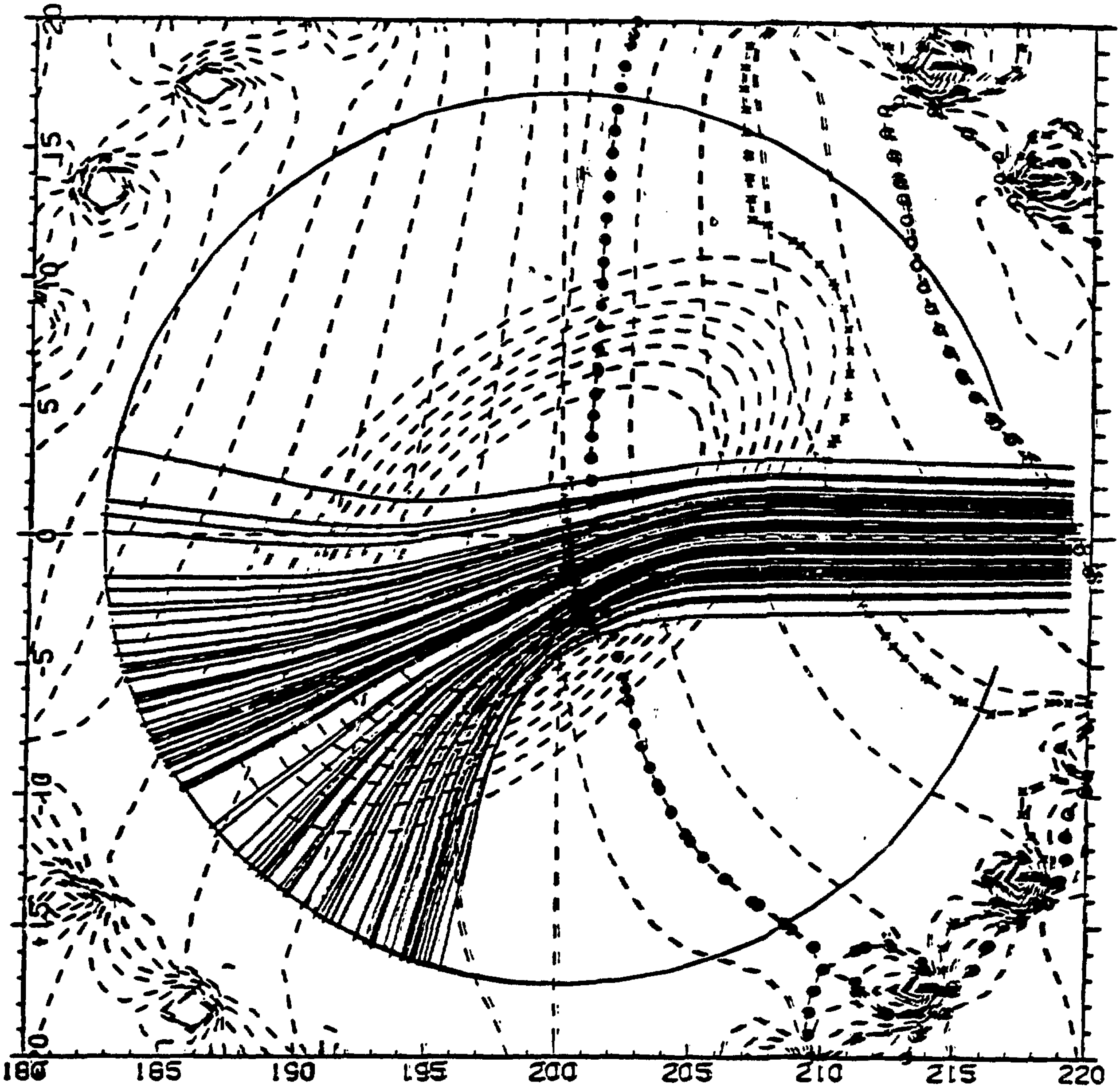

B_0 = 2.5200 TESLA ι_0 = 0.46 ϑ = 90.00° ΔB = 400 GAUSS
O-MODE 1.HARMONISCHE f = 70.0 GHZ ω_{p0}^2/ω^2 = 0.638
T_0 = 985 eV $N_0 = 3.860 \cdot 10^{13}$,
TEMP.-PROF TH.DICHTE-PR.

5.140	7.000
1.680	2.870
0.000	0.000

$\beta(0)$ = 0.0048 $\bar{\beta}$ = 0.00036 P_0 = 124 kW

ECF power deposition profile: theory ⇔ experiment

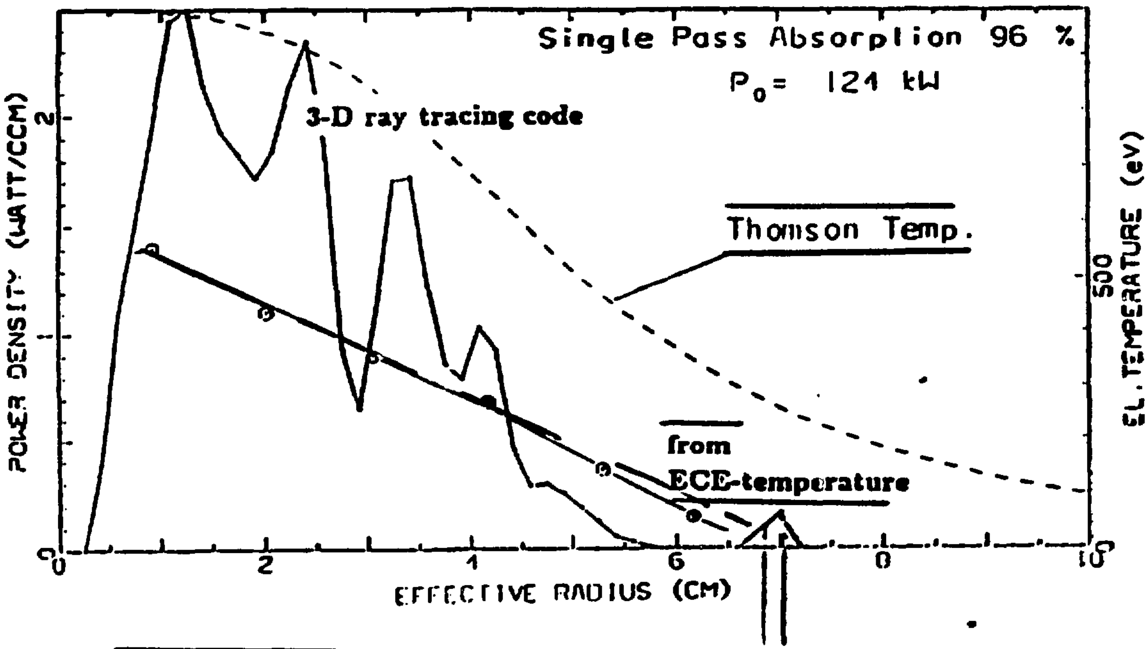

$$p_{\mathrm{ECF}}(r) \approx \frac{3}{2}\, n_e(r) \left\{ \left(\frac{\partial T(r,t)}{\partial t}\right)_{t<t_0} - \left(\frac{\partial T(r,t)}{\partial t}\right)_{t>t_0} \right\}$$

electron energy spectra

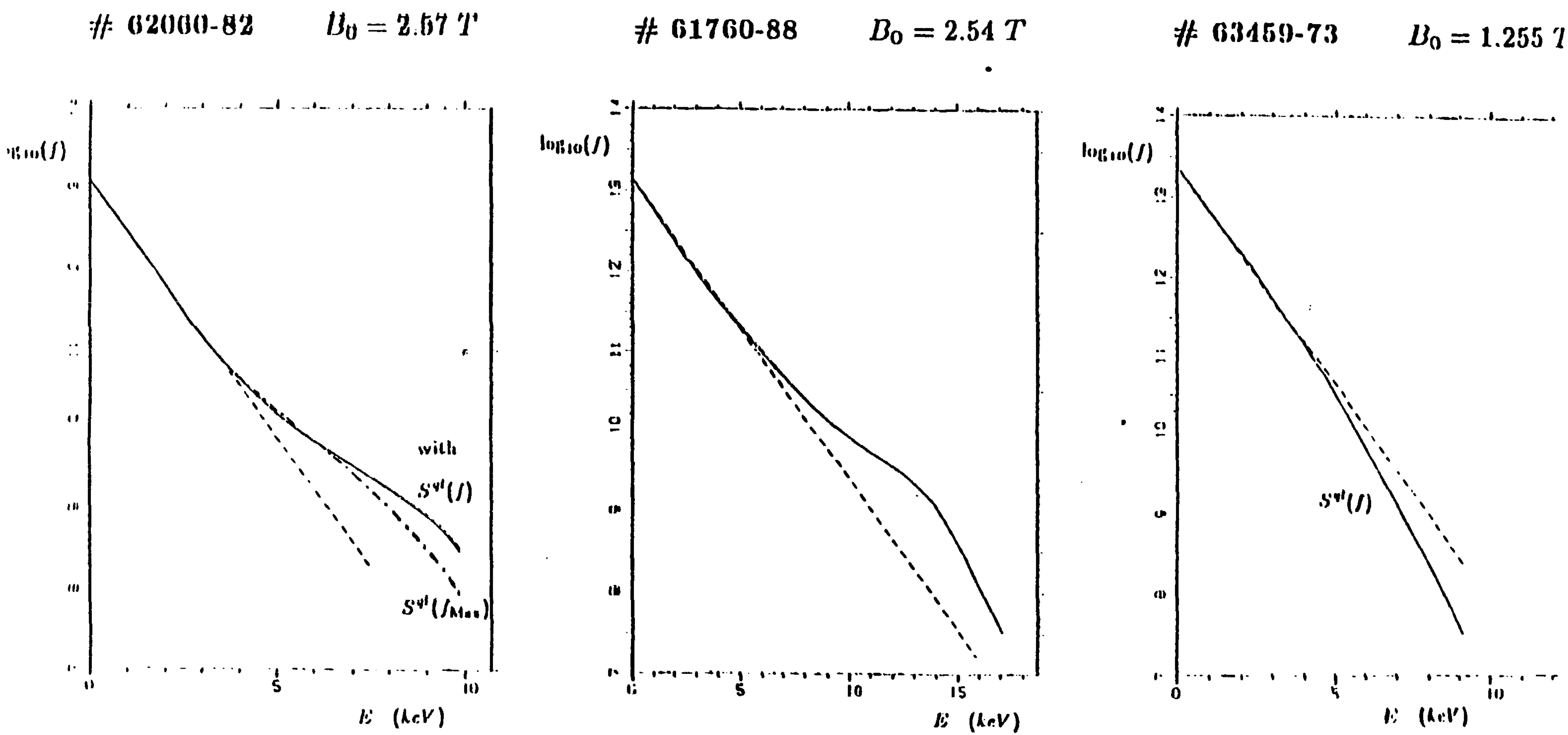

ECF fundamental o-mode

62060-82 $B_0 = 2.57\ T$

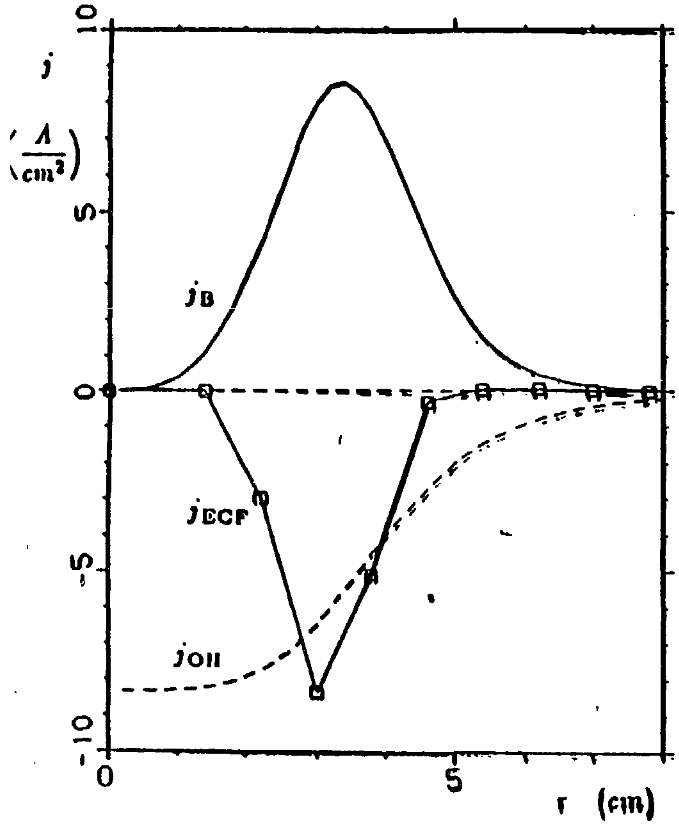

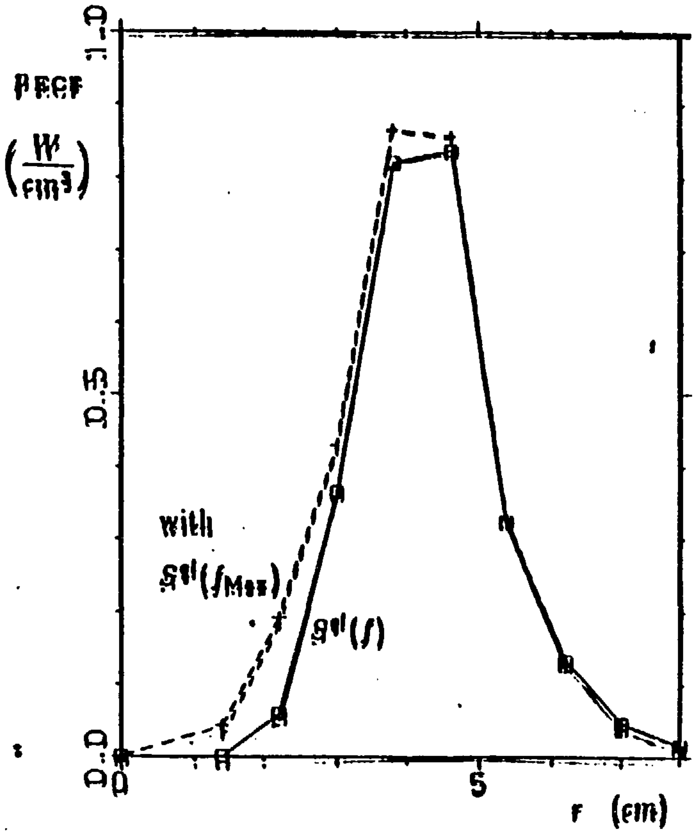

current evolution
(fundamental o-mode)

dW/dt > 0

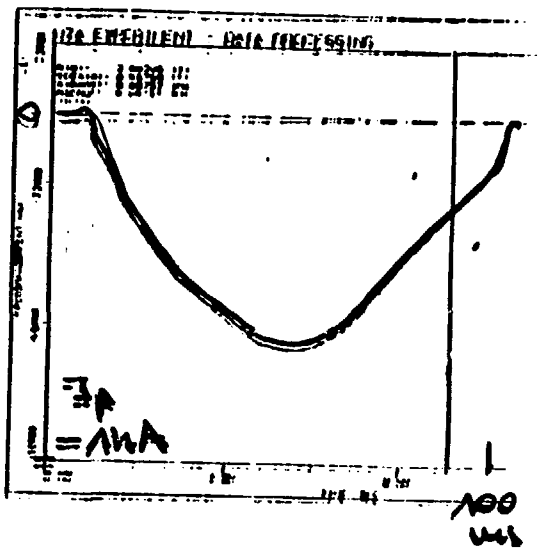

61760-88 $B_0 = 2.54\ T$

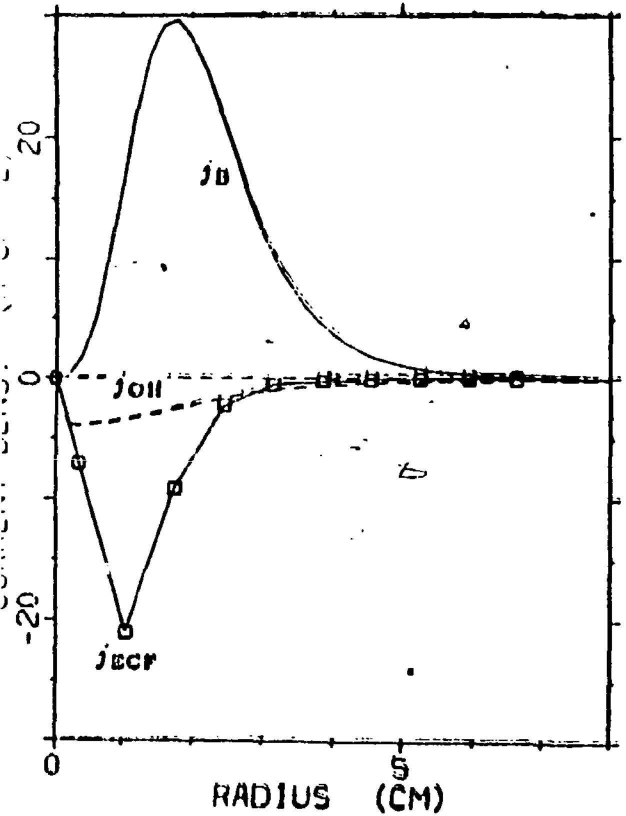

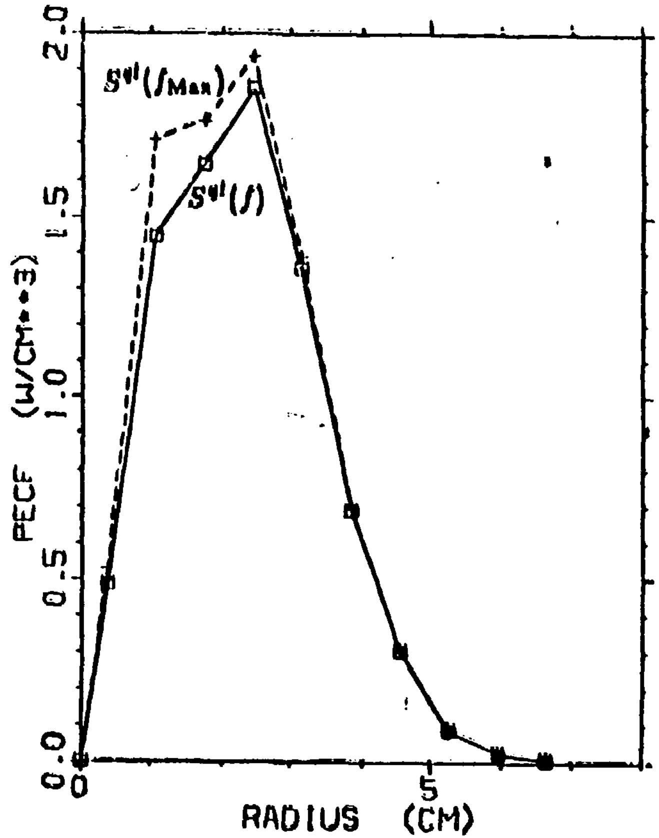

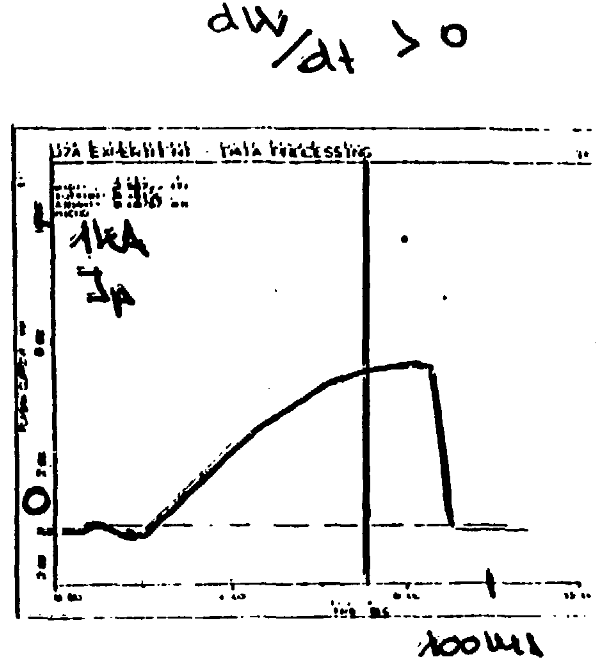

Table 1: *Comparison of current drive calculations with experimental data*

Shots	B_0 (T)	$T_e(0)$ (eV)	$n_e(0)$ (10^{13} cm^{-3})	P_{ECF} (kW)	Z_{eff}	I_B (A)	I_{ECF} (A)	I_{exp} (A)	U_{bal} (V)	U_{exp} (V)
62060-82	2.57	795	1.56	75	3	480	-200	-280	-0.10	0.07±.05
61760-88	2.54	1570	1.18	100	3	840	-220	515	-0.02	0.0 ±.05
61908-96	2.46	680	1.87	70	1.5	680	30	805	+0.01	0.03±.05
63402-21	1.280	292	2.29	105	3	230	-10	140	-0.03	0.03±.03
63459-73	1.255	701	2.06	130	3	1230	120	1015	-0.05	0.04±.03
63432-50	1.220	503	1.78	130	2.5	920	250	1050	-0.02	0.03±.03

ELECTRON DISTRIBUTION FUNCTIONS

62060-82 $B_0 = 2.67\ T$ High j_{ECF}

61700-88 $B_0 = 2.54\ T$ Low j_{ECF}

Deviation of the electron distribution function from the Maxwellian

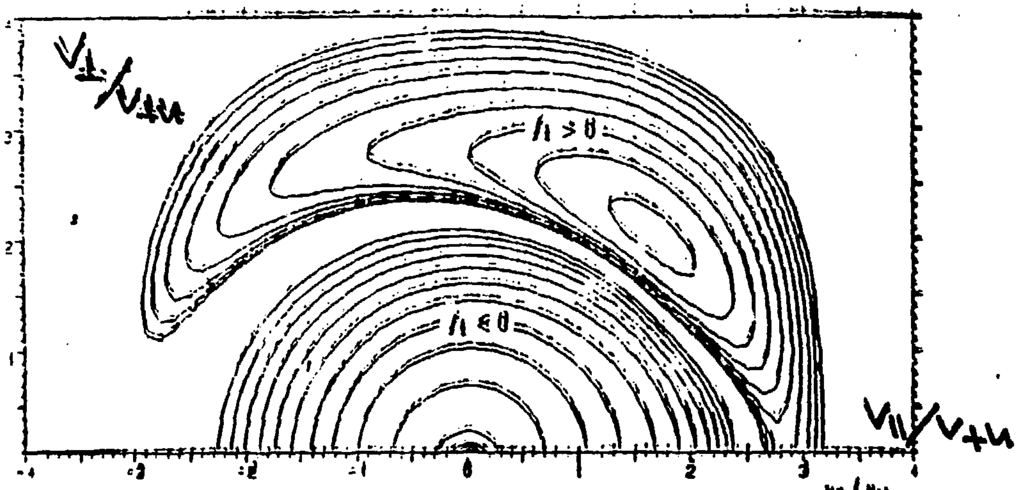

Quasi-linear energy source function $S^{ql}(f)$

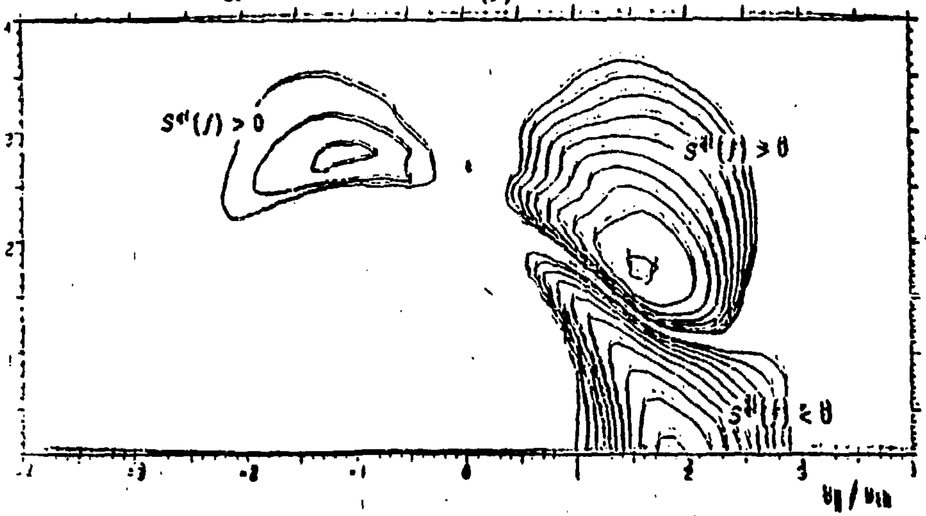

Deviation of the electron distribution function from the Maxwellian

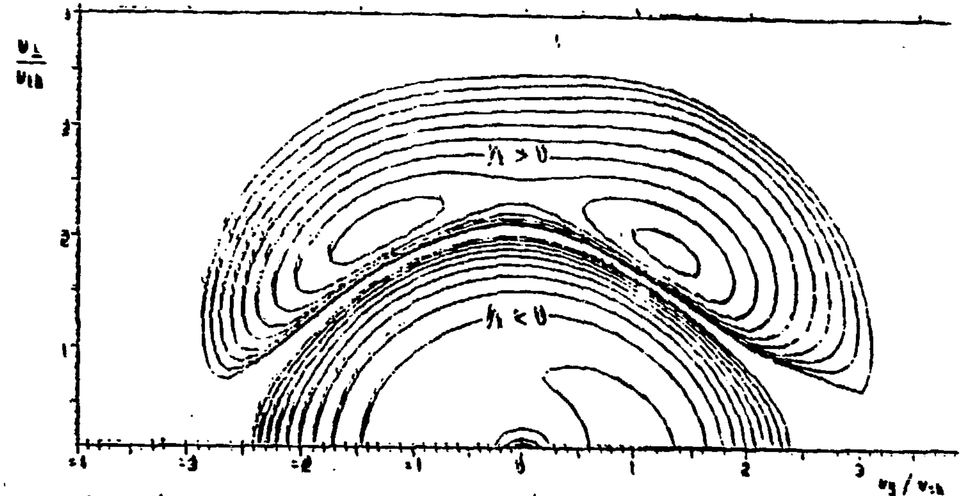

Quasi-linear energy source function $S^{ql}(f)$

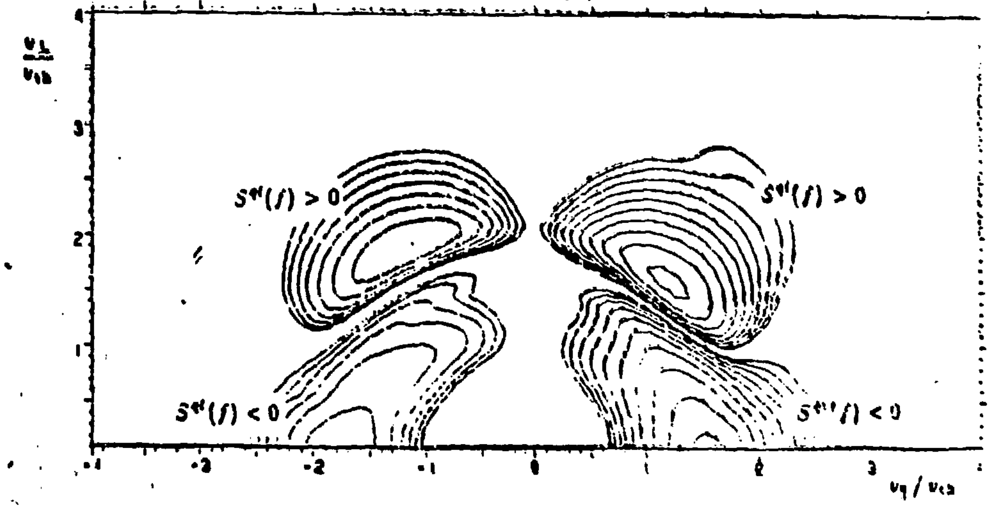

Results

rather good agreement of theoretical predictions and experimental results → multiple reflections

possibility for control of plasma current (bootstrap current) and current density distribution by ECF

outline of the ECF-launching system for W 7AS

W VII-AS RAY TRACING CALCULATIONS

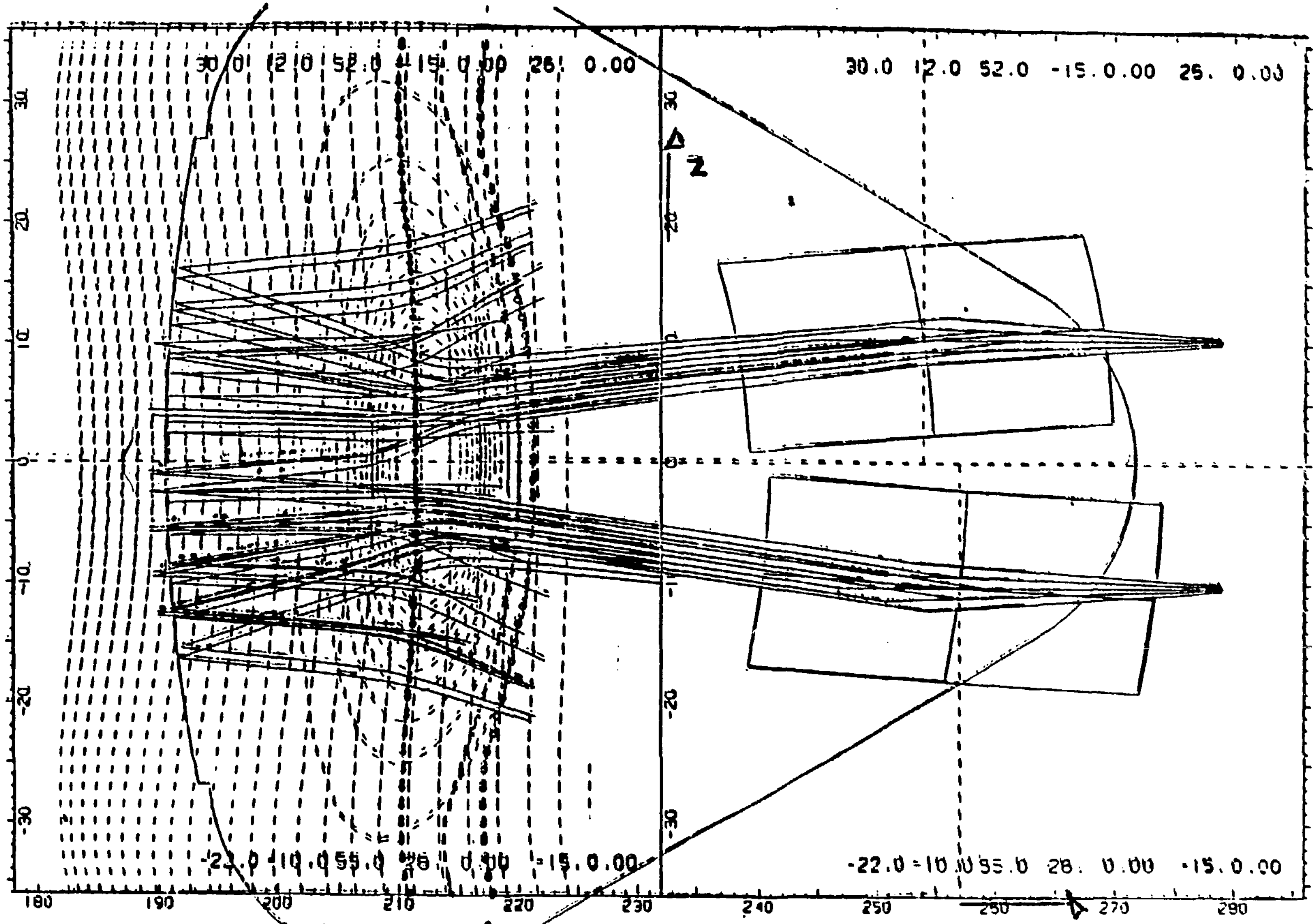

B_0 = 2.7377 TESLA ι_0 = 0.40   θ = 75 86°   ΔB = 500 GAUSS

O-MODE   1.HARMONISCHE   f = 70.0 GHZ ω_{pe}^2/ω^2 = 0.909

T_0 = 1000 eV N_0 = 5.500 10^{13}

TEMP.-PROF	TH.DICHTE-PR.
4.050	0.970
1.500	1.800
0.000	0.000

β(0) = 0.0059   β̄ = 0.00049 $P_{1,1}$ = 100 110 120 130 kW

ECRH AN W7AS $\varphi =$ 36.03

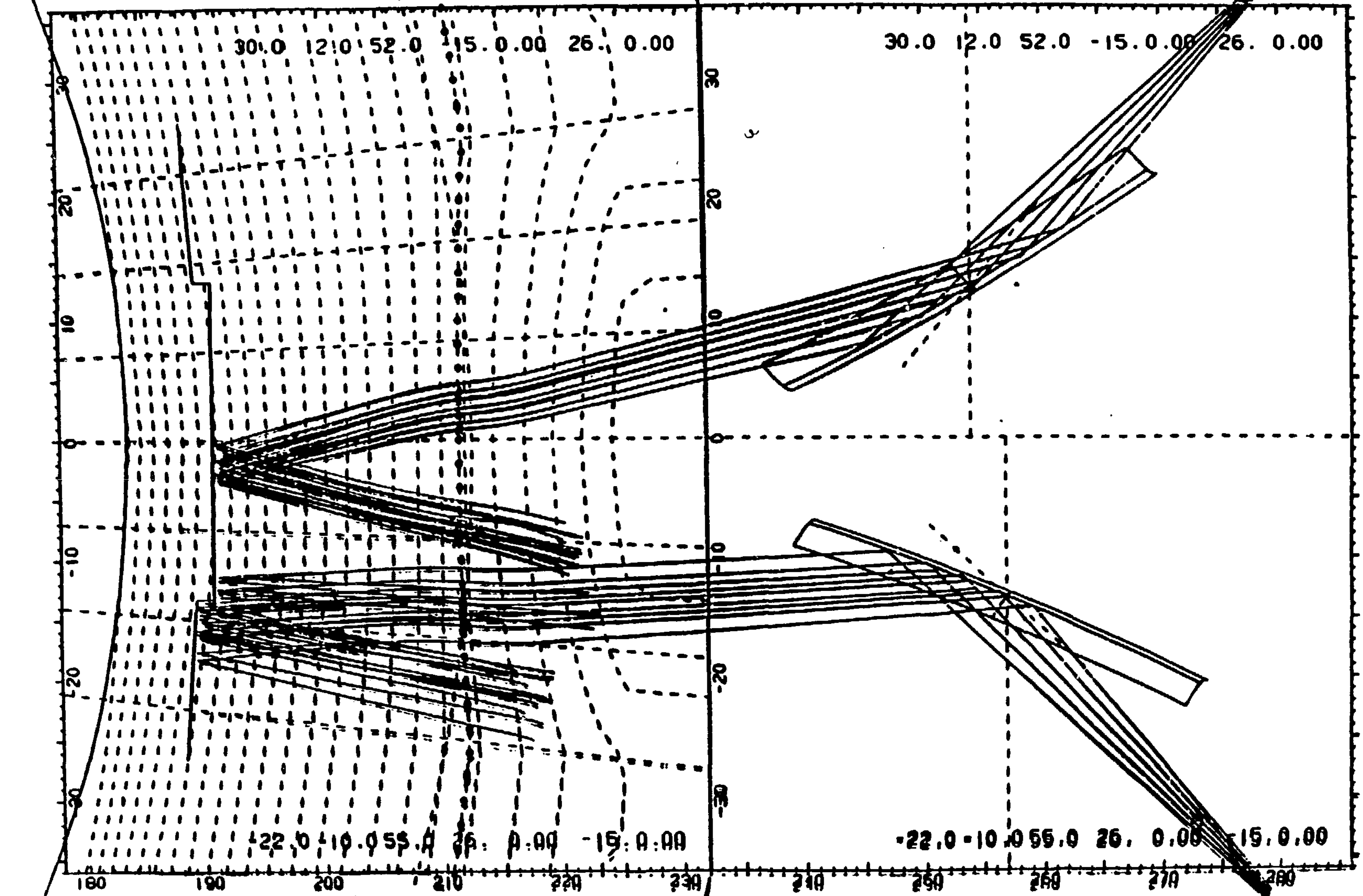

B_0 = 2.7377 TESLA ι_0 = 0.40 Φ = 75 86° ΔB = 500 GAUSS
0-MODE 1.HARMONISCHE f = 70.0 GHZ ω_{pe}^2/ω^2 = 0.909
T_0 = 1000 eV N_e = 5.500 10^{13},

TEMP.-PROF	TH.DICHTE-PR.
4.850	8.970
1.500	1.800
0.000	0.000

$\beta(0)$ = 0.0059 $\bar{\beta}$ = 0.00049 $P_{1...4}$ = 100 110 120 130 kW Absorption 65 %

Effects of E×B drift resonance on Fast Ion Confinement in W7A and Heliotron E

How to avoid falling into Loss Cone

K. Hanatani
PPL, Kyoto Univ.

November 11, 1987
at Oak Ridge

Effects of ExB drift resonance on fast ion confinement
in Wendelstein VII-A and Heliotron E

presented by K. Hanatani

Plasma Physics Laboratory, Kyoto University,
Gokasho, Uji, Kyoto, JAPAN

This paper summarizes recent study on beam-ion confinement in helical systems. Fast neutral beam injection (NBI) in both Wendelstein VII-A and Heliotron E showed effective heating of plasmas /1,2/ even by nearly perpendicular beams. Reasons for the effective heatings in these devices, however, have been considered to be different. In WVII-A, the reason is attributed to the enhanced confinement of beam ions as well as of thermal ions due to the effects of large radial electric field, E_r. In Heliotron E, by contrast, E_r field has been considered to have only small effect on beam ion orbits. We extend previous work on the fast-ion confinement /3,4,5/ and clarify the influence of E_r field.

In order to study the E_r field effects, we have developed an efficient drift orbit solver which works in real space coordinates /6/. To speed up orbit following, we use "field splitting" scheme which decomposes fully 3D filed quantities into helically symmetric and symmetry-braking parts. The E_r filed is calculated from electric potential ϕ which is constant on 3D magnetic surfaces. The orbit solver has been incorporated with Monte Carlo NBI code (HELIOS) /3,4/.

Extensive benchmark tests of Monte Carlo NBI codes have been carried out between (1) ODIN code (IPP, Garching) and HELIOS code (PPL, Kyoto) /7/ and (2) between HELIOS code and DESORBScode (ORNL, Oak Ridge) /8/. The objectives of these benchmark tests are (i) to eliminate possible errors in numerical coding, (ii) to improve physics modeling and (iii) to establish common ground among NBI codes for stellarator/heliotron research.

We interpret NBI experiments on WVII-A and Heliotron E by using the Monte Carlo code including E_r field. We examined how the ExB drift modify the topology of drift orbit. We confirmed numerically that two kinds of ExB drift resonance can exist in toroidal helical device. Under the condition of ExB drift resonances, loss region of fast ion is created in the velocity space because of resonant orbits. It was found that different branch of ExB drift resonance can explain the confinement properties of beam ion in the perpendicular NBI experiments on W7A and Heliotron E /9/.

REFERENCES

/1/ WVII-A Team, NI Group, et al., in Contr. Fusion and Plasma Phys., (Proc. 10th Int. Conf. London 1984) Vol.2, IAEA, Vienna (1985) 371.
/2/ K.Uo, A.Iiyoshi, T.Obiki, et al., ibid. 387.
/3/ K.Hanatani, M.Wakatani and K.Uo, Nucl. Fusion 21 (1981) 1067.
/4/ K.Hanatani, Y.Nakashima, H.Zushi, et al., Nucl. Fusion 25 (1985) 259.
/5/ F.P.Penningsfeld, W.Ott, E Speth, 12th Europ. Conf. (Budapest, 1985) Vol.9F Part1, 397.
/6/ K.Uo et al., IAEA-CN-47/D-I-1, (Kyoto, 1986).
/7/ K.Hanatani, F.P.Penningsfeld, H.Wobig, in Proc. IAEA TCM (Kyoto, 1986).
/8/ R.H.Fowler et al., presentation at this workshop.
/9/ K.Hanatani, F.Sano, Y.Takeiri et al., 14th Europ. Conf. (Madrid), 11D/I (1987).

Code of Ethics for computational physicists

(1) Thou shalt not use a computer program for predicting future experiments

unless

thou art sure that the program can explain existing experiments.

→ Motivation of this Talk

(2) Thou shalt not use a computer program for analizing existing experiments

unless

thou art sure that the program is bug free!

→ Motivation of the Next Talk

Benchmark test.

OUTLINE

① Motivations

② Monte Carlo Code

③ Benchmark tests

④ E×B drift resonance in W7A

⑤ E×B drift resonance in Heliotron E

⑥ Summary

3D NBI CODE

HELIOS

helical Orbit Slowing down Scattering

- Target Plasma
  - 3D vacuum field
- Beam
  - arbitary injection angle
  - beam divergence
- Orbit
  - real space coordinats
  - model field → real field
  - field-splitting scheme
  - E_r field, $\vec{E} = -\nabla\Phi(\psi)$
- Collision
  - slowing down
  - pitch angle scattering
  - energy scattering
- Neutral
  - helical, halo neutral
- CX analizer
  - slowing down spectrum

Benchmark test of NBI codes for Helical Systems

IPP, Garching	PPL, Kyoto	ORNL
ODIN code	HELIOS code	DESORBS code
• Dommaschk potential	• model field	• flux coord. code
FAFNER	• real field Biot-Savart	• real space code

field-splitting scheme

Advantage of real space code

→ can follow orbits outside of flux surface

Field Splitting Scheme : An efficient 3D Interpolation Algorithm

K. Hanatani
PPL Kyoto Univ.

- Motivation
- Basic Idea, Advantages
- Algorithm
- Application
- Efficiency, Accuracy, Convergence
- Generality, Limitation

Field - Splitting Scheme

Decomposition

$\vec{A}, \vec{B}, \vec{V}_D \ldots$ by e.g. Biot Savart Law

any quantity	Principal part	Residual part

$$Q = P + R$$

fully 3D Asymmetric 3D	nearby Symmetry 2D	Symmetry breaking part 3D
toroidal + helical	helical invariant	toroidal perturbation
(r, θ, ϕ)	$(r, \theta - \chi\phi)$	(r, θ, ϕ)
	Short wave length	long wave length

TWO-LEVEL INTERPOLATION

	Bicubic Spline	trilinear interpolation

IPP-CRAY KIH989 2 C2-03 12.08.86 20:31:38

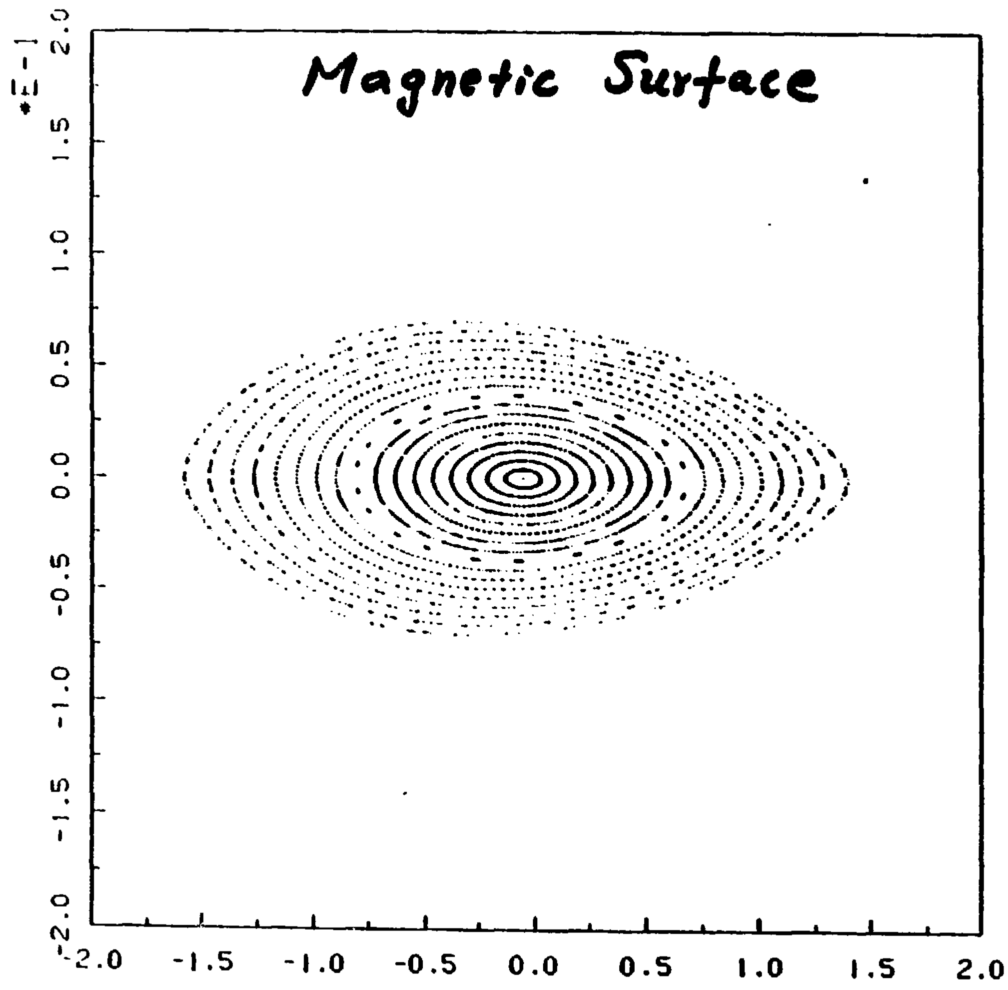

W7A (N+)

$\iota \approx 0.5$

RKAPA = 2.5
R = 2.000
RA = 0.230
BAXIS = 3.200
ALPHA = 40.000
BETA = 0.000
GAMMA = 0.288

8

IPP-CRAY KIH201 2 C2-03 19.08.86 15:04:32

E field

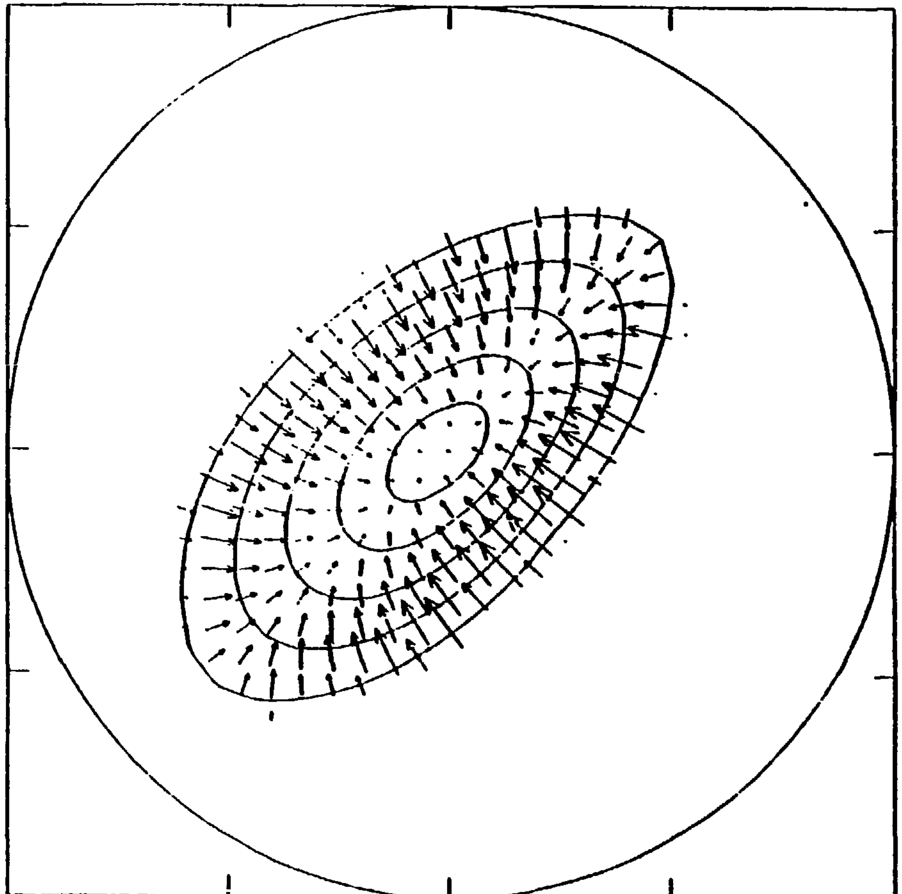

W7A (N+)

RKAPA = 2.5
R = 2.000
RA = 0.230
BAXIS = 3.200
ALPHA = 40.000
BETA = 0.000
GAMMA = 0.288

IPP-CRAY KIH201 3 C2-03 19.08.86 15:04:33

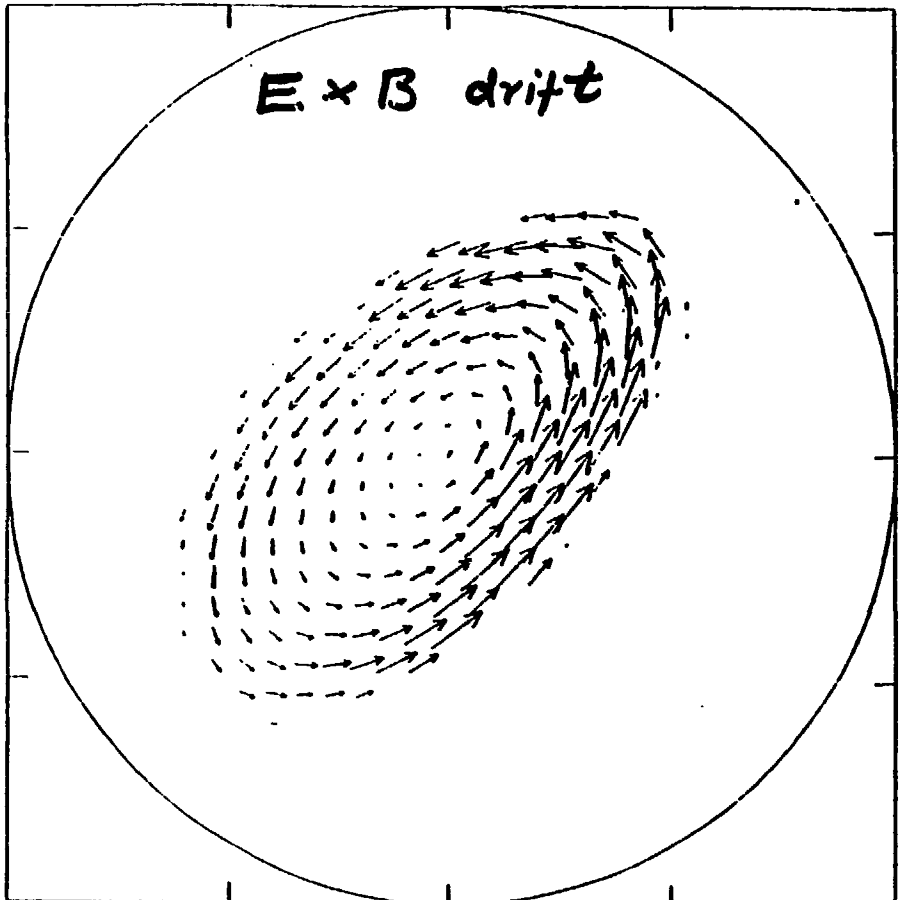

W7A (N+)

RKAPA = 2.5
R = 2.000
RA = 0.230
BAXIS = 3.200
ALPHA = 40.000
BETA = 0.000
GAMMA = 0.200

IPP-CRAY KIH203 3 C2-03 19.08.86 15:05:58

$\vec{G}(\vec{x})$: Drift

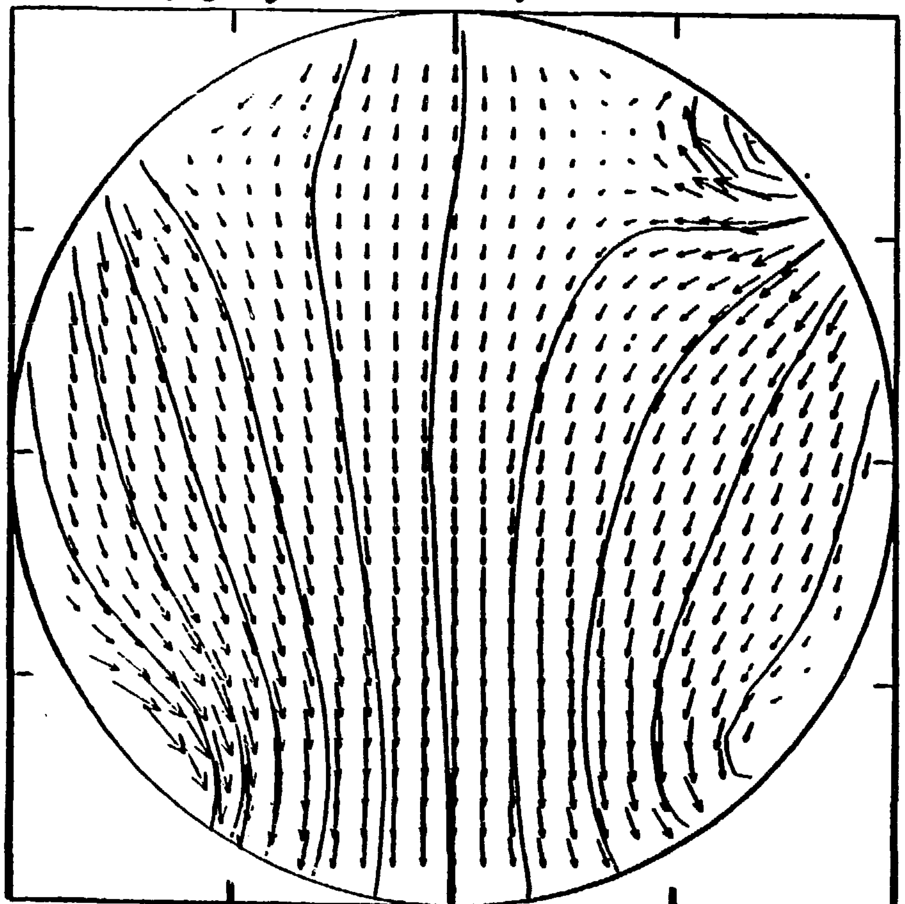

W7A (N+)

RKAPA = 2.5
R = 2.000
RA = 0.220
BAXIS = 3.200
ALPHA = 40.000
BETA = 0.000
GAMMA = 0.280

III

IPP-CRAY KIH202 5 C2-03 19.08.86 15:05:59

$\vec{G}^{(0)}(\vec{x})$: Drift, Hellically Symmetric Part

W7A (N+)

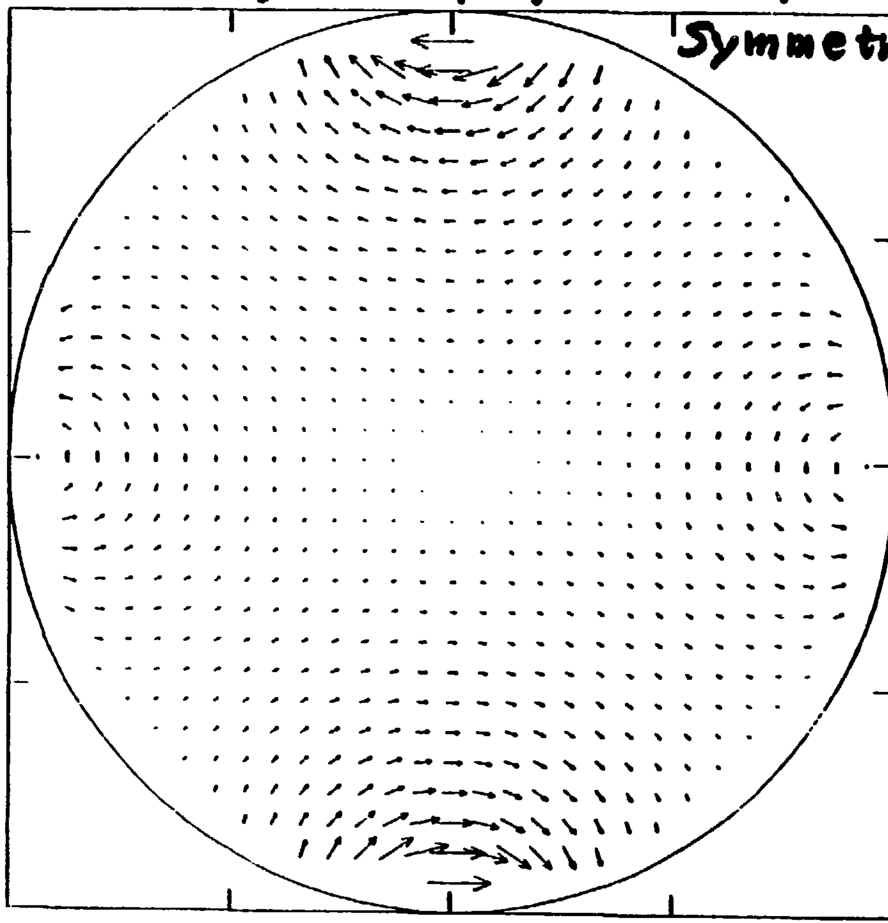

RKAPA = 2.5
R = 2.000
RA = 0.230
BAXIS = 3.200
ALPHA = 40.000
BETA = 0.000
GAMMA = 0.280

(-ARROW-) : HELICAL DRIFT BH

12

IPP-CRAY KIH202 7 C2-03 19.08.86 15:06:00

$\vec{G}^{(1)}(\vec{x})$: Drift, Symmetry-Breaking Part

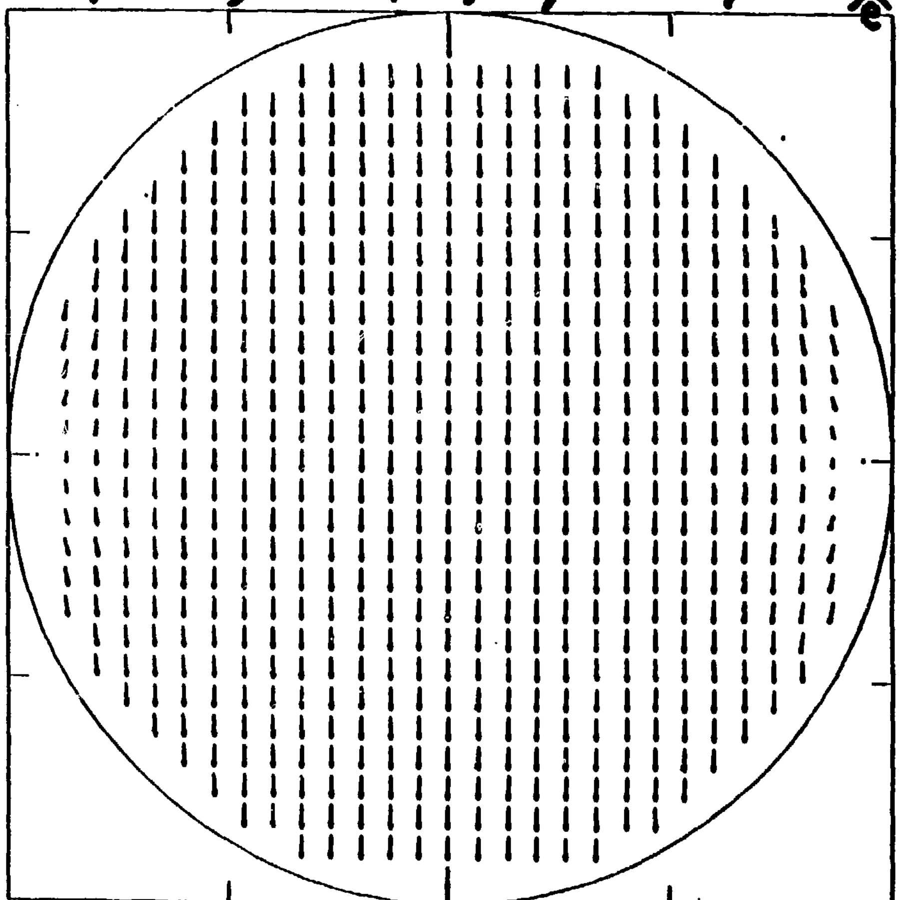

W7A (N+)

RKAPA = 2.5
R = 2.000
RA = 0.230
BAXIS = 3.200
ALPHA = 40.000
BETA = 0.000
GAMMA = 0.280

Nearly Perpendicular Neutral Injection in W7A

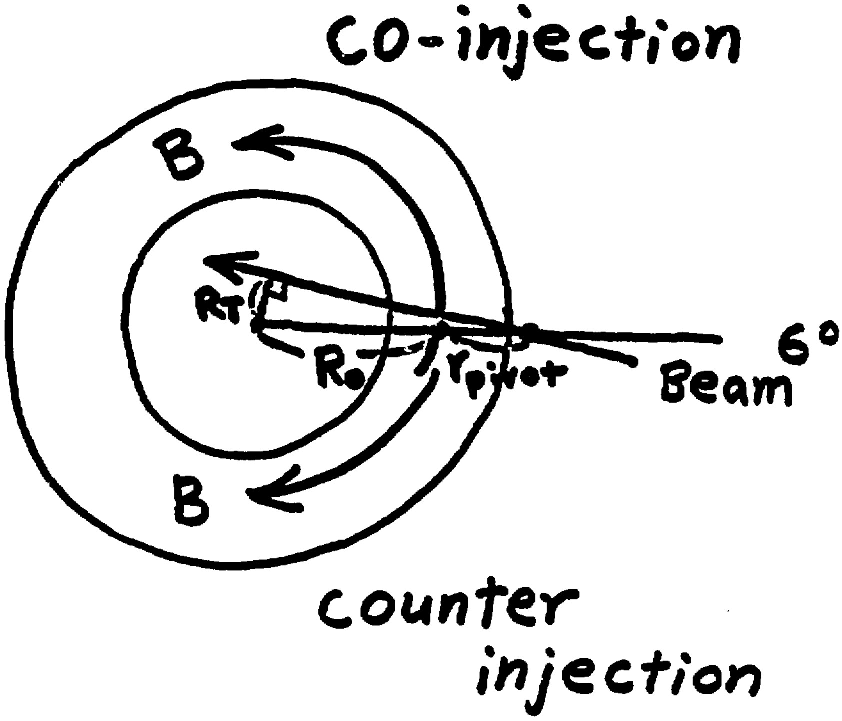

$$\frac{v_{\parallel}}{v} = \frac{R_T}{R} \simeq \frac{(R_o + r_{pivot})\sin\alpha}{R_o}$$

$$\alpha = 6°$$

$$\boxed{\frac{v_{\parallel}}{v} \cong \pm 0.1}$$

the OH current by which the target plasma was produced in a toroidal magnetic field of 3.2 T with a total transform of ι = 0.43 (co) and ι = 0.44 (counter). The plasma current was lowered until t = 130 ms (Fig. 3a) and three neutral beams were switched on, one after the other. The total neutral powers were 760 kW ("co") and 730 kW ("counter") (Fig. 3b). The line density (Fig. 3c) developed similarly in the two cases. In the "co"-discharge, gas puffing was stronger, and therefore the density rose faster. The total plasma energy (Fig. 3d) was already higher in the "counter"-discharge at the beginning and it stayed higher. The radiation (Fig. 3e) developed similarly, becoming stro

15

$\eta_{co} \approx \eta_{counter}$

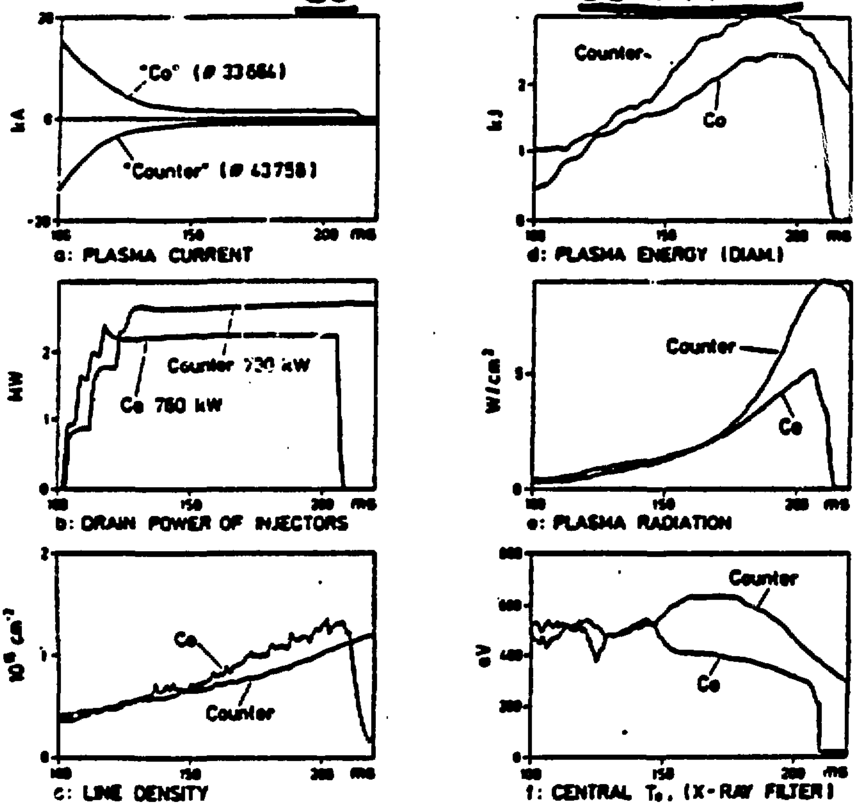

Fig. 3 Comparison of two typical discharges, one with co-injection, the other with counter-injection

W7A TEAM and NI TEAM
4th International Symposium
Roma, 1984

Fast Ion Confinement in W7A

—— already known ——

1. Nearly perpendicular neutral injection in W7A showed experimental heating efficiency higher than that predicted by orbit following Monte Carlo calculations without E_r field.

2. Doppler shift measurement of impurity line emission in NI discharges showed large polidal rotation of plasma, indicating the presence of radial electric potential of $|\phi| \simeq (2-4)\,kV$.

3. ODIN code, when it included E_r field, showed improvement of heating efficiency.
   ⟶ consistent with W7A experiment.

TION /Co
$\Phi \propto r^2$

'iles for a set
ential surfaces
abolic)

field
red by
method

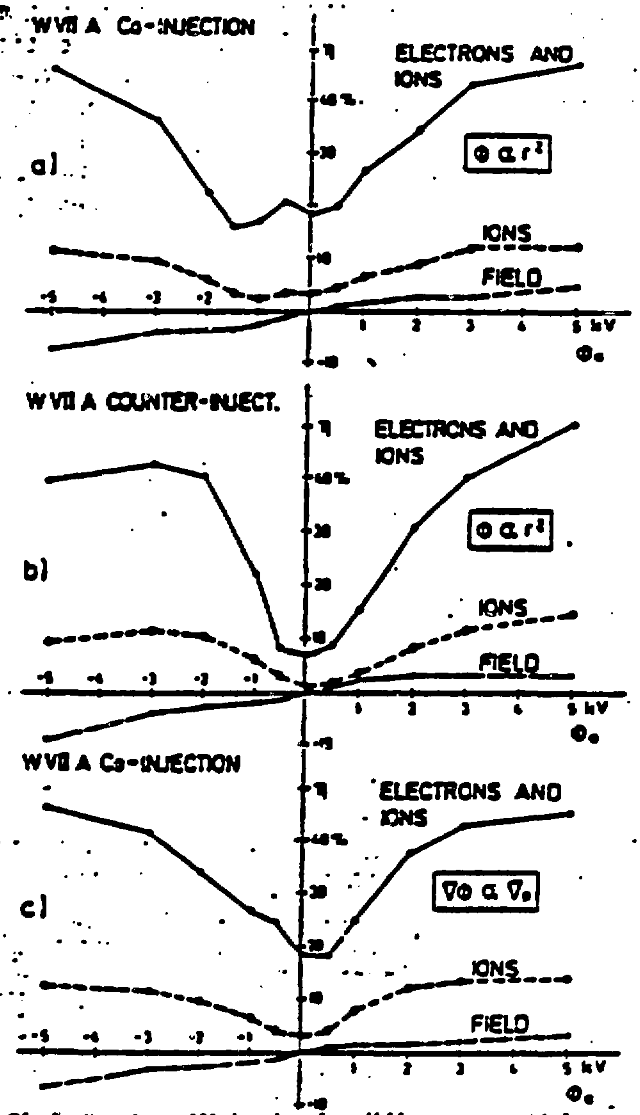

Fig.5: Heating efficiencies for different potentials as calculated by the new version of ODIN for shot Nr. 38000 at 180 ms

W VII A / Co-INJECTION $\Phi \propto r^2$

F (cm^2)

HANATANI 87-11-06 20:17:22 1 5

EOINJ = 27000.0
R = 2.0
AP = 0.0837
IOTA = 0.43
B = 3.2

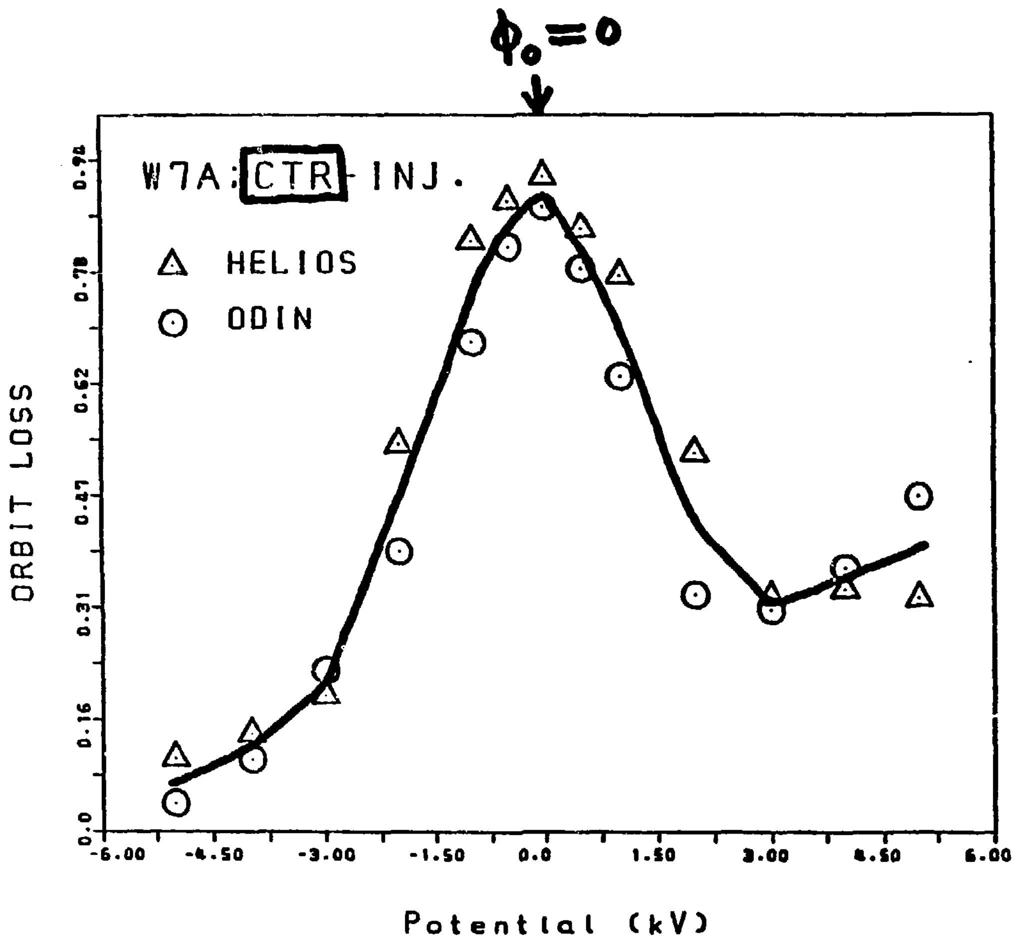

18

HANATANI 87-11-06 20:17:21 0 3

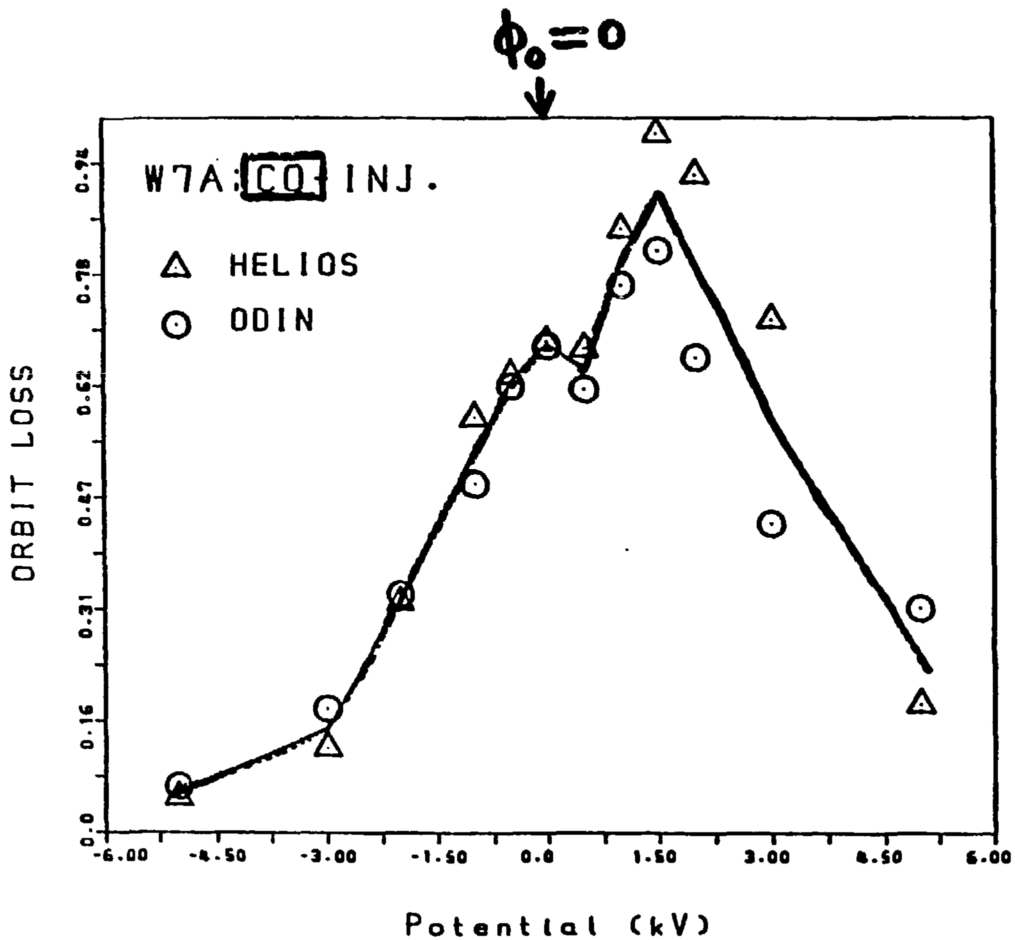

HANATANI 87-11-06 20:17:22 1 5

EOINJ = 27000.0
R = 2.0
AP = 0.0837
IOTA = 0.43
B = 3.2

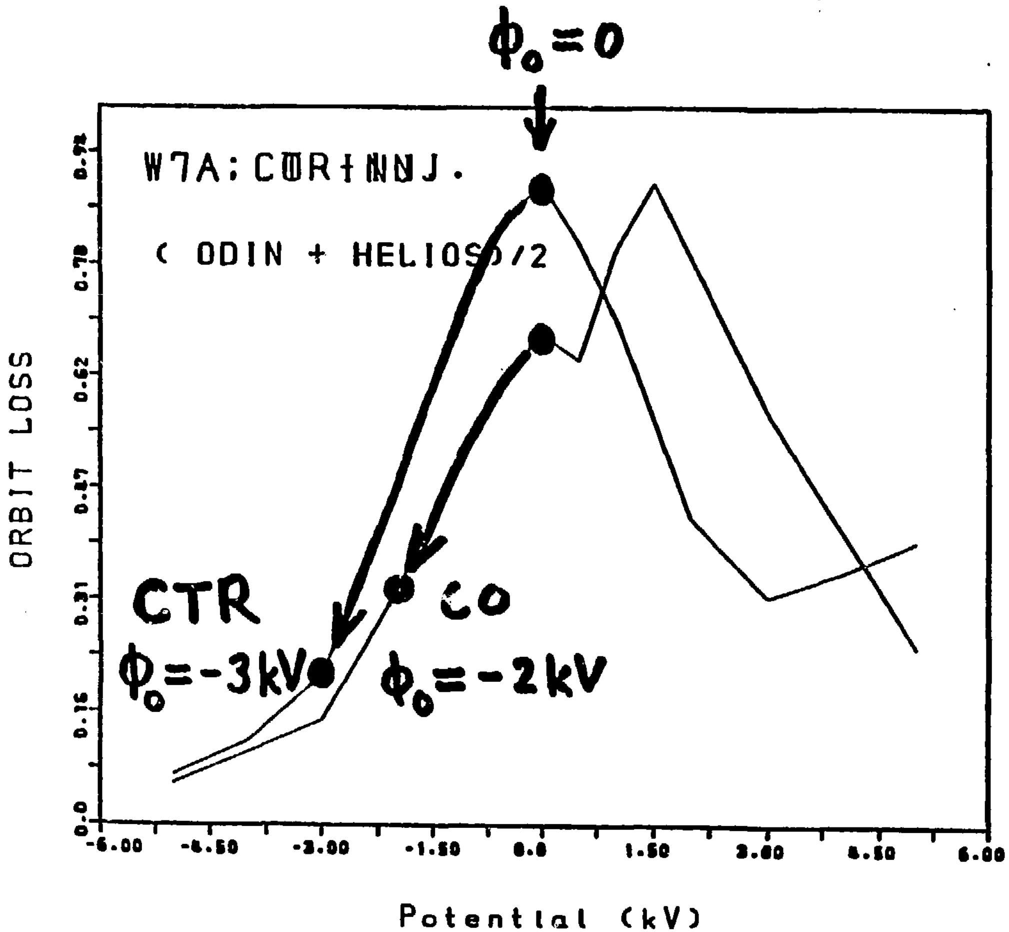

- The presence and the Influence of E_r field in W7A are already basically understood.

→ Both transport of thermal ion and confinement of fast ion are improved.

- However, there are several points need to be clarified.

(about the confinement of fast ions)

Fast ion confinement in W7A

— Points need to be clarified —

① How can the "small" electric potential $\left|\frac{q\phi_0}{E_0}\right| \simeq 0.1$ improve the confinement of perpendiculary injected fast ions ?

→ cf. thermal ions $\left|\frac{q\phi_0}{T_i}\right| \simeq 2-3$.

② How large is the loss of fast ions due to trapping in helical ripples ?

→ WORKING HYPOTHESIS :

Fat banana orbits (not helically trapped orbits) are mainly responsible for the loss of beam ions in W7A.

- $\epsilon_h \ll \epsilon_t$
- large poloidal larmor radius
- cf. transport of electrons and thermal ions

Fast ion confinement in W7A

—— points need to be clarified (continued) ——

③ Why counter-injection was as efficient as co-injection ?

$$\eta_{counter} \approx \eta_{co}$$

④ Which sign of potential ϕ (+ or −) is appropriate for NI heated W7A plasmas ?

→ polarity of ϕ is important because it is related to the origin of ϕ.

→ cf. thermal ion transport.

⑤ Can we generalize the improved confinement of fast ions to other helical systems ?

→ peculiarity of W7A?

→ How about in HE, ATF, W7AS ?

Parameters of W7A Stellarator

$R = 2$ [m]

$a_p = 0.1$ [m]

$B = 3.2$ [T]

$\iota = \frac{R}{r}\frac{B_\theta}{B_\phi} \simeq \frac{R}{a_p}\frac{B_{\theta,a}}{B_\phi} = 0.5$

$E_0 = 27$ keV

$E_0/2 = 13.5$ keV

$E_0/3 = 9$ keV

$T_i \approx 1$ keV

Poloidal Larmor Radius

→ measure of banana width

$$\rho_\theta \equiv \frac{mv}{qB_\theta} = \frac{\sqrt{2mW}}{qB_\theta} \qquad \rho \equiv \frac{mv}{qB}$$

$$W = \frac{1}{2}mv^2$$

$$\rho_\theta\,[\mathrm{m}] = \Big(\underbrace{\iota\cdot\frac{a_p}{R}}_{\simeq 40}\Big)^{-1}\cdot\rho \cong 4.59\times10^{-3}\left(\iota\frac{a_p}{R}\right)^{-1} \times \frac{\sqrt{AW\,[\mathrm{eV}]}}{B_\phi\,[\mathrm{T}]}$$

	W [keV]	$\rho_{i,\theta}$ [m]	$\rho_{i,\theta}/a_p$	
E_0	27	0.298	2.98	large banana
$E_0/2$	13.5	0.211	2.11	
$E_0/3$	9	0.172	1.72	
$\frac{3}{2}T_i$	1.5	0.070	0.70	

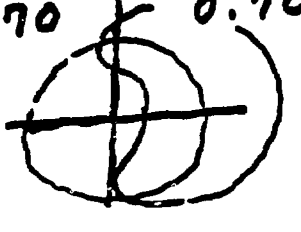

25

W7A TEAM and NI TEAM
4th International Symposium on
Heating in toroidal Plasmas, Roma
1984

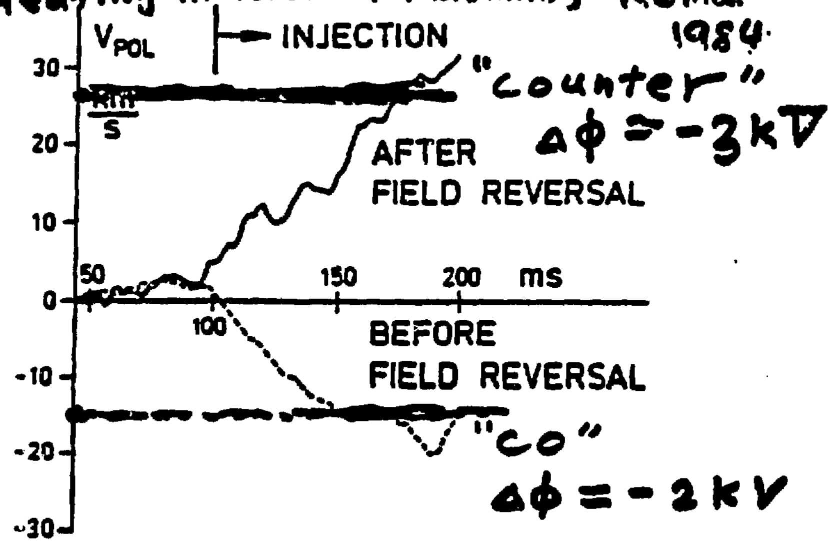

Fig. 5 Observed poloidal drift velocity of the plasma at r = 6.5 cm versus time. Comparison of a co- and a counter-discharge

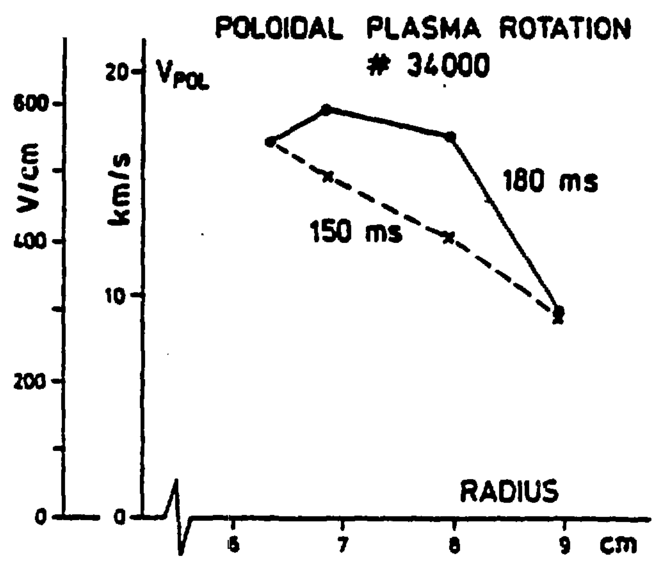

Fig. 6 Observed poloidal drift velocity (and the corresponding electric field strength) versus radius

Estimation of Potential Drop from the Doppler shift measurement

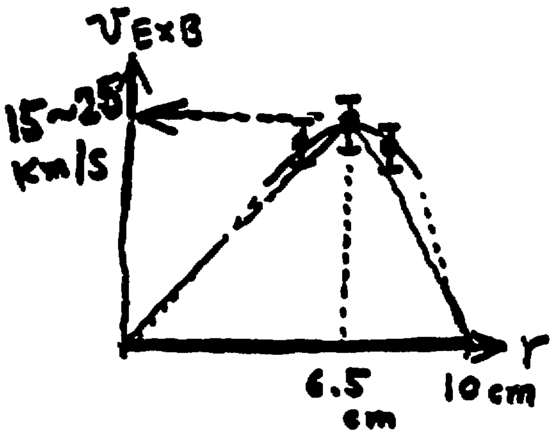

$$v_{E\times B} = \frac{|\vec{E}\times\vec{B}|}{B^2} = \frac{E_r}{B}$$

$$E_r = B \cdot v_{E\times B}$$

$B = 3.2$ T

$a_p = 0.1$ m

$$\phi \simeq \frac{1}{2} a_p \cdot (E_r)_{max}$$

$$= \frac{1}{2} a_p \cdot B \cdot (v_{E\times B})_{max}$$

$$= 0.16 \times (15 \sim 25) \times 10^3 \ \underline{\text{Volt}}$$

$$\phi = (2.4 \sim 4.0) \ \underline{\text{kV}}$$

In this work, we consider

$\phi_0 = -2$ kV for <u>co-injection</u>

$\phi_0 = -3$ kV for <u>counter-injection</u>

as the typical values of potential

$$\left|\frac{q\phi_0}{T_i}\right| \simeq 2-3 \longleftrightarrow \left|\frac{q\phi_0}{E_0}\right| \simeq 0.07 \sim 0.11$$

$$\left|\frac{q\phi_0}{E_0/2}\right| \simeq 0.15 \sim 0.22$$

$$\left|\frac{q\phi_0}{E_0/3}\right| \simeq 0.22 \sim 0.33$$

$$\boxed{\begin{array}{l} T_i \simeq 1 \text{ keV} \\ E_0 = 27 \text{ keV} \end{array}}$$

Logical Structure of this Work

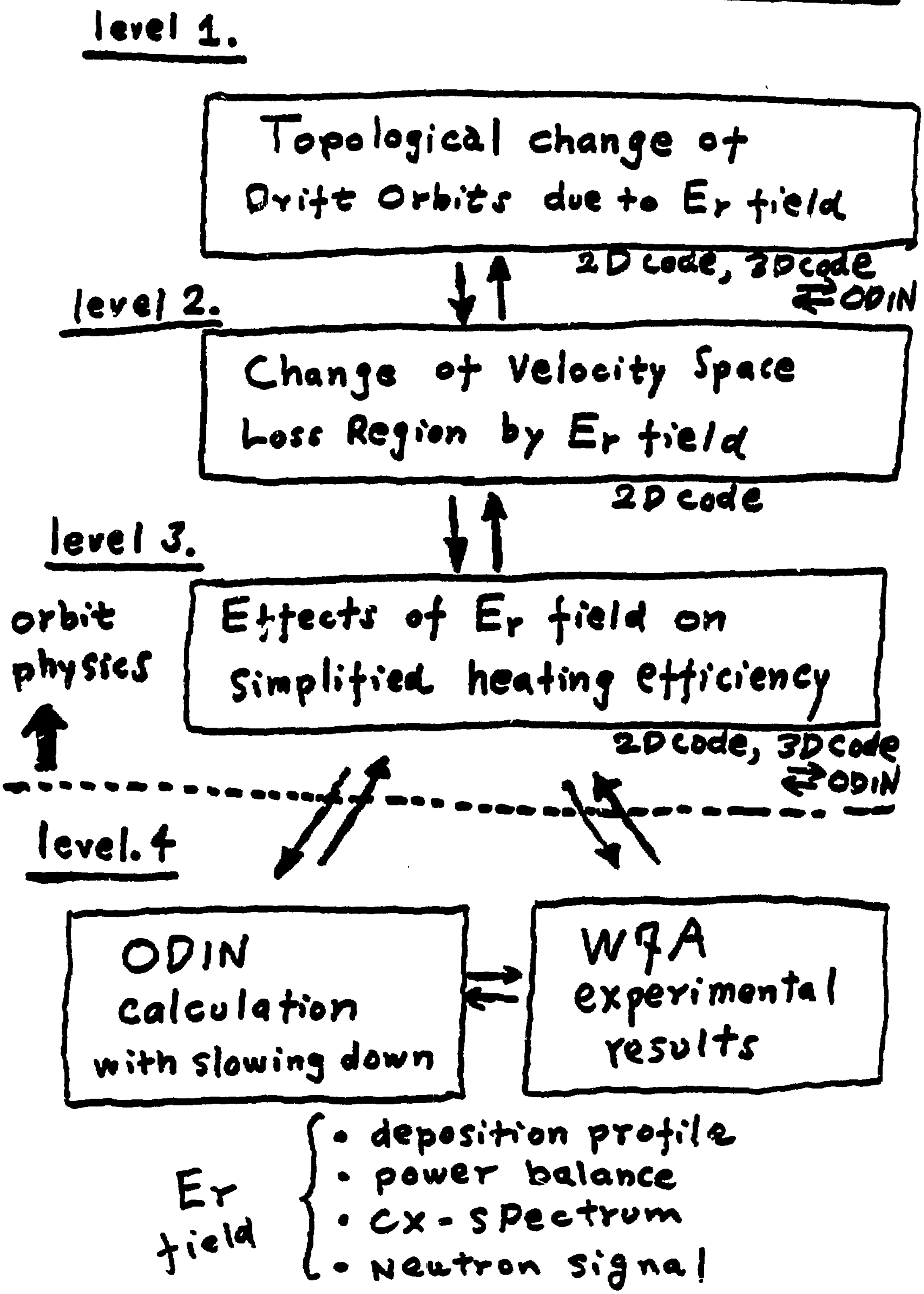

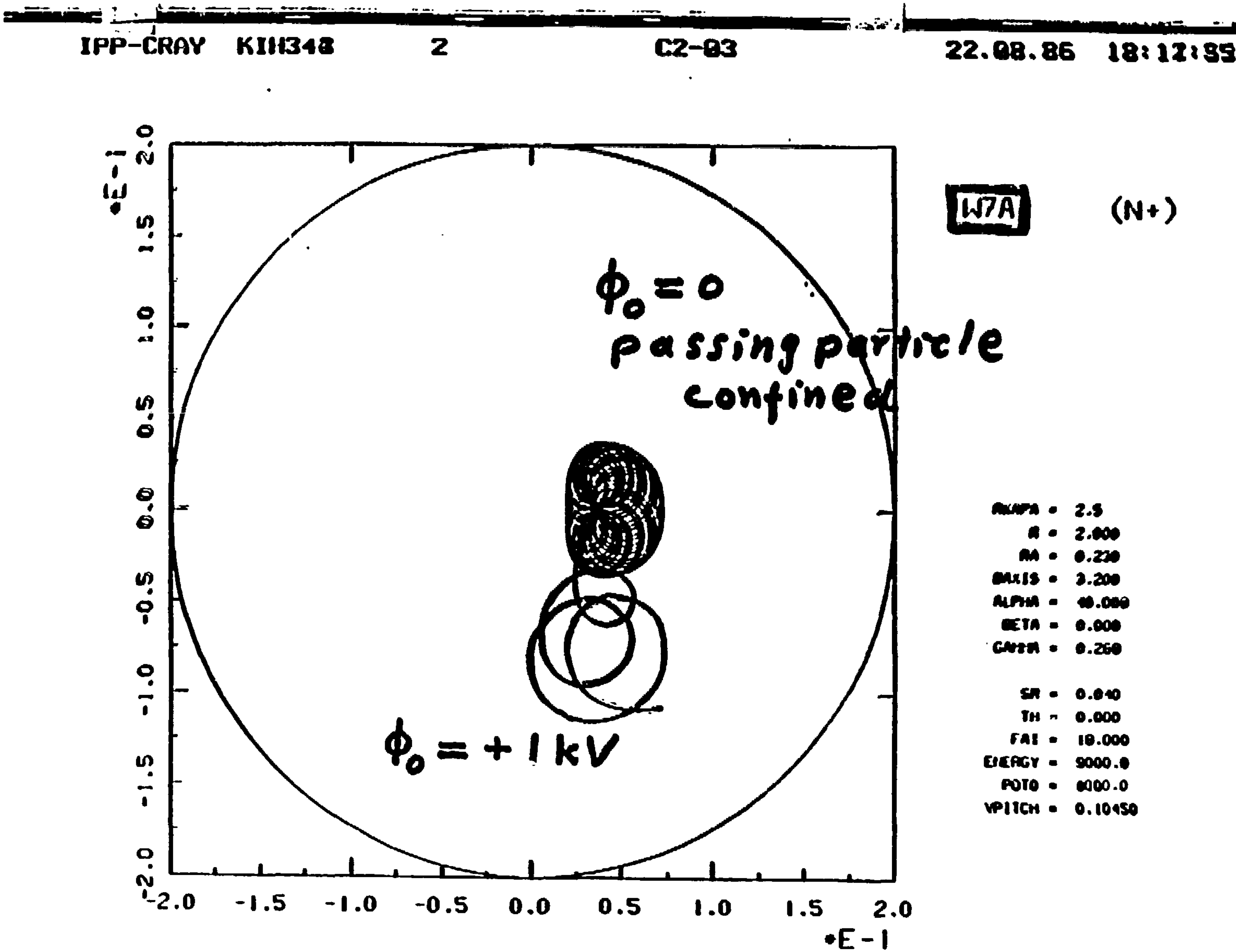
IPP-CRAY KIH348 2 C2-03 22.08.86 18:12:55
W7A
(N+)
$\phi_o = 0$
passing particle
confined
$\phi_o = +1 kV$
*E-1
-2.0 -1.5 -1.0 -0.5 0.0 0.5 1.0 1.5 2.0
*E-1
RKAPA = 2.5
R = 2.000
RA = 0.230
BAXIS = 3.200
ALPHA = 40.000
BETA = 0.000
GAMMA = 0.260
SR = 0.040
TH = 0.000
FAI = 10.000
ENERGY = 9000.0
POTO = 8000.0
VPITCH = 0.10450

IPP-CRAY KIH35D 2 C2-03 22.08.85 18:29:52

W7A (N+)

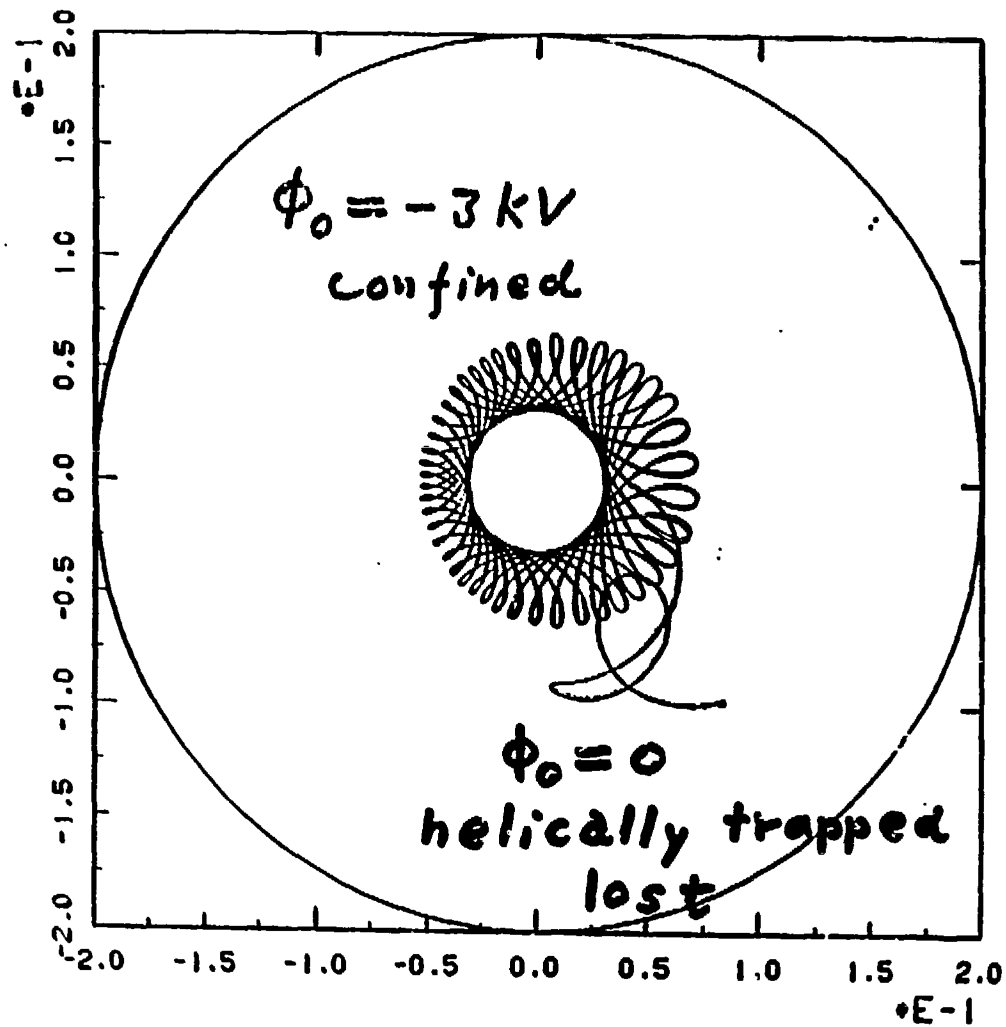

RKAPA = 2.5
R = 2.000
RA = 0.230
BAXIS = 3.200
ALPHA = 40.000
BETA = 0.000
GAMMA = 0.200

SR = 0.040
TH = 0.000
FAI = 18.000
ENERGY = 9000.0
POT0 = -3000.0
VPITCH = -0.10450

Charged Particle Confinement in toroidally-helical field

— without E_r field —

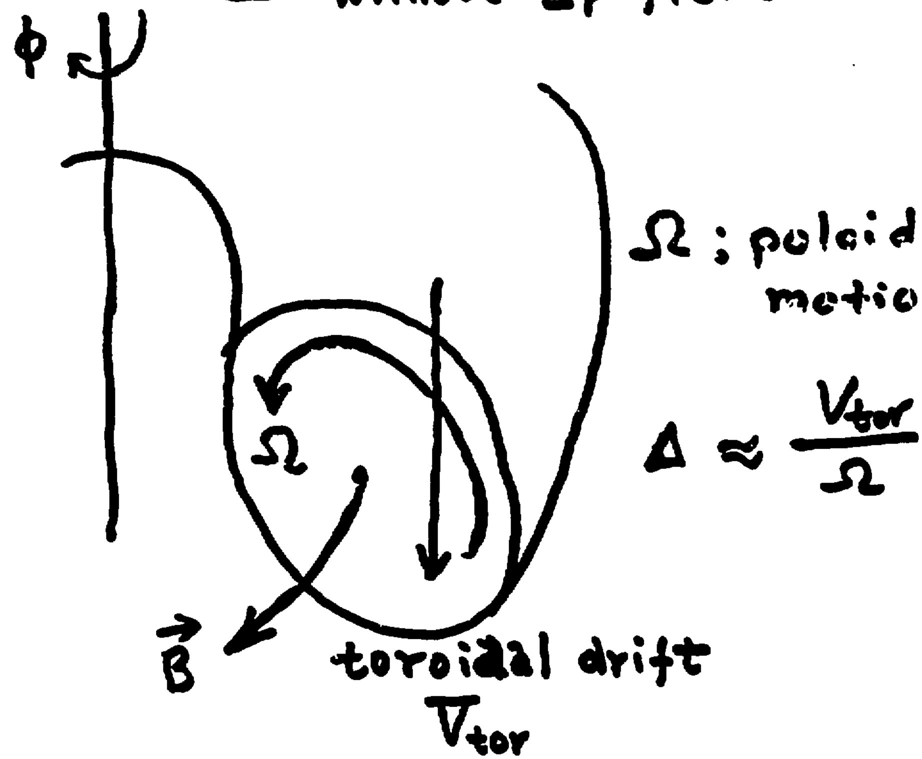

① Rotational Transform, $\Omega_{t} = \frac{\iota\, v_{\parallel}}{R}$

→ confinement of
passing particle
toroidally-trapped particle

② ∇B drift due to helical Ripple

→ confinement of Ω_h
helically-trapped particle

—— with E_r field ——

$E \times B$ drift resonances can occur

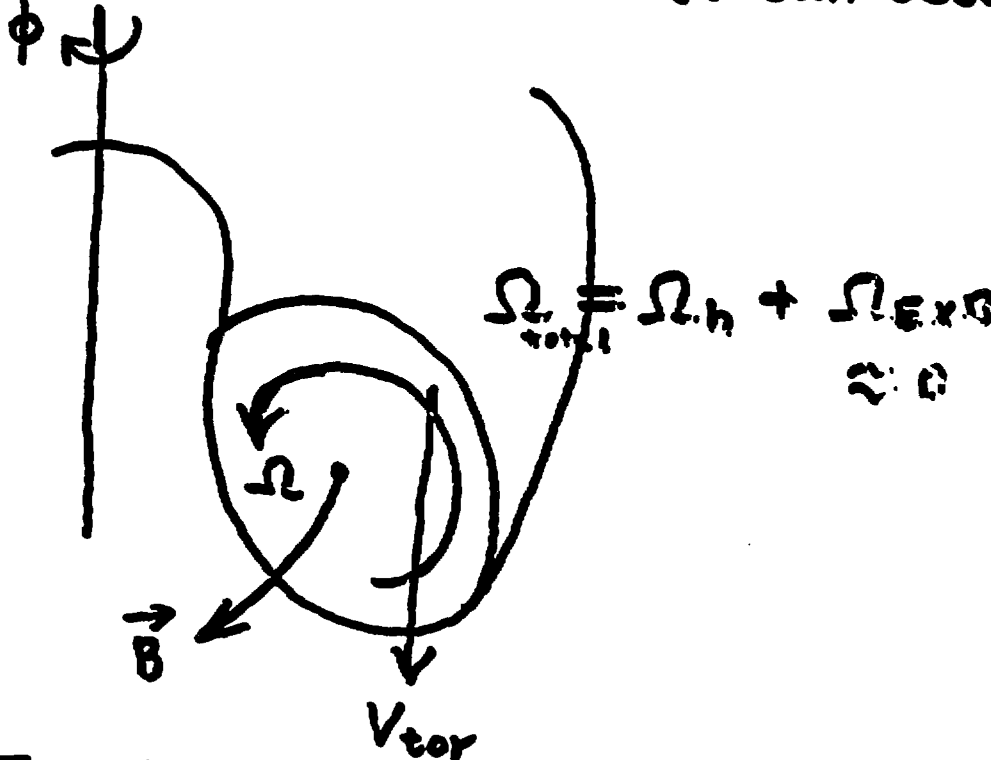

Two types of RESONANCE

① $\boxed{\text{HELICAL RESONANCE}}$

→ Helically-trapped particle
$E \times B$ drift resonates with
$\vec{B} \times \nabla B$ drift due to helical
<u>resonant super banana</u> ripple.

② $\boxed{\text{TOROIDAL RESONANCE}}$

→ passing particle
$E \times B$ drift resonates with
Rotational transform.

<u>resonant banana</u>

$E \times B$ drift Resonance

$\downarrow$

Prompt Orbit Loss

due to resonant orbits

① **W7A Stellarator**

TOROIDAL RESONANCE

$$v_{\parallel} \frac{\iota}{R} + \Omega_{E \times B} \approx 0$$

resonant banana orbit

Hanatani, Pennigsfeld, Wobig
IAEA TCM (Kyoto, 1986)

② **HELIOTRON-E**

HELICAL RESONANCE

$$\Omega_{\nabla B} + \Omega_{E \times B} \approx 0$$

resonant superbanana orbit

Hanatani et al, EPS (Madrid) 1987

Resonant Orbits create Loss Cone

IPP-CRAY KIH984 2 C2-03 15.09.86 12:42:41

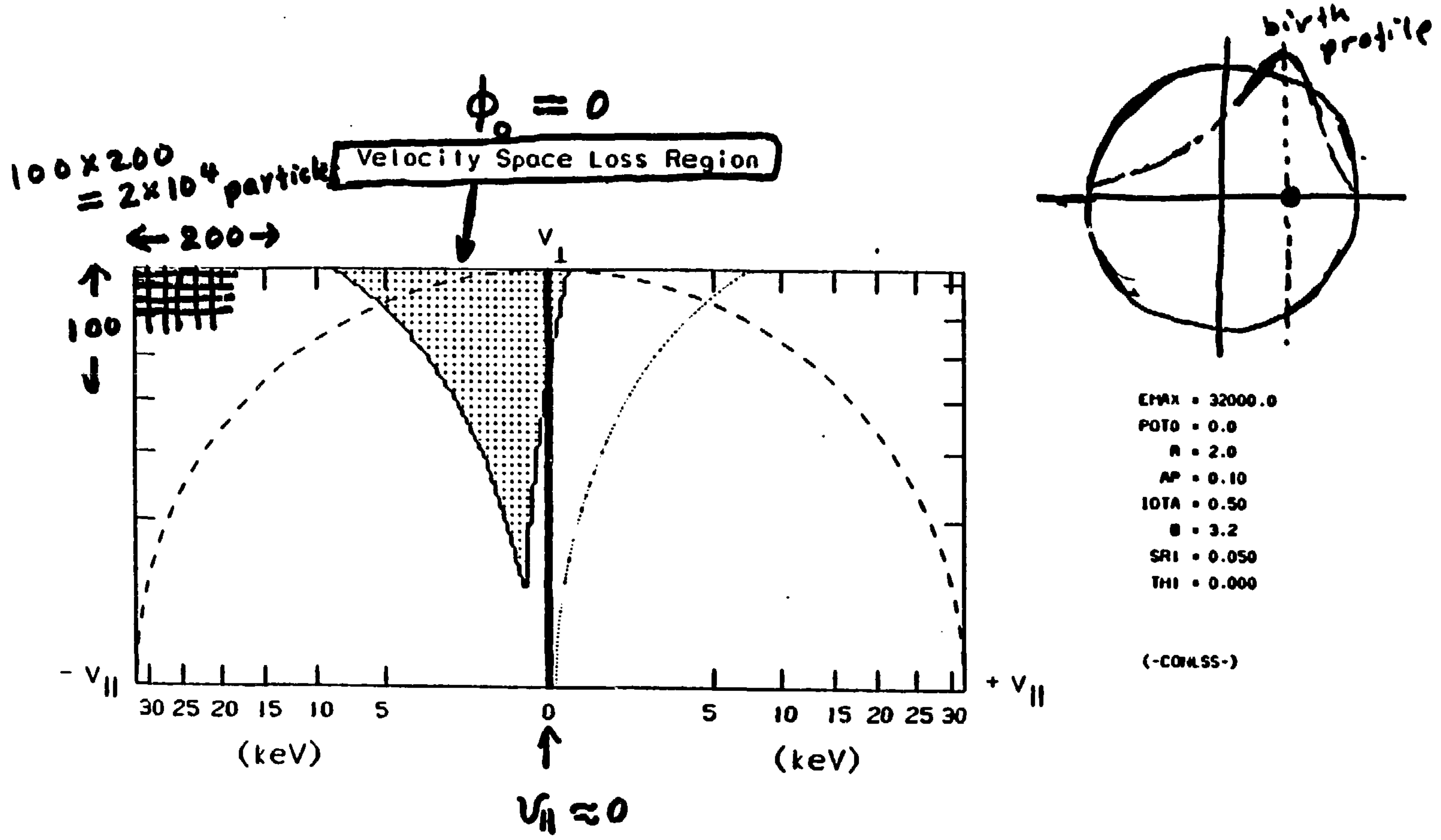

IPP-CRAY KIH104 17 C2-03 19.09.86 13:19:04

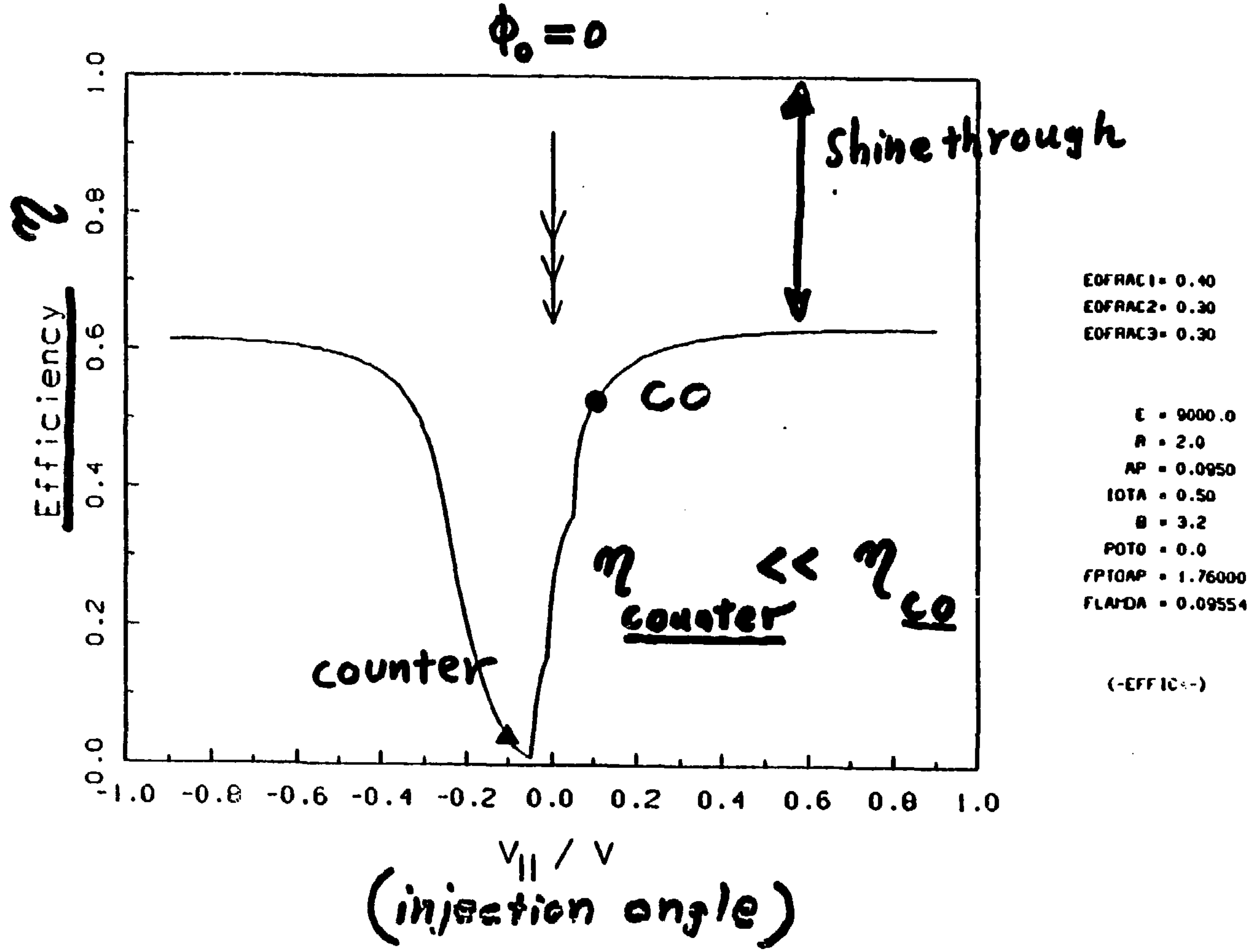

34

IPP-CRAY KIH984 7 C2-03 15.09.86 12:44:55

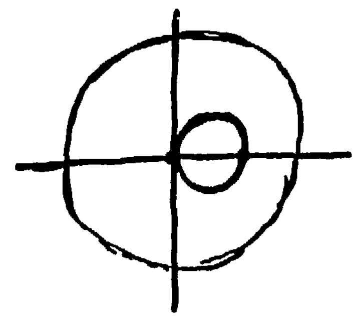

$\phi_0 = -3\,kV$

Velocity Space Loss Region

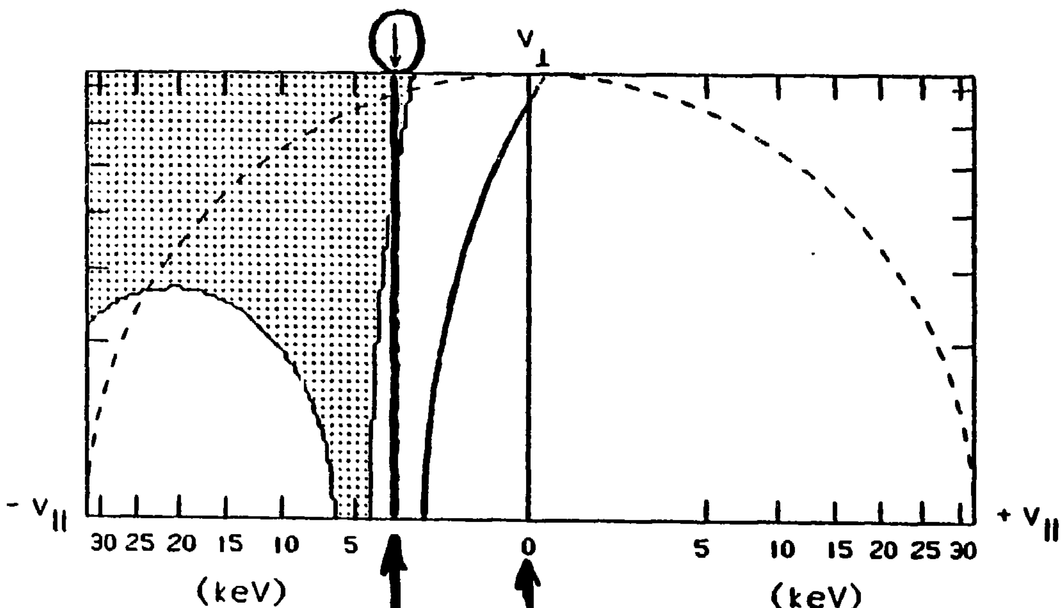

EMAX = 32000.0
POTO = -3000.0
R = 2.0
AP = 0.10
IOTA = 0.50
B = 3.2
SRI = 0.050
THI = 0.000

(-CONLSS-)

$\Omega_t \approx 0$

$\Omega_t + \Omega_{E\times B} \approx 0$

TOROIDAL RESONANCE

35

IPP-CRAY KIH104 21 C2-03 19.09.86 13:20:01

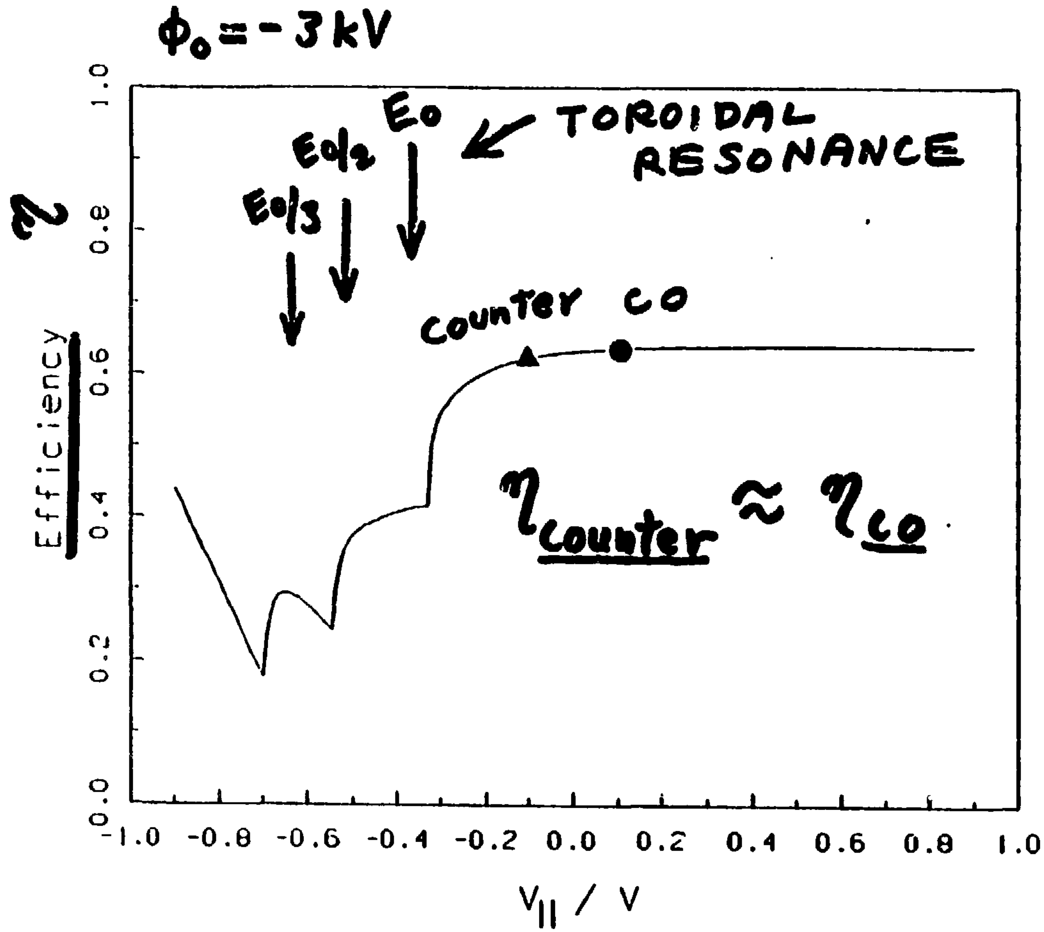

EOFRAC1 = 0.40
EOFRAC2 = 0.30
EOFRAC3 = 0.30

E = 9000.0
R = 2.0
AP = 0.0950
IOTA = 0.50
B = 3.2
POTO = -3000.0
FPTOAP = 1.76000
FLAMDA = 0.09554

(-EFFIC--)

IPP-CRAY KIH984 6 C2-03 15.09.86 12:44:39

$\phi_0 = +2\ kV$

Velocity Space Loss Region

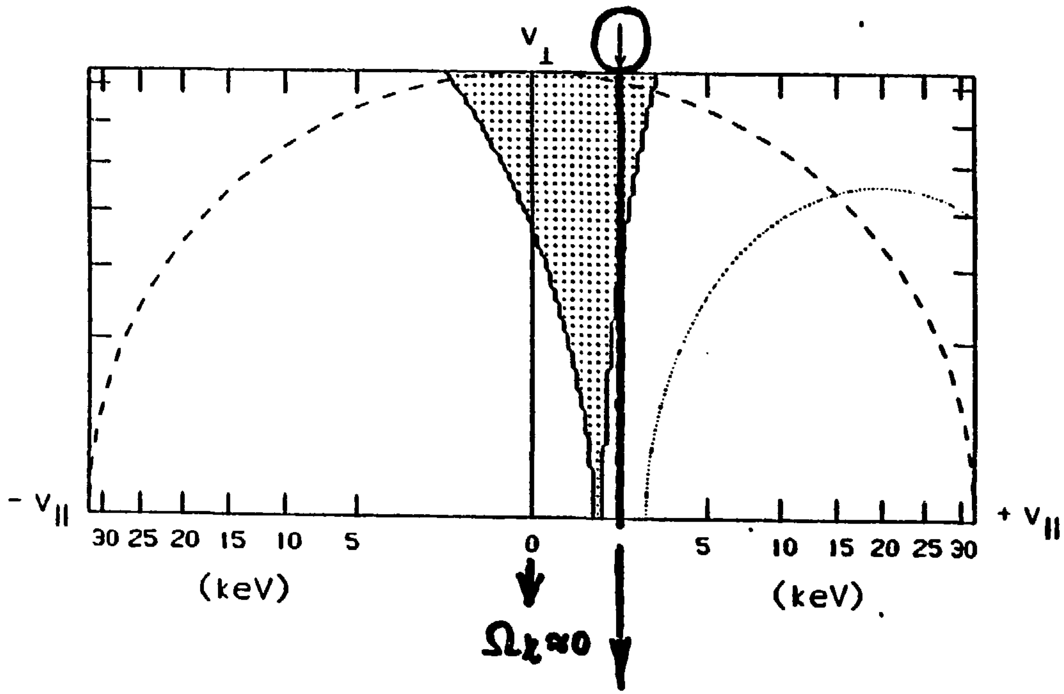

EMAX = 32000.0
POTO = 2000.0
R = 2.0
AP = 0.10
IOTA = 0.50
B = 3.2
SR1 = 0.050
THI = 0.000

(-CONLSS-)

IPP-CRAY KIH104 13 C2-03 19.09.86 13:18:27

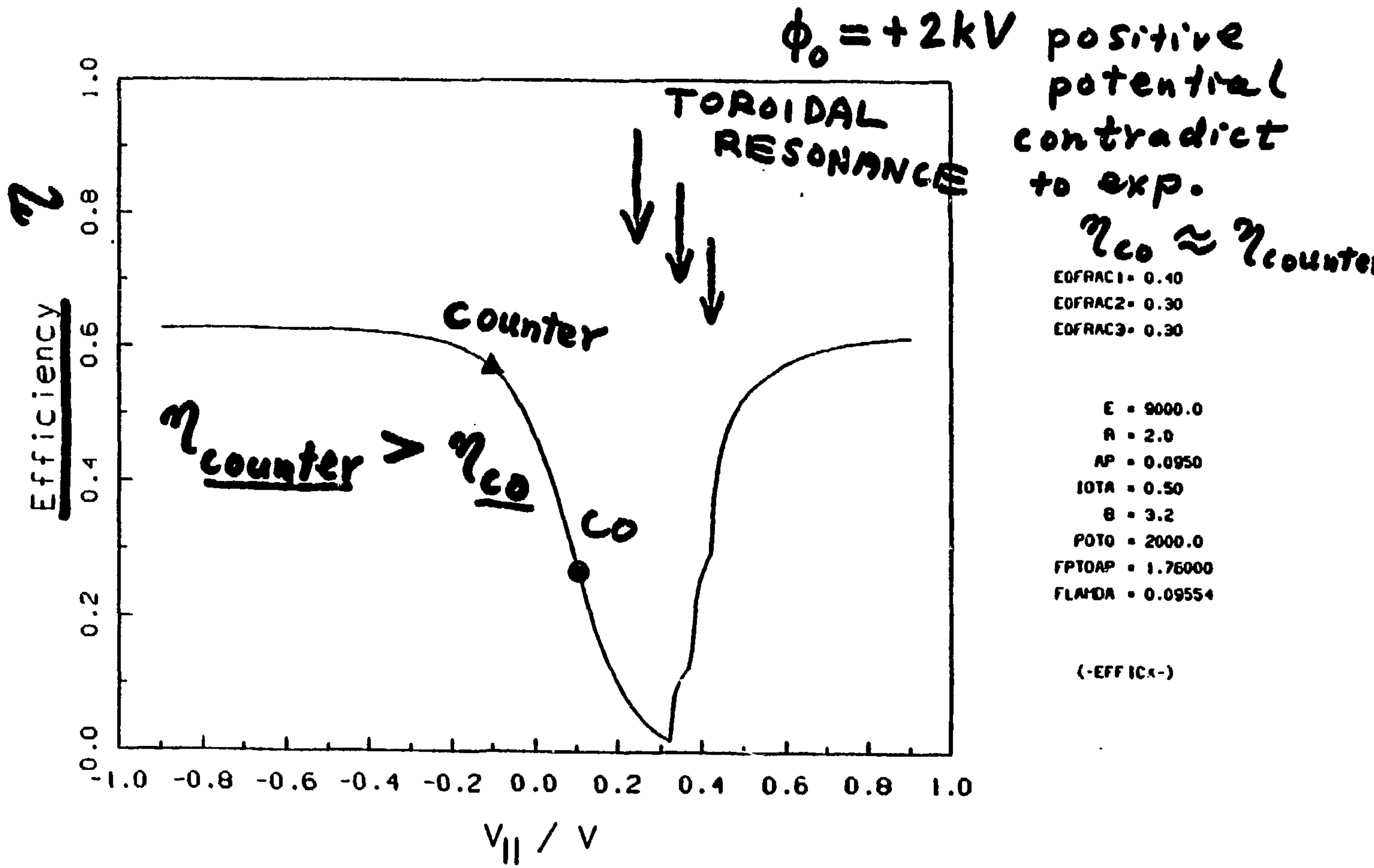

IPP-CRAY KIH124 2 C2-03 22.09.86 10:40:54

Potential dependence

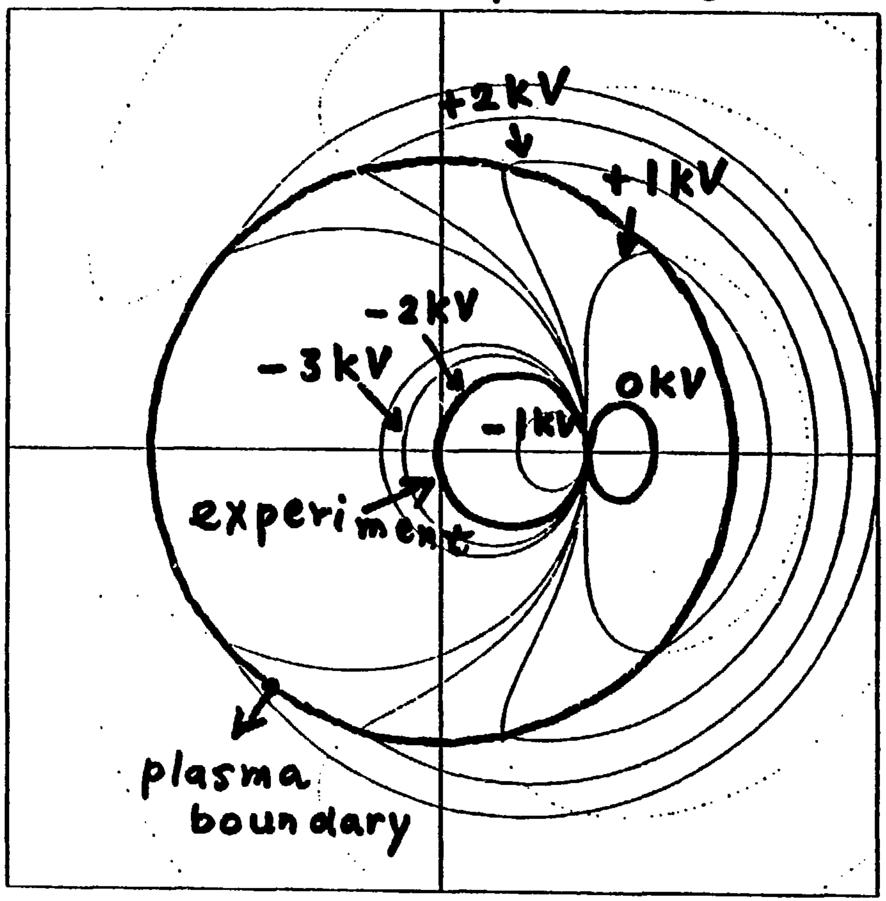

$$\frac{v_{\parallel}}{v} = +0.1$$

"co"

$$E = 27\ keV$$

(-ORBIT3-)
POTO SCAN

ENERGY = 27000.0
R = 2.0
AP = 0.1000
IOTA = 0.50
B = 3.2

Positive potential
deteriorate
confinement

PIT1 = 0.1

59

IPP-CRAY KIH125 2 C2-03 22.09.86 10:43:11

Potential dependence

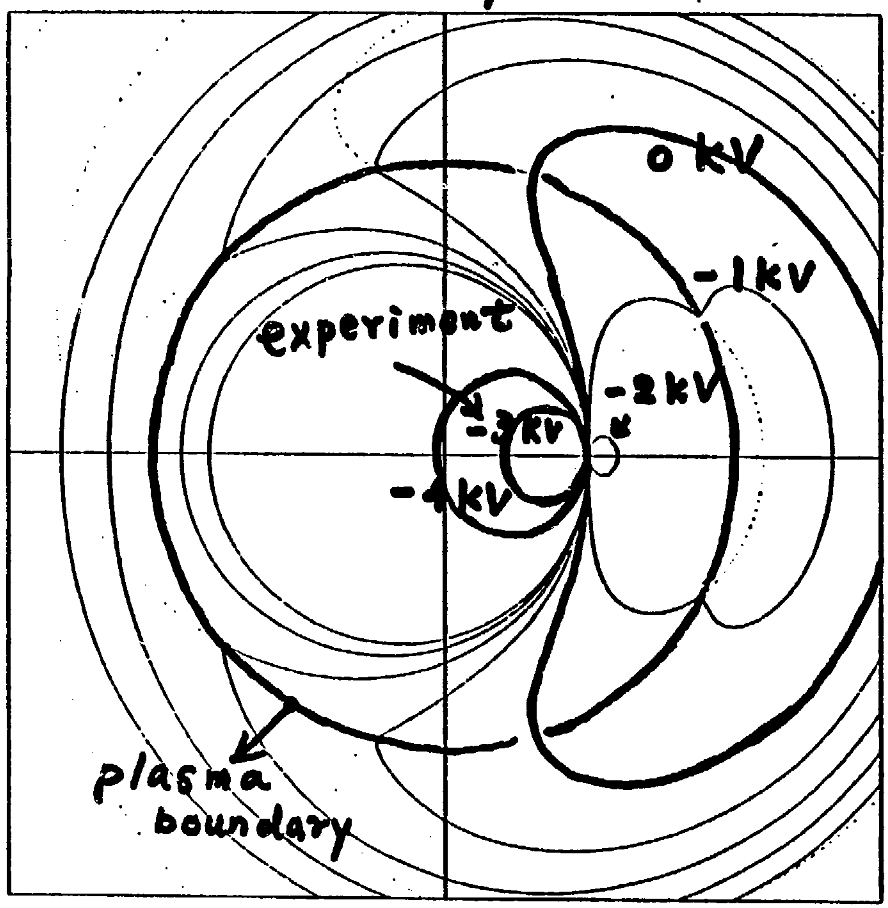

$\frac{v_{\parallel}}{v} = -0.1$

"counter"

$E = 27$ keV

(-ORBIT3-)
POTO SCAN

ENERGY = 27000.0
R = 2.0
AP = 0.1000
IOTA = 0.50
B = 3.2

PITI = -0.1

4i

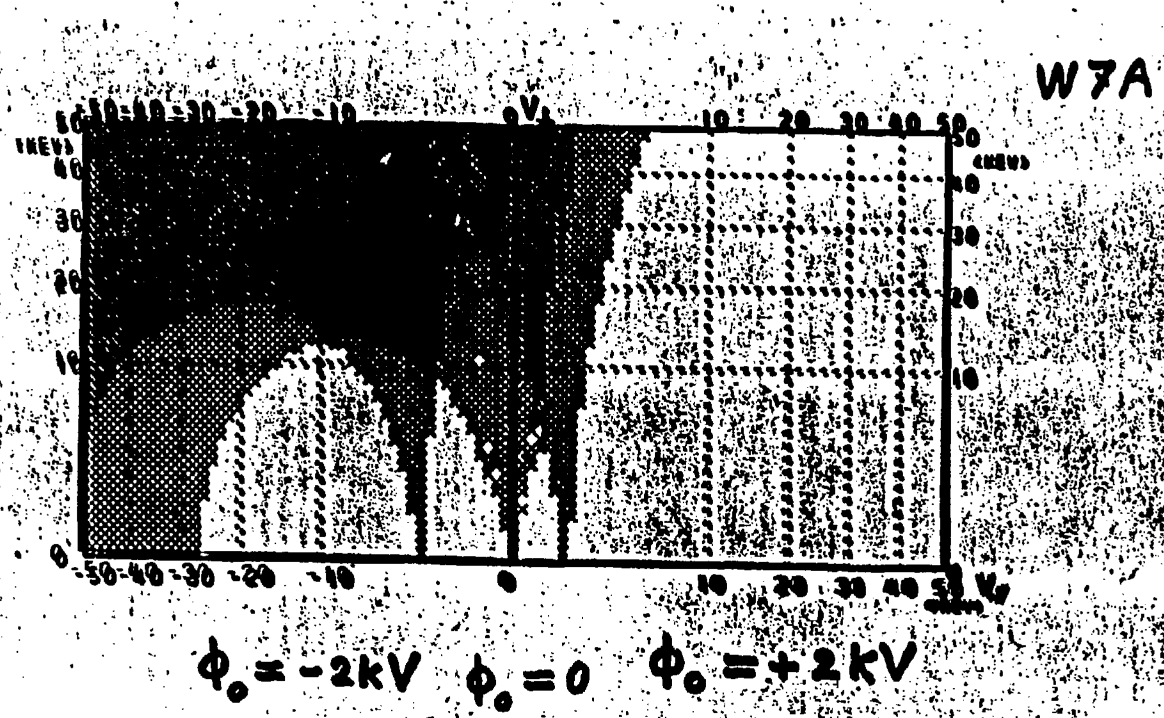

41

Fig 2

HANATANI 87-11-06 22:15:18 0 9

EOINJ = 27000.0
R = 2.0
AP = 0.0837
IOTA = 0.43
B = 2.2

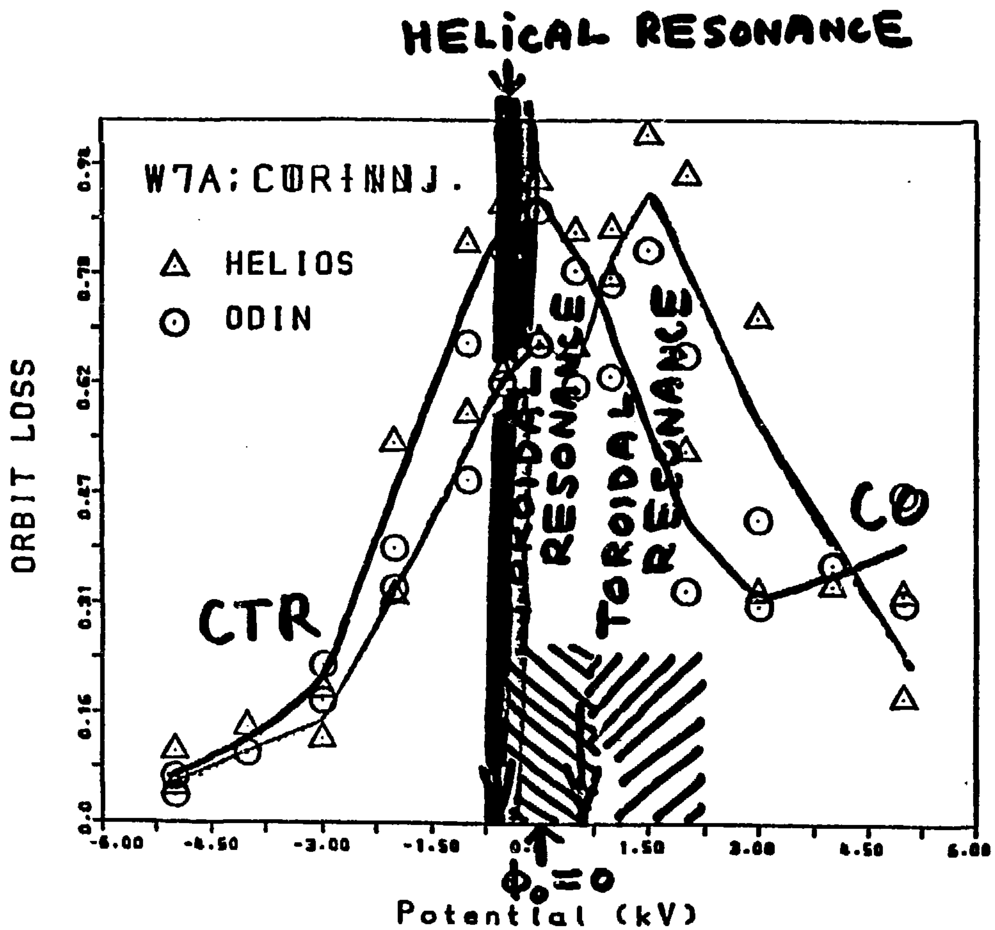

Shift of the Resonance Zone in the velocity space due to potential

TOROIDAL RESONANCE

$$\Omega_{\ell} + \Omega_{E\times B} \approx 0$$

In $\ell = 2$ systems, $\ell \approx$ const

Assume parabolic potential profile

$$\phi = \phi_0 (1 - \psi/\psi_b), \quad \psi \cong \frac{1}{2} B_0 r^2$$

RESONANCE CONDITION

$$\boxed{\lambda \frac{a_p}{\rho_{\theta,a}} - \frac{q\phi_0}{E} = 0} \qquad \lambda \equiv \frac{v_{\parallel}}{v}$$

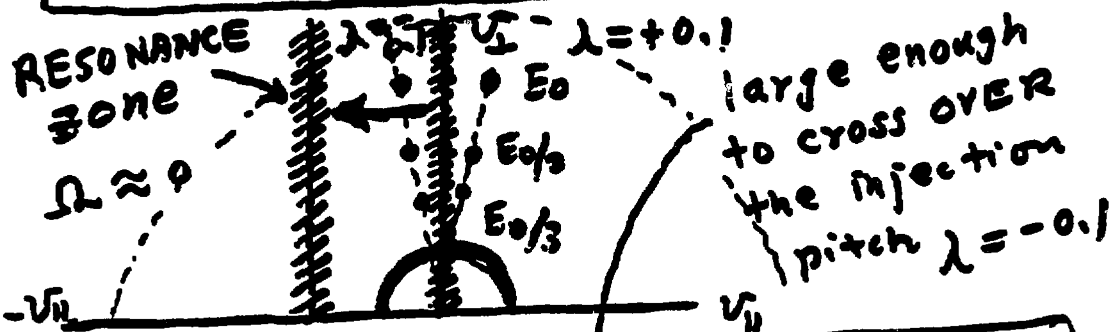

RESONANT PITCH

$$\lambda = \frac{q\phi_0}{E} \cdot \frac{\rho_{\theta,a}}{a_p}$$

$\lambda(27\,\text{keV}) \simeq 0.1 \times 3 \simeq 0.3$

$\lambda(13.5\,\text{keV}) \simeq 0.2 \times 2 \simeq 0.4$

$\lambda(9\,\text{keV}) \simeq 0.3 \times 1.7 \simeq 0.5$

thermal ion

$\lambda(1.5\,\text{keV}) \simeq 2 \times 0.7 \simeq \underline{1.4 > 1}$

global off resonance

$\longrightarrow$ NO RESONANT BANANA

FAST ION coherent in pitch

Thermal ION isotropic in pitch

Effect of E×B drift resonance in Heliotron E

1. INTRODUCTION
2. E x B DRIFT RESONANCE
3. VELOCITY SPACE LOSS REGION WITH E_r FIELD
4. POLOIDAL ROTATION MEASUREMENT
5. CHARGE-EXCHANGE ENERGY SPECTRUM
6. MONTE CARLO CALCULATION
7. SUMMARY

Resonant Superbanana

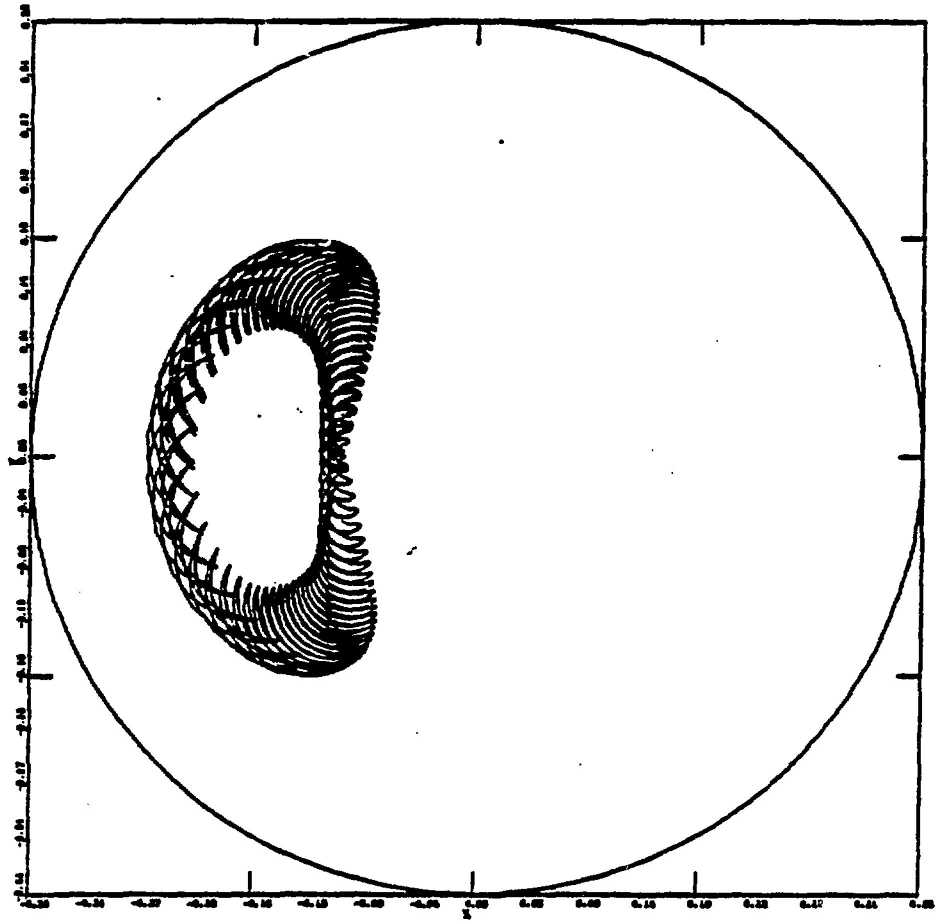

Poloidal Rotation

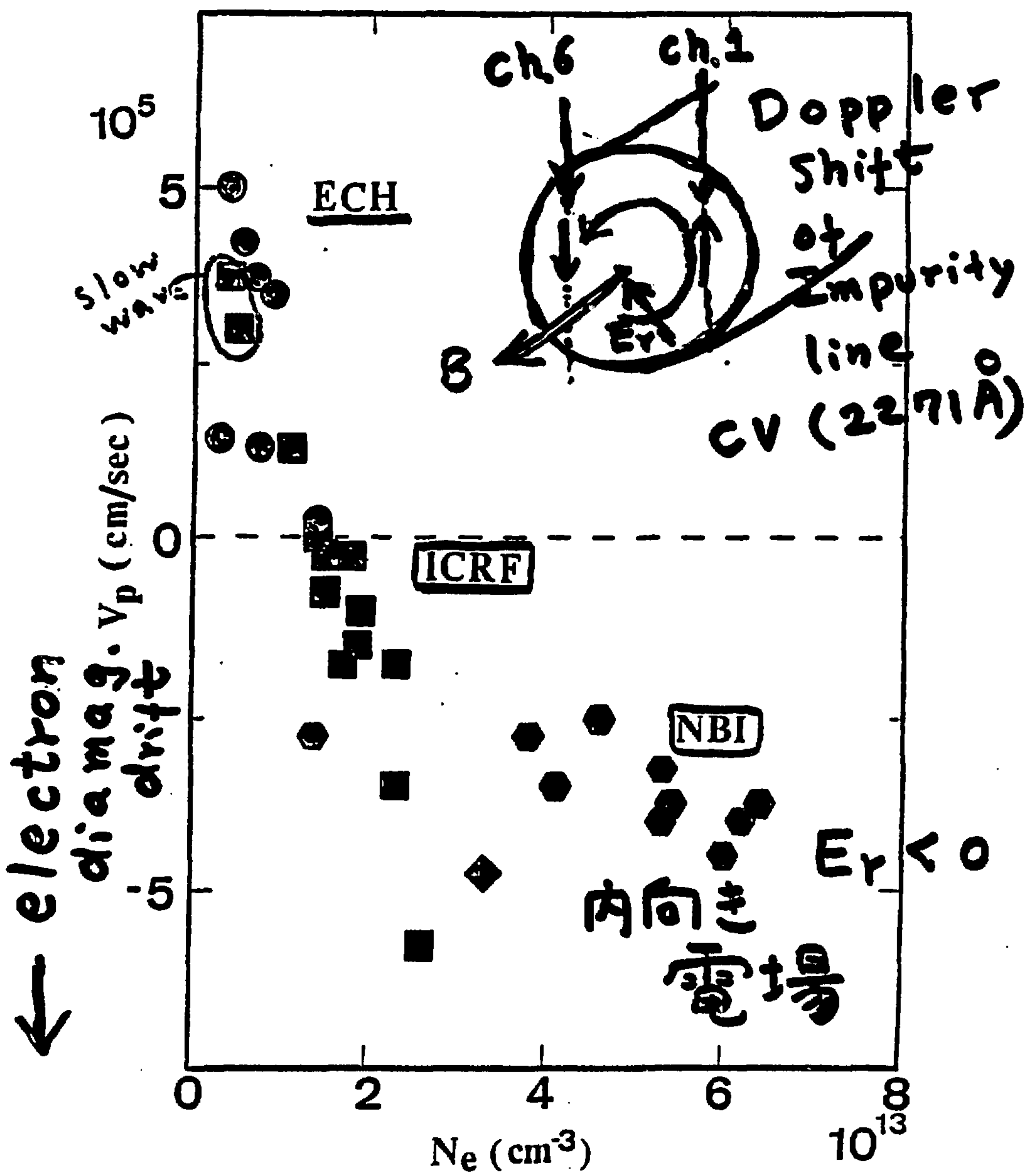

Zushi, Kondo et al.

Modification of Velocity Space Loss Region dueto Er field

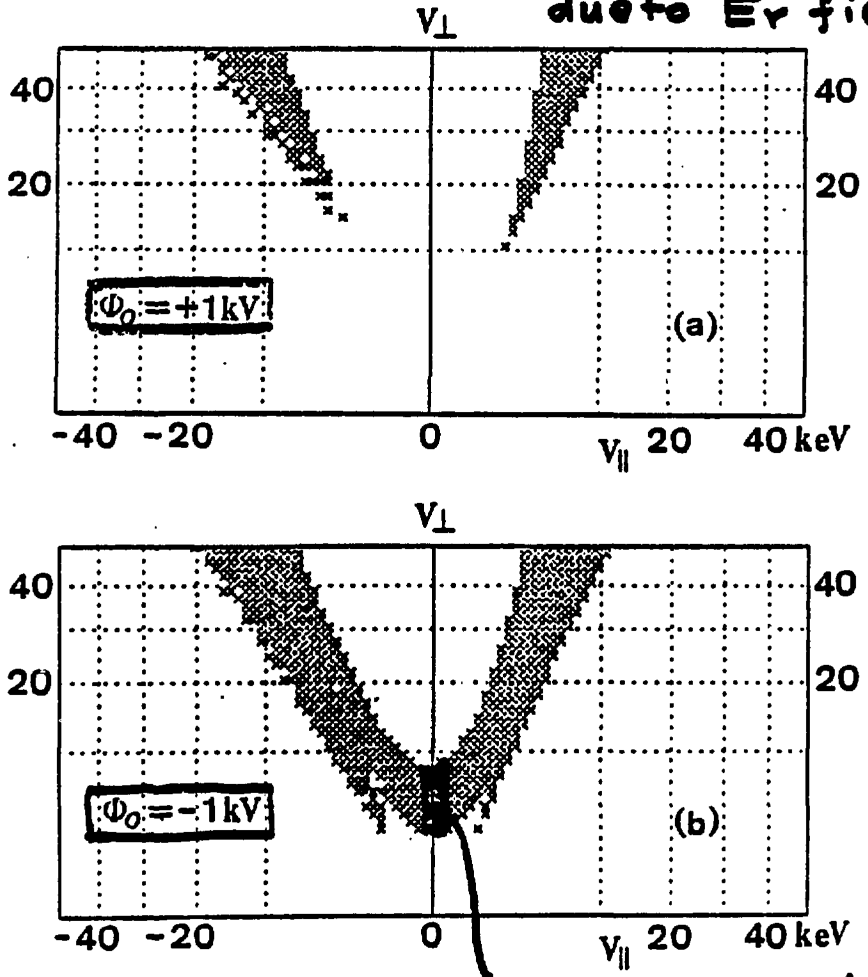

$E_{res} \simeq -q\phi_0/\epsilon_n(a)$

Fig.1 Potential dependence of velocity space loss region in Heliotron E. Calculated at $\bar{r}/a$ = 0.5 out side of the torus. In the calculation, we assumed parabolic potential profile, $\phi = \phi_0(1-\psi/\psi_b)$.
(a) ϕ_0 = +1 kV,
(b) ϕ_0 = -1 kV.

Fix NBI input power and n_e
change B field

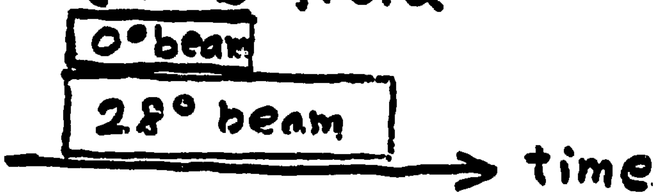

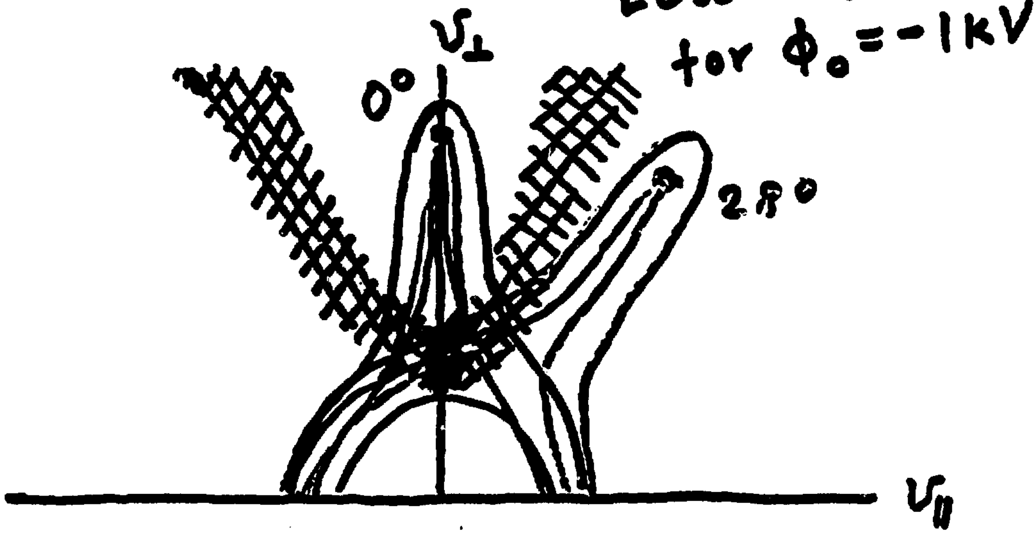

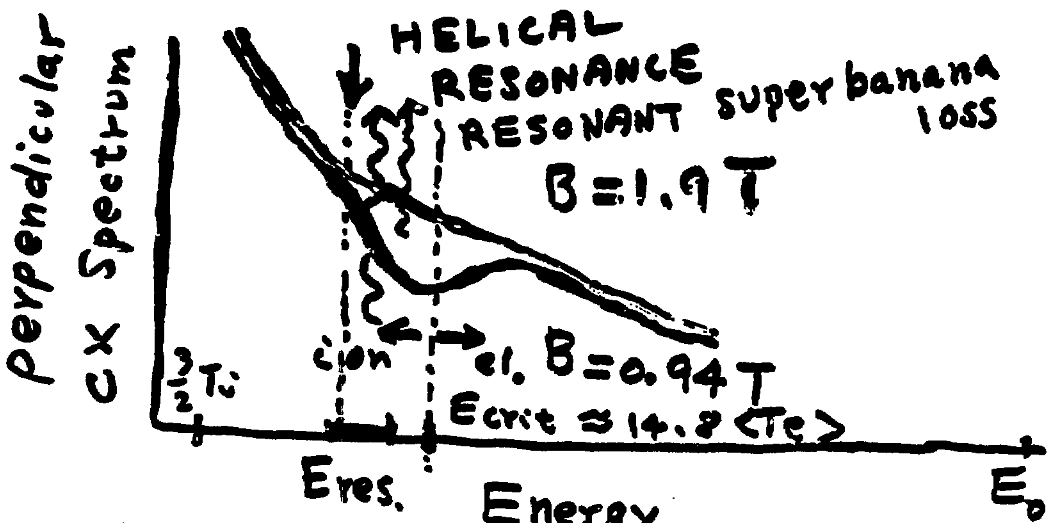

$E_{res.} \simeq \phi_0 / \epsilon_h(a) \approx 3$ keV

CX. Spectrum

Perp. beam → Perp. NPA

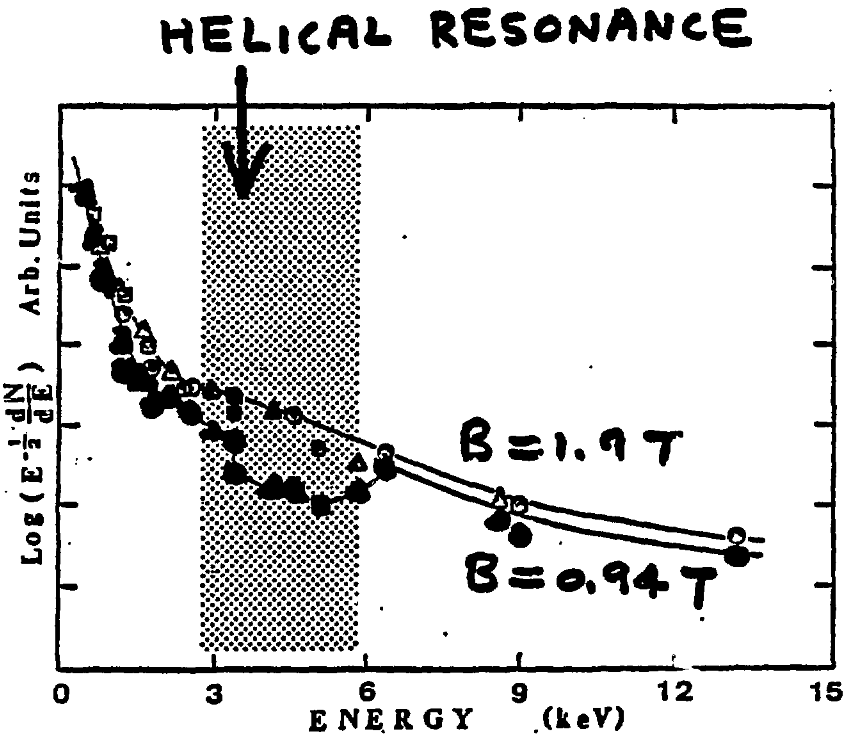

Fig.3 Charge-exchange energy spectrum of an exactly perpendicular beam. Open symbols for B = 1.9T, closed symbols for B= 0.94T. External parameters were fixed except magnetic field, B.

HELIOS コード

Simulation parameters:

- δ-function source
  $E = 4.5\,\mathrm{keV},\ v_{\parallel} = 0$
- starting position
  $(r, \theta, \phi) = (2\,\mathrm{cm}, 180^\circ, 9.47^\circ)$
- $n_e(0) = 9 \times 10^{13}\,\mathrm{cm}^{-3}$
  $T_e(0) = T_i(0) = 400\,\mathrm{eV}$
  parabolic profile
- 100 test particle / RUN

Monte Carlo Calculation of Resonant Superbanana Loss

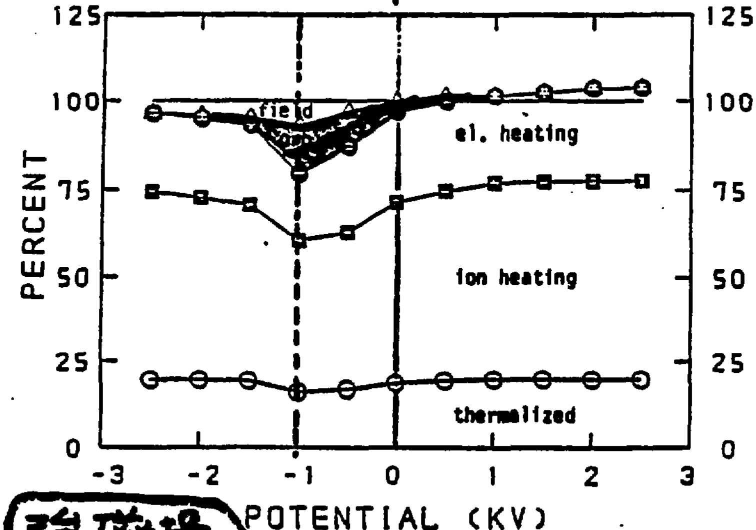

強磁場
Fig. 4 (a); B = 1.9 T

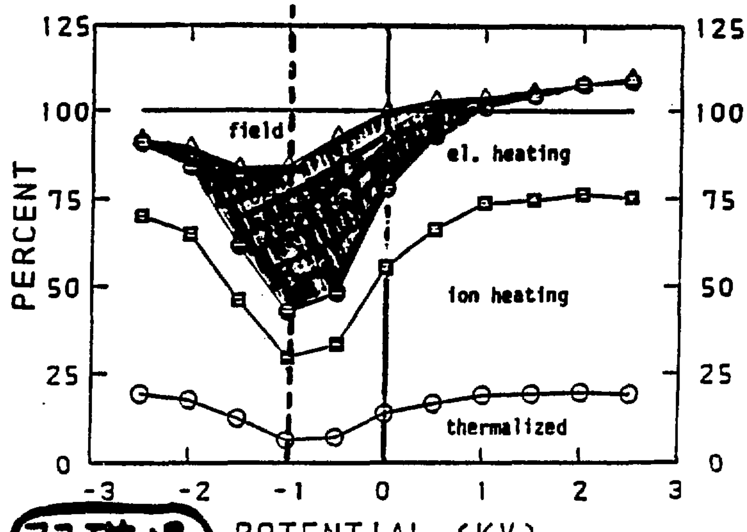

弱磁場
Fig. 4 (b); B = 0.94 T

Effect of ExB drift resonance in Heliotron E

7. SUMMARY

In this paper, we have investigated the role of ExB drift resonance in the confinement of helically trapped fast ions in Heliotron E.

(1) Instead of the toroidal resonance, which plays major role in the beam-ion confinement in the WVII-A device, the helical resonance becomes important in the Heliotron E device.

(2) Confinement of helically trapped fast ions in Heliotron E is improved by positive E_r field and deteriorated by negative E_r field due to the helical resonance.

(3) The poloidal rotation measurement of NBI plasmas suggested the presence of small negative E_r field, which can cause the helical resonance of fast ions in the low energy regime.

(4) The charge exchange energy spectrum showed a correlation with the predicted helical resonance in the Heliotron E configuration.

(5) Monte Carlo calculation showed potential and magnetic field dependences consistent with the measurements of V_p and C.X. energy spectra in the Heliotron E experiment.

SUMMARY

1. Kyoto 3D NBI code upgraded → HELIOS.

2. Benchmark tests of Monte Carlo NBI codes from three different countries have been carried out.

3. E × B drift resonance can explain beam-ion confinement in W7A and Heliotron E.

Benchmarks of Neutral Beam Injection Codes for Stellarators*

R. H. FOWLER, J. A. ROME, R. N. MORRIS,

ORNL

K. HANATANI

Plasma Physics Lab., Kyoto University

The 3-dimensional geometry of stellarators/heliotrons make it more difficult to calculate beam deposition and thermalization. Extensive comparisons between the Oak Ridge and Kyoto codes were undertaken, using a simplified model for the Heliotron-E plasma and magnetic field. The perpendicular injection geometry causes most of the energetic fast ions to be helically trapped. The high transform and shear of the heliotron configuration helps to confine these orbits, but energy losses in the model cases ranged from 20% to 50%. Although the codes use different coordinate systems and collision operators, when they solve the same problem, the answers are equivalent. For perpendicular injection, very little, if any, acceleration of the slowing process can be tolerated.

* *Research sponsored by the Office of Fusion Energy, U.S. Department of Energy, under Contract No. DE-AC05-84OR21400 with Martin Marietta Energy Systems, Inc.*

BENCHMARKS OF NBI CODES FOR STELLARATORS

I. Introduction - motivation

II. Description of thermalization codes – orbit equations, collision operators, etc.

III. Sensitivity and/or Numerical Issues

IV. Benchmarks for Heliotron-E perpendicular injection with model field

V. Heliotron-E results using a filament model

VI. ATF results for perpendicular and tangential injection

VII. Conclusions

Importance of Benchmarking NBI Codes

- Beam inputs are a significant part of the power balance but are seldom directly measured

- Calculations serve as a guide to determine optimal injection angles

- Calculations are expensive, so the appropriateness of analytic moments should be determined

Codes and Cases Considered

HELIOS – Kyoto real space code

MAGCOM – ORNL magnetic coordinate code

DESORBS – ORNL real space code

CASES:

Perpendicular and parallel injection into Heliotron-E and ATF

ORNL MAGCOM CODE

- Boozer coordinates, natural for profiles and electric field treatment
- Only mod $B = \sum_{n,m} A_{n,m}(\psi) \cos(n\phi - m\theta)$ needed
- $A_{n,m}(\psi)$ are least-squares fitted
- Relatively fast but loss boundary cannot be extended much beyond outer flux surface

ORNL DESORBS CODE

- Real space cylindrical coordinates
- ψ is interpolated using 3-D splines
- For complex fields vector B is interpolated using 3-D splines
- More difficult to treat electric fields
- Slower than MAGCOM but allows treatment of complete geometry

Guiding Center Equations in Magnetic Coordinates

$\dot{\psi} = (\dot{P}_\theta g - \dot{P}_\phi I)/\gamma,$ $\qquad \dot{\rho}_c = [-(\rho_c g' - \iota\!\!\!-)\dot{P}_\theta + (\rho_c I' + 1)\dot{P}_\phi]/\gamma,$

$$\dot{\theta} = \left(\delta \frac{\partial B}{\partial \psi} + e\frac{\partial \Phi}{\partial \psi}\right) \frac{\partial \psi}{\partial P_\theta} + \frac{e^2 B^2}{m} \rho_c \frac{\partial \rho_c}{\partial P_\theta},$$

$$\dot{\phi} = \left(\delta \frac{\partial B}{\partial \psi} + e\frac{\partial \Phi}{\partial \psi}\right) \frac{\partial \psi}{\partial P_\phi} + \frac{e^2 B^2}{m} \rho_c \frac{\partial \rho_c}{\partial P_\phi},$$

where $\rho_c = mv_{\parallel}/eB$, B is obtained by FFT,

$$B = \sum_{n,m} A_{n,m}(\psi)\cos(n\phi - m\theta)$$

The toroidal current within a flux surface is $I(\psi)/(2 \times 10^{-7})A$, and the poloidal current outside a flux surface is $g(\psi)/(2 \times 10^{-7})A$.

$\gamma = e[g(\rho_c I' + 1) - I(\rho_c g' - \iota\!\!\!-)],$ $\qquad \delta = e^2 \rho_c^2 B/m + \mu.$

$\dot{P}_\theta = -\delta \frac{\partial B}{\partial \theta},$ $\qquad \dot{P}_\phi = -\delta \frac{\partial B}{\partial \phi}.$

$\frac{\partial \psi}{\partial P_\theta} = \frac{g}{\gamma},$ $\qquad \frac{\partial \rho_c}{\partial P_\theta} = -\frac{(\rho_c g' - \iota\!\!\!-)}{\gamma},$

$\frac{\partial \psi}{\partial P_\phi} = -\frac{I}{\gamma},$ $\qquad \frac{\partial \rho_c}{\partial P_\phi} = \frac{(I'\rho_c + 1)}{\gamma}$

Guiding Center Equations in Real Space

$$\frac{d\mathbf{R}}{dt} = \frac{\hat{\mathbf{B}}}{qB} \times \left(\mu \nabla B + m v_{\|}^2 \frac{\hat{\mathbf{B}}}{B} \cdot \nabla \mathbf{B}\right) + v_{\|} \hat{\mathbf{B}},$$

$$\frac{dv_{\|}}{dt} = -\frac{\mu}{m} \hat{\mathbf{B}} \cdot \nabla B,$$

$$\hat{\mathbf{B}} = \frac{\mathbf{B}}{B},$$

$$\mu = \frac{1}{2} m \frac{v_{\perp}^2}{B} = \frac{1}{2} \frac{m}{B} \left(v^2 - v_{\|}^2\right) \ ,$$

$$v_{\|} = \frac{d\mathbf{R}}{dt} \cdot \hat{\mathbf{B}}(\mathbf{R}).$$

Slowing Down of Fast Ions

$$\frac{\partial f}{\partial t} = \frac{1}{\tau_s v^2} \frac{\partial}{\partial v} \left(v^3 + v_c^3\right) f$$

$$f = \frac{\delta \left(v - v_o\right)}{v_o^2}$$

$$\frac{\partial \langle v \rangle}{\partial t} = -\frac{\left(v_o^3 + v_c^3\right)}{\tau_s v_o^2}$$

On plasma ions:

$$\Delta v_i = -\frac{v_c^3}{v_o^2} \frac{\Delta t}{\tau_s}$$

On plasma electrons:

$$\Delta v_e = -v_o \frac{\Delta t}{\tau_s}$$

Pitch Angle Scattering

$$\frac{\partial f}{\partial t} = \frac{1}{2\tau_s}\frac{v_c^3}{v^3}\frac{\partial}{\partial \zeta}\left[\left(1-\zeta^2\right)\frac{\partial t}{\partial \zeta}\right]$$

Sample $\zeta = \frac{v_{\parallel}}{v}$ from the Gaussian:

$$P(\zeta) = \frac{1}{\sqrt{2\pi}\sigma}e^{-\frac{1}{2}(\zeta-\langle\zeta\rangle)^2/\sigma^2}$$

where $\sigma^2 = \langle\zeta^2\rangle - \langle\zeta\rangle^2$

let $f = \delta(\zeta - \zeta_o)$

$$\sigma^2 = \frac{v_c^3}{v^3}\frac{\Delta t}{\tau_s}\left(1-\zeta_o^2\right)$$

$$\langle\zeta\rangle = \zeta_o\left(1 - \frac{v_c^3}{v^3}\frac{\Delta t}{\tau_s}\right)$$

Charge Exchange with Re-absorption

$$\xi = \int_o^L e^{-n_o\sigma_{cx}l} n_o \sigma_{cx} dl$$

$$Ln_o\sigma_{cx} = v\Delta t n_o \sigma_{cx} = \frac{\Delta t}{\tau_{cx}} > -ln\xi$$

The neutral is tracked by transforming from guiding center coordinates to particle coordinates with a random phase for the gyro-motion

Profile Parameters For Heliotron-E Cases

$$T_i(\psi) = T_e(\psi) = T_o(1 - \psi^{S_1})^{R_1} + T_t$$

$$N_i(\psi) = N_e(\psi) = N_o(1 - \psi^{S_2})^{R_2} + N_t$$

$$E_o = 26 \text{ keV}$$

	High Density	Medium Density	Low Density
R_1	0.5	2	1
R_2	0.86	1	1
S_1	1	2.575	1
S_2	1	1	1
T_0	376 eV	406 eV	540 eV
T_t	5 eV	10 eV	60 eV
N_o	1.37×10^{14} cm^{-3}	8.7×10^{13} cm^{-3}	4.45×10^{13} cm^{-3}
N_t	1.00×10^{11} cm^{-3}	0.3×10^{13} cm^{-3}	4.50×10^{11} cm^{-3}

HELIOTRON NEUTRAL DENSITY PROFILES

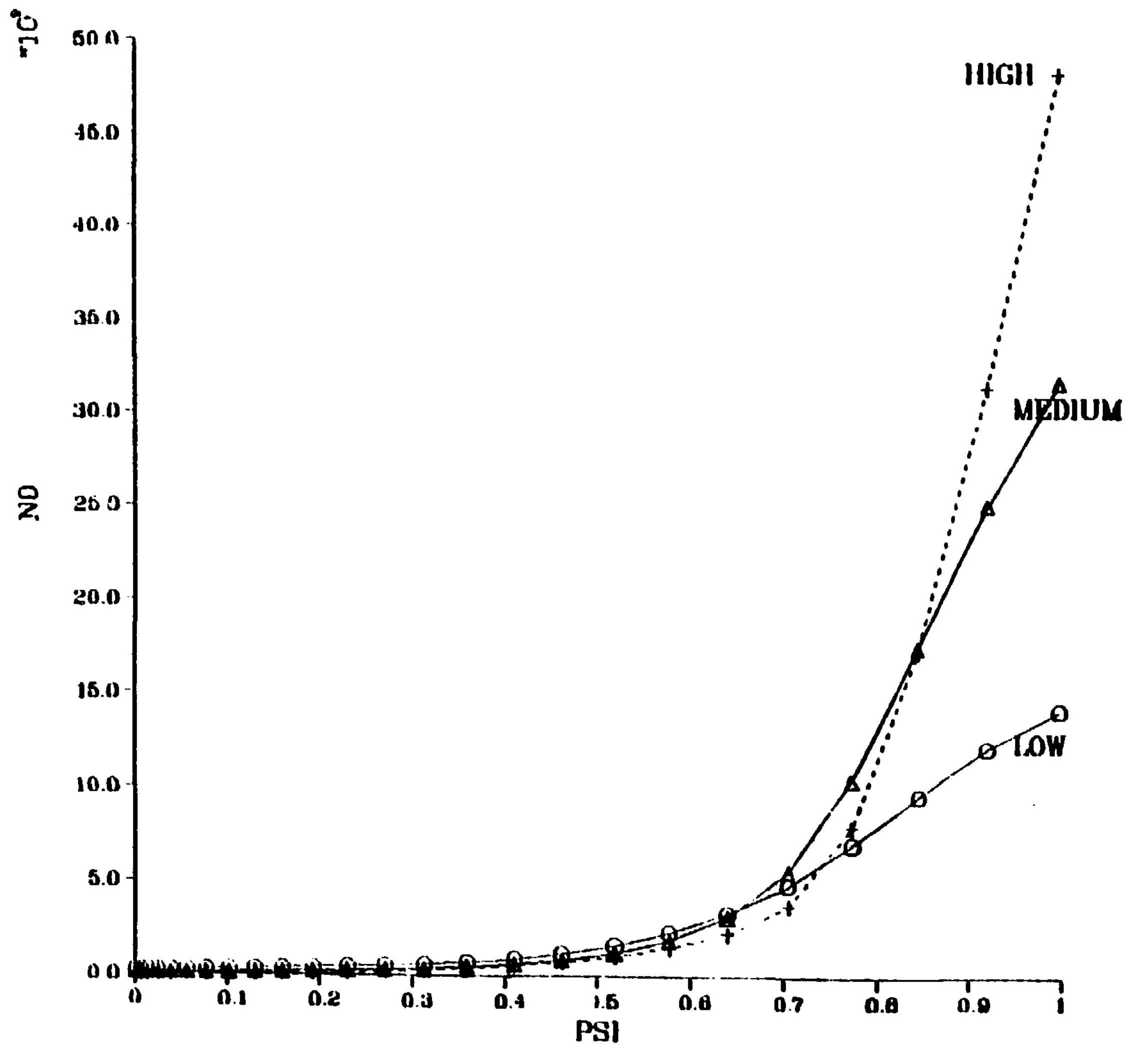

Sensitivity Questions

- Numerical/Statistical - How many particles are sufficient? Random numbers, etc.
- Magnetic field – Are simple models accurate?
- Boundary model used to determine orbit losses – Can the outer flux surface be used?
- Acceleration of slowing down process – Can computer time be saved without loss of accuracy?
- Frequency of collisions – What is a reasonable number of collisions? Should collisions be "independent" of orbit integration?

Reducing Collisions Saves A Small Amount of Computer Time — Is it Worth the Risk?

Model magnetic field (NF 21(1981) 1067).
Heliotron-E low density case N0 = 4.45e13, T0 = 540 eV, τ_s = 12 ms
100 particles
Boundary at last closed surface

Collisions (1000's)	Orbit Loss(%)	GE(%)	Gi(%)
2	39.9	42.6	15.7
10	52.7	35.3	11.0
20	51.8	35.5	12.2
30	51.5	35.7	12.4
40	45.4	39.2	14.8
143	45.6	39.1	14.5
	47.8	37.9	13.4

- Collisions should be every time step in order to accurately sample at turning points where trapping and detrapping occurs

Acceleration Techniques Drastically Reduce Computational Time But When are They Valid?

Scheme 1

Compute τ_s for problem. Then choose n_c = # of collisions. The Δt for the collision operator is given by

$$\Delta t_c = \frac{\tau_s}{N_c}$$

Δt_c, N_c are the same for all acceleration factors; i.e., there is **always** N_c collisions with Δt_c for each collision. The "acceleration" is given by changing the orbit following time $t_{\text{orbit}} = \dfrac{\tau_s}{N_g}$, N_g = acceleration factor.

N_c collisions during t_{orbit} time.

Scheme 2

Let Δt_{DE} = integration time step of GC eqs. Collision after each step with $N_g \Delta t_{DE} = \Delta t_c$ for the collision operator (pitch angle and slowing down).

$$N_g = \text{goose factor}$$

$$t_{\text{orbit}} = \text{time for all particles to thermalize or be lost.}$$

ACCELERATION of SLOWING DOWN PROCESS

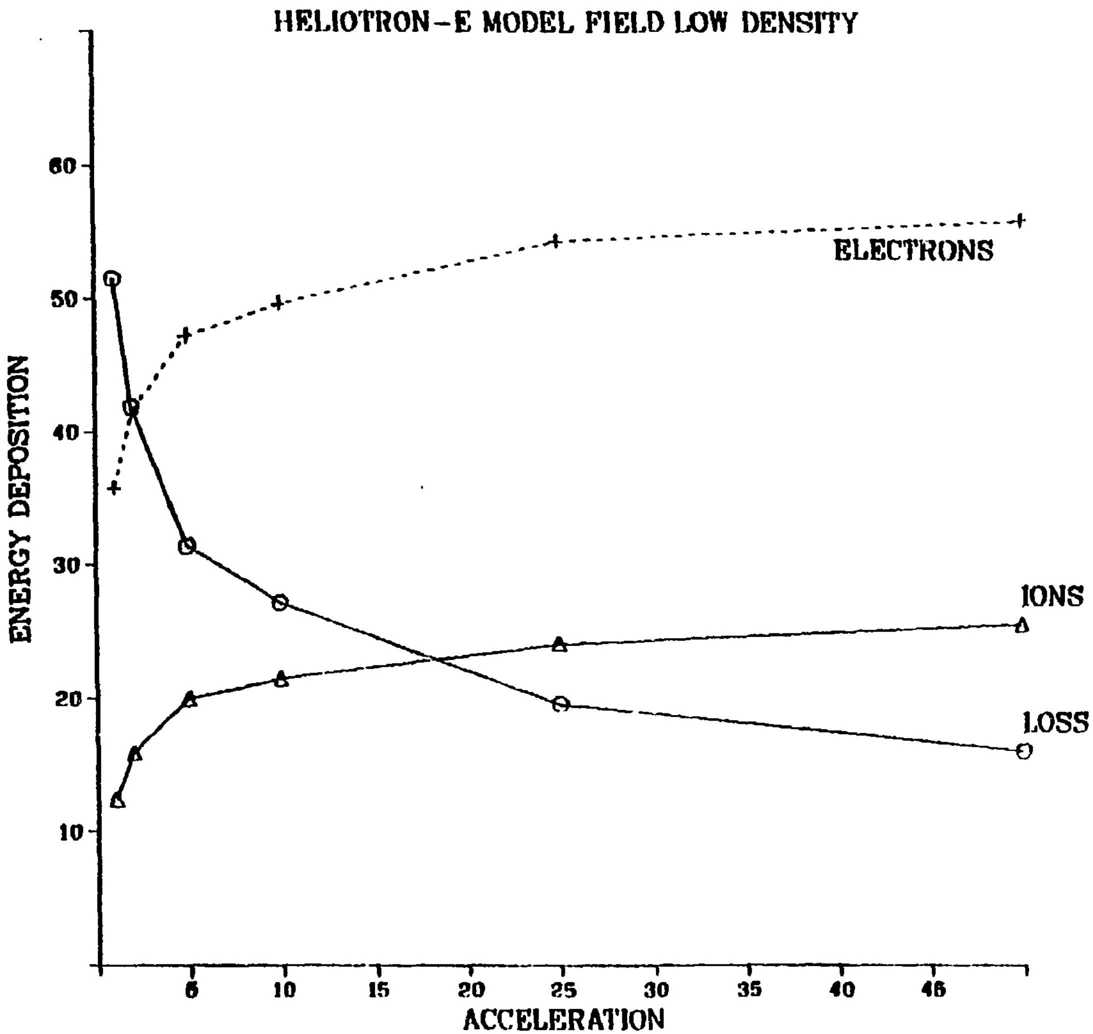

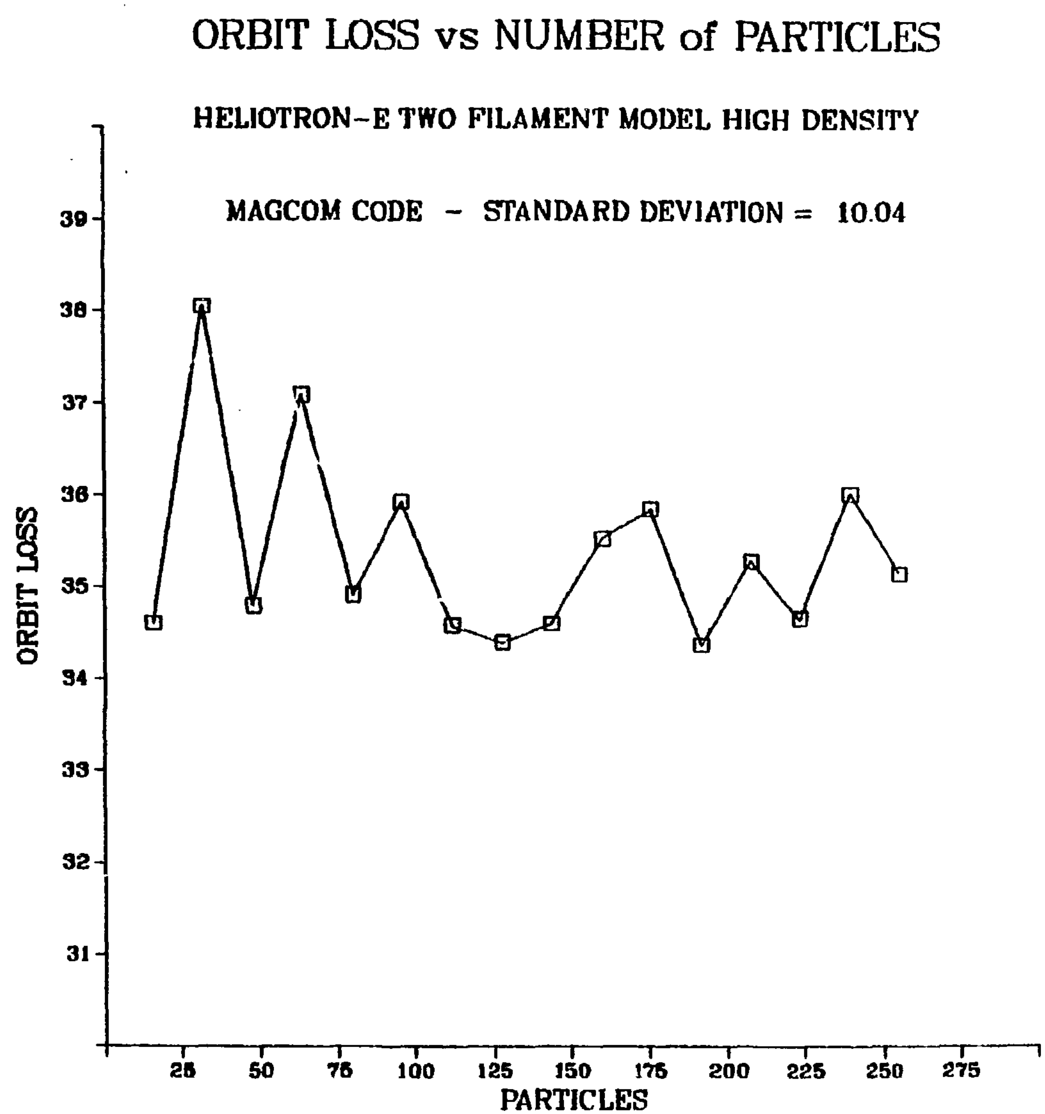

ORBIT LOSS vs NUMBER of PARTICLES
HELIOTRON-E TWO FILAMENT MODEL HIGH DENSITY
MAGCOM CODE - STANDARD DEVIATION = 10.04
ORBIT LOSS
39
38
37
36
35
34
33
32
31
25
50
75
100
125
150
175
200
225
250
275
PARTICLES

ORBIT LOSS vs NUMBER of PARTICLES

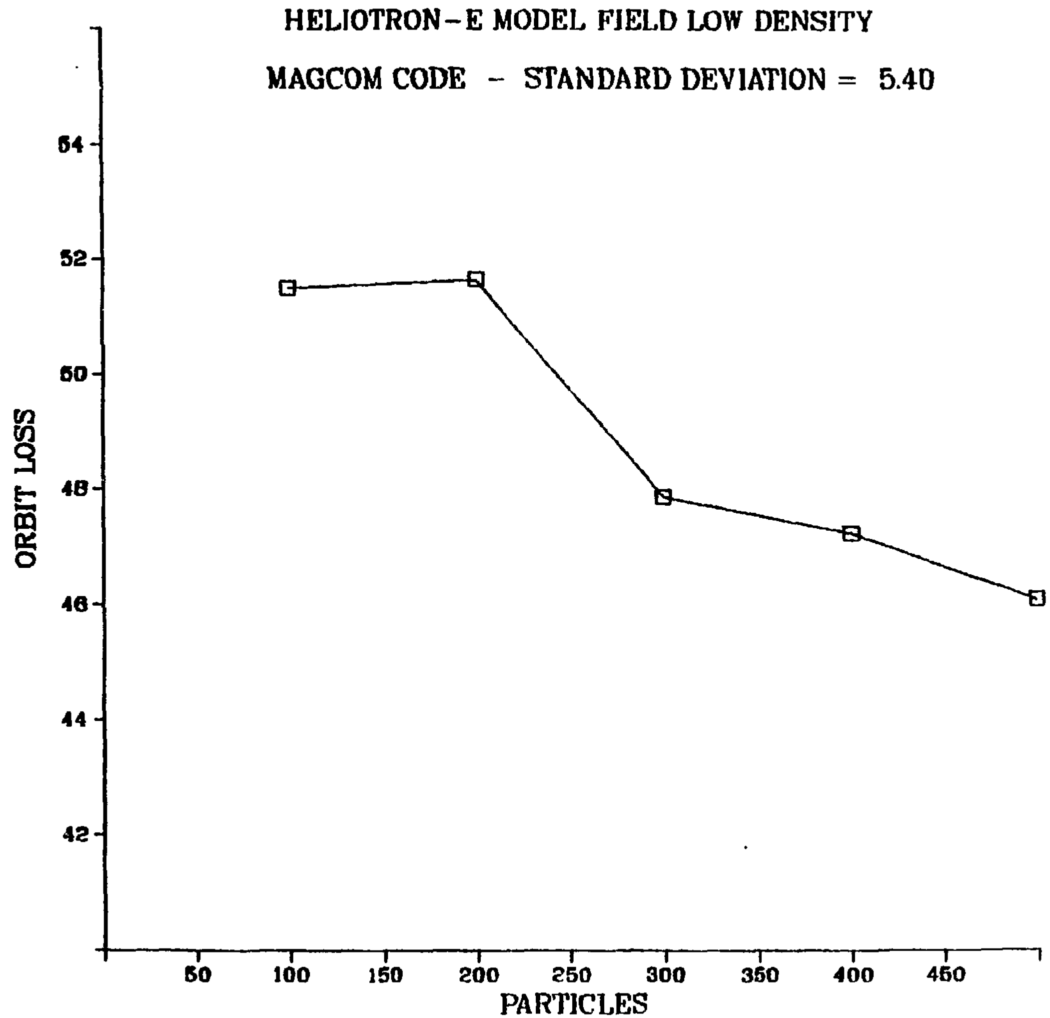

Model Helical Field Used for Benchmarks

Hanatani, Wakatani, Uo, Nucl. Fusion **9**(1981)1067

$$\vec{B} = B(0)\vec{h} + \nabla\psi \times \vec{h}$$

$$\vec{h} = (\hat{z} + \rho\hat{\theta})/(1+\rho^2)$$

$$\psi = -\frac{\pi}{L}B_{cz}(0)\{\alpha^* + e_0 - e_1\rho_c K_2'(2\rho_c)\cos 2(\theta - \frac{2\pi z}{L})\}\rho^2$$

$$\rho_c = 2\pi a/L,\ \rho = 2\pi\tilde{r}/L$$

a = minor radius

L = pitch length

toroidal correction factor $(1 - r/R\cos\theta)$

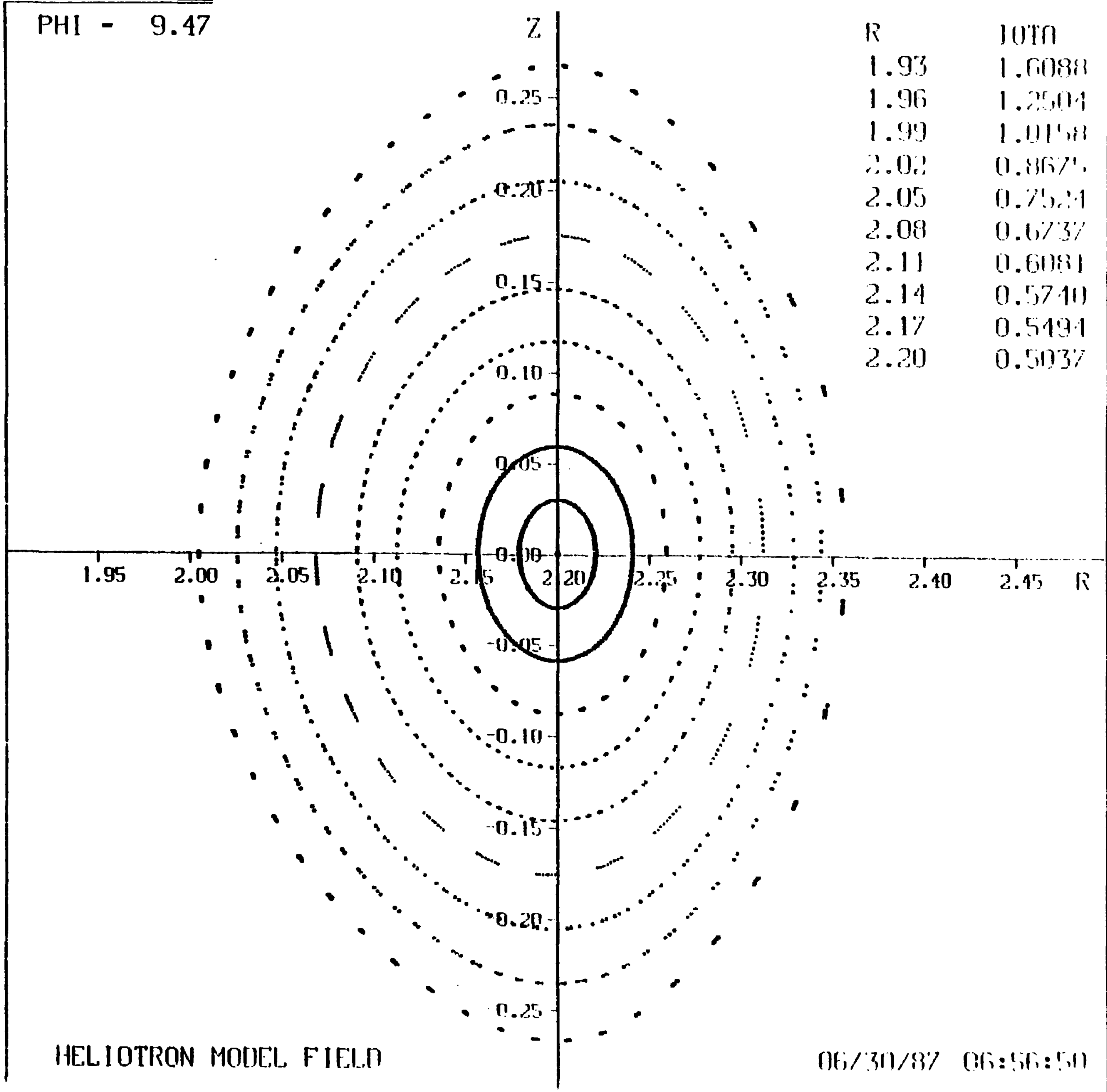
PHI - 9.47
Z
R IOTA
1.93 1.6088
1.96 1.2504
1.99 1.0158
2.02 0.8675
2.05 0.7524
2.08 0.6737
2.11 0.6081
2.14 0.5740
2.17 0.5494
2.20 0.5037
0.25
0.20
0.15
0.10
0.05
0.00
-0.05
-0.10
-0.15
-0.20
-0.25
1.95
2.00
2.05
2.10
2.15
2.20
2.25
2.30
2.35
2.40
2.45
R
HELIOTRON MODEL FIELD
06/30/87 06:56:50

Beam Line

E Component

Top View

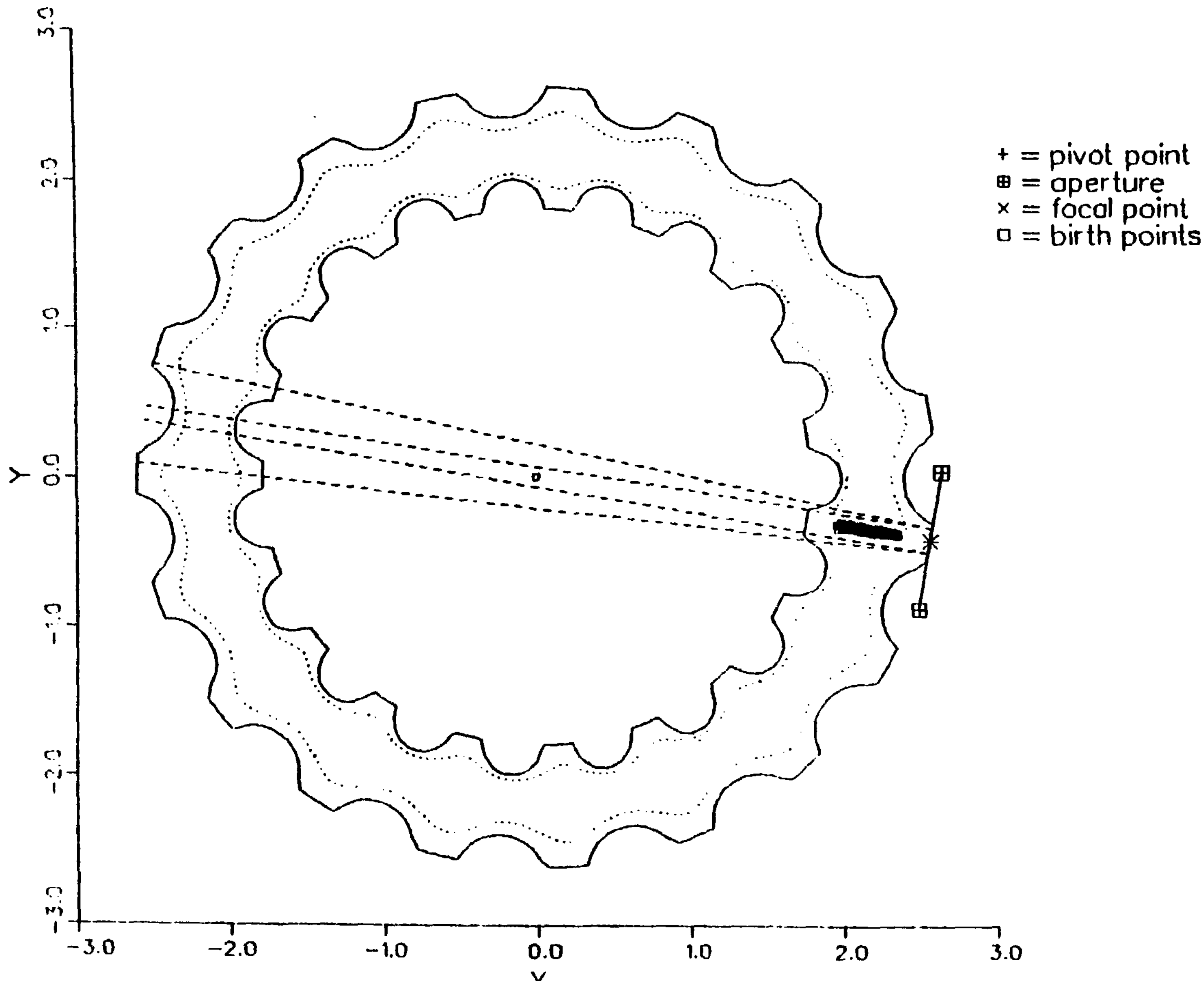

Fast Ion Density

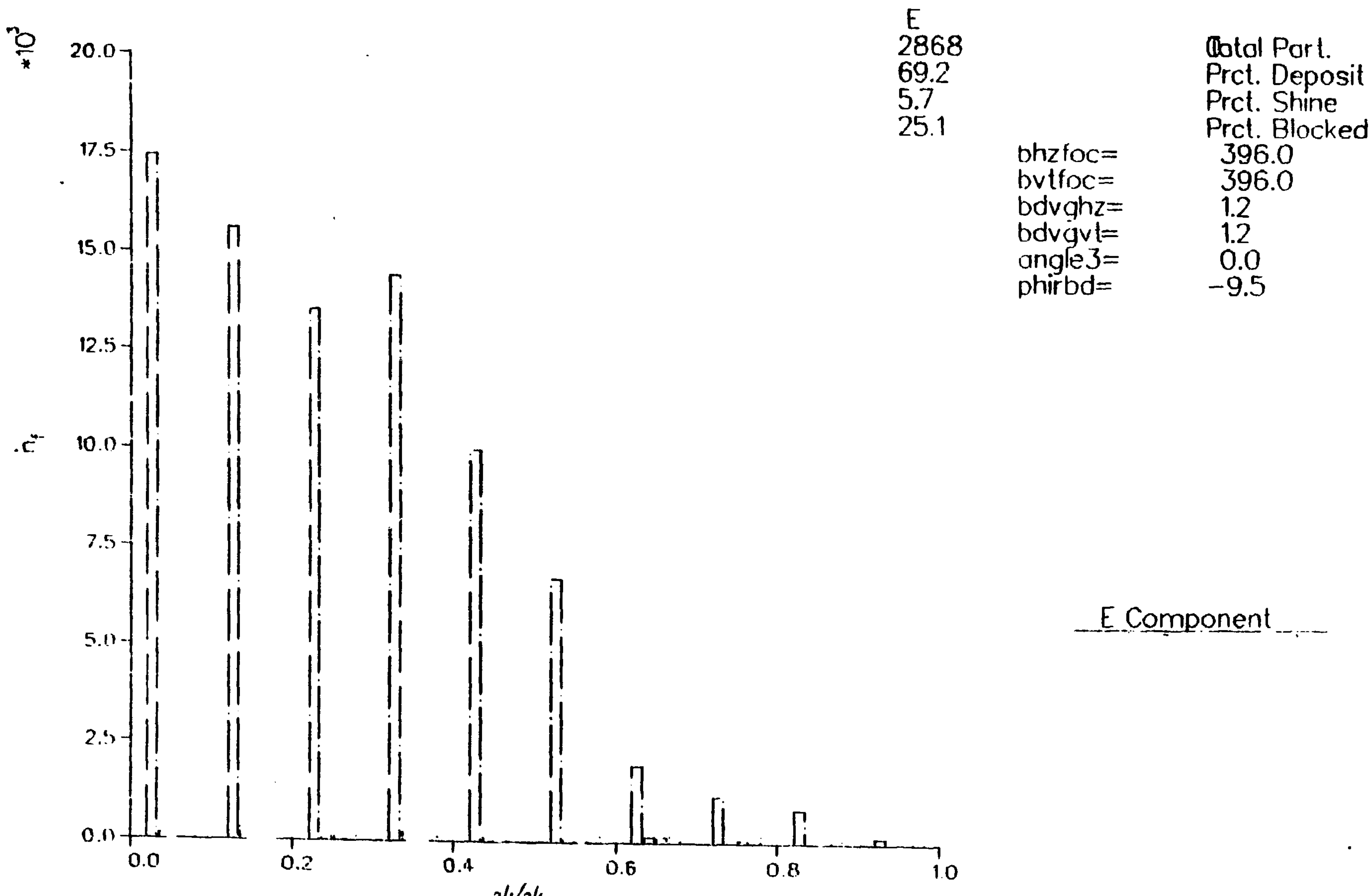

Benchmark STEPS

Kyoto and ORNL CODES

- Cases benchmarked – Perpendicular injection into high (I) and low density (II) Heliotron-E plasmas with a model magnetic field (Hanatani, et al., Nucl. Fusion **9** (1981) 1067)

- Beam deposition agrees – 92% (I) and 65% (II) beam absorption, shinethrough agrees

- Collisionless orbit loss (I) agrees – 28.5% with boundary at last closed flux surface

- Numerically calculated collisionless orbit shift of deeply trapped particles agrees with analytical prediction

- Collisionless orbits match for Kyoto and ORNL flux coordinate codes

$$\frac{\Delta}{a} = -0.15 \quad \text{analytic}$$

$$\Delta = \frac{-V_\perp}{\Omega_k} \qquad V_\perp = -\epsilon_t \omega_0 r \qquad \epsilon_t = a/R_0$$

$$\Delta' = \frac{0.8124 - 0.5}{2} = 0.156$$

$$\Omega_k = -2l\left(\frac{E(k)}{K(k)} - \frac{1}{2}\right)\epsilon_h \omega_0$$

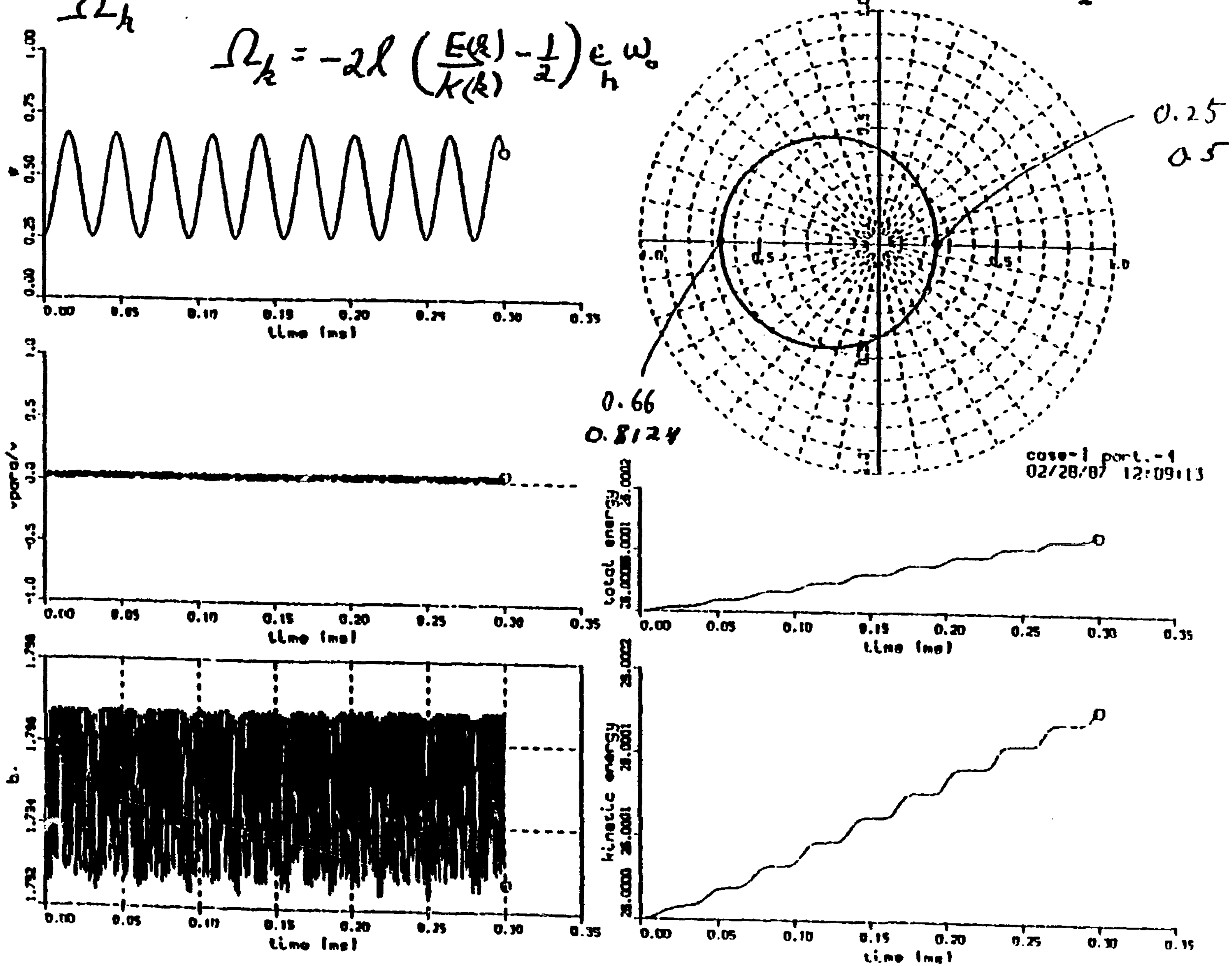

Collisionless orbit

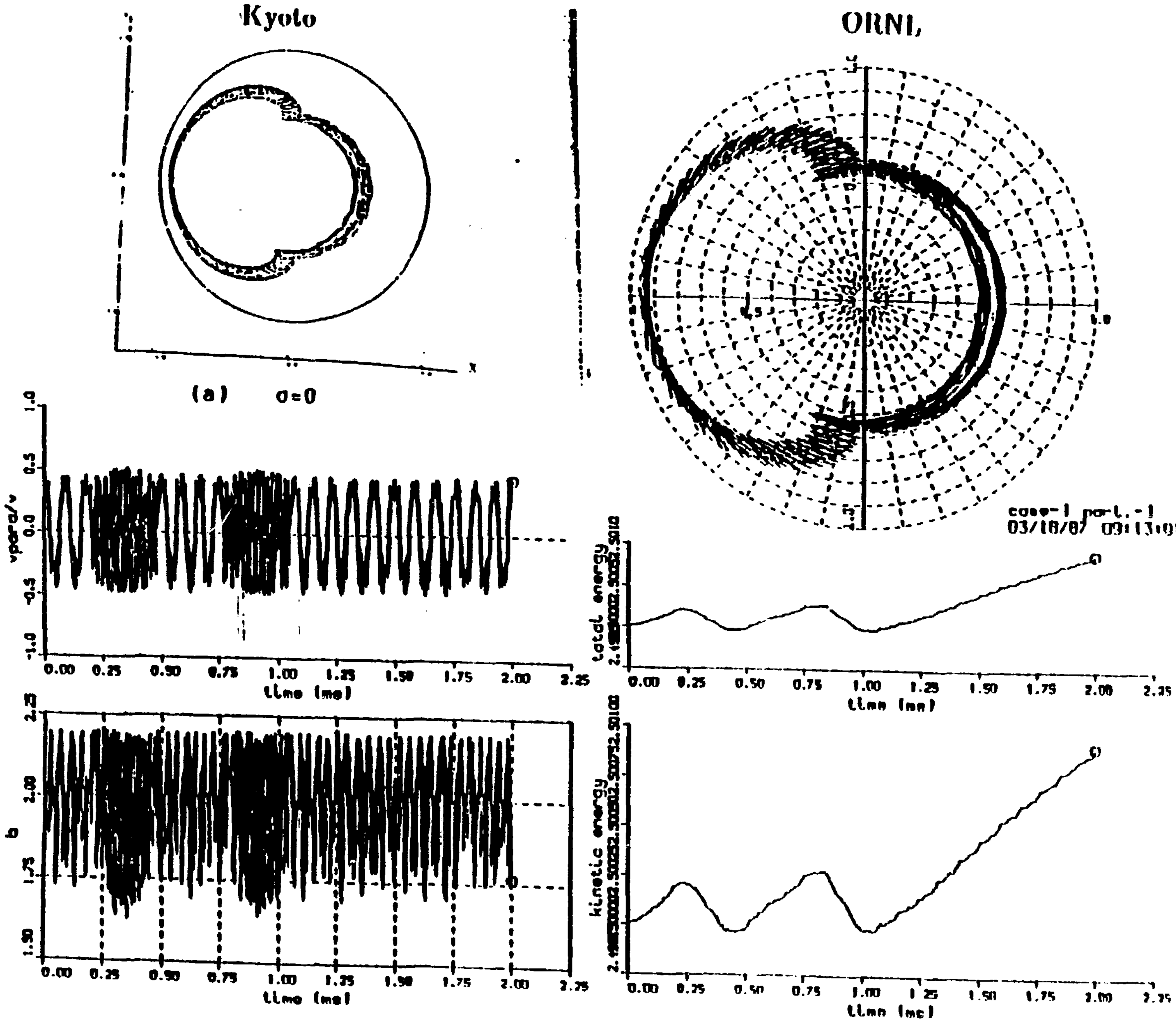

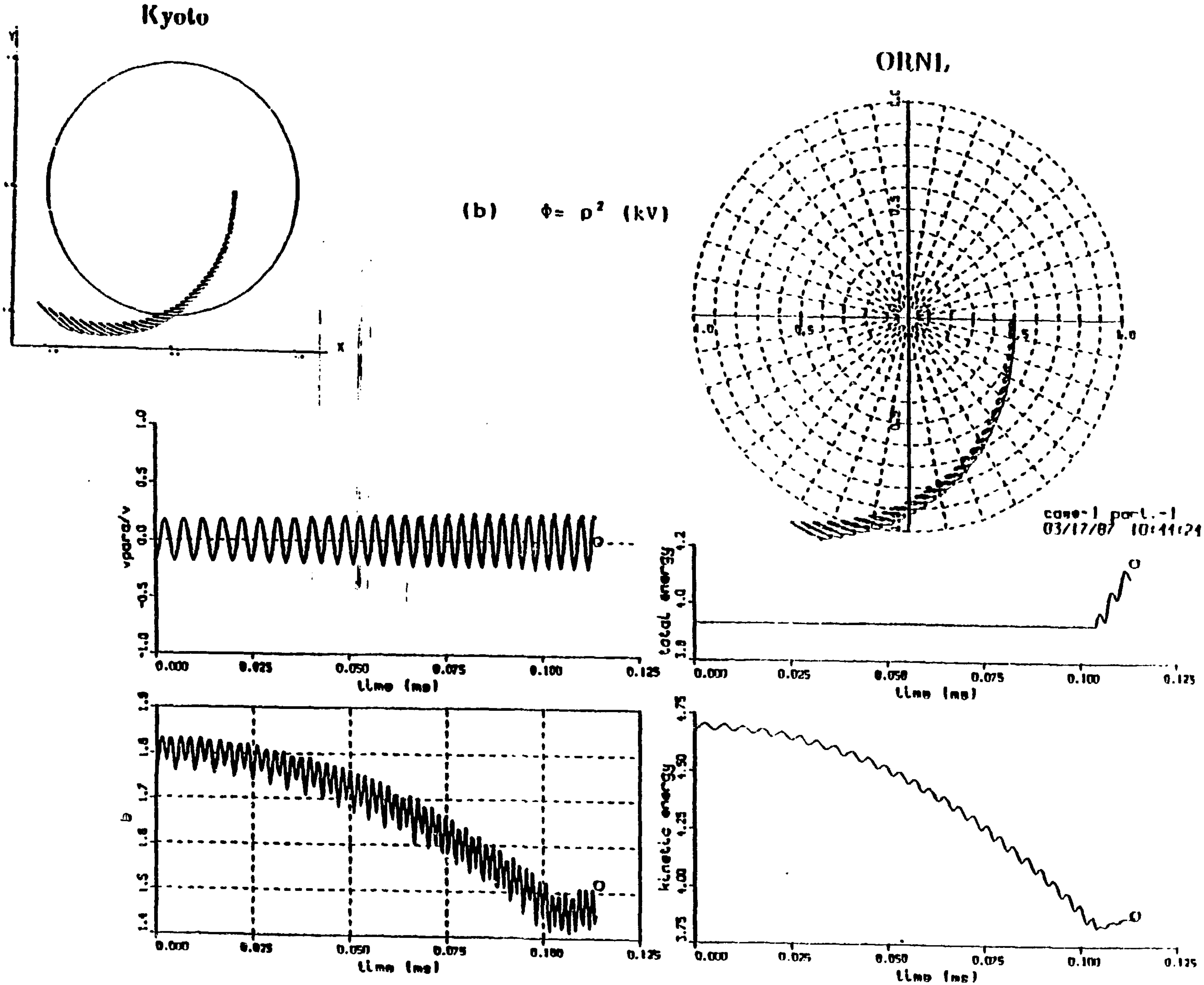
Kyoto
ORNL
y
x
vpara/v
time (ms)
q
total energy
kinetic energy
case-1 part.-1
03/17/87 10:41:24

(b) $\Phi = \rho^2$ (kV)

- Thermalization at birth positions for Case I

	Number of Fast Ions	Energy to Electrons	Energy
HELIOS	1000	73.3%	26.7%
MAGCOM	512	71.8%	23.3%

- Complete thermalization process, no charge exchange, boundary at last closed flux surface

Code	Density Case	Number of Fast Ions	Energy Orbit Loss	Energy to Electrons	Energy to Ions
HELIOS	High	100	40.3%	46.8%	13.0%
MAGCOM	High	100	43.1%	44.8%	11.0%
DESORBS	High	100	42.8%	44.1%	11.4%
HELIOS	Low	512	47.4%	39.2%	13.3%
MAGCOM	Low	500	46.1%	39.9%	13.6%

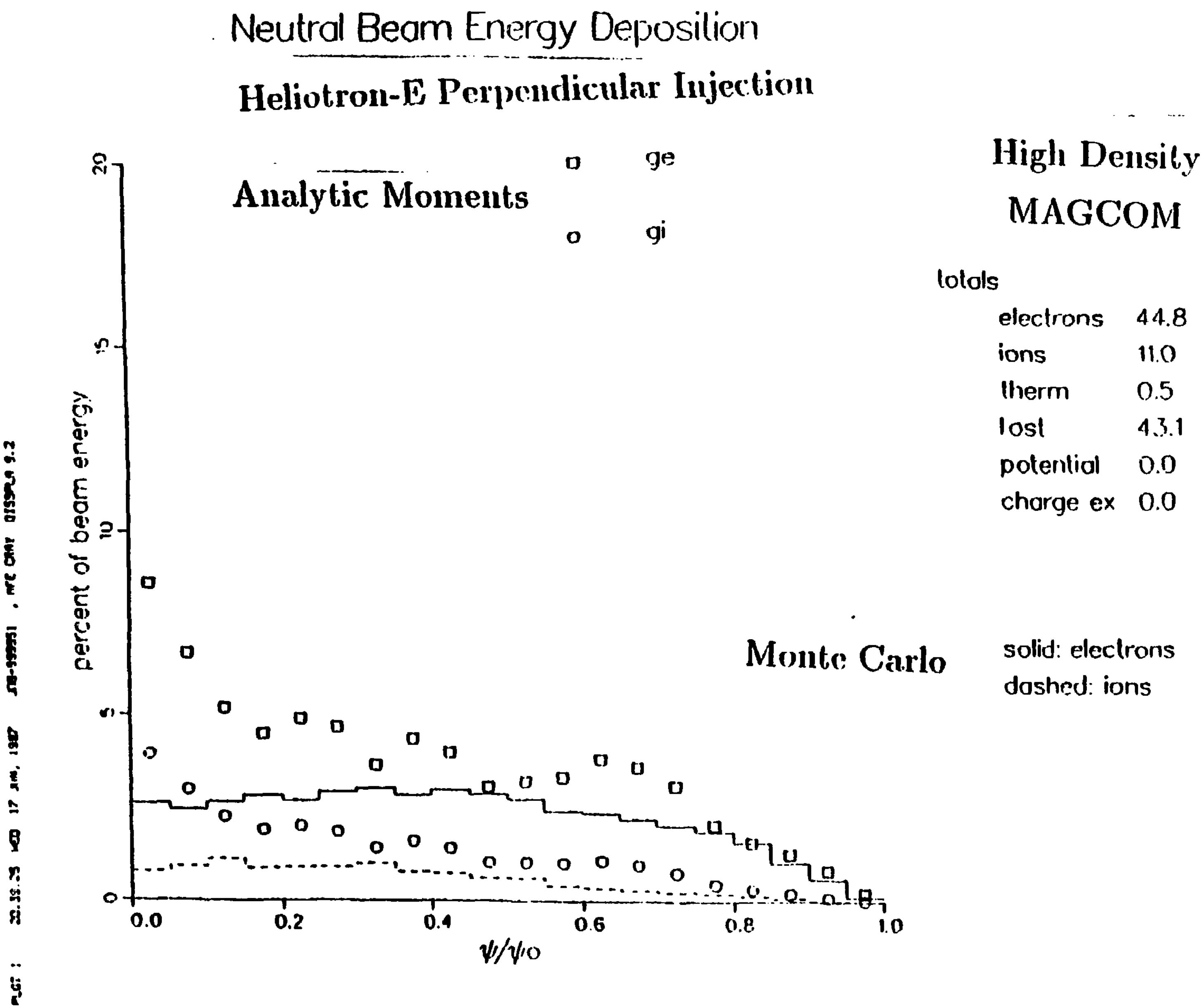
Neutral Beam Energy Deposition
Heliotron-E Perpendicular Injection
Analytic Moments
ge
gi
High Density
MAGCOM
totals
electrons 44.8
ions 11.0
therm 0.5
lost 43.1
potential 0.0
charge ex 0.0
Monte Carlo
solid: electrons
dashed: ions
percent of beam energy
0
5
10
15
20
0.0
0.2
0.4
0.6
0.8
1.0
ψ/ψo

Heliotron-E

HF coils

Two filaments, 380 segments

$I_H = 1.16$ MA (2 T)

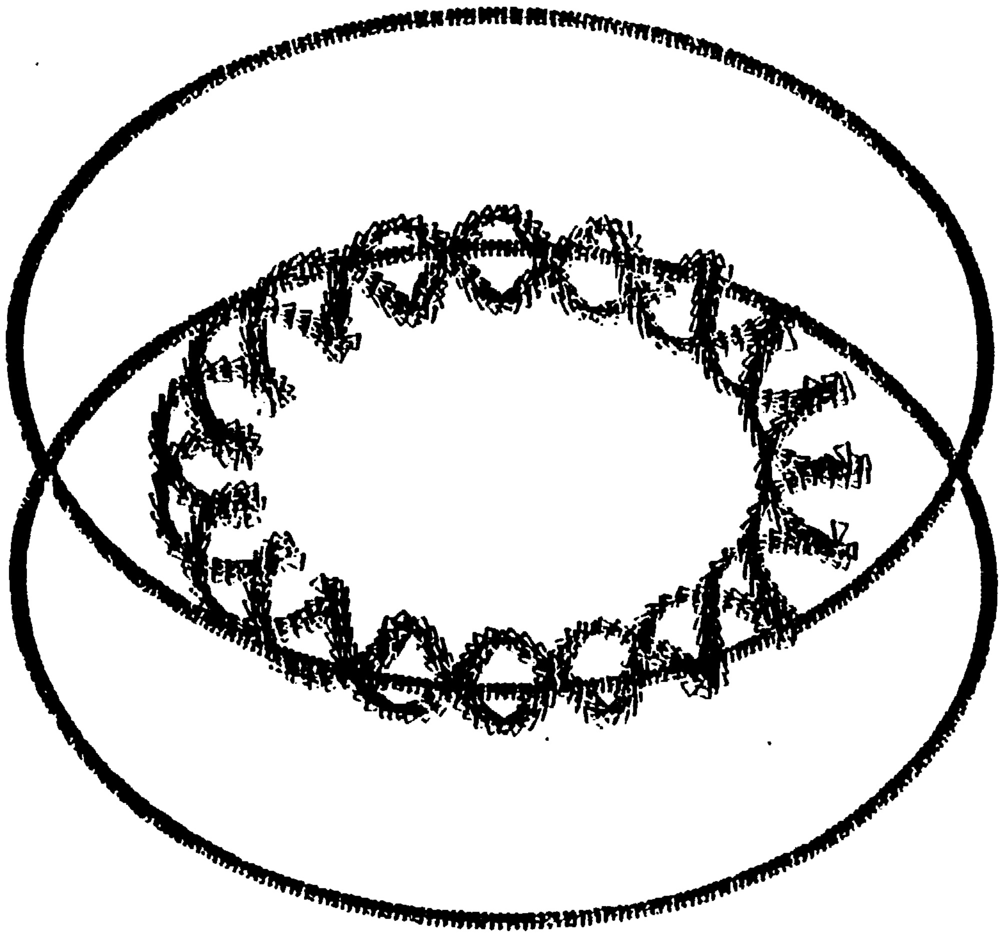

VF coils

$Z_v = \pm 1.2$ m

$r = 3.5$ m

$I_v = -0.9894 I_H$

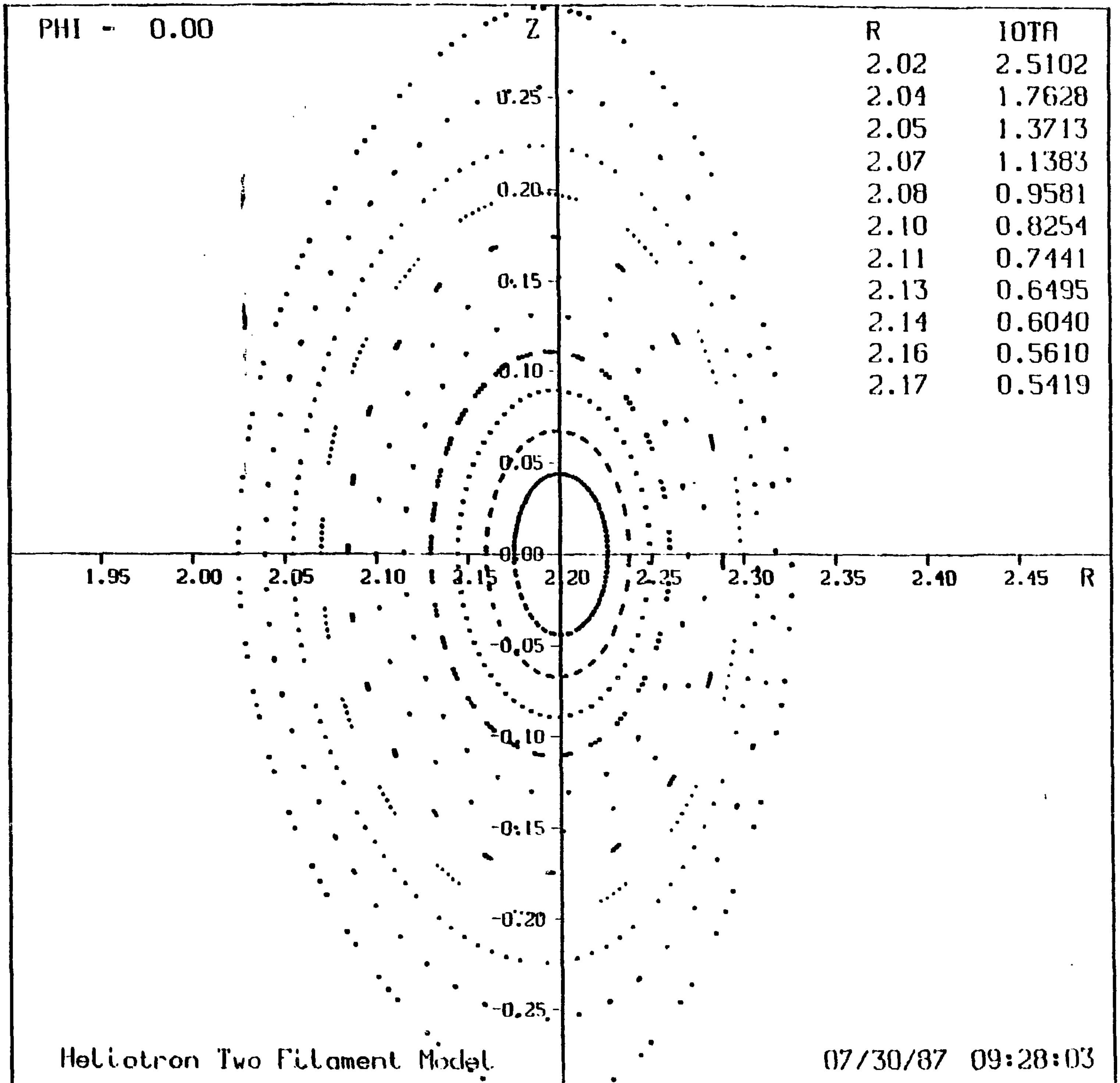
PHI - 0.00
Z
R
IOTA
2.02 2.5102
2.04 1.7628
2.05 1.3713
2.07 1.1383
2.08 0.9581
2.10 0.8254
2.11 0.7441
2.13 0.6495
2.14 0.6040
2.16 0.5610
2.17 0.5419
0.25
0.20
0.15
0.10
0.05
0.00
-0.05
-0.10
-0.15
-0.20
-0.25
1.95
2.00
2.05
2.10
2.15
2.20
2.25
2.30
2.35
2.40
2.45
Heliotron Two Filament Model
07/30/87 09:28:03

ENERGY DEPOSITION vs BOUNDARY

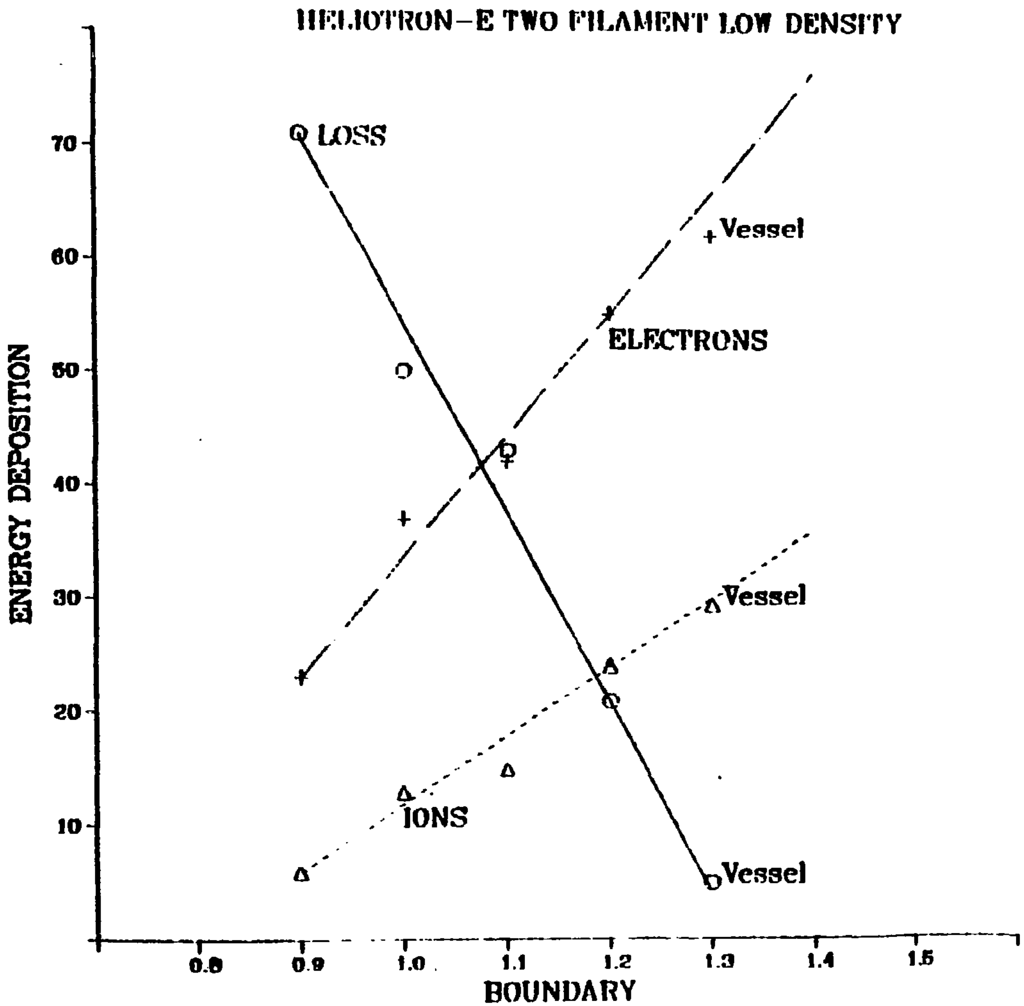

ENERGY DEPOSITION vs BOUNDARY

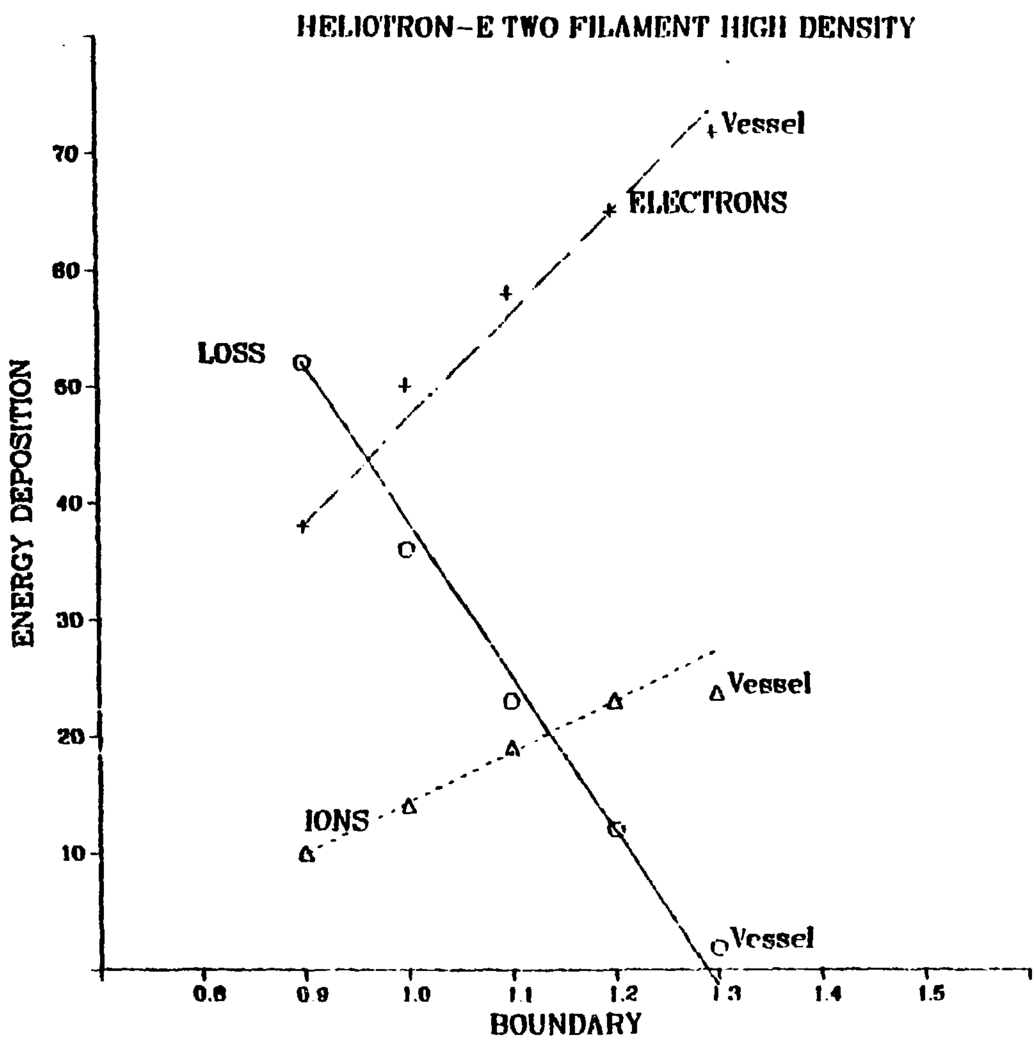

Many helical orbits leave and re-enter the outer flux surface.

Charge exchange loss

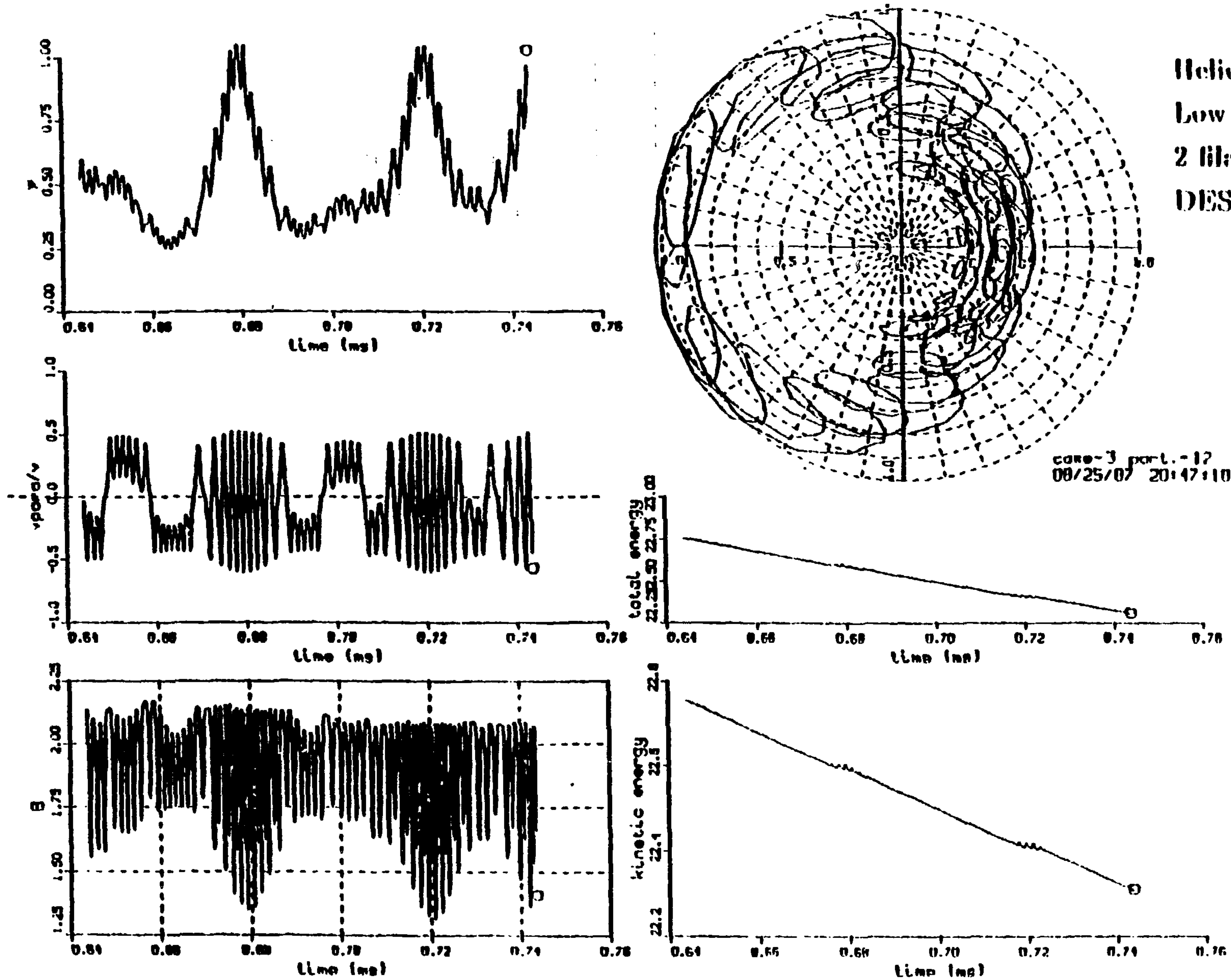

Heliotron-E

Low Density

2 filament model

DESORBS

Heliotron-E

Two Filament Model

Perpendicular Injection

Vacuum Vessel Geometry

DESORBS

Density Case	Energy Orbit Loss	Charge Exchange Loss	Energy to Electrons	Energy to Ions
High	0.08%	10.3%	66.1%	21.5%
Medium	0.06%	12.2%	64.5%	21.2%
Low	7.32%	21.8%	49.9%	19.2%

$Z_{eff} = 1$

Discrepancy with HELIOS

Work in progress!

Profile Parameters For ATF Cases

$$T_i(\psi) = T_e(\psi) = T_o(1-\psi) + T_t$$

$$N_i(\psi) = N_e(\psi) = N_o(1-\psi) + N_t$$

$$\Phi = \Phi_o(1-\psi)$$

$$T_o = 1000\ eV,\ T_t = 50\ eV$$

$$N_o = 4\times 10^{13}\mathrm{cm}^{-3},\ N_t = 1\times 10^{12}\mathrm{cm}^{-3}$$

$$\Phi_o = 0 \text{ or } 2\ kV$$

$$E_o = 40\ \mathrm{keV}$$

ATF Six Filament Model

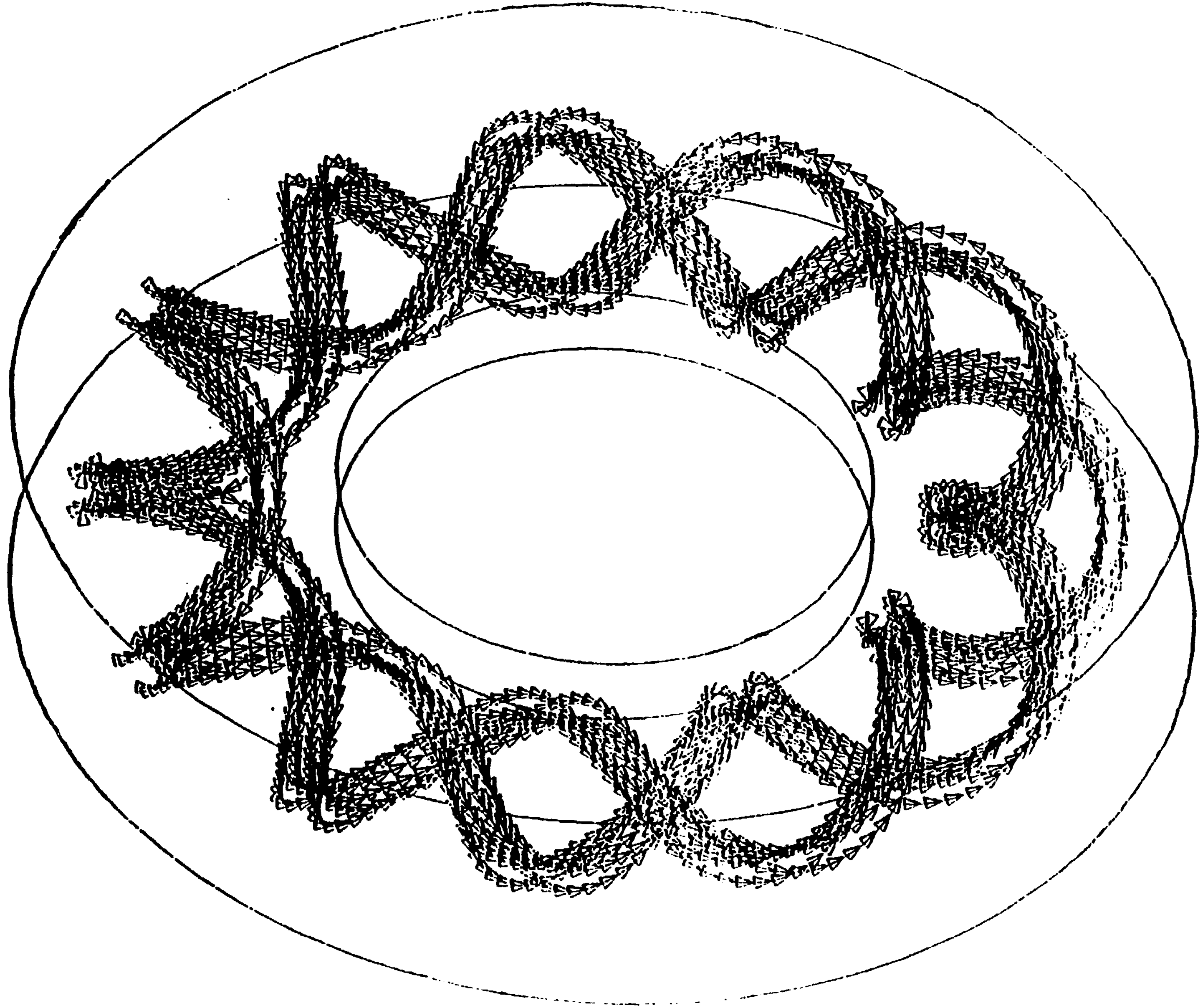

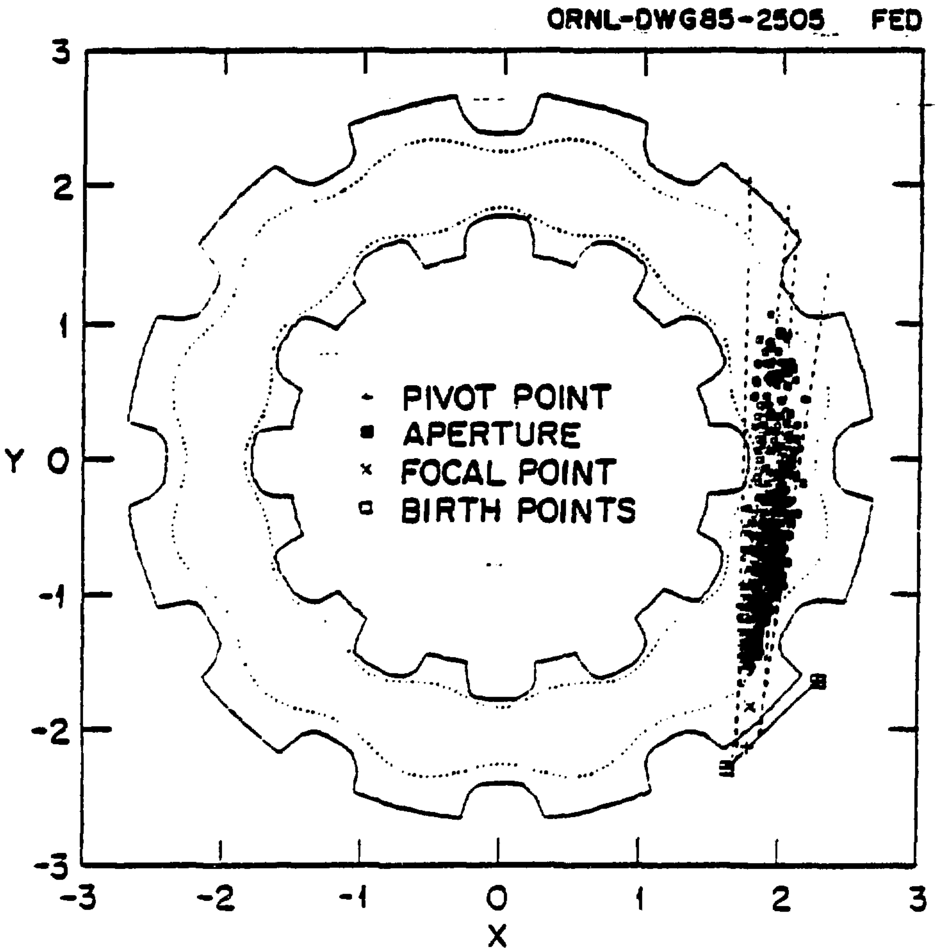

ORNL-DWG85-2505 FED
PIVOT POINT
APERTURE
FOCAL POINT
BIRTH POINTS
Y
X
3
2
1
0
-1
-2
-3

ATF Tangential Injection

Monte Carlo and Analytic Moments Results

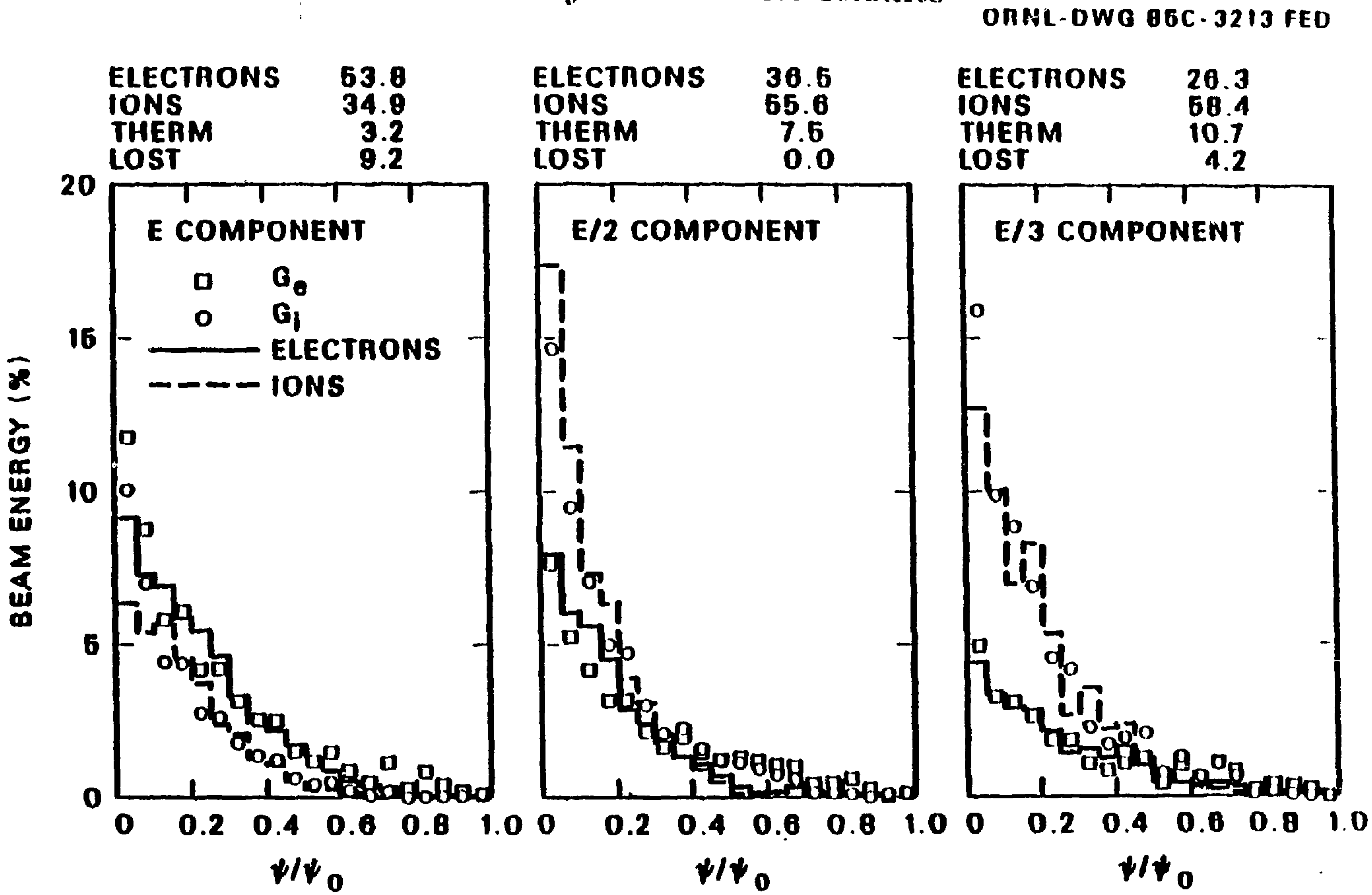

$\Phi_0 = 2kV$ (Electric field)

ATF Tangential Injection

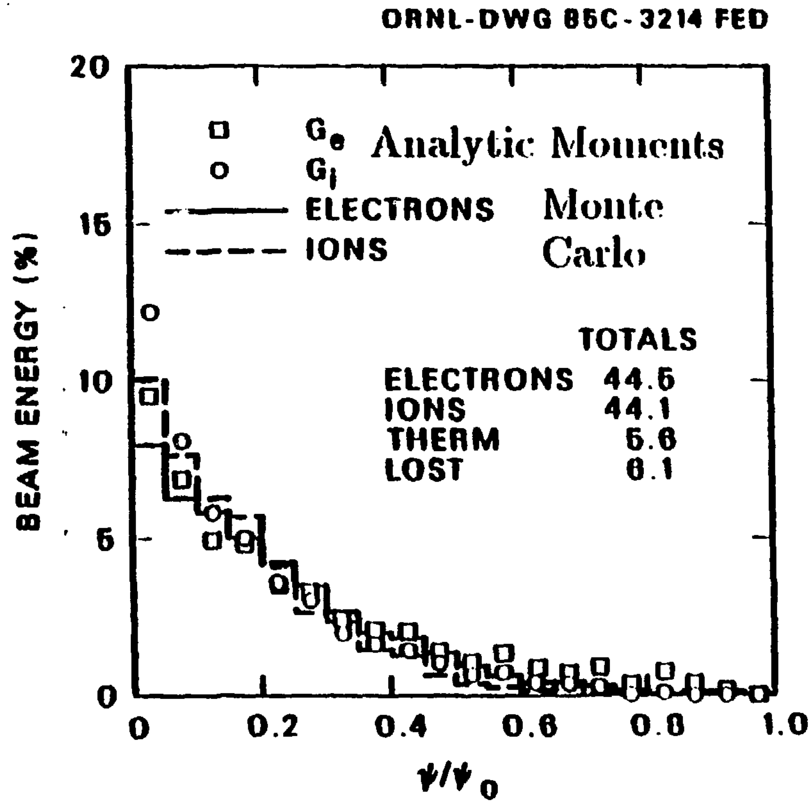

$\bar{\Phi}_0 = 2$ kV (Electric field)

ATF

Six Filament Model

Vacuum Vessel Geometry

Injection	Energy Orbit Loss	Energy to Electrons	Energy to Ions
Perpendicular	64.2%	26.9%	7.53%
Tangential	7.99%	49.1%	36.5%

$\Phi_0 = 0$ (no $\vec{E}$)

$Z_{eff} = 1$

Conclusions

- Results are very sensitive to:
  - Magnetic field model. Also the fields in real space and flux space must correspond exactly to get agreement.
  - Outer boundary model for perpendicular injection where many helical orbits leave and re-enter the outer flux surface and sample large regions of the plasma. However, outer flux surface is adequate for ATF tangential injection.
- The number of collisions should be large enough to accurately sample at turning points where trapping and detrapping occurs.
- Acceleration of slowing down process should not be used for perpendicular injection which produces large numbers of helical orbits. Acceleration can be used for ATF tangential injection which produces mostly passing particles.
- Perpendicular injection into Heliotron-E for our "best" model produces a small orbit loss while for ATF the orbit loss is $\sim$65%.
- The analytic moments method can be used for ATF tangential injection but not for any perpendicular injection cases.

ECH COMMISSIONING AND FUTURE PLANS FOR ATF

T. L. WHITE, T. S. BIGELOW

PRESENTED AT THE

U.S.-JAPAN STELLARATOR/HELIOTRON WORKSHOP

FUSION ENGINEERING DESIGN CENTER

OAK RIDGE, TENNESSEE

WEDNESDAY

NOVEMBER 11, 1987

OUTLINE

- INTRODUCTION
  - SYSTEM DESCRIPTION
  - UNIQUE FEATURES
- HIGH-POWER TEST RESULTS
  - CALIBRATION OF WAVEGUIDE MODE ANALYZER
  - OVERALL SYSTEM EFFICIENCY
- ECH COMMISSIONING TASKS
- FUTURE PLANS
  - NEAR TERM
  - LONG TERM

INTRODUCTION

- THE PRIMARY APPLICATION FOR THE ATF ELECTRON CYCLOTRON HEATING (ECH) SYSTEM IS TO PRODUCE CURRENT FREE TARGET PLASMAS FOR SUBSEQUENT HEATING WITH HIGH-POWER NEUTRAL BEAMS.

- 53.2 GHz WAS CHOSEN TO MATCH THE 1.9 TESLA PEAK FIELDS PRODUCED BY THE ATF HELICAL FIELD POWER SUPPLY ($\omega = \omega_{ce}$).

- MOST OF THE HIGH-POWER NBI EXPERIMENTS WILL BE DONE AT 0.95 TESLA TO INVESTIGATE HIGH β OPERATION, THEREFORE, THE INITIAL OPERATION OF THE ECH SYSTEM WILL BE AT THE SECOND HARMONIC ($\omega = 2\,\omega_{ce}$).

- SINCE ATF WILL ULTIMATELY RUN STEADY STATE, THE ENTIRE ECH SYSTEM (POWER SUPPLY, GYROTRON OSCILLATOR, AND WAVEGUIDE TRANSMISSION SYSTEM) WILL HAVE STEADY-STATE CAPABILITY.

TLW: 11/5/87.2

ECH SYSTEM DESCRIPTION

- ECH POWER SOURCE IS A 53.2 GHz 200 kW cw GYROTRON OSCILLATOR THAT PRODUCES >90% OF ITS POWER IN THE TE_{02} MODE.

- SOME UNIQUE FEATURES OF THE SYSTEM ARE

  - EVACUATED WAVEGUIDE 2.5 IN. I.D.

  - QUASI-OPTICAL TE_{02} MODE TRANSMISSION WITHOUT INTERMEDIATE MODE CONVERSIONS.

  - SOPHISTICATED POWER MONITORING SYSTEM.

  - POWER SUPPLY AND GYROTRON CAN OPERATE SHORT PULSE TO STEADY STATE.

  - WAVEGUIDE SYSTEM ALSO HAS STEADY-STATE CAPABILITY WITH THE ADDITION OF SOME MODEST COOLING.

- INITIALLY, THE ECH LAUNCH INTO ATF WILL BE FROM THE TOP USING A SIMPLE OPEN WAVEGUIDE RADIATING THE TE_{02} MODE.

TLW: 11/5/87.6

ATF GYROTRON POWER SUPPLY

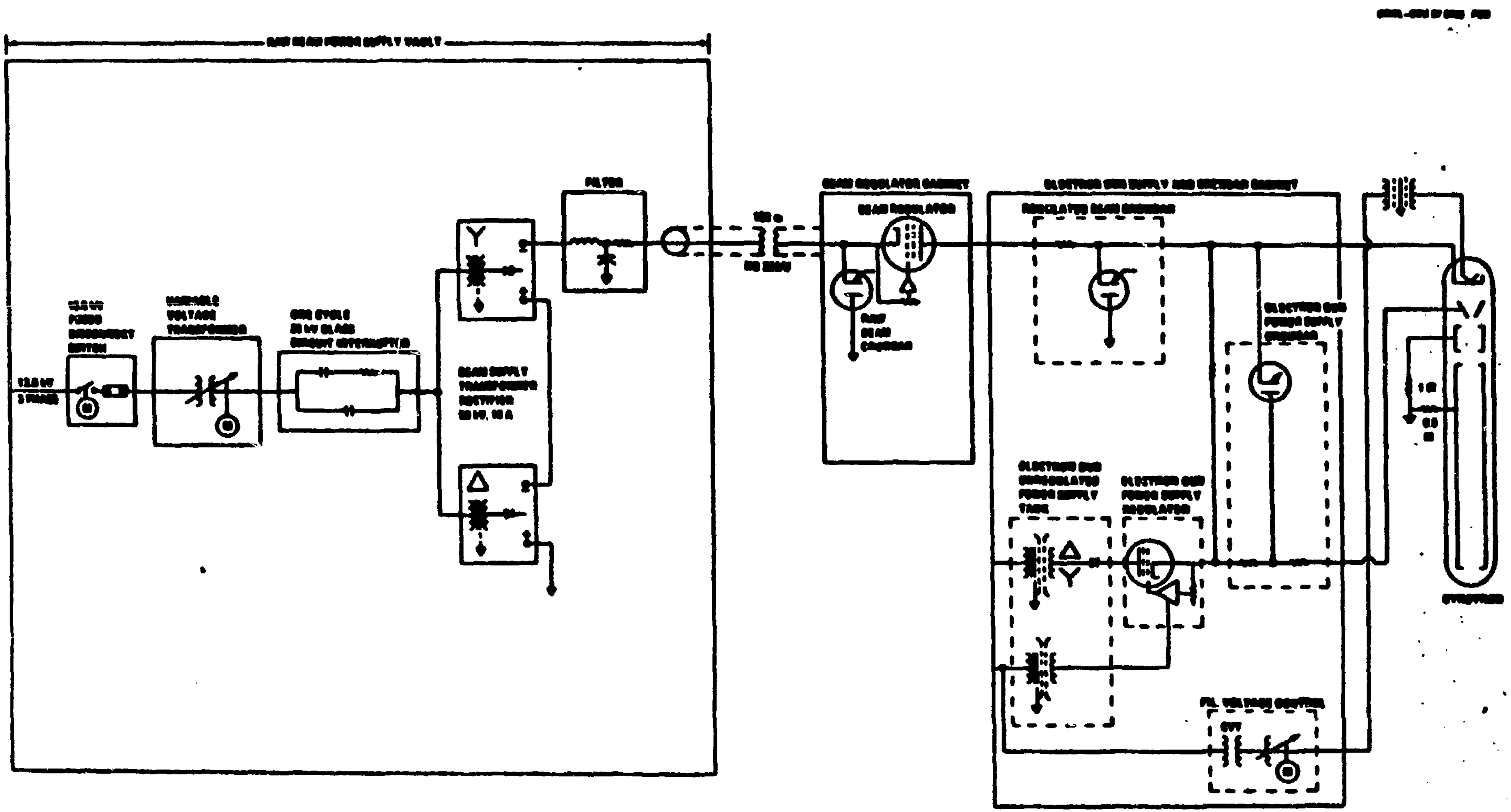

THE ATF ECH WAVEGUIDE TRANSMISSION SYSTEM

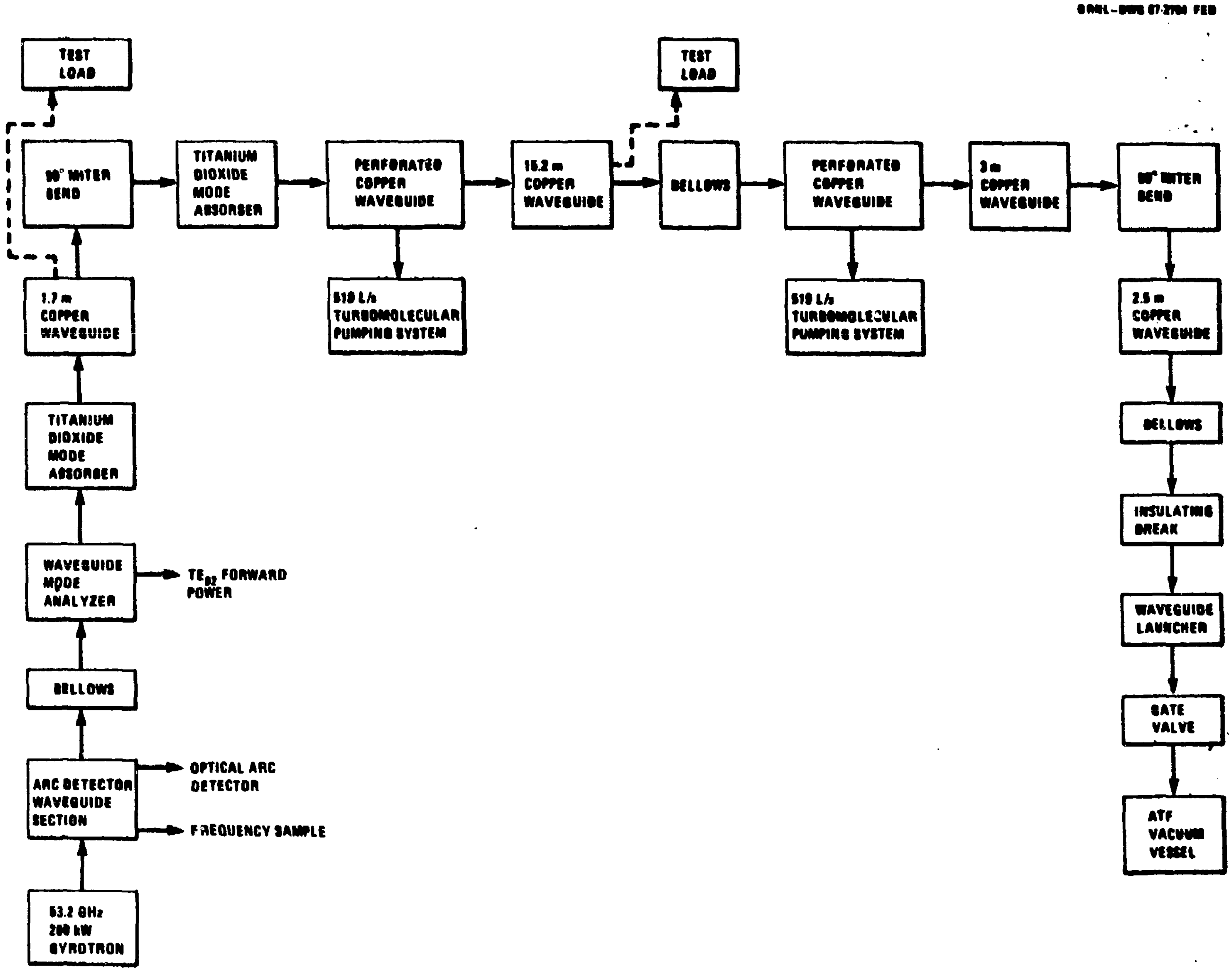

HIGH-POWER TESTS

- ECH POWER IS MEASURED CALORIMETRICALLY BY ACCURATELY MEASURING THE TEMPERATURE RISE AND WATER FLOW THROUGH A WATER-COOLED MICROWAVE 'TEST' LOAD.

- THE GYROTRON POWER IS PULSED ON AND OFF CONTINUOUSLY AT PEAK POWERS $\leq$200 kW.

- NORMALLY, THE AVERAGE POWER IS HELD TO LESS THAN 20 kW TO PROTECT UNCOOLED BELLOWS AND PUMPOUT SCREENS IN THE WAVEGUIDE SYSTEM.

- THE CALORIMETRIC POWER IS USED TO CALIBRATE A WAVEGUIDE MODE ANALYZER THAT CAN MEASURE INSTANTANEOUS POWER.

WAVEGUIDE MODE ANALYZER

ORNL-DWG 85-3447R FED

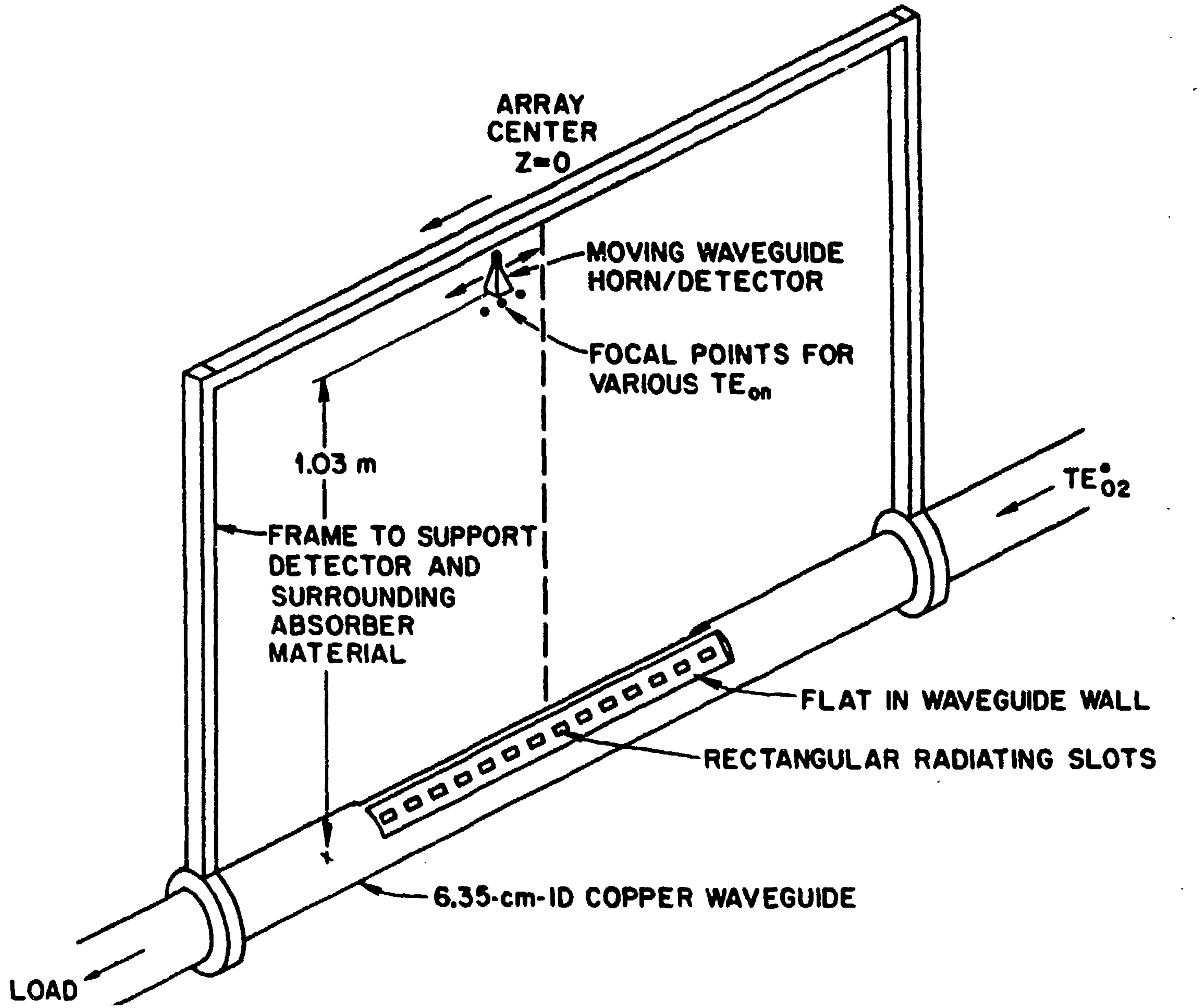

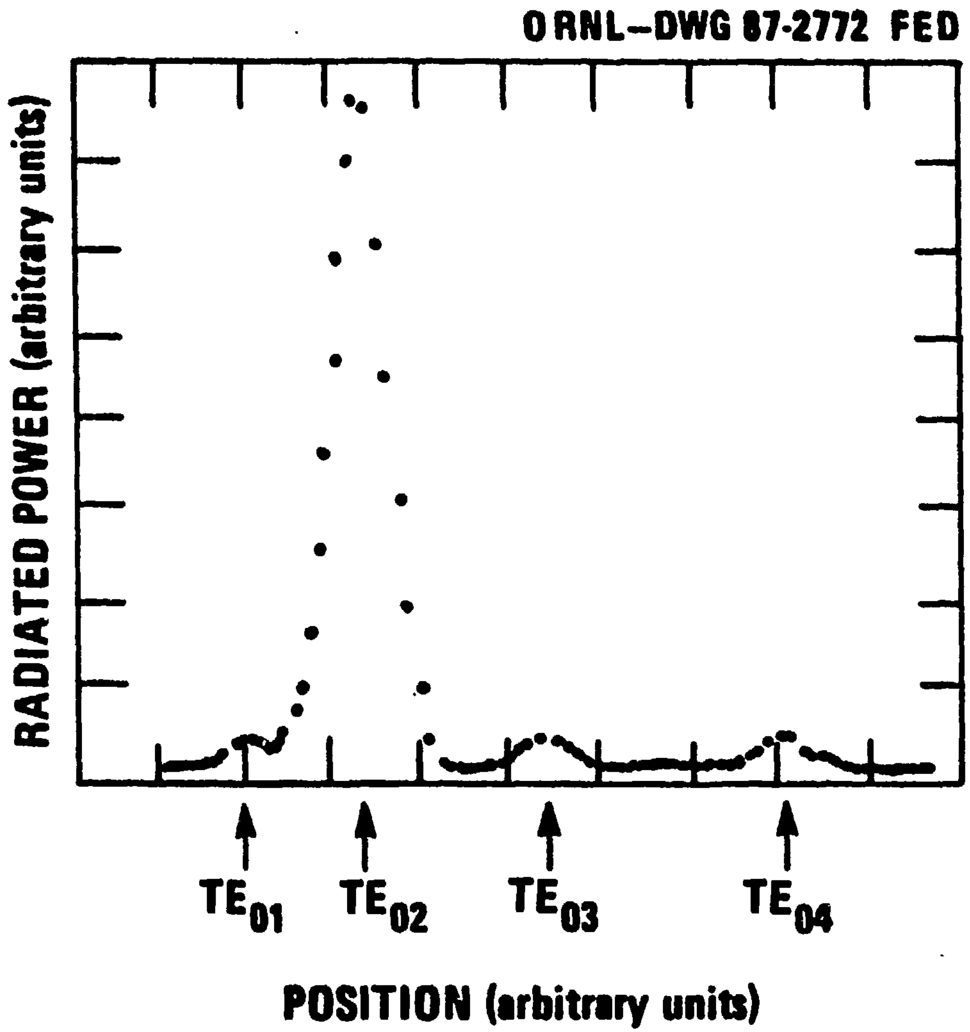

T. L. WHITE, T. S. BIGELOW, H. D. KIMREY, "INITIAL HIGH-POWER TESTING OF THE ATF ECH SYSTEM," EC-6, JOINT WORKSHOP ON ECE AND ECRH, SEPTEMBER 15-17, 1987.

WAVEGUIDE TRANSMISSION LOSSES (PEAK) vs TIME FOR A SINGLE BEND SYSTEM

ORNL-DWG 87-3041 FED

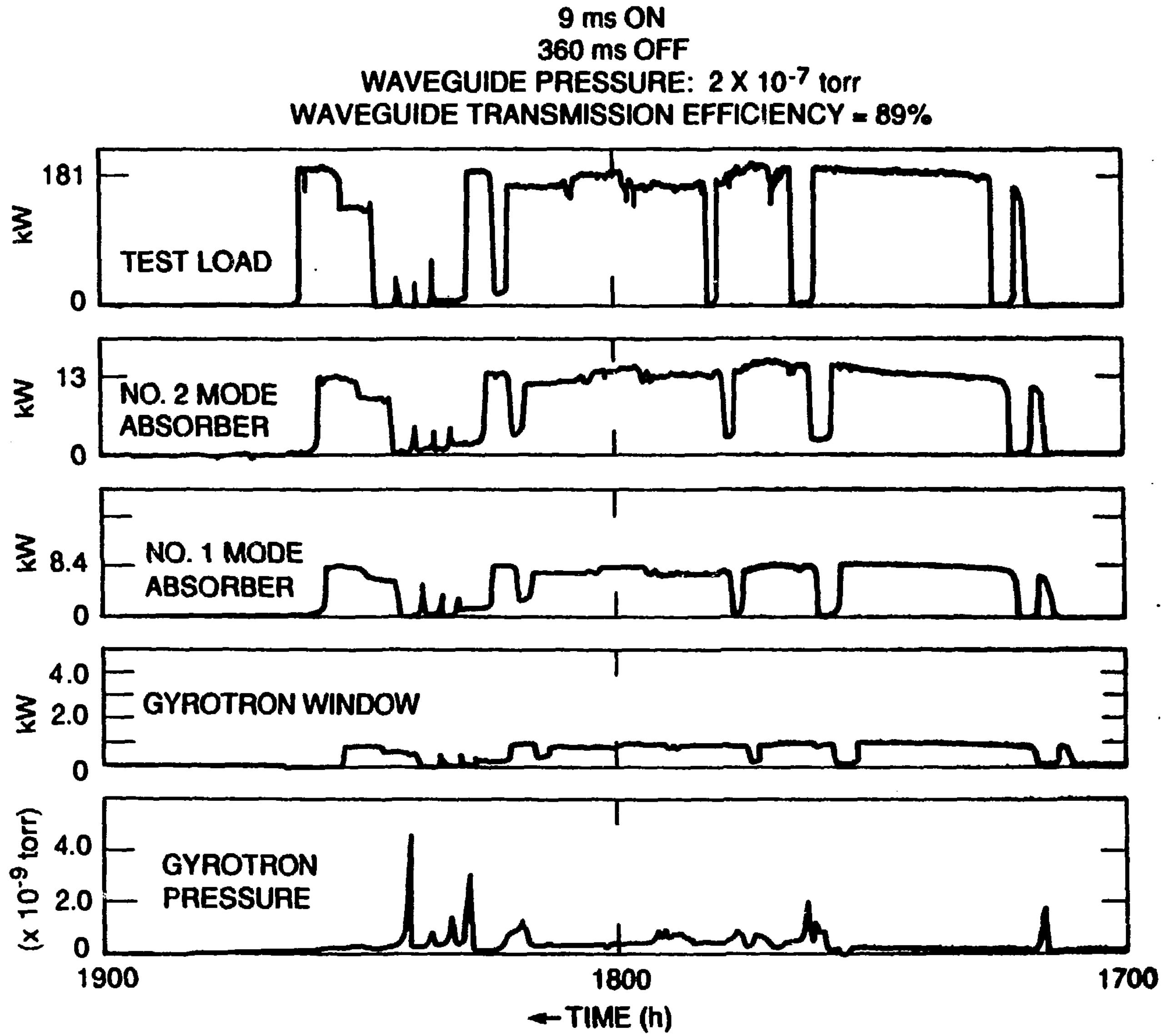

WAVEGUIDE MODE ANALYZER OUTPUT vs TIME

ORNL-DWG 87-3042 FED

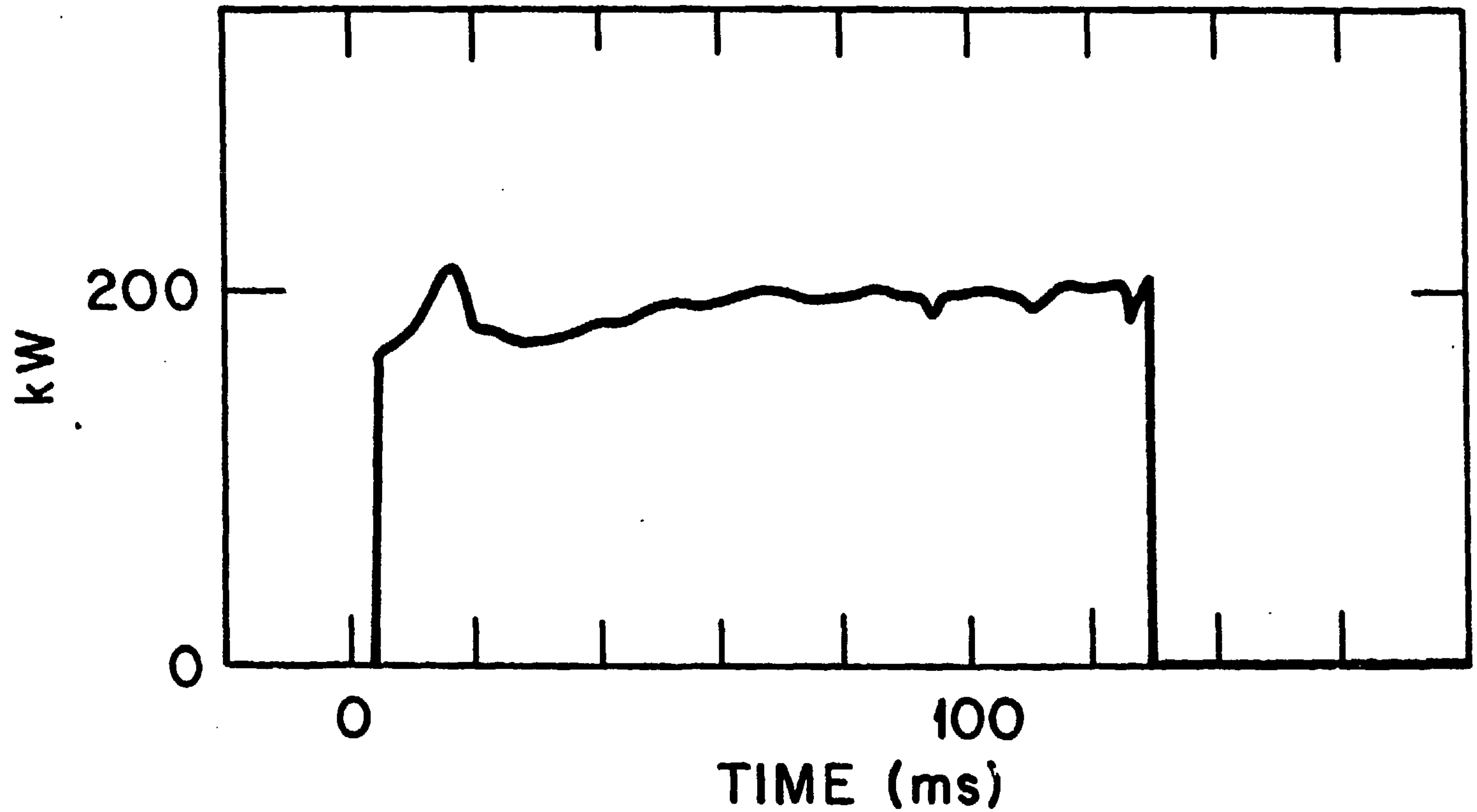

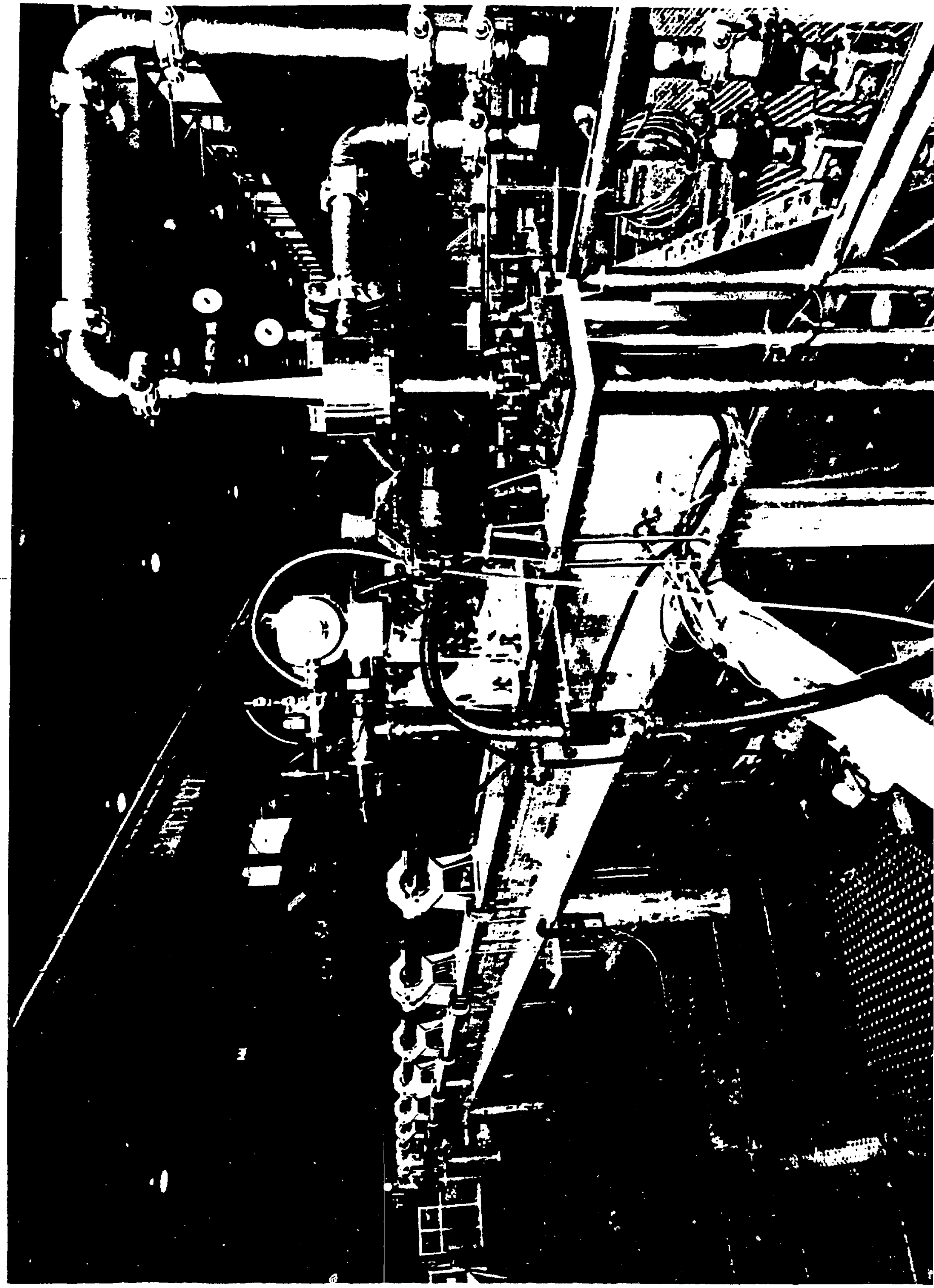

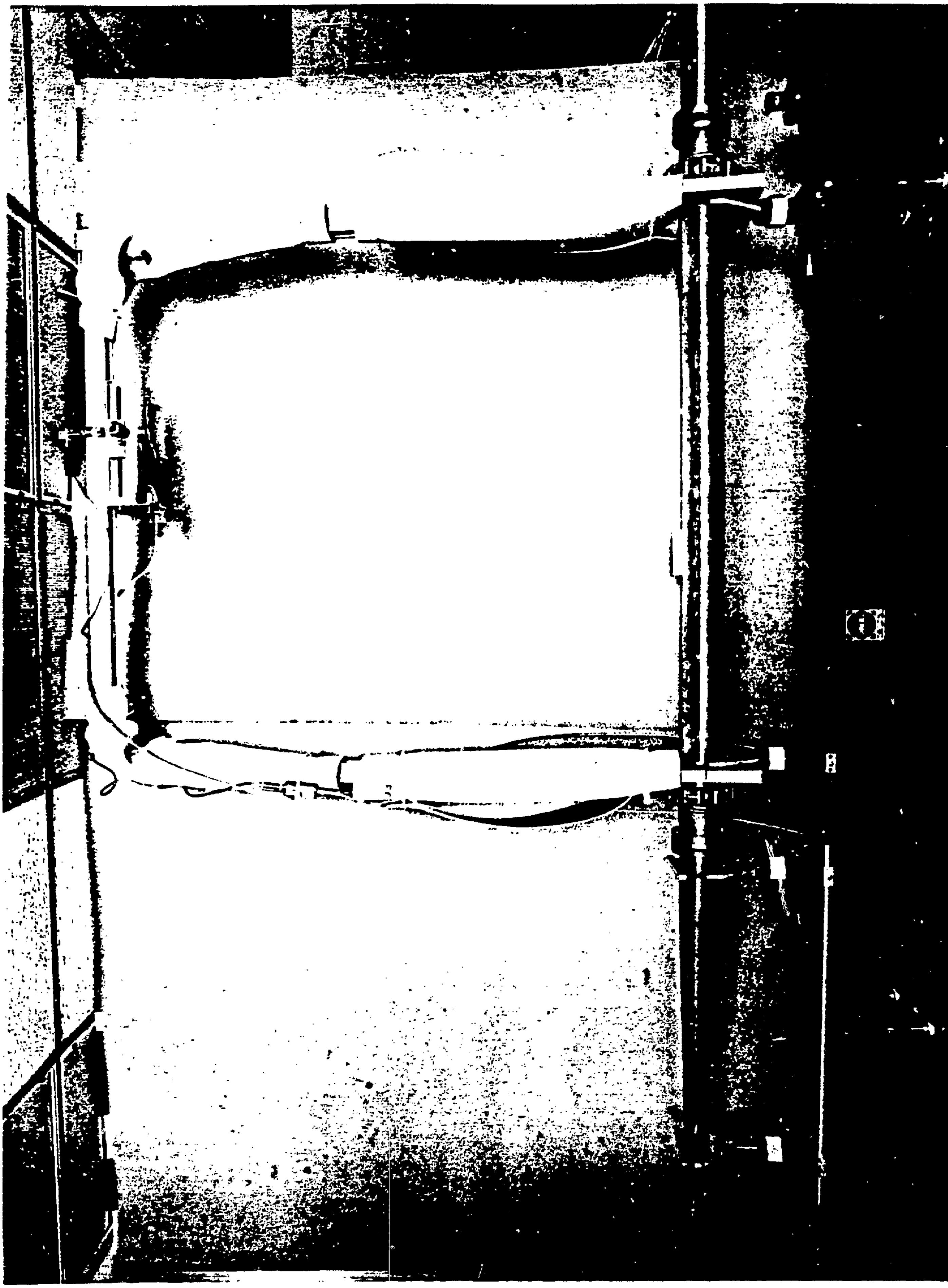

HIGH-POWER TESTS (CONT)

- THE WAVEGUIDE MODE ANALYZER WILL BE THE PRIMARY POWER DIAGNOSTIC DURING ATF OPERATION.

- THE OVERALL ECH WAVEGUIDE SYSTEM EFFICIENCY WITH TWO BENDS IS 87%.

- WAVEGUIDE PRESSURE DURING OPERATION IS LOW (10^{-7} TORR SCALE).

TLW: 11/5/87.3

ECH COMMISSIONING TASKS

- INVESTIGATE GYROTRON "TUNE-UP" MODES WITHOUT MAGNETIC FIELD OR GAS PUFF
  - REQUIRED TO SET UP GYROTRON FOR OPTIMUM POWER SHOT AFTER SHUTDOWN
  - REQUIRED TO ASSURE PEAK POWER AVAILABLE BETWEEN 5 MINUTE ATF SHOTS
  - 200 kW SHORT PULSE OPERATION ≤10 ms FOR REPETITION RATES ≤2 Hz TO LIMIT AVERAGE POWER INTO ATF VACUUM VESSEL TO ≤4-5 kW

ECH COMMISSIONING TASKS (cont.)

- MICROWAVE RADIATION SURVEY NEEDED TO EVALUATE POTENTIAL HAZARDS TO EQUIPMENT, PERSONNEL
  - MICROWAVE PROTECTION SYSTEM CONSISTS OF AN ARRAY OF FOUR CALIBRATED DETECTORS PLACED AROUND THE ATF AND GYROTRON ENCLOSURES (INTERLOCKED WITH ECH OPERATION)
  - PORTABLE DETECTOR USED TO SURVEY ECH WAVEGUIDE AND OTHER AREAS

TLW: 11-11-87.8

ECH COMMISSIONING TASKS (cont.)

- EXPLORE POTENTIAL INTERACTIONS OF THE ECH SYSTEM WITH THE ATF HELICAL FIELD POWER SUPPLY
  - 13.8 kV POWER GRID PERTURBATIONS WERE SIGNIFICANT WHEN ISX-B AND EBT-S WERE OPERATING SEVERAL YEARS AGO
  - WHILE GYROTRON POWER SUPPLY HAS FAST REGULATION CONTROL, OTHER SYSTEMS SUCH AS THE GYROTRON MAGNETS DO NOT
  - TIME VARYING B_{HF} MAY CAUSE GROUND LOOP NOISE IN ECH GROUNDING SYSTEM
  - TIMING ECH SHOT FOR CURRENT FLATTOP MAY SOLVE THESE PROBLEMS

ECH COMMISSIONING TASKS (cont.)

- OPTIMIZE ELECTRON DENSITY AND TEMPERATURE AT A FIXED ECH INPUT POWER BY VARYING GAS PUFF, HELICAL FIELD CURRENT, AND VERTICAL FIELDS
  - INVESTIGATE THE REPEATABILITY OF EACH OF THE ABOVE EXPERIMENTALLY CONTROLLED PARAMETERS
  - THERE IS A NARROW "WINDOW" IN $\omega_{ceo}/\omega_{\mu}$ FOR PLASMA PRODUCTION AND HEATING
  - MARK CARTER WILL DISCUSS ATF "PRESSURE WINDOW" FOR ECH BREAKDOWN

TLW: 11-11-87.8

FUTURE PLANS

- NEAR TERM (1 YEAR)
  - INSTALL 2ND 200 kW 53.2 GHz ECH WAVEGUIDE SYSTEM
  - UPGRADE POWER SUPPLY TO OPERATE TWO GYROTRONS SIMULTANEOUSLY
  - UPGRADE SIMPLE OPEN WAVEGUIDE (TE_{02}) LAUNCH WITH FOCUSED, POLARIZED BEAM LAUNCH

TLW:11-11-87.2

ORNL-DWG 87-2793 FED

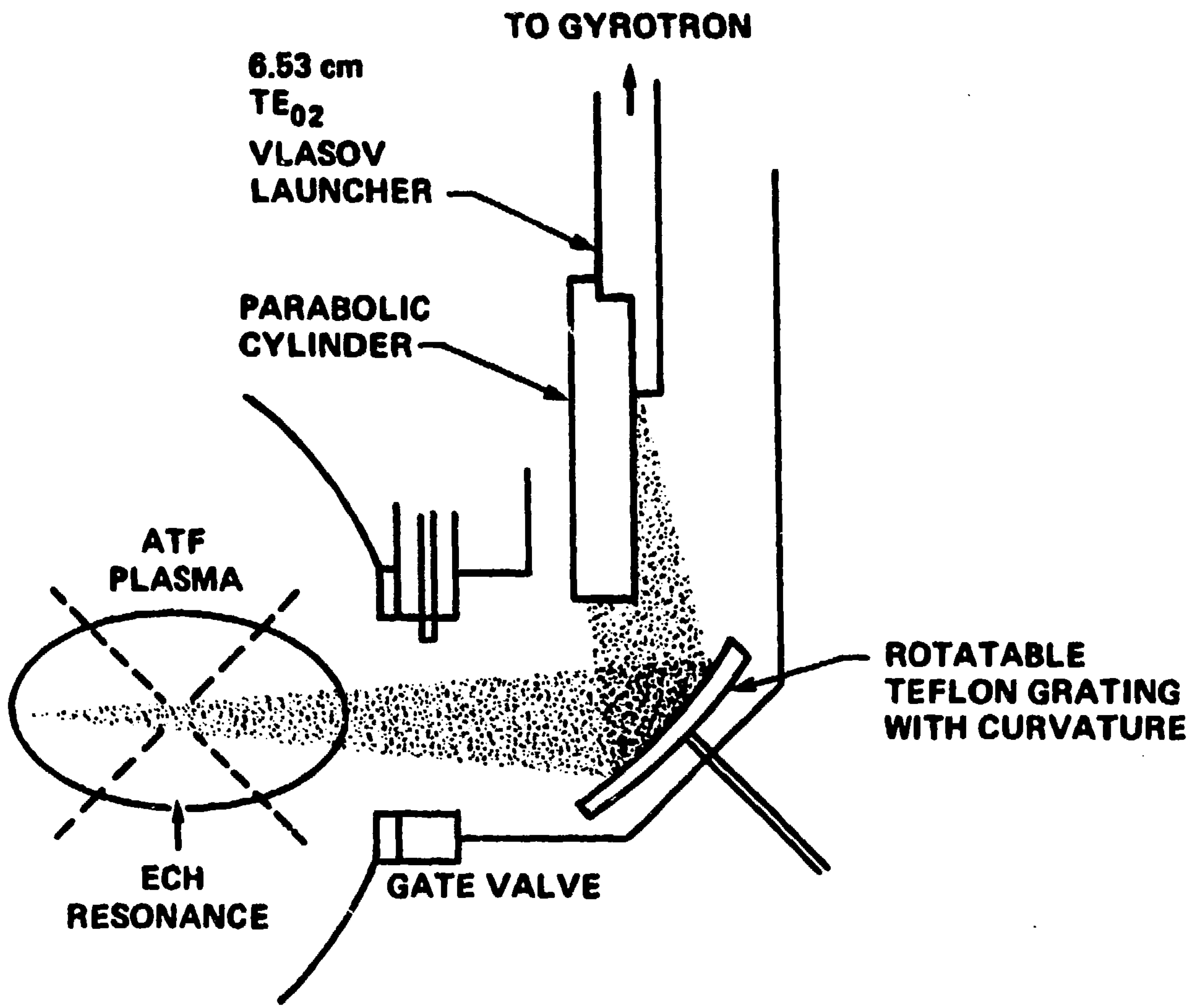

T. S. BIGELOW AND T. L. WHITE, "ATF ECH WAVEGUIDE COMPONENT DEVELOPMENT AND TESTING," 12TH INT. CONF. ON INFRARED AND MILLIMETER WAVES, ORLANDO, FLORIDA, DECEMBER 14-18, 1987.

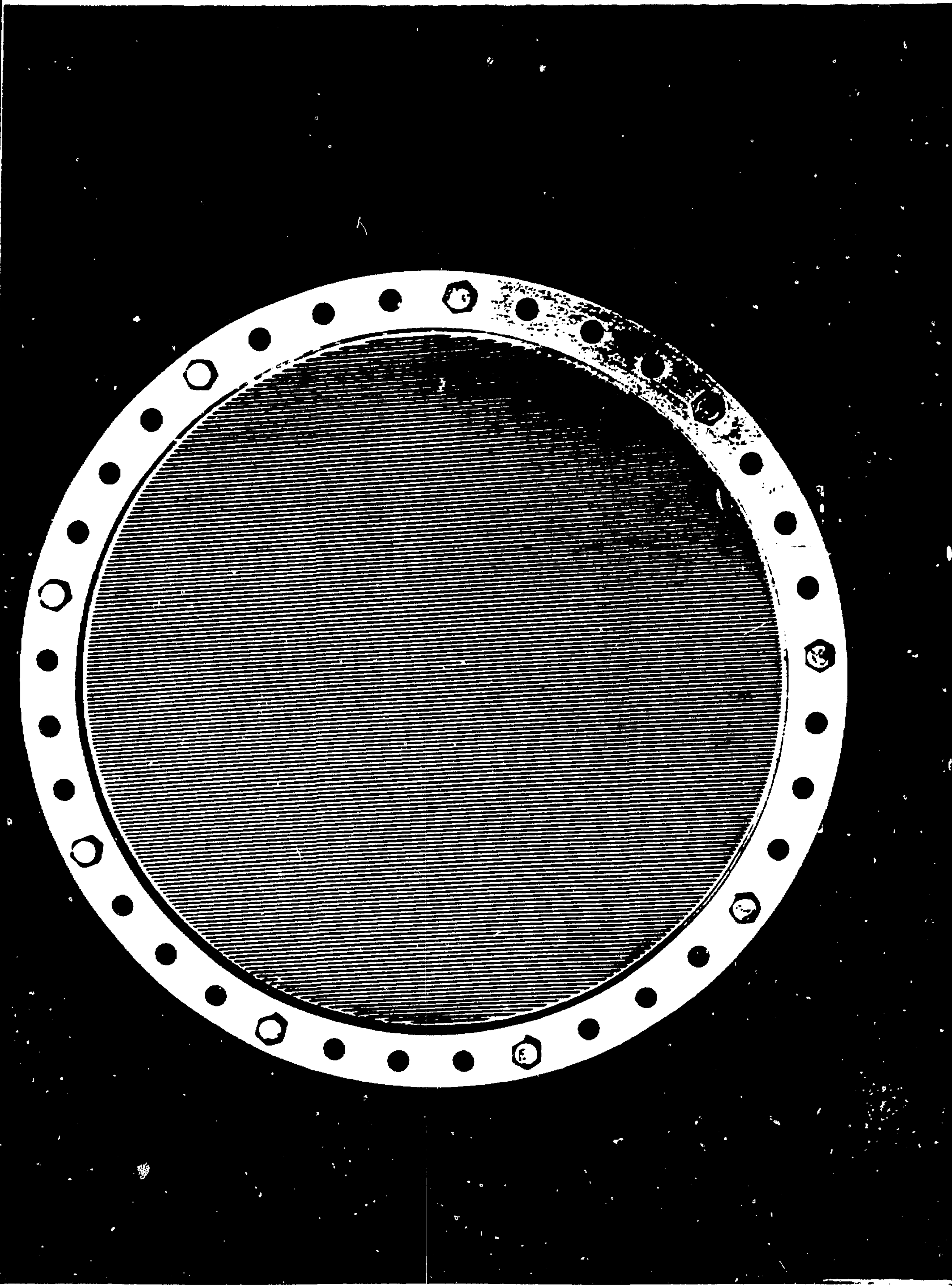

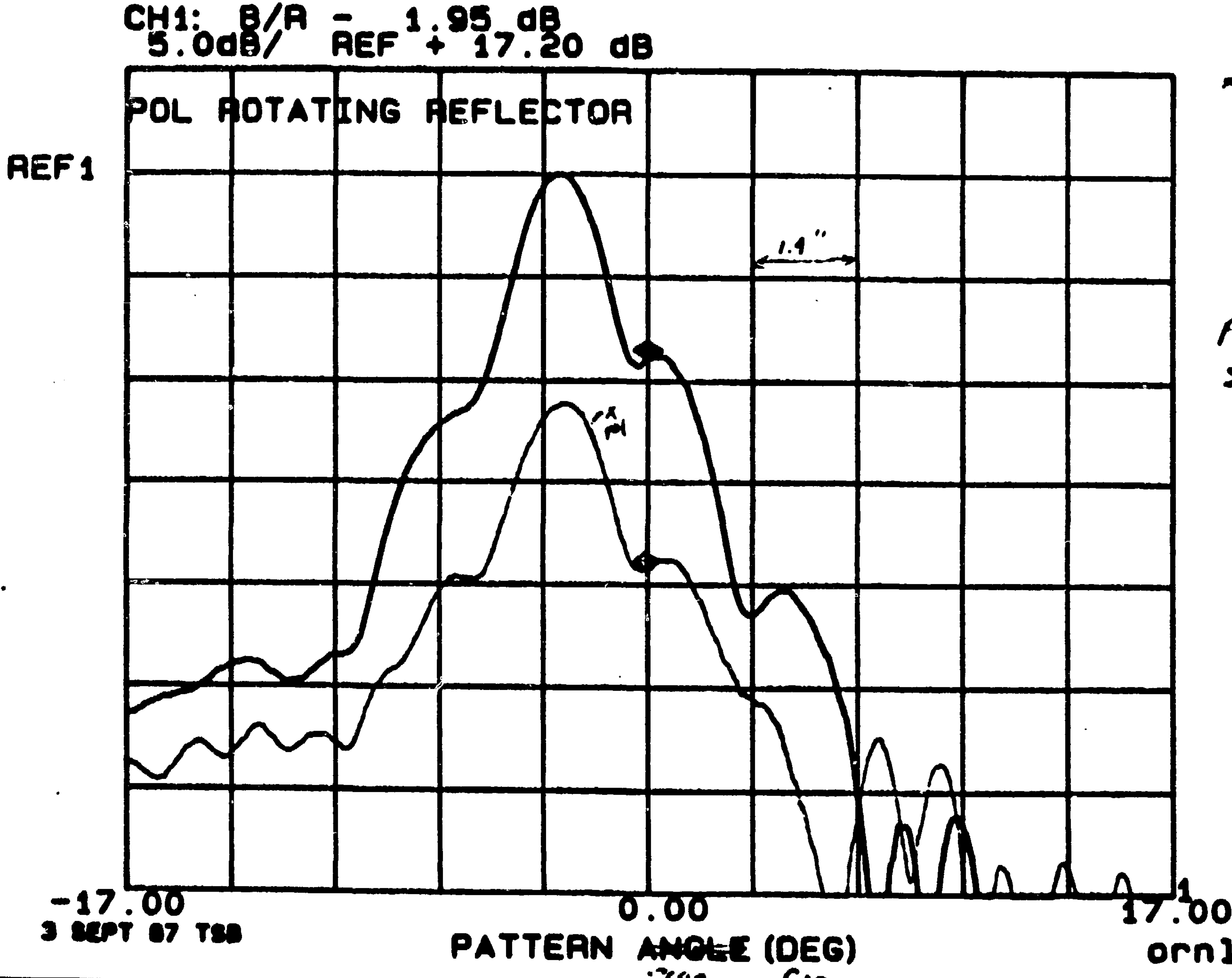

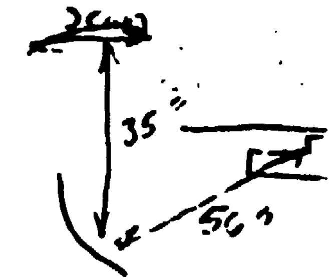

pol rotate 90° setting
.33" deformation
x-pol by rotating receiving horn

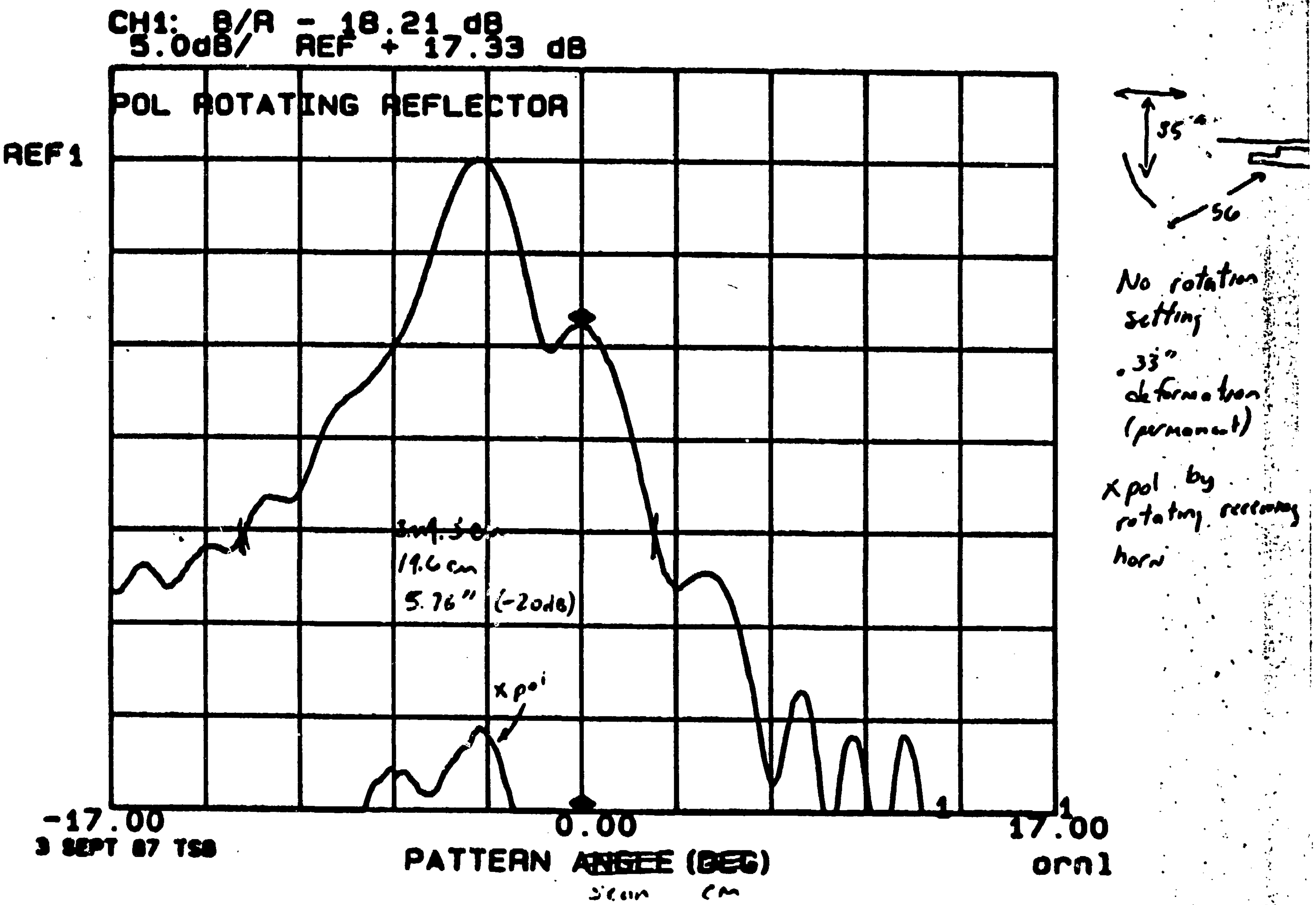
CH1: B/R - 18.21 dB
5.0dB/ REF + 17.33 dB
POL ROTATING REFLECTOR
REF1
3M.5 on
19.6 cm
5.76" (-20dB)
x pol
-17.00
0.00
17.00
3 SEPT 87 TSB
PATTERN ~~ANGLE~~ ~~(DEG)~~
scan cm
ornl
35"
56
No rotation setting
.33" deformation (permanent)
x pol by rotating receiving horn

FUTURE PLANS (cont.)

- **LONGER TERM (3-4 YEARS)**
  - SUPPORT STEADY STATE ATF PROGRAM WITH ~2 MW OF ECH POWER
  - ECH IS THE PREFERRED HEATING APPROACH BECAUSE:
    - POWER DEPOSITION CAN BE LOCALIZED AND CONTROLLED BY VARYING FREQENCY (MAGNETIC FIELD) AND BEAMING
    - MINIMAL INTERACTION WITH THE WALLS AND THE EDGE PLASMA
    - LESS DEMANDING ACCESS AND LAUNCHING REQUIREMENTS
    - PHYSICS IS WELL UNDERSTOOD
    - HIGHLY SUITABLE FOR NON-HEATING APPLICATIONS

TLW:11-11-87.3

FUTURE PLANS (cont.)

- 53.2 GHz BEST CHOICE FOR STEADY-STATE OPERATION (0.95 TESLA, SECOND HARMONIC X-MODE)

- 106 GHz BEST FOR HIGH DENSITY OPERATION (1.9 TESLA, SECOND HARMONIC X-MODE) BUT LIMITED ON ATF TO 3-4 SEC

- CHOICE OF FREQUENCY WILL BE DETERMINED BY ATF PROGRAM DIRECTION AS WELL AS PROGRESS IN GYROTRON DEVELOPMENT

PLASMA PRODUCTION, Mark Carter OR

Outline

- Prior to plasma formation, start with only a few free electrons in machine
- Motivation and basics of 2nd harmonic ECH startup in Heliotron-E & ATF
  - nonlinear orbits required
- Simple power balance for 1st harmonic ECH startup
  - linear phenomenon
- Range of |B| for ECH production in ATF
- ICRH production possibilities
  - Uragan III data
  - hypothesis for observed behavior

A few free electrons are always available from various sources

- $\sim$ 200 millirad/year natural background radiation in ATF vacuum vessel with fields on $\rightarrow$ few tens of free $\bar{e}$'s in $\sim$ 1sec depending on fill pressure

- Field ramp in torsatrons induce a loop voltage which might produce additional free electrons

  - Heliotron-E tries very hard to prevent electron runaway by strong gas puffing and introducing field errors

  - Wendelstein VII a has no induced loop voltage but can still breakdown with second harmonic ECH

- If rf is strong enough, population will grow exponentially so it doesn't take too many to get started

I. Motivation for 2^{nd} harmonic ECH analysis

- For high βeta experiments in ATF, the 53 GHz microwaves will be resonant at the second harmonic
  - Heliotron-E can get reasonable plasma with $\gtrsim 80$ kW
  - Early ATF has 1 gyrotron (< 200 kW) and ATF is larger $\Rightarrow$ lower power density than Heliotron for given input

- Interesting nonlinear physics problem for second harmonic interactions
  - linear energy absorption $\sim (k\rho)^2 \omega_b$ is <u>very</u> small for cold (~ 0.025eV) electrons

    $\Rightarrow$ linear theory can't explain breakdown
  - <u>But</u> if resonance occurs at a local minimum of $|\underline{B}|$ along $\underline{B}$, nonlinear effects are important

    $\Rightarrow$ nonlinear orbits make breakdown possible

Solution to relativistic equations of motion on a gyroperiod time scale

- trapped at bottom of well ($v_{\parallel} = 0$)
- ~0.025eV initial energy

$\Rightarrow$ periodic energy excursions give possibility of ionization

$f = 18\,\mathrm{GHz}$, $|E_-| \approx 100\ \mathrm{V/cm}$, $k_{\parallel} = 0$, $k_{\perp} = \frac{\omega}{c}$

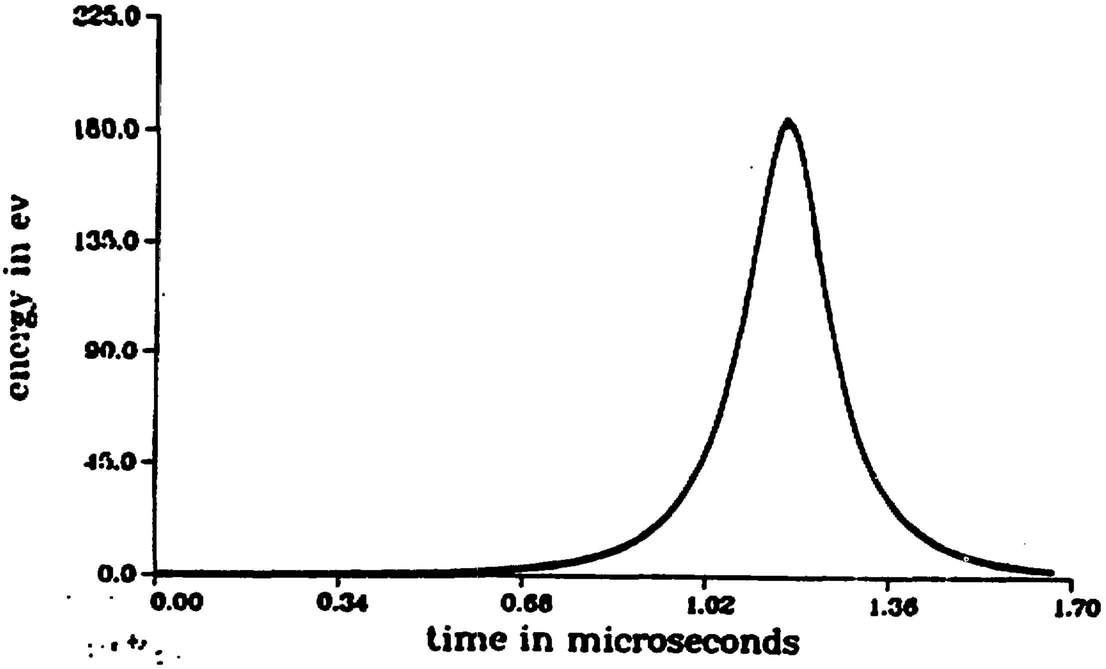

For 2nd Harmonic ECH, Large Perpendicular Energy Excursions occur if Electrons are trapped near Resonance

- Cold electrons are easily trapped when passing through the resonance region
- A few cold electrons always exist because of natural background radiation (ie. μ-meson cosmic ray bombardment)
- Energy time behavior is approximated by*:

$$E(t) \simeq \frac{E_{exc}}{2}\left[1 - \cos(\nu_{rf} t)\right]$$

where: $E_{exc} \approx 3.2\,\varepsilon mc^2$; $\nu_{rf} \approx \varepsilon\omega$

$$\varepsilon \equiv \frac{2e|E_-|}{mc\omega}$$

ω = microwave driving frequency

$|E_-|$ = modulus of right hand polarized component of microwave electric field strength

m = electron rest mass

c = speed of light in vacuum

e = magnitude of electron charge

* Phys. Fluids 29, 100 (1986)

$\psi = 0.3$
$\iota = 0.4$

Near the X-Point
A Well Exists in $|\underline{B}|$ along $\underline{B}$
ON THE INSIDE OF THE TORUS

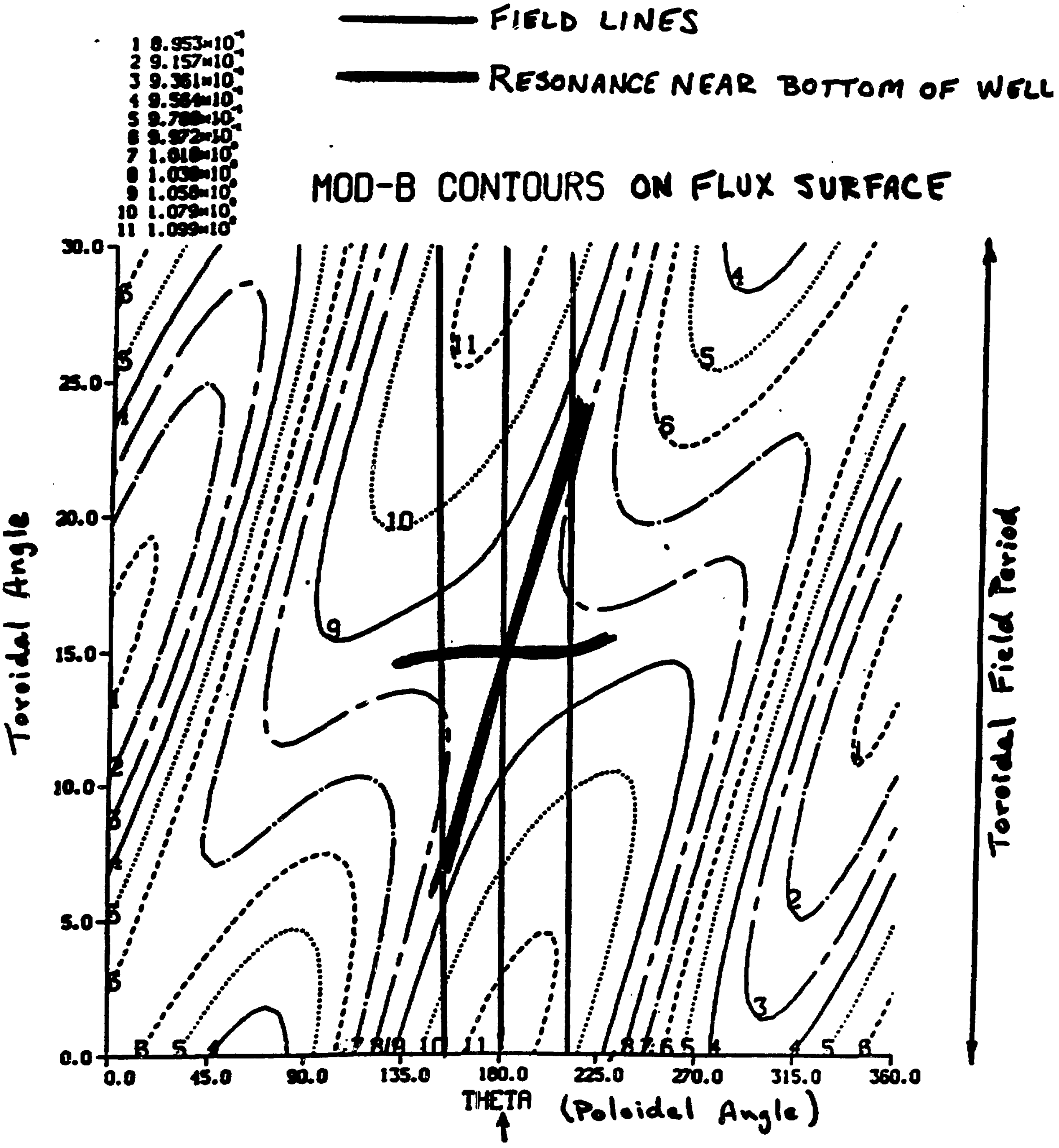

Resonance Layer is Wide if it occurs Near the Saddle Point

- Nonlinear Excursions are strongest near weak $\nabla|B|$

ORNL-DWG 84-3811R FED

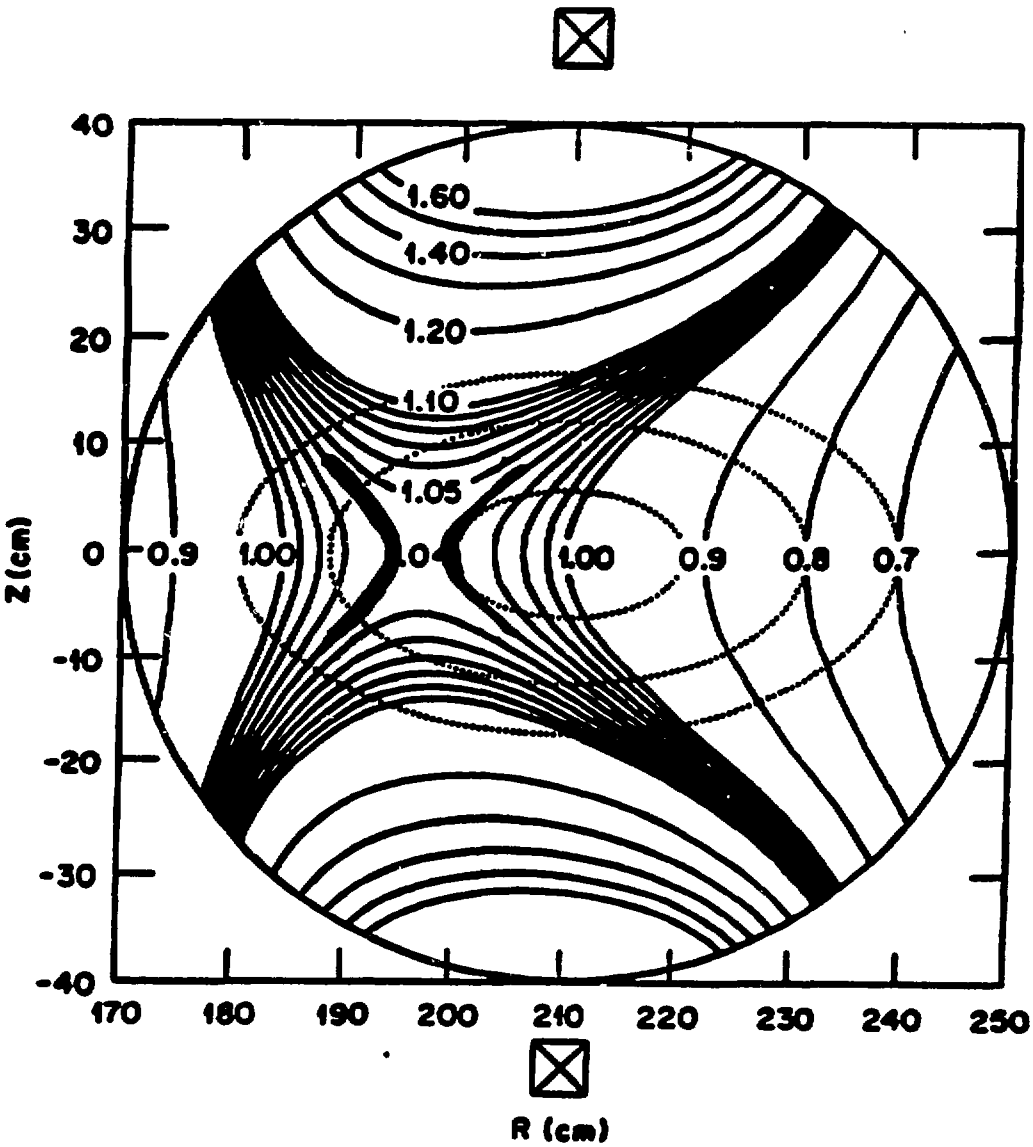

Cold electrons are easily trapped near resonance when excursion frequency, $\nu_{rf} \simeq \varepsilon\omega$, exceeds the bounce frequency, ω_b.

a)

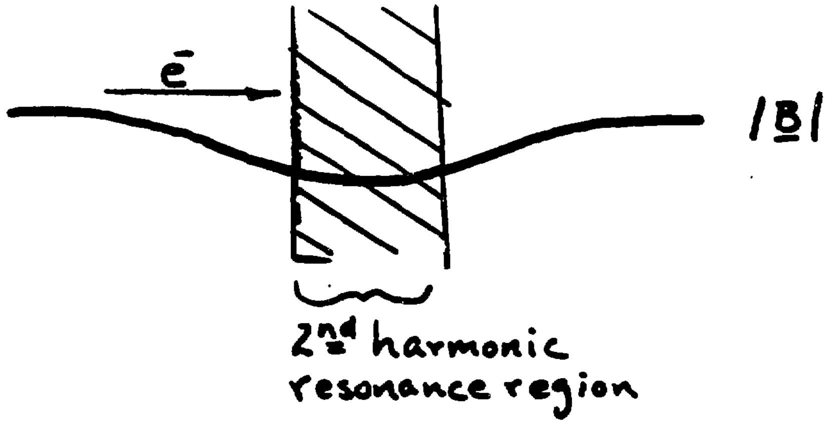

cold electron slowly enters resonance region and perpendicular energy rapidly increases

b)

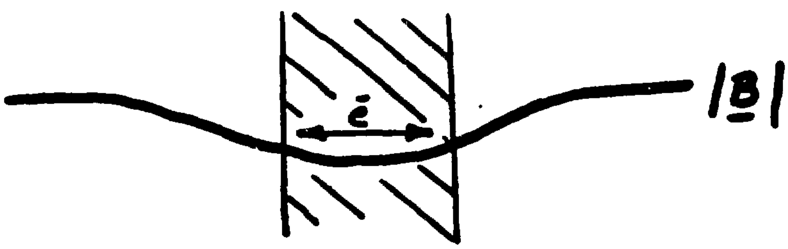

electron becomes magnetically trapped near resonance and undergoes energy excursions

Schematic shows the regions in velocity space occupied by each group

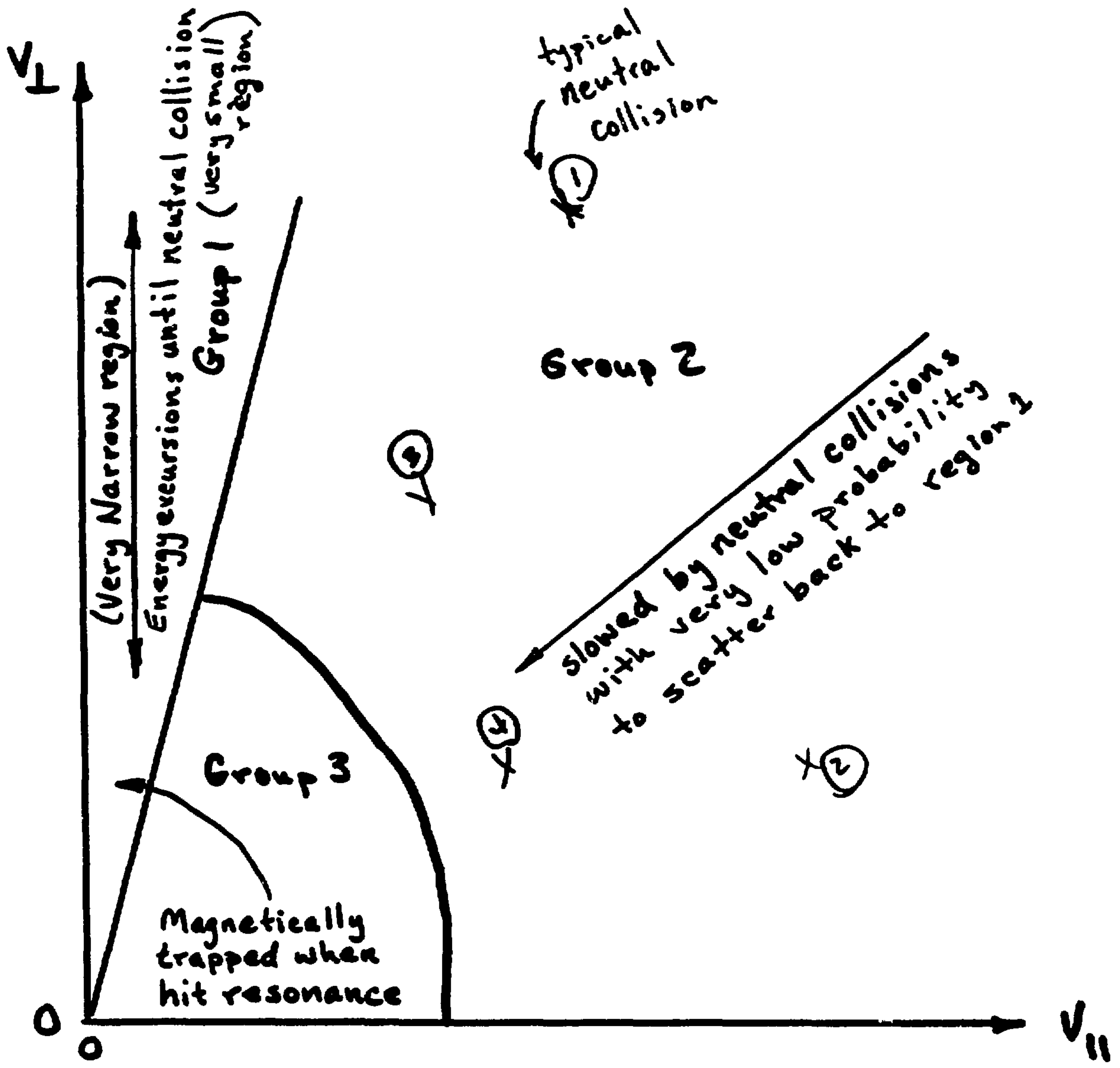

- Electrons in groups 1 and 2 cause new electrons to be born in group 3 (assumption)

- First neutral collision by group 1 electron de-traps it (moves to group 2)

ELECTRON MULTIPLICATION MODEL IS SIMILAR TO FISSION CRITICALITY MODELS*

- Duderstadt, Hamilton Nuclear Reactor Analysis, Wiley and Sons, New York pp 75, 2

$$\begin{cases} k \equiv \dfrac{\text{Number of electron in second generation}}{\text{Number of electrons in first generation}} \Big\} \text{ Multiplicati Factor} \\ \dfrac{\delta n}{\delta t} \approx \dfrac{dn}{dt} \approx \dfrac{(k-1)n}{\ell} \quad \text{is rate equation} \\ \ell \equiv \text{Average time required to complete cycle} \end{cases}$$

- Let: $K = \sum_m C_m$; $\ell = \sum_m P_m t_m$ where $P_m = \dfrac{C_m}{K}$

  where: - C_m is the number of 2nd generation electrons appearing through channel m

  - P_m is the probability of 2nd generation electron appearing through channel m
  - t_m is the time required for an electron to proceed through channel m

- 3 channels in model
  - channel 1: ionization in Group 1 collision
  - channel 2: ionization during slowing down
  - channel 3: original electron recycles

→ GROWTH RATE $\equiv \gamma = \dfrac{K-1}{\ell}$

Electric Field Strength is most important parameter

- Estimate for cavity with surface area, A_c
- Assume vacuum

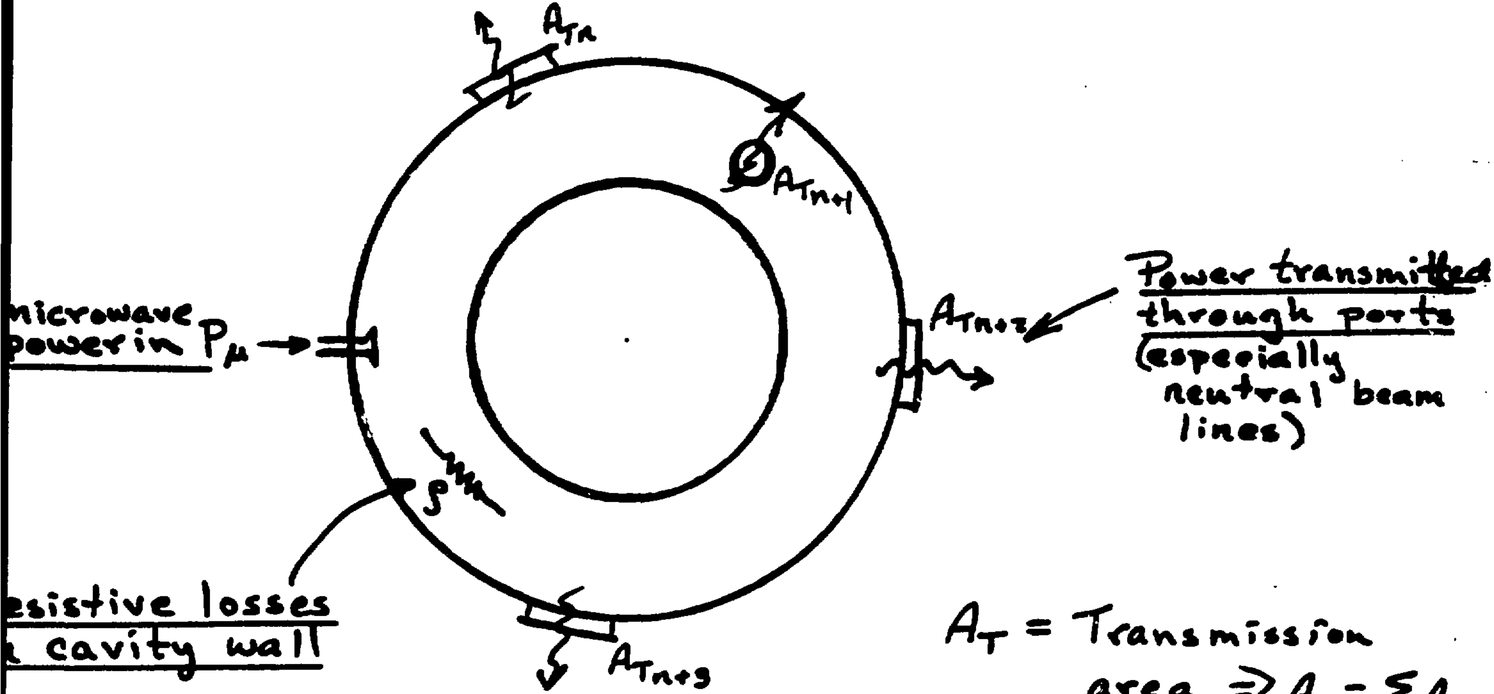

A_T = Transmission area $\Rightarrow A_T = \sum A_{T_n}$

- Assume $\frac{1}{2}$ power in the right hand polarized component, $|E_-|$

$$|E_-| \approx 19.4 \left[\frac{P_\mu}{A_T + 9\times10^{-4}\sqrt{f\rho_c'}\,A_c} \right]^{1/2} \frac{\text{Volts}}{\text{meter}}$$

P_μ in watts, A_c = cavity surface area in m^2, f in GHz, ρ = resistivity in $\mu\Omega m$, A_T in m^2

- Simple cross section approximation, 36 eV ~~to form~~ electron, ion pair

Estimates for Heliotron-E using 2^{nd} harmonic

- Fixed $|E_-|$; power estimates by comparison to experimen

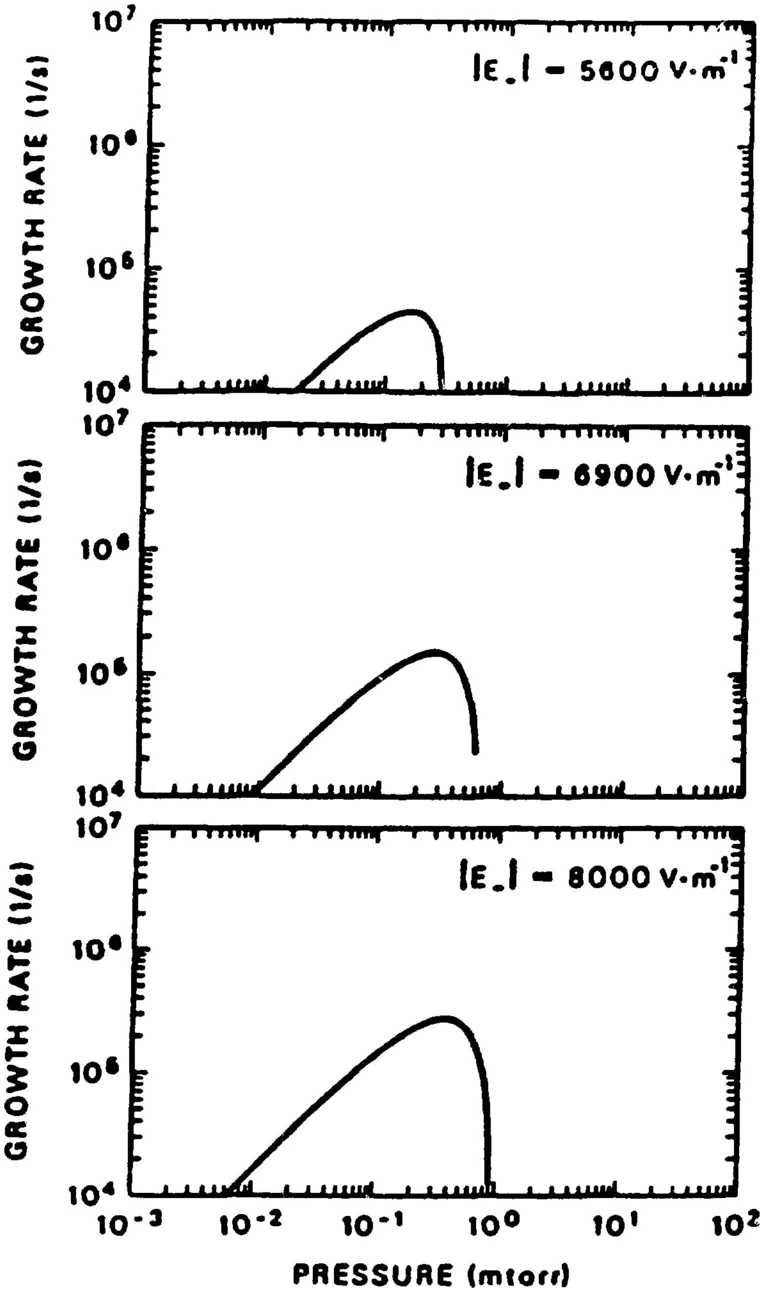

~ 100 kW ?

~ 150 kW ?

~ 200 kW ?

FIG. 6. Growth rate for parameters similar to Heliotron-E: a_c = 25 cm, R = 210 cm, $\omega/2\pi$ = 53 GHz, N_f = 19.

Second Harmonic ECH Breakdown in ATF Depends Strongly on Vessel Transmission Area

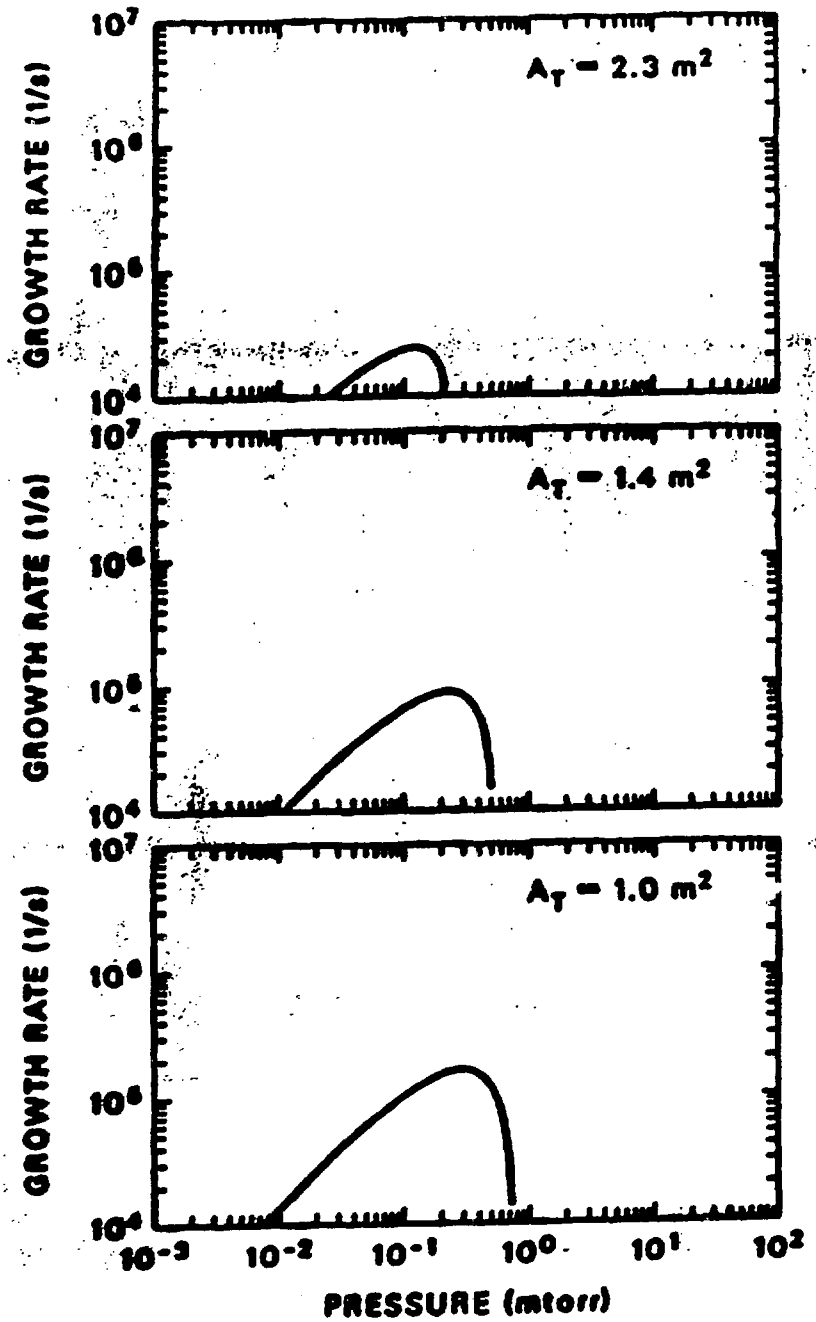

FIG. 7. Growth rate for parameters similar to ATF: $a_c = 40$ cm, $R = 210$ cm, $\omega/2\pi = 53$ GHz, $N_f = 12$.

Long Scale Lengths required for 2nd harmonic

- The resonance layer can not be "thinner" than the gyroradius of an ionizing electron

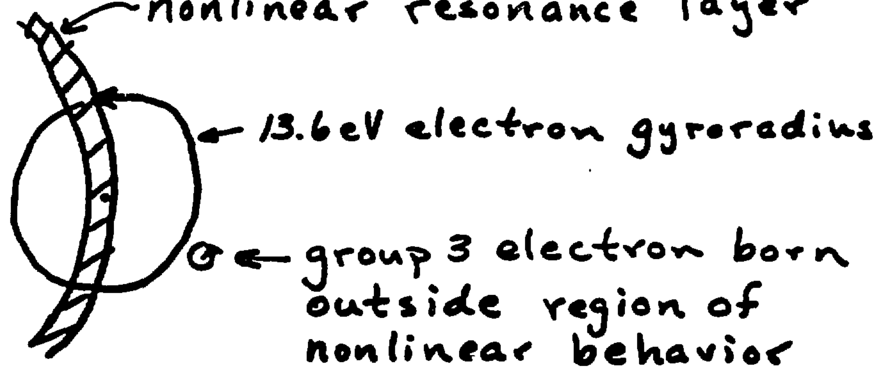

- If ionization electrons are born on field lines which do not pass through a nonlinear interaction region, they must diffuse back to nonlinear resonance instead of just making a field period transit

  ⇒ becomes difficult to complete cycle on a reasonable time scale

⇒ Resonance near mod B X point or axis leads to narrow range of magnetic field

2nd harmonic ECH breakdown described by linear power balance model

Quasilinear (Kennel + Englemann) rf operator averaged over torus

$$\frac{\partial f}{\partial t} \approx \frac{R}{a\Omega_{res}} \frac{\pi e^2}{m} \frac{|E_-|^2}{4} \frac{1}{v_\perp} \frac{\partial}{\partial v_\perp} v_\perp \frac{\partial f}{\partial v_\perp}$$

$$\Rightarrow \frac{P}{n_e} \approx \frac{1.6}{B_{res}} \frac{R}{a} |E_-|^2 \frac{eV}{sec}$$

$|E_-|$ in V/m
B_{res} in Tesla
R = major radius
a = minor radius

↑ Power absorbed per electron

$|E_-|$ estimate including plasma loading

$$|E_-|^2 = (19.4)^2 \left[\frac{P_\mu}{A_T + 9\times10^{-4}\sqrt{f\,\delta_c}\,A_c + \frac{1\times10^{-16}}{B_{res}} \frac{R}{a} n_e V} \right]$$

n_e = electron density ; V = plasma volume

Average electron model

$$\frac{dE}{dt} \approx \frac{P}{n_e} - \underbrace{\nu_{en} E_e}_{\text{neutral collisions}} - \underbrace{\frac{E}{\tau}}_{\text{transport}} \quad ; \quad \frac{dn_e}{dt} \approx n_e \left[\underbrace{\frac{\sigma_i}{\sigma_T}(E)\,\nu_{en}}_{\text{ionization}} - \underbrace{\frac{1}{\tau}}_{\text{transport}} \right]$$

$\Rightarrow$ Equilibrium, $\frac{dE}{dt} = \frac{dn}{dt} = 0$

$\Rightarrow$ Estimate τ and iterate for solution

Confinement Model for 1st harmonic ECH startup

- Assume hyperbolic $|B|$ surfaces

$$|B|^2 \approx \begin{cases} B_o^2 - (2B_o\varepsilon_2 - \varepsilon_2^2)h^2x^2 & ; y=0 \\ B_o^2 + (2B_o\varepsilon_2 + \varepsilon_2^2)h^2y^2 & ; x=0 \end{cases}$$

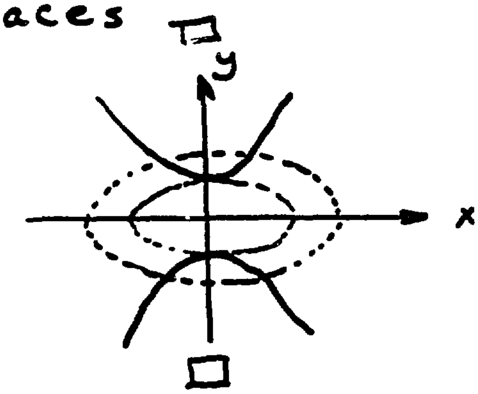

$$\psi \propto \left[x^2+y^2 - \frac{\varepsilon_2}{B_o}(x^2-y^2)\right]$$

$$h \equiv \frac{m}{\ell R} \quad ; \quad \varepsilon_2 \equiv 2B_o h a_c K'(2ha_c)$$

$\ell = 2$; R = major radius ; a_c = coil radius

- Let ψ_{res} be flux surface tangent to resonant surface and crudely model confinement time for electrons born in resonance region by:

$$\tau \approx \tau_{max}\left(1 - \psi_{res}/\psi_{max}\right)^{s}$$

(s is adjustable)
typically $s=2$

$\Rightarrow$ reasonable properties

a) no confinement if resonance is outside last closed flux surface

b) best confinement when resonance covers all closed flux surfaces

"Heliotron-like" parameters appear to be reasonable

– Note: Cutoff not accounted for

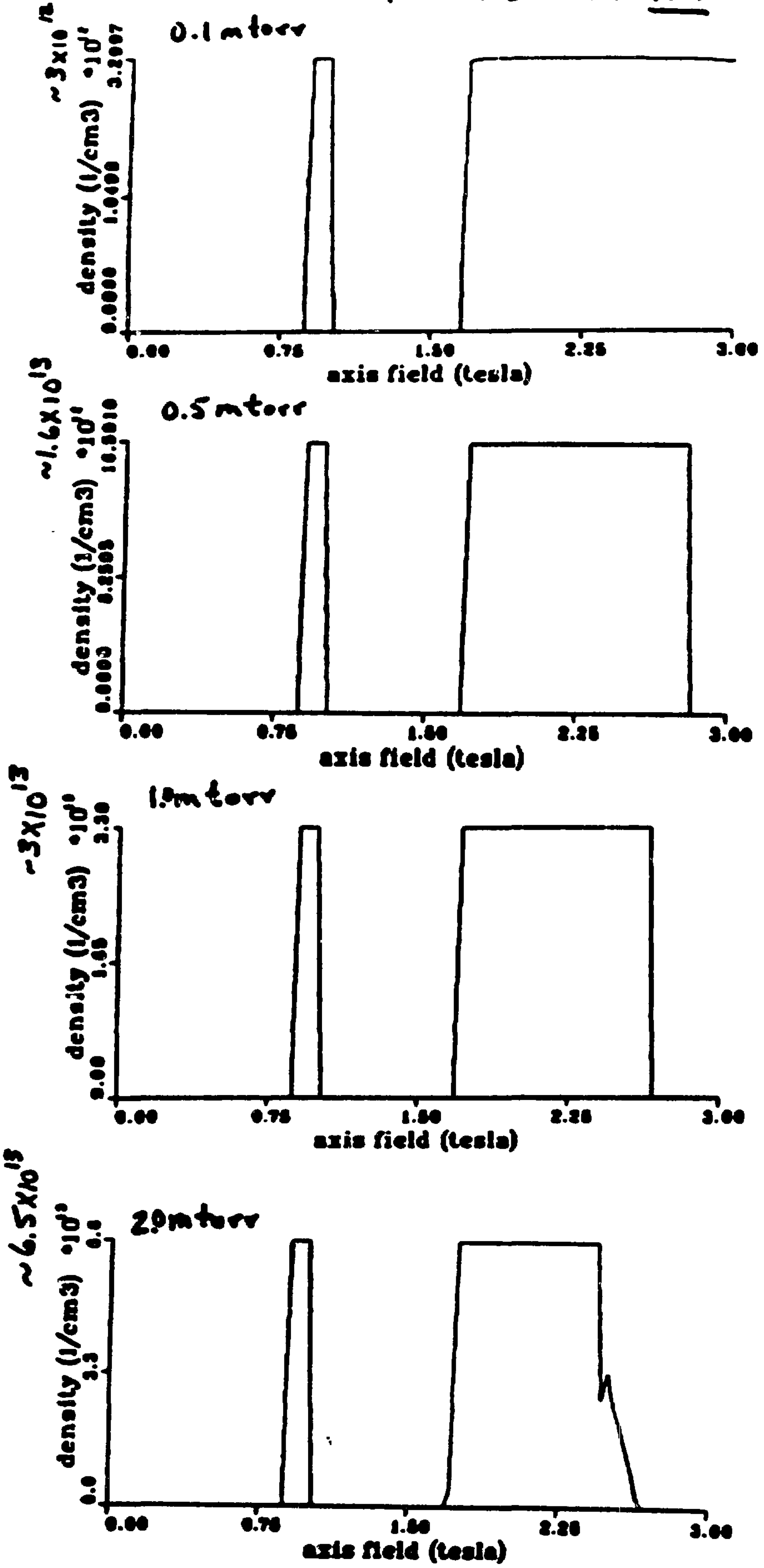

Parameters

200 kW @ 53 GHz

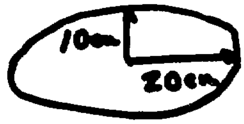

$m = 19 \quad \ell = 2 \quad \gamma = 2$

$R = 2.1\,m$

$A_t = 0.5\,m^2 \quad A_c = 5\,m^2$

$\rho = 0.5\,\mu\Omega m$

$\tau_{max} = 0.03$ sec

(A_T, A_c are uncertain for Heliotron-E)

Second harmonic fails at ~3.0 mtorr

Reasonable plasmas in ATF for 1^{st} and 2^{nd} harmonic

- Note: Plasma cutoff not accounted fo

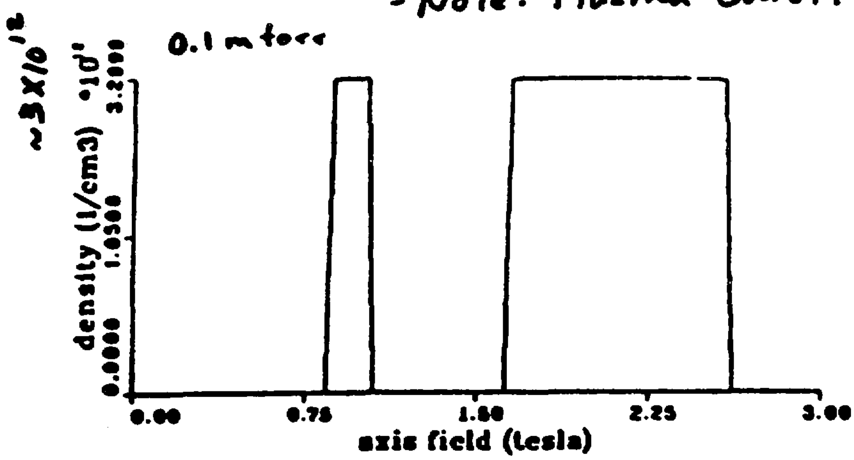

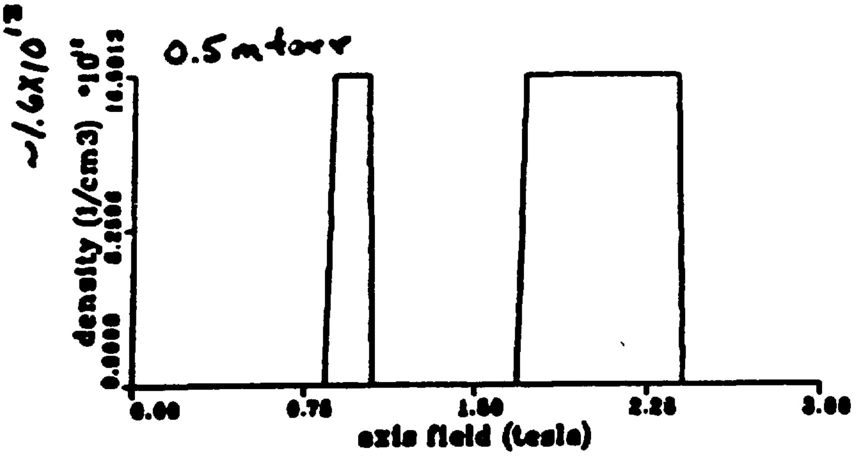

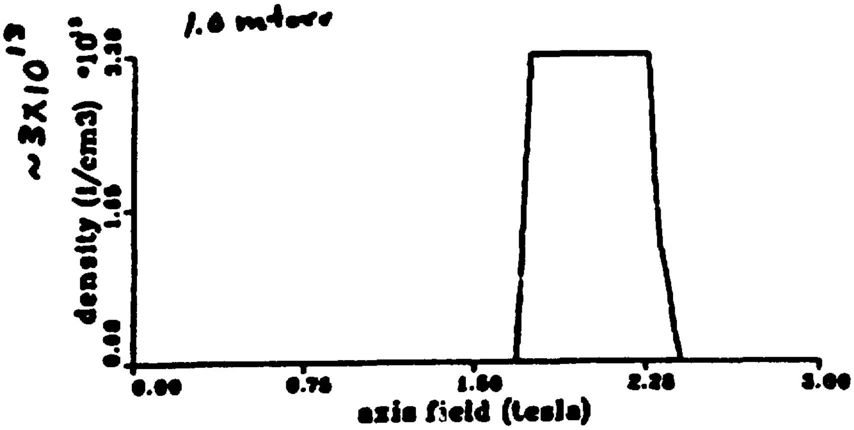

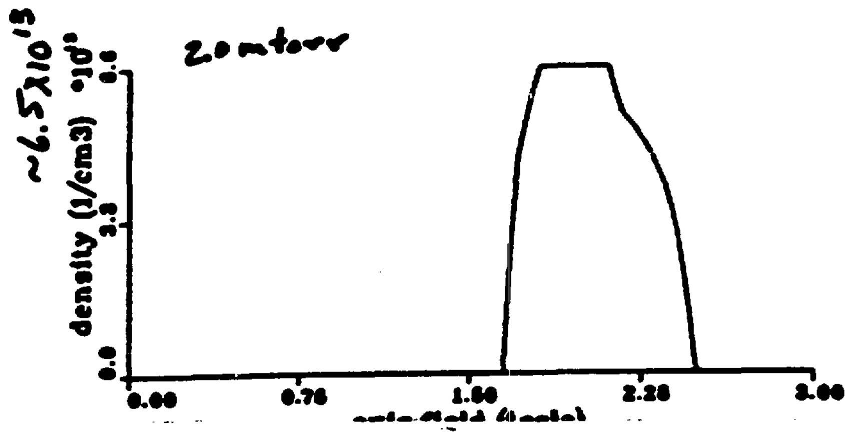

Parameters

200 kW @ 53GHz

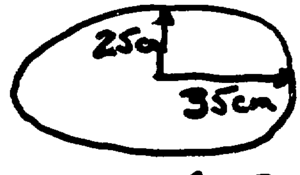

m = 12 ℓ = 2 ρ =

R = 2.1m

$A_t = 1m^2$ $A_c = 90$m

$\rho = 0.5 \mu\Omega m$

$\tau_{max} = 0.05$ sec

Note: A_t is most uncertain parameter

Pressure too high for 2^{nd} harmonic

Breakdown inhibited when antenna voltage is too high or too low

- Voltage usually increased after plasma reaches a few $10^{11}\ cm^{-3}$ density

neutral pressure (torr) 1.500×10^{-6}
magnetic field (gauss) 4.400×10^{3}
rf frequency (MHz) 5.431×10^{0}

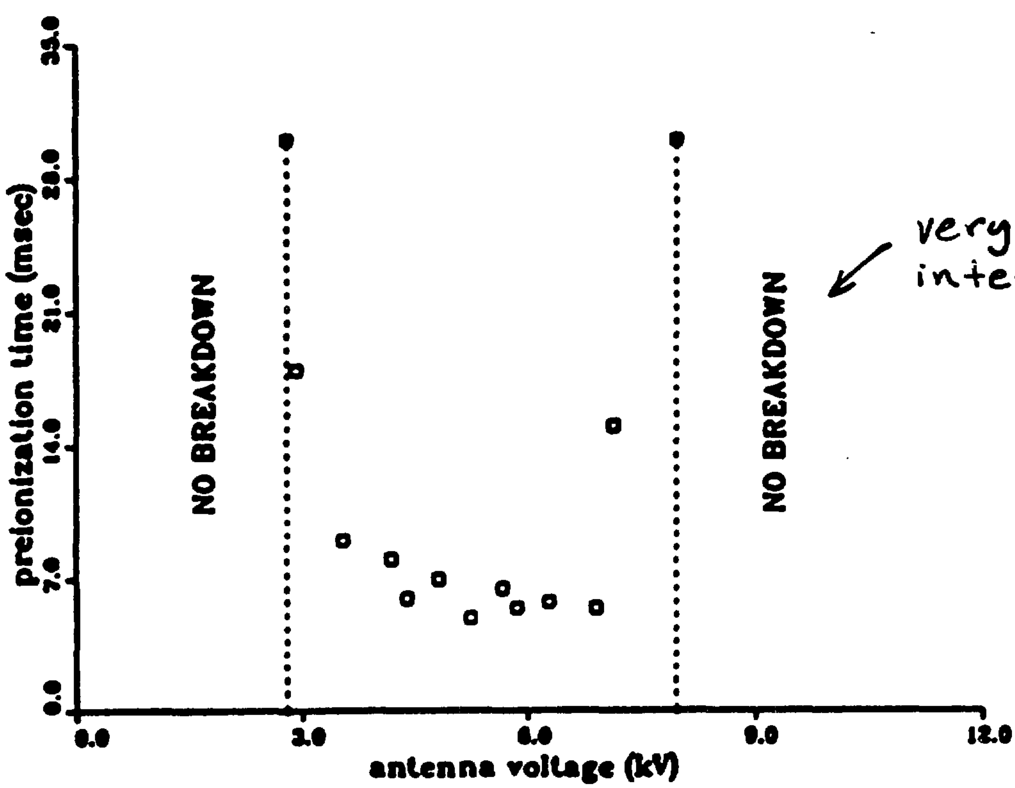

very interesting

ICRF plasma production in Uragan III represented by 2 stages

1) IONIZATION PHASE ⇐ remainder of talk

2) Buildup phase

- several models; Alfven, parametric

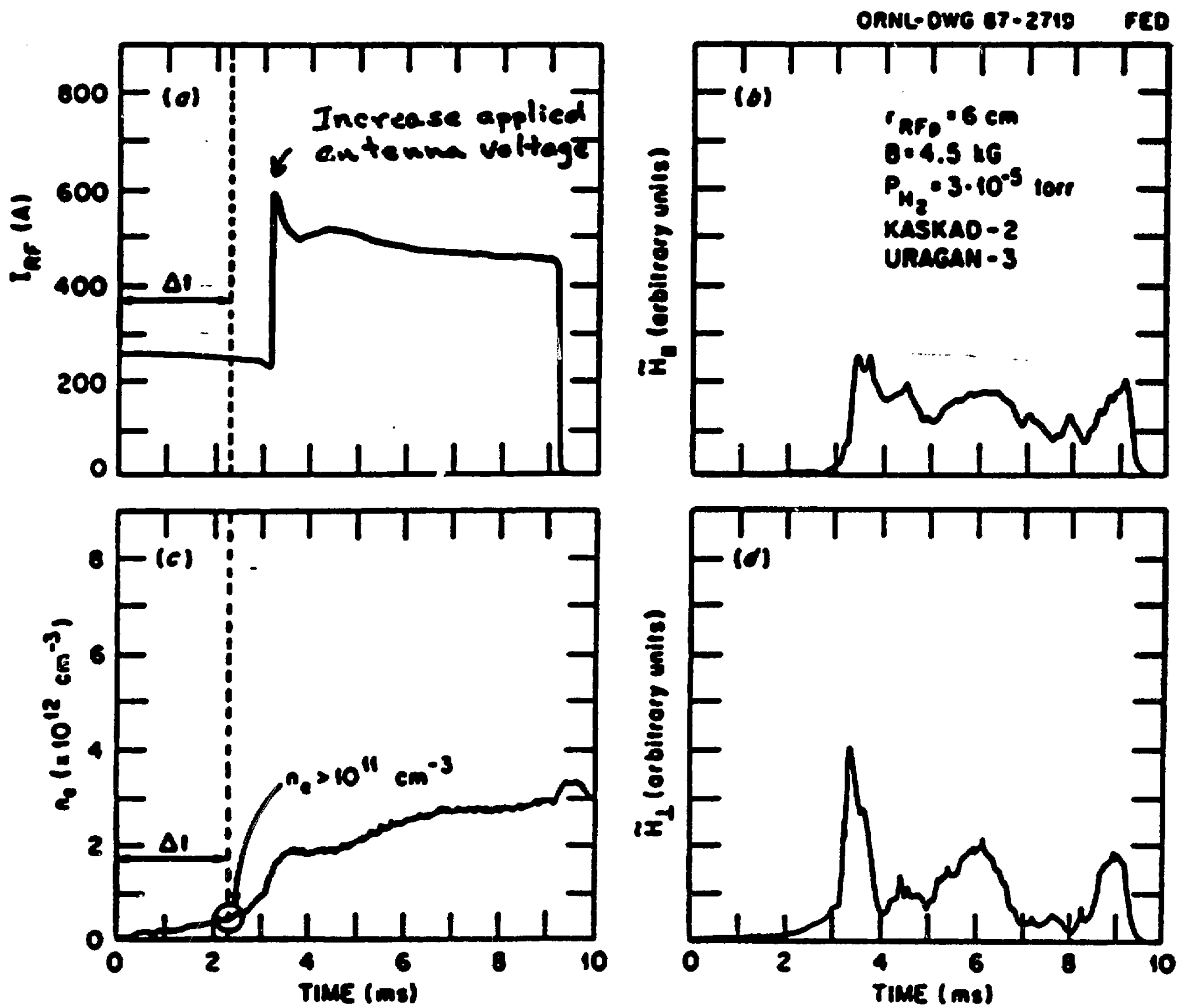

fields ~ 1/3 of way around torus from antenna

First ATF antenna is much different from Uragan III !

Experiments of interest use different types of antennas

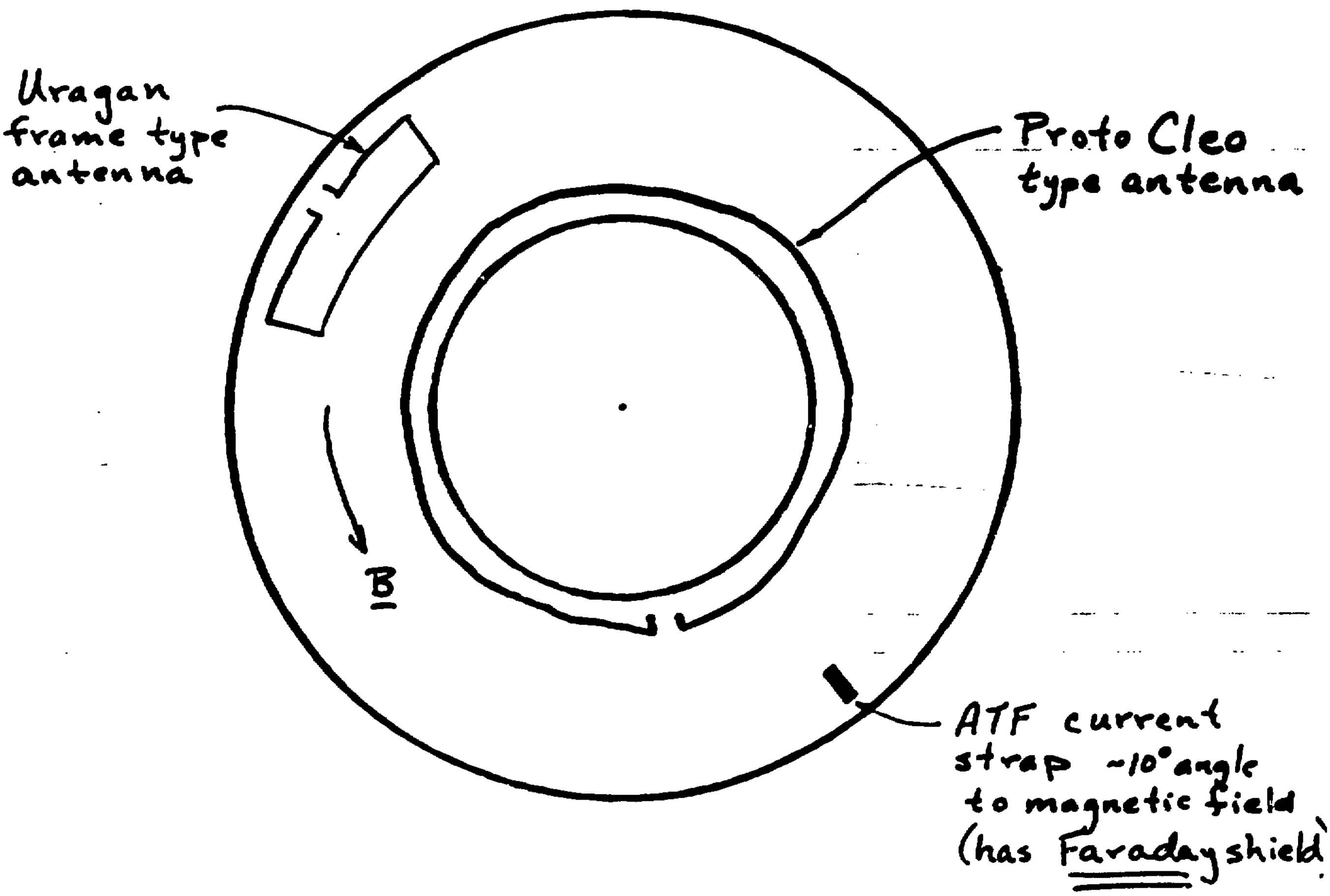

? How much vacuum electric field parallel to static magnetic field is required to break down the neutral gas ?

? Is there a "gap" in plasma density between shorting out of $\underline{E} \cdot \underline{B}$ and propagation of the primary heating mode ?

Plasma Production by Radio Frequency Waves

- Cyclotron heating of free ions in a weakly ionized gas is severely limited by charge exchange

But $\Longrightarrow$ Some power will couple directly to free electrons

- more likely candidate for breakdown
- Vacuum wavelengths ~ c/f are usually too large to fit into cavity (unless a toroidal mode is excited)

$\Rightarrow$ Electric fields parallel to $\underline{B}$ are probably localized (toroidally) near the antenna in ATF, Uragan III

- Assume a form of the electric field

$$E_{\parallel} \approx \underbrace{E_0 \cosh^{-1}\left(\frac{z}{\lambda}\right)}_{\substack{\text{localized} \\ \text{near antenna}}} \cos\underbrace{\left(\cancelto{0}{k_r} z - \omega t\right)}_{\text{not propagating}}$$

? Does electron experience the localized field in a time less than $1/f$ or does it "slosh" in the Electric field ?

Consider 1-D Equation of Motion for model evanescent parallel electric field

$$\frac{d^2 z}{dt'^2} = \frac{q V_A \lambda}{m L_A^2} \frac{\cos(\omega t')}{\cosh(z/\lambda)}$$

Let $\mathfrak{z} \equiv z/\lambda \qquad t \equiv \omega t'$

$$\frac{d^2 \mathfrak{z}}{dt^2} = \frac{q V_A}{m L_A^2 \omega^2} \frac{\cos(t)}{\cosh(\mathfrak{z})} \equiv \delta_m \frac{\cos(t)}{\cosh(\mathfrak{z})}$$

- For electrons, δ_m can be $\gtrsim 1$

  For ions, δ_m is typically $\ll 1$

for electrons: $\delta_m \approx \dfrac{45 V_A}{(L_A f)^2}$, $\left\{ \begin{array}{l} V_A \text{ in Volts} \\ L_A \text{ in cm} \\ f \text{ in MHz} \end{array} \right.$

$\Rightarrow$ Different types of orbits for different initial conditions and δ_m values

$\Rightarrow$ electrons "expelled" if $\delta \gtrsim 1$

Simple cases and dimensionless parameters

- In the homogeneous limit, electron drifts with superimposed oscillation

  - Oscillation energy is:

$$W_{osc} \simeq 22 \left[\frac{E_{\parallel}}{f}\right]^2 eV \quad \begin{cases} E_{\parallel} \text{ is rf field in V/c} \\ f \text{ is rf frequency in M} \end{cases}$$

- For inhomogeneous problem, orbit becomes nonlinear in region where $W_{osc} \gtrsim W_i$ (W_i is energy initially)

  - for model, this occurs for

$$\cosh(z/\lambda) \lesssim \frac{5 V_A \lambda}{\sqrt{W_i}\, L_A^2 f} \equiv \alpha$$

(solution if $\alpha > 1$)

  - the value of $\delta \equiv \dfrac{\delta m}{\cosh(z/L)}$ at this location is:

$$\delta_p \equiv \frac{v_i}{\lambda \omega} \simeq \frac{10\sqrt{W_i}}{\lambda f} \quad \begin{cases} W_i \text{ in eV} \\ \lambda \text{ in cm} \\ f \text{ in MHz} \end{cases}$$

(this is ratio : $\dfrac{\text{rf time}}{\text{transit time}}$)

Numerical Integration

$V_A = 38700$ Volts $\quad L_A = 25.4$ cm $\quad \lambda = 5$ cm $\quad f = 30$ MH

$\underline{\delta \gtrsim 1 \,,\ \delta_p < 1}$ $\Rightarrow$ "Bounces off" rf region

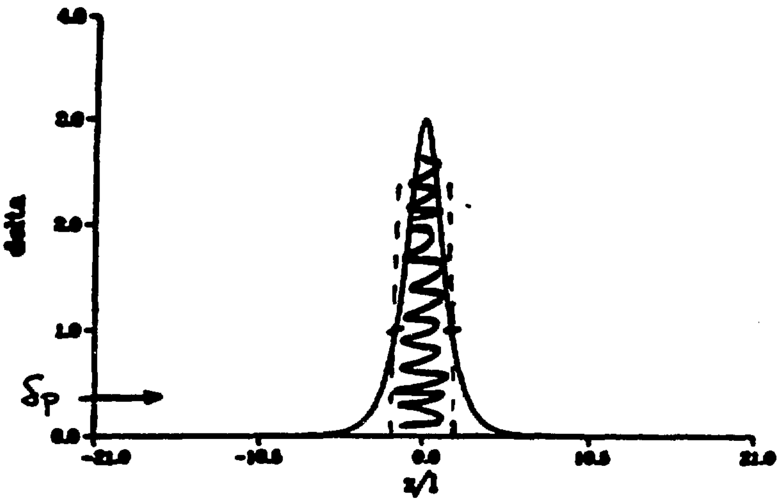

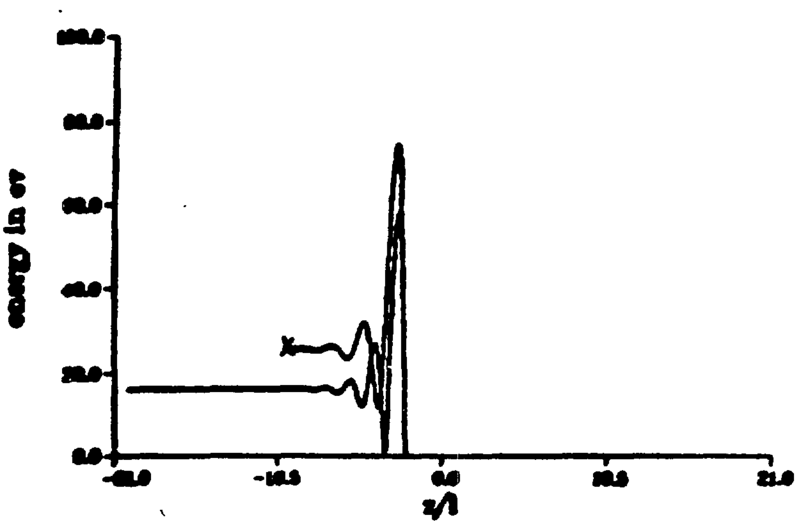

Another simple model: for where $\delta > 1$

- Evanescent fields

$$k_\perp \approx \frac{i}{c}\sqrt{\omega_{pe}^2 + k_\parallel^2 c^2 - \omega^2}$$

$$\perp \text{ behavior} : \quad E_\parallel \approx E_{\parallel 0}\, e^{\int_0^x i k_\perp dx'}$$

- Assume parabolic density profile

$$n \sim n_e \frac{x^2}{L_p^2}$$

- Assume $k_\parallel \approx \dfrac{2\pi}{\lambda}$, $k_\parallel c \gg \omega$

Bernstein Mode launch configuration

parallel extent = 2.5E+01 cm = λ
antenna length = 2.5E+01 cm = L_A
antenna voltage = 3.5E+04 Volts = V_A
rf frequency = 1.0E+01 MHz = f

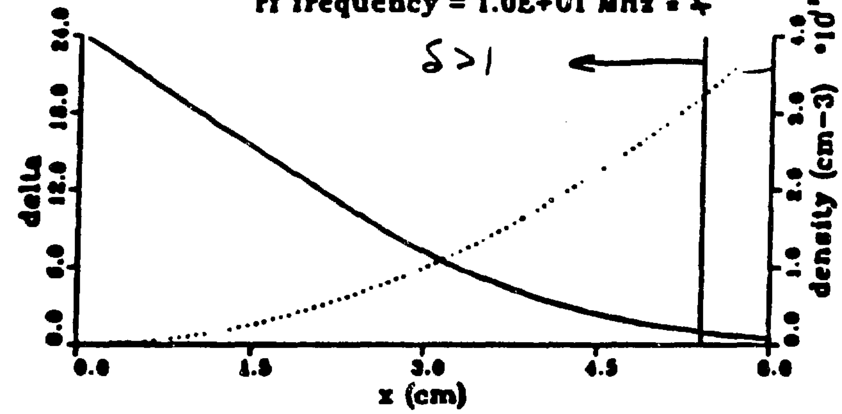

parallel extent = 2.5E+01 cm
antenna length = 2.5E+01 cm
antenna voltage = 3.5E+04 Volts
rf frequency = 2.5E+01 MHz

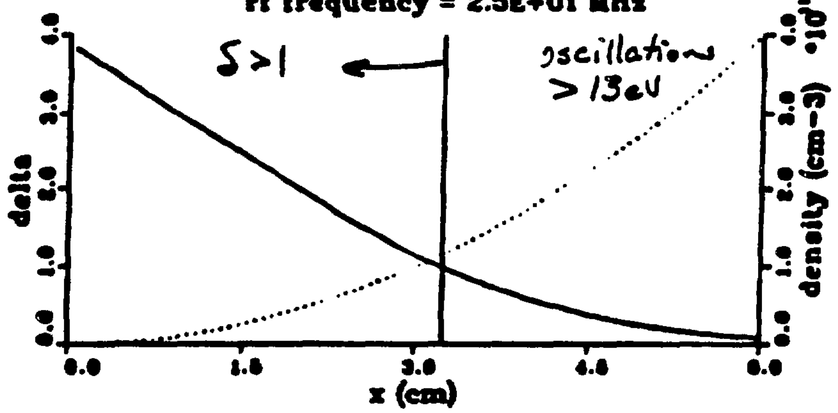

parallel extent = 2.5E+01 cm
antenna length = 2.5E+01 cm
antenna voltage = 3.5E+04 Volts
rf frequency = 4.0E+01 MHz

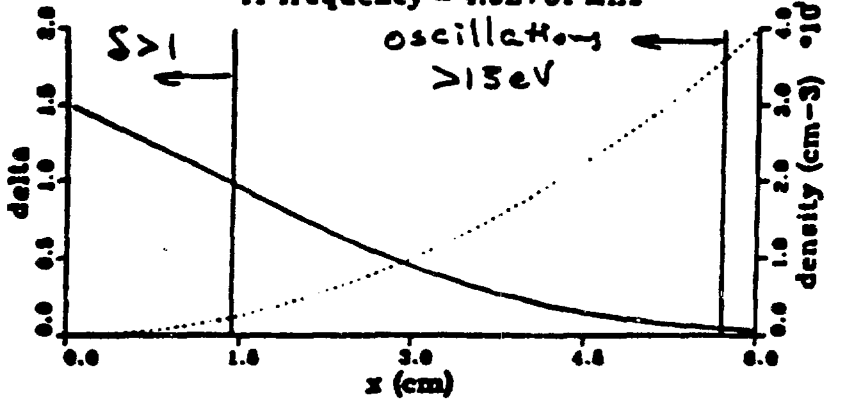

Summary

- 2^{nd} harmonic ECH startup probable in ATF
  - gas control important

- 1^{st} harmonic ECH startup works well if resonance lies inside closed flux surface region

- ICRF startup will probably require dedicated antenna with long parallel wavelengths in ATF